Terms and Conditions of Use of Digitised Theses from Trinity College Library Dublin

Copyright statement

All material supplied by Trinity College Library is protected by copyright (under the Copyright and Related Rights Act, 2000 as amended) and other relevant Intellectual Property Rights. By accessing and using a Digitised Thesis from Trinity College Library you acknowledge that all Intellectual Property Rights in any Works supplied are the sole and exclusive property of the copyright and/or other IPR holder. Specific copyright holders may not be explicitly identified. Use of materials from other sources within a thesis should not be construed as a claim over them.

A non-exclusive, non-transferable licence is hereby granted to those using or reproducing, in whole or in part, the material for valid purposes, providing the copyright owners are acknowledged using the normal conventions. Where specific permission to use material is required, this is identified and such permission must be sought from the copyright holder or agency cited.

Liability statement

By using a Digitised Thesis, I accept that Trinity College Dublin bears no legal responsibility for the accuracy, legality or comprehensiveness of materials contained within the thesis, and that Trinity College Dublin accepts no liability for indirect, consequential, or incidental, damages or losses arising from use of the thesis for whatever reason. Information located in a thesis may be subject to specific use constraints, details of which may not be explicitly described. It is the responsibility of potential and actual users to be aware of such constraints and to abide by them. By making use of material from a digitised thesis, you accept these copyright and disclaimer provisions. Where it is brought to the attention of Trinity College Library that there may be a breach of copyright or other restraint, it is the policy to withdraw or take down access to a thesis while the issue is being resolved.

Access Agreement

By using a Digitised Thesis from Trinity College Library you are bound by the following Terms & Conditions. Please read them carefully.

I have read and I understand the following statement: All material supplied via a Digitised Thesis from Trinity College Library is protected by copyright and other intellectual property rights, and duplication or sale of all or part of any of a thesis is not permitted, except that material may be duplicated by you for your research use or for educational purposes in electronic or print form providing the copyright owners are acknowledged using the normal conventions. You must obtain permission for any other use. Electronic or print copies may not be offered, whether for sale or otherwise to anyone. This copy has been supplied on the understanding that it is copyright material and that no quotation from the thesis may be published without proper acknowledgement.

New Carbon Nanotube Composites

By

Rowan Blake

A thesis submitted to the University of Dublin, Trinity College for the degree of Doctor of Philosophy.

Department of Chemistry
University of Dublin
Trinity College

September 2005

DECLARATION

This thesis has not been submitted as an exercise for a degree at any other university. Except where stated, the work described therein was carried out by me alone.

I give permission for the Library to lend or copy this thesis upon request.

Signed: 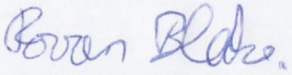

Declaration;

This thesis has not been submitted as an exercise for a degree at any other University. Except as otherwise indicated, the author carried out the work described herein alone.

I give permission to the library to lend a copy of this thesis upon request.

Rowan Blake.

Rowan Blake

List of abbreviations

AFM	Atomic Force Microscopy
atm	atmospheres
BE	Binding energy
CPP	chlorinated polypropylene
CPE	chlorinated polyethylene
CVD	Chemical Vapor Deposition
t-Bu	tert-butyl
n-Bu	butyl
DMTA	Dynamic Mechanical Thermal Analysis
DSC	differential scanning calorimetry
EDX	Energy Dispersive X-ray Analysis
HRTEM	High Resolution Transmission Electron Microscopy
IR	Infrared
MWNT	Multi Walled Carbon Nanotubes
NT	nanotube
NMP	N-metyhl pyrolodine
PE	polyethylene
PPV	poly (m-phenylenevinylene-co-2,5-dioctyloxy-p-phenylenevinylene)
PS	polystyrene
PVC	polyvinylchloride
RBM	Radial breathing modes
SEM	Scanning Electron Microscopy
SPM	Scanning probe microscope
SWNT	Single Walled Carbon Nanotubes
TCD	Trinity College Dublin
TEM	Transmission Electron Microscopy
TGA	Thermo gravimetric analysis
THF	tetrahydrofuran
UTS	Ultimate tensile strength
XPS	X-ray photoelectron spectroscopy

Summary

The main goal of this research is to prepare new chemically functionalised carbon nanotubes and their composite materials and to investigate their properties. This work is focused on the use of organometallic chemistry for the functionalisation and modification of carbon nanotubes.

In chapter 2, preparation and purification of arc discharged nanotubes were initially explored. However, due to the price reduction in CVD nanotubes from Nanocyl CVD nanotubes were used in the following studies. The lithiation reaction using n-BuLi was performed on the purified annealed nanotubes giving highly air and moisture sensitive and extremely reactive adducts. The lithiated nanotubes have been reacted with selected metal (Au, Sn, Pb, Ge) and metalloid (Si) halides. These reactions resulted in the loss of lithium halide and the formation of covalent metal to carbon, nanotube, bonds, producing a metal coating on the nanotubes. Lithiated carbon nanotubes have also been found to be very strong reducing agents, which can reduce gold from its salts giving gold metal nanoparticles on the nanotube surface. The products of the reactions have been characterised by TEM, HRTEM, IR, Raman and XPS spectroscopy.

In chapter 3, lithiated nanotubes have been treated with a range of alkyl halides with various carbon chain length: octyl, decanyl, hexadecanyl and docosanyl. These reactions yielded new alkyl functionalised carbon nanotubes. TGA results have shown that the decomposition temperature of alkyl functionalised nanotubes is substantially lower than for the non functionalised nanotubes. Sedimentation studies have shown that the solubility of alkyl functionalised nanotubes in THF increase with alkyl chain length reaching an optimum for hexadecanyl. Reactions of di-halogenated alkyls (1,6 di-bromohexane and 1, 12-di-bromododecane) with lithiated carbon nanotubes resulted in the formation of a number of tip to tip and tip to wall junctions cross-linking different nanotubes.

The alkylated carbon nanotubes were then mixed in solution with a range of polymers (chapter 4) chlorinated polypropylene, chlorinated polyethylene, polyvinyl chloride and polystyrene. Polymer films with alkylated nanotubes composite films have been prepared

by solution casting. The mechanical properties of these composites (Young's modulus, tensile strength and toughness) have been studied using a tensile tester. This research has shown that the mechanical properties of alkylated carbon nanotube polymer composites strongly depend on the nature of polymer, length of the alkyl chain and vol.% of nanotubes. In general, for the selected polymers hexadecanyl functionalised nanotubes provided the optimum alkyl chain length for overall polymer reinforcement. The most significant improvement in mechanical properties was observed for polyvinyl chloride and polystyrene composites. Chlorinated polypropylene and chlorinated polyethylene composites have shown more modest increases.

Lithiated carbon nanotubes were then reacted with halogenated polymers such as chlorinated polypropylene and polyvinyl chloride (chapter 5). The reactions resulted in elimination of lithium halide and covalent bonding of the polymer to the nanotubes giving polymer grafted nanotubes. New nanocomposite materials have been studied by transmission electron microscopy, TGA and IR spectroscopy. Subsequently, polymer grafted nanotubes have been used to prepare a range of polymer carbon nanotube composites by solution casting technique. The addition of the polymer-grafted nanotubes to the chlorinated polypropylene polymer matrix resulted in the most significant increase in mechanical properties. As the nanotube content is increased to 0.6 vol %, the Young's modulus increased by a factor of 3, while both the tensile strength and the toughness increased by factors of 3.8 and 4, respectively. The PVC composites reinforced with CPP grafted nanotubes demonstrated more than a ten fold increase in the toughness of the films. The covalent functionalisation of nanotubes enabled an efficient dispersion and excellent interfacial stress transfer, potentially leading to new ultra-strong polymer composite materials.

Chapter 6 contains the experimental details for the procedures and techniques described in this work. Chapter 7 presents final conclusions and the future outlook for the research performed in this project. Overall this work produced a number of very interesting carbon nanotube composites which could potentially be used commercially for polymer

reinforcement and development of new devices for nanoelectronics. We also believe this work should contribute to both materials chemistry and nanotechnology.

'*Our business is to realise the world as we see it, not to reform it as we know it.* '

'The Model Millionaire' ***by***

Oscar Fingal O'Flaherty Wills Wilde

Acknowledgements

I would like to take this opportunity to express my sincere appreciation and gratitude to my supervisor Dr. Yurii K. Gun'ko for all of his help, advice and his belief in me where others would have doubted.

The Financial support given by Higher Education Authority, PRTLI, is greatly acknowledged.

I must also thank all of the staff in the chemistry department.

To the group Ian O' Conner, Michelle Byrne, Serena Corr, Mick Maloney, Anna Zukova, Arunas Teiserskis, Sivakumar Balakrishnan and Stephen Byrne thanks for your help and laughs.

To all the of the guys in the physics department who have helped me in particular; Dr. Jonny Coleman, Karen Hosie, Dr. Manuel Ruether, Dr. Martin Cadek, Rory Leahy, Dr. Tatania Perova, Valeria Nicolosi. To everyone in the CMA where I spent the first few years, in particular Neal Leddy and David John thank you very much for your help.

To Fiona Paolozzi and Fiona Doherty whom have given me the ability to achieve things that before I would have thought never possible I owe you so much. Thank you.

To my dearest friends all of whom have played an immense part in this thesis and my life I thank you; Dr. Aine Whelan, Andrew Felton, Dr. Andrew Harte, Andrew O'Neill, Anna Dunphy, Catherine McLaughlin, David Kinlen, Deborah Moore, Eoin Quinlan, Garret O'Moore, Dr. Hugh Hayden, Iain Macaulay, Joanne Hayes, Ken Bryan, Dr. Kevin Ryan, Dr. Michael Seery, Moira Kelly, Richard Wallace, Dr. Róisín Reilly, Sheena MacDonald, Dr. Úna Hanafin and Wesley Earl.

To Richard and Rona Felton my sincerest thanks for all of your support both emotional and intellectual throughout the last four years.

To Joe Neavyn, John Blake, Lorna Neavyn, Dr. Micheal Miniter, Monica Dowdall-Blake and Rose Miniter thank you for your support and help.

To Brian and Anna Hussey thank you for your encouragement, words of support, belief and love.

Dorothy Blake who has been a pillar of support through my entire life and someone who I have depended on throughout my life I owe you so much. Thank you.

To Sonya Felton I love you and thank you so much for bearing me for the last seven years.

To Katherine Blake to whom I owe everything I can only try to express in words how much I am indebted to you, love you and owe you. Thank you.

Table of Contents: **Page No.**

List of Figures, Schemes and Tables : Page No.

Chapter 1

Figures

Chapter2

Figures

Schemes

Chapter 3

Figures

Schemes

Chapter 4

Figures

Tables

Equations

Chapter 5

Figures

Tables

This thesis is dedicated to the ones I love…

To Dorothy, Katherine and Sonya

Chapter 1

Introduction

1.1 General introduction into carbon nanotubes

Carbon, in sp^2 hybridisation, is known to form several interesting structures. Most familiar is that of graphite which has been known for centuries and more recently there has been the discovery of C_{60}, by Kroto *et al.*[1] After the discovery of this molecule, a number of structures from C_{70} to C_{1800} have been produced.[2] Initially C_{60} could only be obtained in small amounts however in 1990 Wolfgang Kratschmer and Donald Huffman discovered a way of making C_{60} in relatively large, milligram, amounts[3] through the arc discharge method. This involved two carbon electrodes which when an arc was generated, through the application of a DC current in an inert atmosphere, produced the C_{60} molecules in a deposit formed on the cathode.

In 1991 the Japanese microscopist, Sumio Iijima, who was studying the material deposited on the cathode during the arc discharge method of formation of fullerenes, discovered tubular structures of carbon,[4] which would become known as carbon nanotubes. Schematic images of a multi-walled (MWNT) and single-walled (SWNT) carbon nanotubes are shown in figure 1.1. The nanotubes are made up of cylindrical tubes of rolled graphite layers. MWNTs consist of several cylindrical tubes of different diameters encapsulated in each other. In each of the nanotubes the carbon-atom hexagons are arranged in a helical fashion about the needle axis. The tips of the tubes are normally closed by curved, polygonal, or cone shaped caps.

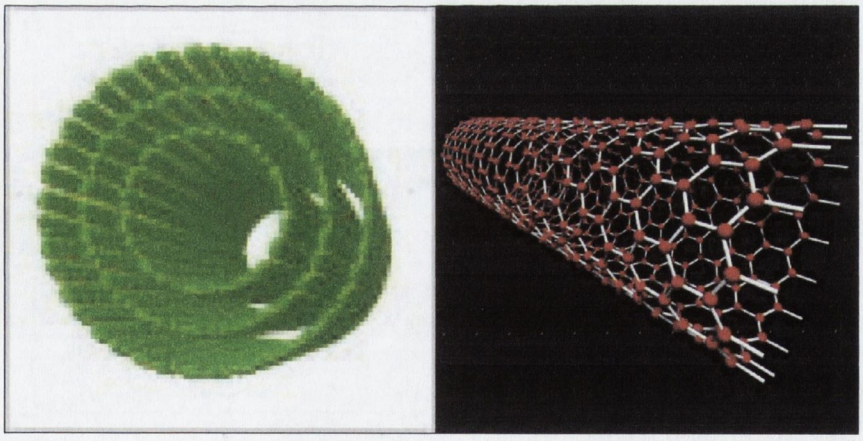

Figure 1.1 Multi Walled Nanotube (MWNT), left, and Single Walled Nanotube (SWNT), right[5]

1.2 Preparation of carbon nanotubes

In 1991 Iijima discovered multiwalled nanotubes, seven years later in 1998 Iijima, and Ichihashi[6] as well as Bethune *et al.*[7] discovered single walled nanotubes (SWNTs). Nanotubes are produced predominantly *via* three methods; arc-discharge, laser ablation and chemical vapour deposition (CVD), also known as catalytic growth. There are also different modifications of these techniques, such as the method by Zhu *et al.* [8] who used the arc discharge method under water, however in general these are the prevailing forms of nanotube production. Initially MWNTs were prepared by Iijima using the Kratschmer-Huffmann generator. They were grown on the cathode which was in an argon filled chamber at 100 Torr, the set up is shown in figure 1.2. The MWNTs ranged from 4 to 30 nm in diameter and up to 1 micron in length.

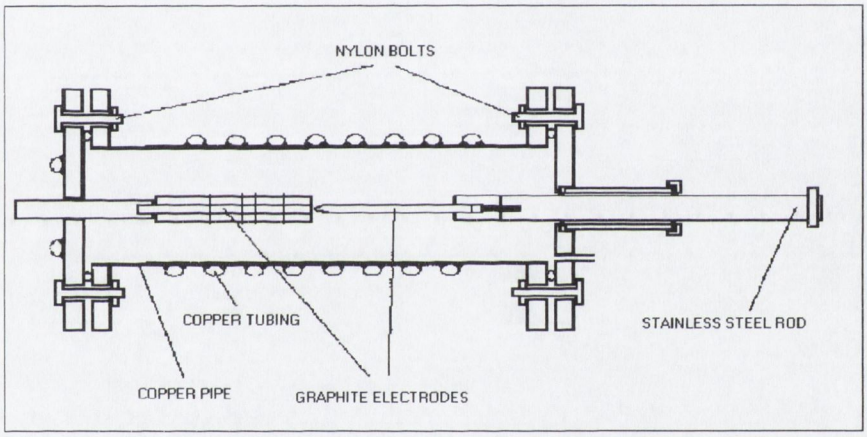

Figure 1.2 Kratschmer-Huffmann Generator[9]

In this set up both cathode and anode are carbon electrodes and the DC current is applied whilst the system is under an inert pressurised atmosphere. Smalley, who was originally involved in the discovery of C_{60} proposed a method of producing nanotubes *via* the use of laser-ablation.[10] Yacaman *et al.*[11] were the first people to grow nanotubes catalytically *via* chemical vapour deposition (CVD).

Iijima *et al.* reported on the growth morphology of the arc discharge MWNTs. They discovered that there are many variations in the shape of the hexagonal rings, especially close to the tip.[12] Ebbesen and Ajayan[13] reported a variation of the technique used by Iijima in which they achieved large scale synthesis of MWNTs, ~75% of the starting material, this involved a helium atmosphere as well as slight variation on the DC current applied. The

nanotubes had diameters between 2 and 20 nm and lengths ranging in micrometers, the tips were capped with pentagons.

Working on the laser ablation method reported by both Iijima and Bethune, Journet *et al.*[14], figure 1.3, obtained large quantities of SWNTs using a helium atmosphere and filling the anode with a mixture of metal catalysts and graphite powder. The material produced was analysed by scanning electron microscopy (SEM) and contained ~ 80% of SWNT ropes.

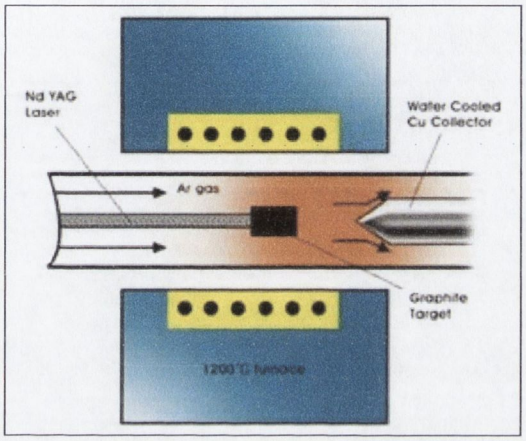

Figure 1.3 The laser ablation production of carbon nanotubes (CNTs)[15]

Smalley's laser ablation method [10] of SWNT production delivered high yields of nanotubes, greater than 70%, and again involved the use of catalysts both Ni and Co. This is all carried out in a furnace at the very high temperature of 1200 °C. The nanotubes that were produced were reported as being uniform in diameter these nanotubes formed ropes that were 5-20 nm in diameter.

Yacaman *et al.*[11] used the CVD method to produce MWNTs. This was performed by passing a carbon source, generally ethylene or acetylene through a furnace at 550 to 750 °C and nanotubes are grown over a catalyst, present in the furnace, after cooling. In general the catalysts used are iron, nickel or cobalt nanoparticles. The heat or energy source is used to break the carbon source into reactive carbon which reacts on the catalysts surface and forms nanotubes. Excellent alignment as well as positional control on the nanometre scale is possible by using the CVD method.[16,17] By choosing the appropriate catalyst it is possible to grow preferentially SWNT or MWNTs.[18] Figure 1.4 shows the setup for a CVD chamber and how the CVD nanotubes are produced.

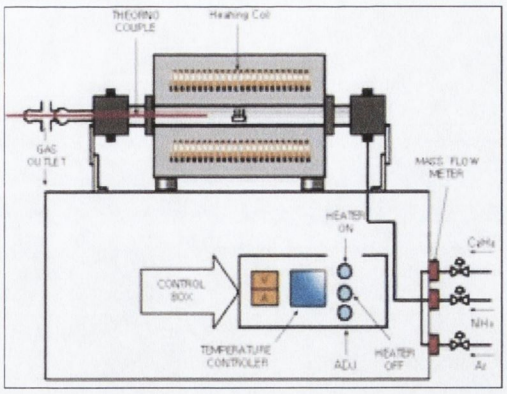

Figure 1.4 Chemical Vapour Deposition apparatus for carbon nanotube production[19]

The growth mechanism of carbon nanotubes is still the subject of much debate. The mechanisms of formation are more than likely based on a combination of several of the published theories.[18-22] However, one thing that is certain is the drastically different synthetic requirements for SWNTs and MWNTs, exemplified by the necessity of the catalysts presence in the arc discharge method of production. This suggests that the mechanism of the formation of these nanotubes is quite different.

It has been observed experimentally that MWNTs grow in two directions both by lengthening and thickening. There comes a point when the nanotubes terminate or close and cease growing, during the formation MWNTs remain open at both ends. Guo *et al.*[20] suggested that the open ended structure is supported by a *lip-lip* interaction between the walls. Tight binding calculations on MWNTs showed that the edge is stabilised by a bridging carbon which supports this theory.

Charlier *et al.*[21,22] performed first principle molecular dynamic simulations on the growth process of both SWNTs and double walled nanotubes (DWNTs). They found that, at experimental temperatures in the absence of catalyst and in accordance with experimental findings the SWNTs close. The form of a SWNT and its diameter depends on the form of catalyst in both the arc discharge and laser ablation production methods. Sinnott *et al.*[18] suggests that the metal catalyst particle floats or is supported on the graphite wall which builds up the wall as it floats. It presumes that the catalyst particles are spherical or pear-shaped, in which case the deposition will take place on only one half of the surface (this is the lower curvature side for the pear shaped particles). The carbon diffuses along the concentration gradient and precipitates on the opposite half, around and below the bisecting diameter. While floating, they prevent the formation of pentagons and dome closure and allow

the formation of hexagons.[23] As the catalyst forms more and more hexagons it gradually becomes poisoned by excess carbon clusters which results in tip closure.

In some cases nanotube skeletons or filaments can form by extrusion in which the nanotube grows upwards from the metal particles that remain attached to the substrate. This is the formation that is observed in laser ablation method. Molecular dynamic calculations have been carried out which support this theory.[24] Another proof of this theory is that the ends of the SWNTs produced in the laser ablation method contain the majority of metal clusters. Depending on the size of the catalyst particles, SWNT or MWNT can be grown. In arc discharge, if no catalyst is present in the graphite, MWNT will be grown on the C_2 particles, where C_n stands for n fold coordinated carbon atom, that are formed in the plasma.

1.3 Structure of nanotubes

Nanotubes exist as different types; arm-chair, zigzag and chiral. These names are attributed to the layout or structure of the carbon atoms around the nanotubes' surface. They can be described by the chiral vector (n,m) where n and m are integers of the vector equation $R = na_1+ma_2$. The chiral vector is determined by the diagram in figure 1.5. The grey hexagons drawn in figure 1.5 represent those of the graphitic plane which when rolled form the nanotubes' wall. The blue lines represent the nanotube; if it was possible to cut along those lines and then connect the ends together this would form the nanotube. Point A represents where the line intersects an atom. The yellow line coming from point A is indicative of the arm chair form of the nanotube. Point B is the point nearest to this line which intersects another carbon atom. The atoms shown as points are now connected with the chiral vector R. The wrapping angle can be calculated by finding the angle between the chiral vector and the armchair line.

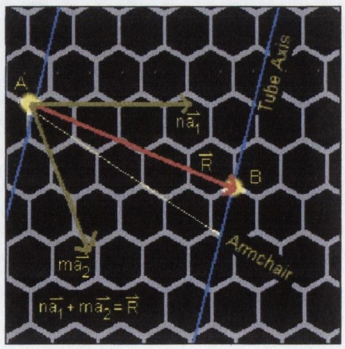

Figure 1.5 the diagrammatic representation for the calculation of the chiral vector for nanotubes[25]

If this angle is equal to 0 ° then the nanotube is of the armchair form. If the angle is equal to 30 ° then it is a 'zigzag' type and if it is between these two values then it is chiral. The vector in figure 5 of na_1 is that of the 'zigzag' form. If the vector of na_1 and ma_1 are added they represent that of a chiral nanotube.[26] The chirality of a nanotube affects many its properties including its conductance and density. The armchair form shows metallic behaviour, the zigzag is semi-conducting and the conductivity of the chiral nanotube depends on the chirality. In figure 1.6 the three forms of nanotubes are pictorially represented which makes it easier to visualise.

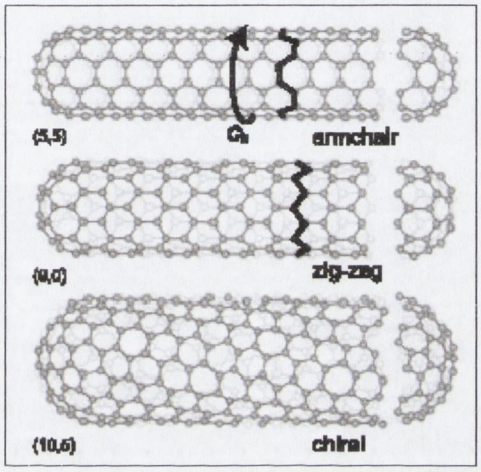

Figure 1.6 pictorial representations of armchair, zigzag and chiral forms of nanotubes[27]

Nanotubes, in particularly SWNTs frequently form bundles or ropes. In these structures nanotubes are packed closely together in an orderly manner. Thess *et al.* [8] measured the properties of these ropes of nanotubes. They found that the SWNTs in a triangular lattice had a lattice constant of 17 A and that the nanotubes are packed in a hexagonal close packed array.[28] In general SWNTs are packed much more tightly together than MWNTs and it is more difficult to separate SWNTs from these ropes.

1.4 Analytical techniques used for nanotube characterisation

Raman spectroscopy

Initially, Raman spectroscopy was performed on ropes of nanotubes and then later, on isolated single SWNTs and MWNTs.[29,30] The Raman spectra of SWNTs usually exhibit four main bands: at 2600 - 2700 cm^{-1} there is the *G'* band, at ~1580 -1600 cm^{-1} is the *G* band, the *D*

band at ~1350 cm^{-1} and the radial breathing modes (RBMs) which are generally found below ~400 cm^{-1}, figure 1.7.

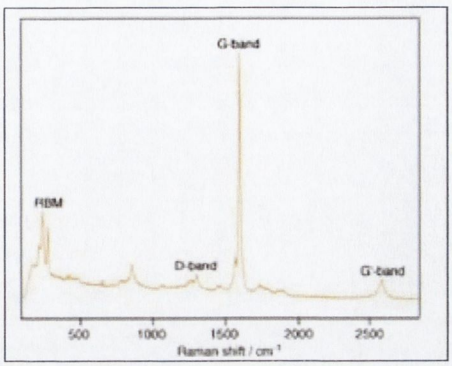

Figure 1.7 Raman spectrum of SWNTs exhibiting RBM, D, G and G' bands[31]

The G band, graphitic band, in the Raman spectra is that of tangential C-C stretching mode. This peak is derived from the optically allowed mode E_{2g} of 2D graphite. The G band is an intrinsic feature of carbon nanotubes one of the most important features of this peak is that from the shape it is possible to infer whether the nanotubes are conducting or not. It is the area of graphitisation of the nanotube and from it the degree of graphitisation can be estimated. Due to the structure of arc discharge nanotubes which are perfectly straight the G band of these nanotubes is very large. Conversely, the D, disorder, band is the dispersive disorder-induced band, which corresponds to the sp^3 carbon atoms, if the nanotube was an ideal nanotube this peak would be due solely to the carbon atoms on the tip. In a CVD nanotube however, which are exceptionally curvy and defective from the theoretical structure, there is a relatively large D band with respect to the G band. The G' band is due to a second order Raman scattering.[32]

The RBMs which are found at the lower-frequency side of the spectrum are those peaks which arise from the movement of the nanotubes. As is the case with all molecules the nanotubes are not stationary objects. The perfect cylindrical picture which is evoked by theoretical nanotubes like those in figure 1.6 is not in reality how they exist. The RBMs are dependant on the diameter of the nanotubes. The nanotubes are in a constant state of movement, molecular movement and this movement changes the size of the nanotube both laterally and horizontally. It is this which is accounted for in the RBM peaks of the Raman spectrum. Noticeably the RBMs are much more pronounced in the SWNTs spectrum because they have a greater

freedom of movement due to the fact they are not inhibited by the inner walls as in the MWNTs.

Infrared spectroscopy IR

There are between seven and nine IR active modes in SWNTs which are strongly dependent on symmetry.[33] The frequencies are at 868 and 1575 cm^{-1} according to Kaster *et al.*[34,35] and Kuhlmann.[24] This form of characterisation was used initially to observe any residual catalyst or other impurities however, as more chemistry such as organic chemistry is performed on nanotubes this technique is fast becoming much more important. For example, Saito *et al.*[36] characterised the MWNTs which they had chemically altered by amino compounds using this technique.

X-ray photoelectron spectroscopy (XPS)

XPS is another technique which provides information of the structure of the nanotubes outer surface. Again it is a technique which is becoming more popular as more chemistry is performed on the outer surface of the nanotubes. For instance, Droppa *et al.*[37] studied the incorporation of nitrogen into nanotubes. They examined the C1s and N1s regions of the XPS and what they noticed was that not only do the peaks broaden but also they are shifted to higher binding energies. Lee *et al.*[38] who studied sidewall fluorination of SWNTs also studied the C1s spectra of the SWNTs. They suggest that there are three peaks in the spectrum of pristine SWNTs, they are at 284.3 eV for sp^2 carbon, 285 eV for sp^3 carbon and 288.5 eV for any carboxyl groups.

Transmission and Scanning Electron Microscopy

The principle of an electron microscope is based on is that electrons are fired, from an incandescent tungsten or lanthanum hexaboride crystal, in a vacuum through a column. These electrons are focused by a series of magnets which narrow the beam of electrons. In order to accelerate the electrons, so as to ensure sample penetration, an anode with an orifice is placed above the sample. The electrons which are in the centre of the beam rush through the orifice and also the sample. The electrons, in the case of transmission electron microscopy (TEM), are fired through the sample being analysed and the image is seen on a fluorescent screen which is a shadow of the sample. In scanning electron microscopy (SEM) reflected and

secondary electrons are processed by an electron detector to form a three dimensional image on a monitor.

SEM is a very good technique for studying the surface morphology of objects. It is possible to reach very high magnitudes which are facilitated by it being in a vacuum. The vacuum allows electrons to be fired at the sample; however, because of this the subjects must be excellent conductors in order to dissipate the electrons. If a non-conducting sample was used it would lead to a build up of electrons and would not allow adequate imaging. This is also a problem with this method because in order to make nanotubes suitable for this form of microscopy they must be covered by a thin layer up to 20 nm, of gold. The problem is visible in figure 1.8, when trying to observe changes in the structure or surface of the nanotubes this technique is entirely unsuitable. The reason being, that the nanotubes depicted in the SEM image on the left of figure 1.8 are on average 50 nm in width however the actual width of the nanotubes which can be seen on the right of the figure, is actually half this at 25 nm. Thus any minute changes to the surface of the nanotubes would be hidden by the large coating of gold.

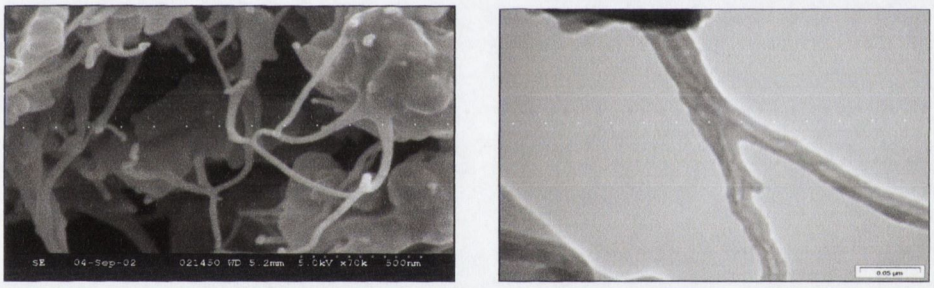

Figure 1.8 Examples of an SEM image, left, and TEM image, right, of CVD MWNTs

TEM, however, is a very useful technique and there are no papers published on carbon nanotubes that are acceptable without this technique included. Again the samples are placed in a high vacuum and electrons are fired at the sample whereas SEM works on the basis that electrons are deflected from the surface of the subject in view the TEM works on the basis that the electrons are transmitted through the species to form the image. The samples are dropped on a copper grid, which has either a formvar polymer or a carbon film coating, by suspending the sample in a solution suitable for the particular coating.

1.5 Mechanical, thermal and electrical properties of carbon nanotubes

Mechanical properties

Nanotubes are reported to have outstanding mechanical properties. This is due to the very strong sp^2 bonding of the carbon atoms of the side walls.[39] The expected Young's modulus for both SWNTs and MWNTs lies in the region of 1.28 TPa, which can be compared to steel (ASTM-A36) of 190 GPa. Treacy *et al.*[40] reported an elastic modulus of 1.25 TPa by measuring the intrinsic vibrations of the nanotubes with the use of a TEM. A year previously Wong *et al.*[41] discovered the tensile modulus of a MWNT to be 1.28 TPa. They measured the modulus by using the tip of an atomic force microscope (AFM). An AFM works on the principle similar to a record needle, there is a single crystal on the end of a lever. As the tip is moved up by what is present on the surface, the lever records this. In their experiment the nanotube was held in position by a glue, silicon oxide, and the tip was used to push the nanotube out of its equilibrium position and the force required to do so was recorded. The types of deformation of the nanotubes varied from a plastic deformation to complete fracture which allowed the modulus to be calculated. E. Hernandez *et al.* showed that with use of tight binding calculations the modulus was strongly dependent on size and chirality of the SWNTs with results of 1.22TPa for (10,0) and (6,6) to 1.26TPa for the large (20,0).[42]

The Young's modulus, ultimate tensile strength and toughness of carbon nanotubes was initially studied by Yu *et al.* in 2000 when they managed to do a stress-strain measurement on individual arc-MWNTs inside an electron microscope.[43] For a range of tubes they obtained modulus values of 0.27-0.95 TPa. More interestingly they showed fracture of MWNT at strains of up to 12% and with strengths in the range 11-63 GPa. This allows the estimation of nanotube toughness at ~1240 J/g. Young's modulus is calculated from the slope of the graph shown in figure 1.9.

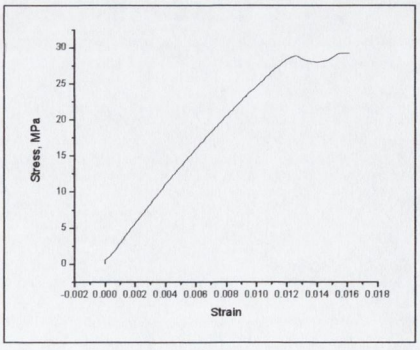

Figure 1.9 Stress/Strain graph of nanotube reinforced PS

UTS, or breaking point of the material is the highest point on the Y axis of the stress strain curve. And toughness is calculated from the stress strain graph as the integral under the curve.

Measurements of mechanical properties for SWNTs are more difficult, because they form bundles held together by π-π interactions. Intertube shear slippage within SWNTs bundles presents a serious limitation to their mechanical properties. The low shear modulus means that effective moduli and strengths for bundles are far below those expected for individual SWNT. It is extremely difficult to de-bundle SWNT. However Garaj and co-workers showed that SWNT could be fused together in bundles by electron irradiation.[44,45] By fine-tuning the dose and irradiation energy they found that they could increase the bundle bending modulus to 750 GPa, close to that of individual SWNT. The maximum tensile strength of a nanotube was found to be 30 GPa.[46]

Solubility

Alone carbon nanotubes are incredibly insoluble in most common solvents. In order to solubilise nanotubes or prepare stable solutions, nanotubes must be chemically functionalised or an appropriate surfactant must be used to disperse them.[47] However, the problem with using a surfactant is that it would prevent any chemical modification of the nanotubes and removal of the surfactant is also difficult. The best suggested solvents for nanotubes to date are *N,N*-dimethylformamide (DMF) and *N*-methylpyrrolidone (NMP).[48]

Thermal Conductivity

The exact nature of the thermal conductivity appears to be a topic of some debate. Although it is generally accepted that conductivity depends heavily on the temperature. In the early stages of nanotube research Hone *et al.*[49] discovered that the thermal conductivity of SWNTs was temperature dependent. They suggested that the conductivity was linear from 7 K to 25 K from 25 K to 40 K the slope of the line increases and rises monotonically with temperature to above room temperature. The same year Che *et al.*[50] numerically calculated the conductivity of a (10,10) nanotube to approach 2980 W/mK as the current applied increased. Also in the same year Yi *et al.*[51] studied the specific heat properties of CVD MWNTs in the temperature range of 4 to 300 K to which they discovered linear dependence of the specific heat on the temperature over the entire temperature interval. The thermal conductivity they discovered was found to vary as T^2, which is similar to graphite. It did not show a maximum due to

Umklapp scattering. Recently the thermal conductivity of an individual MWNT was measured using a micro-fabricated suspend device[52]. The recorded thermal conductivity at room temperature was 3000 W/mK. This is two orders of magnitude greater than those calculated by Hone *et al.*[49] but is close to that of Che *et al.*[50]

Electrical Transport

Electrical transport, or conductivity of carbon nanotubes, has attracted researchers due to the wide variety of possible applications, from nanoscale electronic devices to conductive polymer composites on the macroscale. The conductance of a SWNT is quantized and a nanotube acts as a ballistic conductor. Conversely they also have constant resistance and a tolerance for high current density. Frank *et al.*[53] studied the conductance of nanotubes with the use of a SPM. They made two contacts at either end of the nanotube with a Mercury surface. From this they revealed that the nanotube behaved as a ballistic conductor with quantum behaviour. As additional MWNTs were touched to the mercury surface the conductance jumped by 1 G_0 increments. The value of the conductance, G_0, was calculated as 1/12.9 $k\Omega^{-1}$ where $G_0 = 2e^2/h$. The coefficient was found to have some peculiar values such as 0.5 G_0. Later in 1999, Sanvito *et al.*[54] calculated the conductance of MWNTs and supported the values discovered by Frank.[53] They found that some of the quantum conductance was blocked by interwall reactions. These reactions were able to redistribute the current over the individual tubes across the structure non-uniformly. Thess *et al.*[10] calculated the resistance of ropes of SWNTs to be in the order of 10^{-4} Ω/cm at 300 K. They used a four point technique in order to measure this value. One of their values was in the region of $0.34 * 10^{-4}$ Ω^{-cm} which would mean that these are the most highly conductive carbon fibres known. Frank *et al.*[53] obtained a current density of the nanotube of greater than 10^7 A/cm^2.

1.6 Chemical functionalisation of CNTs

The discovery of carbon nanotubes was achieved by a physicist and microscopist and subsequently these objects drew a large amount of scientific interest from every corner of the world. Initially, the interest was almost exclusively focused on physical properties, with new reports of the outstanding mechanical thermal and electrical properties being published almost monthly. However, except for a few reports neither of the other two main bodies of science, chemistry and biology, entered into the fray until the beginning of 2000s. With problems such as ineffective interfacial stress transfer being discovered and the acknowledged glass ceiling

for the physical research methods of polymer reinforcement the other branches of science have much to offer this area of research. The potential exists to raise the bar of research into this very new area of science and ultimately develop unprecedented and invaluable new materials.

The following account gives a brief introduction to the chemistry that has been performed on CNTs as well as the major analytical techniques, which have been used.

In 2002 M. Aizawa and M.S. P. Shaffer[55] silylated nanotubes with five silylating agents and narrowed them down to two effective agents. The nanotubes chosen were CVD nanotubes which were oxidised so as to introduce polar functional groups on the nanotubes. The conditions were reasonably straightforward once again with 20 mgs of CNTs dispersed in NMP. 40 mmol of reagent was added to the dispersion in an inert atmosphere. The products were analysed by IR, EDX and UV/Vis.

In 1999 Boul *et al.*[56] reported the sidewall functionalisation of SWNTs. The intention was to manipulate the nanotubes sufficiently so that instead of getting suspensions of nanotubes they would obtain actual solutions. Their goal was to solvate the nanotubes but allow for reversible functionalisation so the nanotubes could be left unaltered. The nanotubes which they used were produced by the laser ablation method. In this report they undertook two methods of functionalisation, after the preliminary fluorination of the sidewalls. The first method was lithiation of the fluorinated nanotubes using a range of alkyl-lithium species and the second was to from a nanotube Grignard reagent using alkyl-magnesium bromides in THF. In each case they use the same chain lengths; -methyl, -ethyl, -butyl, -hexyl, -octyl and -dodecyl. After functionalisation they tested the nanotubes stability and solubility in a range of solvents after which they were able to remove the alkyl chains by oxidation. They compared the nanotubes before oxidation and after oxidation through AFM and noticed no shortening in the length of the nanotubes. They came to the conclusion that the oxidation did not destroy the SWNTs.

In 2005 S. Chen *et al.*[57] functionalised SWNTs with the use of sec-butyl lithium (sec- BuLi). Due to the reactivity of the reagents being used all reactions were carried out in an inert atmosphere. The nanotubes were sonicated in THF for 4 hrs to obtain a good dispersion and subsequently the sec-Buli was added through a syringe to 25 mg of HiPCO SWNTs. Then carbon dioxide was bubbled through the reaction vessel in order to functionalise the nanotubes

with both alkyl and carboxyl groups. Characterisation of these nanotubes was carried out by Raman and IR spectroscopy as well as TGA. After functionalisation they noticed that the nanotubes were stable in water at 0.5 mg/ml.

Recently in 2005 Wei *et al.*[58] coated CVD MWNTs with several metal sulfides using the known nanotube surfactant sodium dodecyl sulphate (SDS). After suspending the MWNTs in an aqueous solution of SDS the nanotubes were then sonicated in a solution of the relevant metal salt. Subsequently sodium sulfide was added and after a 30 hr reaction the final products were obtained. The products were analysed by TEM and photoluminescence. The images of the coated nanotubes which they obtained were very impressive with nanoparticles of 30 nm surrounding the walls of the nanotubes. The authors suggest that these new materials could have potential applications in field emitters or nanometre optoelectronic devices.

A similar type of functionalisation was carried out by Hernadi *et al.*[59], who again functionalised CVD MWNTs with metal oxides. This was carried out by using aluminium isopropoxide, tetraethyl orthosilicate (TEOS) and tetraethyl orthotitanate as the reactants. The nanotubes were placed in a suspension of the reactants without any solvents. In the case of the reactant being a solid it was heated to just above its melting point after which water was added to hydrolyse organometallic compounds. The products were then analysed by TEM and EDX. The MWNTs were observed to have a homogeneous coating around the exterior which was the metal deposit.

The formation of novel donor-acceptor compounds has been known for many years and recently phthalocyanine molecules were combined with fullerene molecules in an effort to obtain an optoelectronic system[60]. In a very recent paper published by H.B. Xu *et al.*[61] it is suggested that a similar device could be made by substituting the fullerene molecule by a SWNT. In this case the SWNT would act as the electron acceptor and the charge transfer would come from the chosen porphyrin which was erbium bisphthalocyanine which would be covalently attached to the nanotubes. The methods of characterisation carried out were IR, DSC, TGA, UV/Vis and Raman spectroscopy. Once again the nanotubes chosen for the reaction were CVD nanotubes that were purified by strong acid oxidation. The residual carboxyl groups were seen as adventitious as they would be incorporated into the covalent link to the porphyrin. The nanotubes were refluxed with $SOCl_2$ for 24 hrs and then were treated with the bispthalocyanine in DMF with a catalytic amount of pyridine at 95 °C for 10 days. The nanotubes were then bound to the erbium compound *via* amide bonds. The authors

observed these bonds through the shift in the Raman spectrum thus the authors suggest that these products be used as photo-detectors.

Koos *et al.*[62] studied MWNTs which they connected *via* a diaminopropane linker group. In this study they exploited the fact that nanotubes once oxidised by strong acids are not only opened at the tips of the tubes but also the oxidation leaves carboxylic acid groups at the ends of the nanotubes. Once functionalised the authors studied the surface of the MWNTS with a scanning tunnelling electron microscope (STEM) and found that the surface had been modified by the functional groups which had attached themselves. As well as this they studied the sample with TEM and found an image of one tube connecting to the side wall of another nanotube.

Similar to Koos work was the work carried out by Zhao *et al.*[63] who functionalised MWNTs with isocyanate groups in 2004. Again in their experiment they used nanotubes that had been oxidised and still had carboxylic acid groups bound to the surface of the nanotubes. As in the case of the majority of functionalisation on nanotubes and in particular MWNTs they have seen an increased stability of the nanotubes in solution. The method of functionalisation was through the use of toluene 2,4-diisocyanate in anhydrous acetone at 50 °C for a 24 hr period. The functionalised nanotubes were then characterised by a series of techniques including IR, XPS and TGA. In the TGA they noticed that the degradation temperature of the functionalised nanotubes was much lower than that of the pure nanotubes. This is consistent with the paper published by A. Garg and S.B. Sinnott[64] who carried out molecular dynamics simulations which suggested that on covalent functionalisation the nanotubes weaken irrespective of the nanotubes structure.

A cycloaddition reaction was performed on SWNTs by Holzinger *et al.*[65] in 2004. They proposed that through the use of nitrenes they could attack the nanotube sidewall in an electrophilic [2+1] or undergo a transition into a triplet state by intersystem crossing, figure 1.10. Whichever process occurs the outcome would be the same that of the formation of aziridine ring formation. These are composed of a three membered ring with two carbon atoms which constitute the side wall of the nanotubes. More functionality could be then added to the nanotubes through these rings.

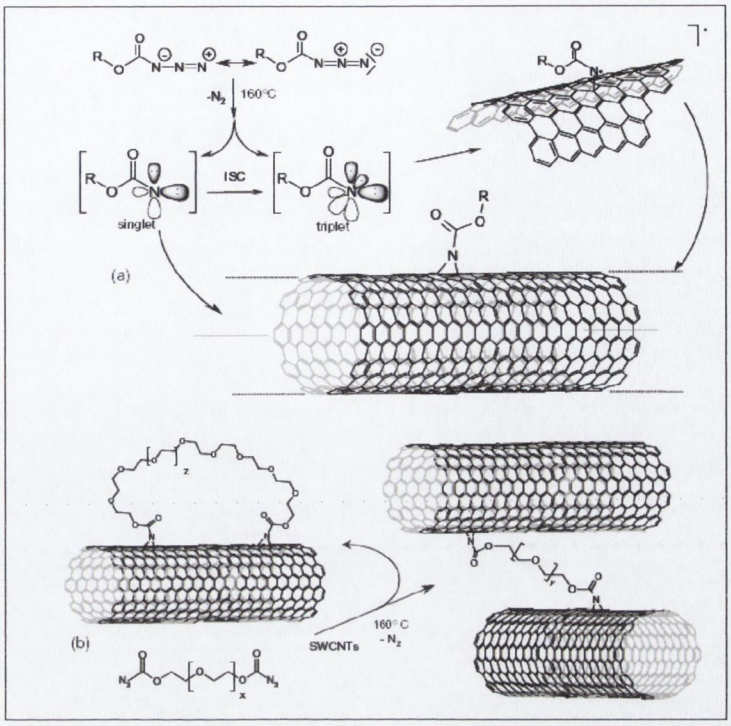

Figure 1.10 The schematic presentation of the nitrene reaction with nanotubes

Barthos *et al.*[66] functionalised SWNTs with; trifluoromethane, trichloromethane, hexafluoropropene and tetrachloroethylene. As in the previous cases the nanotubes they chose to manipulate were CVD grown. The method they used to functionalise the nanotubes was through ball-mixing in an atmosphere of the chosen functionality at room temperature.

Q. Li *et al.*[67] non-covalently functionalised SWNTs in 2004. Their argument was that by non-covalently functionalising nanotubes, the nanotubes pure structure would not be degraded and further manipulation through the covering molecule would be possible. Once again the nanotubes chosen for manipulation were CVD SWNTs. The nanotubes were combined with thionine which has two amino groups symmetrically distributed on either side of three benzene rings. The method of synthesis was a very straightforward one; the nanotubes were placed in an aqueous solution and sonicated with thionine for 12hrs at room temperature. The nanotubes were analysed by a number of common nanotube analysis techniques including SEM, TEM, AFM and Raman as well as TGA. Similar to Zhao *et al.*[63] the TGA spectra show that the degradation temperature of the functionalised nanotubes decreases significantly as compared to pristine nanotubes. The TEM analysis of the MWNTs functionalised with thionine compare well with the AFM images of the SWNTs.

In-situ polymerisation

In situ polymerisation is another method of nanotube functionalisation. In 1999, J. Fan *et al.*[68] functionalised carbon nanotubes with polypyyrole. They characterised the functionalised nanotubes in the standard ways; Raman, IR and TEM. They also measured the conductance of the composites they fabricated from the nanotubes. Later Shaffer *et al.* attempted to form high strength polystyrene-nanotube composite films by following a similar method of in situ polymerisation of polystyrene.[69] Very recently Jiang *et al.*[70] functionalised MWNTs *via* in-situ polymerisation of polyimide with the intention of investigating the resulting composites conductive properties. The result was an impressive increase in the polymers conductivity by eleven orders of magnitude.

Another recent publication showed the chemical modification of CVD MWNTs by Yang *et al.*[71]. In this case the MWNTs were functionalised with polyvinylimidazole, the nanotubes were modified by in situ free radical polymerisation. Again the authors have characterised their sample by standard methods of TEM, IR as well as XRD and SEM. This form of polymerisation offers another creative method of incorporating nanotubes within polymers. A. Eitan *et al.*[72] functionalised the surface of MWNTs with the intention of forming nanotube polymer composites. Again in this application CVD nanotubes were chosen and oxidised to add the functional groups. These nanotubes were then functionalised with di-epoxy groups.

Recently in January of 2005 Banerjee, Benny and Wong published a review[73] on all functionalisation carried out on SWNTs. The overview of the functionalisation of SWNTs from this review is presented in figure 1.11.

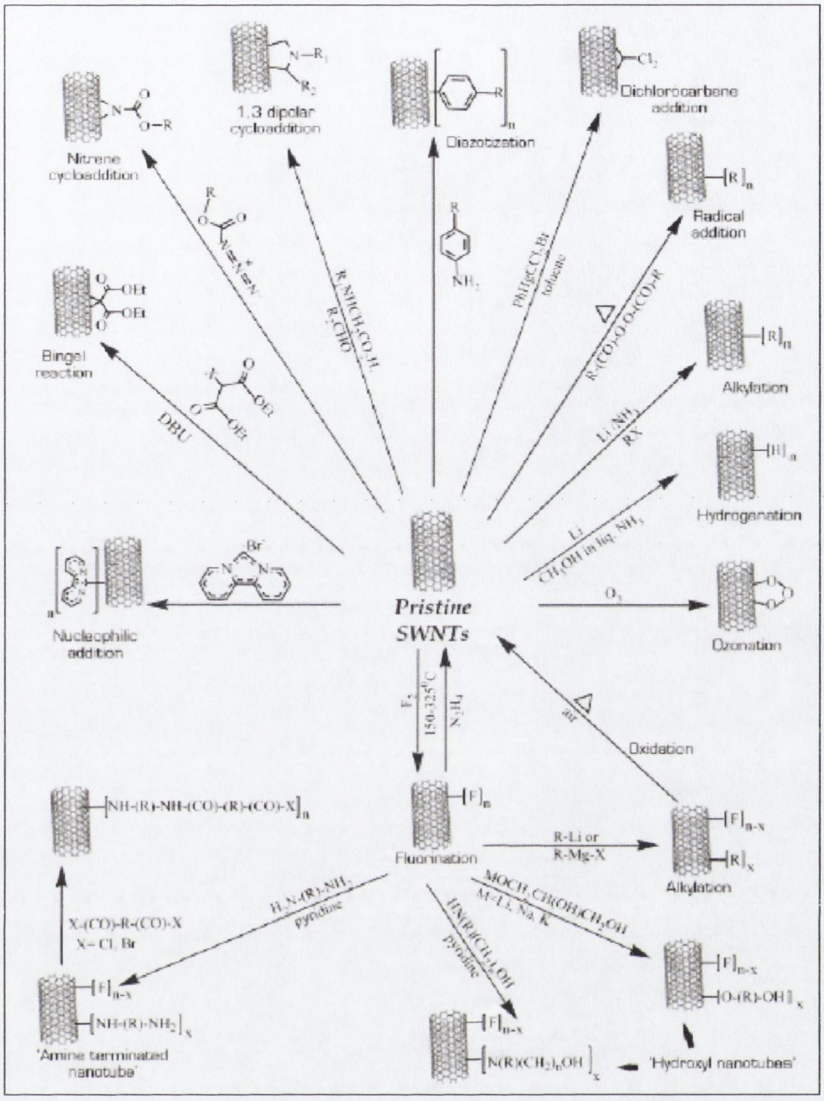

Figure 1.11 An overview of the functionalisation of SWNT to date.[73]

1.7 Introduction to CNTs for polymer reinforcement

The combination of unprecedented physical and chemical properties of carbon nanotubes makes them an ideal candidate as a filler material in composites.[74] CNTs as compared to carbon black are much more effective as conductive filler particles.[75] Researchers have envisaged taking advantage of their conductivity to produce conductive plastics with exceedingly low percolation thresholds.[76] In another area, it is thought that their massive thermal conductivity can be exploited to make thermally conductive composites.[77] However, probably the most promising area in nanotube composite research involves the reinforcement of plastics using carbon nanotubes as fillers.

In fact, the largest commercial use of nanotubes at the moment is at very low loadings (3-5 wt%) within thermoplastic matrices for the purpose of anti-static dissipation, particularly in the automotive and electronics industries.[78]

After over a decade of research on carbon nanotubes none of the expected potential has been realised through NT composite materials. The potential of achieving exceptional improvements in plastic strengths through the involvement of CNTs retains researchers' interest in polymer reinforcement.

One of the most common ways of preparing nanotube polymer composites involves mixing dispersions with solutions of polymer and then evaporating the solvent (polymer solution casting). Shaffer *et al.* demonstrated that carboxyl functionalised nanotubes are more stable than pristine nanotubes in aqueous solutions and thus taking a polymer soluble in water facilitates good dispersion in that polymer solution. Polymer films can then be cast by allowing the water to evaporate.[79,80] The polymer casting method has also been applied to nanotube/polystyrene films. This was done by Hill *et al.* who stabilised a solution of both SWNT and MWNT in polystyrene with the use of a copolymer.[81] They facilitated this by first oxidising the nanotubes and subsequently carrying out an esterification reaction on the carboxyl groups of the nanotubes. The composite film was fabricated using wet casting. A more physical than chemical approach was carried out by Qian *et al.* who used high energy sonication with the use of a sonic tip to disperse the MWNTs in toluene and subsequently mixed this solution with a solution of polystyrene in toluene.[82] The method of mixing polymers with a solvent they are readily soluble in and allowing the solvent to evaporate off is limited by the solvents.

Another method of composite formation is to use a thermoplastic and melt processing. In this method shear mixing is used to produce a homogeneous dispersion of nanotubes in the plastic. Andrews *et al.* used this method to disperse CVD nanotubes in several polymers; high impact polystyrene, acrylonitrile butadiene styrene and polypropylene.[83] Haggenmueller *et al.* used a combination of solvent casting and melt mixing to disperse SWNTs in polymethylmethacrylate.[84] Potschke *et al.* and Sennett *et al.* used polycarbonate as another thermoplastic polymer to fabricate nanotube composites.[85,86]

A different method of nanotube composite material formation was to place both the nanotubes and monomers in a reaction vessel and to carry out an in-situ polymerisation reaction. This

new approach was introduced by Cochet *et al.*[87] in 2001 when they made a MWNT and polyaniline composite. The nanotubes that they used were arc-discharge nanotubes. Through this method they were able to obtain a very high loading of 50 wt%. Shortly after the discovery of the mechanical properties of CNTs, work on obtaining a composite material which would mediate these properties began. In 1999 eight years after the original discovery of MWNTs Shaffer and Windle[39] used a Dynamic Mechanical Thermal analyser (DMTA) to run an in depth study of the mechanical properties of their MWNT and PVA composites. The results that they obtained were far from impressive. By applying the rule of mixtures they discovered that the modulus of a nanotube in their system was 150 MPa which is well bellow the expected value of 1.28 TPa and even below that of a CVD grown nanotube of 500 GPa. The low value is indicative of poor interfacial stress transfer as opposed to inherently weak nanotubes. The problem is symptomatic of the structure of the nanotubes sidewalls which are very similar to graphite, one of graphite's common uses is for frozen lock lubrication. The property of graphite which mediates these common uses is the fact that the hexagonal planes held together by weak Van-der-Waals forces allow the planes to slip by each other readily. Thus this characteristic is carried through in the structure of the nanotubes. In order to improve the mechanical properties of composite materials made from nanotubes this must be overcome. Typically an increase in the strength of composite materials is seen in the low wt% of nanotube concentration. Recently in 2002 Cadek *et al.* obtained an increase in modulus of a factor of 1.8 in composites made from arc-discharge nanotubes in PVA. This increase was obtained with a 1 wt% of nanotubes. Qain *et al.*[82] studied the mechanical properties of polystyrene nanotube composites. In this case the nanotubes used were CVD MWNTs, they obtained 42% increase in the modulus with 1 wt % of nanotubes. A loading of 1 wt% of MWNTs in an ultra high molecular weight polyethylene film increased the polymers strain energy by 150%.[88]

For SWNTs a process has been reported which allowed a colossal 60 wt% of SWNT in PVA. Fibres were spun from this process and the mechanical properties were measured. These fibres reported an energy absorbing capacity nearly 3.5 times that of spider silk (165 J/g).[89] Slippage between the SWNTs was suggested as the mechanism responsible for the enhancement in the toughness. The slippage increases the amount of elongation of the film after yielding and thus as toughness is a function of both yielding and elongation this is the reason for the increase. An addition of 1 wt% of MWNTs to isotactic polypropylene affected the polymer's crystallisation as was exhibited in the Differential Scanning Calorimetry (DSC).[90] An increase

in a polymer's crystallinty would readily increase the polymer's Young's modulus but could, potentially, decrease the polymer's toughness.

Thus after nearly a decade of intensive research, the potential of nanotubes as reinforcement for polymers has not been fully realised; the mechanical properties of derived composites have still fallen short of predicted values.

1.8 Nanotubes and ceramic composites

Ceramics are second only to polymers in their popularity for the incorporation of CNTs. The ceramics have very high stiffness and very good thermal stabilities. For example, the breaks used in high spec cars such as Aston Martins must withstand very high temperatures, when required to break from 217 to 0 mph. These are generally manufactured of ceramics. The problem with ceramics is that they have low breaking strengths that is to say they are brittle. As CNTs have exceptional thermal conductivity properties and would be expected to increase the overall toughness of the composite this would be an excellent combination. The obstacles to making good composite materials that have been observed are similar to the problems found in polymer composites. Obtaining a homogeneous mixture between the Al_2O_3, ceramic, and the nanotubes is a tricky problem. Peigney *et al.*[91] engineered a technique which involved the catalytic growth of nanotubes followed by hot pressing of the powders together to form the final composite. The initial mechanical properties of these composite materials were not as high as was expected and in some cases a combination of the iron catalyst and the oxide gave a stronger product than when the nanotubes were combined.[92] In order to combine ceramics and nanotubes effectively and to allow for stress transfer between the two different matrices it was discovered that at very small grain sizes polycrystalline ceramics become super plastic which facilitates thermo mechanical processing. This allowed the in situ production of nanotubes in ceramics.

Zhan *et al.*[93] studied the interaction of SWNTs and ceramics. The method which they used to prepare the composites was through spark plasma sintering, which allowed a high percentage of SWNTs to be incorporated, 10 vol%. Before the composite was sintered it was mixed thoroughly through ball-mixing this which produced a homogenous dispersion. The increase they obtained through this method was excellent with a two fold increase as compared to the original Al_2O_3 matrix.

As well as aluminium oxide ceramic several authors have looked at combining nanotubes with silca. Seeger *et al.*[94] described a method involving preparing a gel of MWNTs with tetraethoxysilane (TEOS) and sintering this at 1150 °C in argon. The main flaw of this technique is that it resulted in partial crystallisation of the SiO_2 resulting in a bad mixture. An adaptation of this was to use a Nd:YAG laser[95] to allow rapid heating of the mixture which would inhibit the formation of the crystals.

1.9 Nanotubes in Biology

In order to emphasize the fact that nanotubes offer other areas of science the chance to unite in the study of these new exceptional materials, there follows a brief review of the major work being carried out in the most unlikely of branch of science that should be interested in CNTs: biology.

The shape of nanotubes which is similar in structure to a syringe needle has suggested their potential application as a drug delivering tool. In 2005 Venkatesan *et al.*[96] took the hormone which is responsible for red blood cell production, erythropoietin (EPO), and filled a range of nanoparticles with this potential drug. This drug would help people who have renal failure, cancer, bone marrow transplantation and AIDs. The problem with this drug as with many new drugs is that the only route of administration is intravenous which can be very distressing for patients. The ultimate goal for all drugs is that they can be administered orally. The authors suggest that the structure of nanotubes would facilitate oral administration as they would be able to withstand the harsh conditions of the gastro intestinal tract from acidic to basic. The results that they obtained were that the SWNTs which they used offered the highest increase in serum EPO levels through administration *via* the jejunum, which is the second part of the small intestine after the duodenum.

CNTs have been suggested as enzyme anchor sites. In 2003 Yu *et al.*[97] proposed the construction of SWNT arrays on silicon, or forests as they called them on to which they added the enzyme horseradish peroxidase and myoglobin which were attached to the ends of the arrays through covalent functionalisation with carbodiimide. They argue that these enzyme bound nanotubes, would be used in immunoassays and DNA hybridisation assays where peroxidase enzymes are used as tags. In 2004 Lim *et al.*[98] suggested their potential application for glucose sensing. The potential here is that the nanotubes functionalised with glucose enzymes could monitor blood glucose levels and help people control their illness. The enzyme

which breaks down glucose alleviates hydrogen peroxide as one of the by-products. The amount of peroxide present could then be analysed by an electrochemical detector. After experimenting with their theory they achieved a five fold increase in effectiveness of the NT bound enzyme electrodes as opposed to a non nanotube bound enzyme activity.

Nanotubes have even been known to 'put on' weight, in 2004 Chen *et al.*[99] functionalised carbon nanotubes with lipophilic molecules. After functionalisation their, overweight, nanotubes were soluble in liquid paraffin. They suggested that these nanotubes could have good potential as lubricating additives.

1.10 Aims of this work

The main objective of this work is to develop new functionalised carbon nanotubes and their composites using organometallic approaches. We believe that the use of organometallic techniques will allow us to enter into a new area in carbon nanotube functionalisation and modification. These aspects are very important for the potential applications of carbon nanotubes in nanotechnology.

The first task will be to develop effective purification techniques for carbon nanotubes. Then the aim will be to functionalise both SWNTs and MWNTs using lithium alkyls. In our research the lithiated nanotubes will serve as macromolecular ligands for different organometallic reactions. Initially reactions of the lithiated nanotubes with selected metal (Au, Ge, Sn, Pb) and non-metal (Si) halides will be studied. We expect that all these reactions will result in products with stable silicon-carbon or metal-carbon bonds. This would allow us to investigate these new materials without using special handling techniques (high vacuum or extra clean and dry inert gases). The new nanocomposites will be characterised by various techniques such as: TEM, TGA, XPS, elemental analysis, Raman and IR spectroscopy.

One of the most important tasks of this project is to prepare new ultra-strong polymer composite materials using chemically modified multiwalled carbon nanotubes as additives and as a result providing an efficient bonding of nanotubes to the polymer matrix and good interfacial stress transfer. An organometallic approach using BuLi will be used for carbon nanotube modification with the followed by binding the lithiated nanotubes to alkyl halides or halogenated polymers.

Then the functionalised carbon nanotubes will be used to reinforce high and low molecular weight polystyrene (PS), polyvinyl chloride (PVC), chlorinated polyethylene (CPE) and chlorinated polypropylene (CPP). This will be achieved by mixing of polymer with an optimal amount of the functionalised carbon nanotubes in organic solvent containing the selected polymer and by the preparation of films of nanotube-polymer composites via solution casting methods. Mechanical properties of the films will then be investigated using a Zwick-100 tensile tester. It is our expectation that through the interaction between the alkyl or polymer chains grafted to carbon nanotubes and surrounding chains, interfacial stress transfer will be

enhanced. TGA and DSC tests will be undertaken to analyse the thermal transitions of the nanotube-polymer composites to see if the nanotubes affect the crystallinity of the polymers.

One more of the objectives of our work is also to perform sedimentation studies for functionalised carbon nanotubes in organic solvents to measure the solubility of the nanotubes in pure solvent and then with the addition of nanotubes and polymers in the solvent. The successful outcome of the project will contribute to the development of both nanoscale physics and the chemistry of nanotubes and related materials.

1.11 References

[1] H.W. Kroto, J.R. Heath, S.C. O'Brien, R.F. Curl, R.E. Smalley, *Nature*, **318**, 162 (1985)

[2] R. Pis Diez, M.P. Intiguez, *Int. J. Quantum Chem.*, **56,** 689, (1995)

[3] W. Kratschmer, L. Lamb, K. Fostiropoulos, D. Huffman, *Nature,* **347**, 354 (1991)

[4] S. Ijima, *Nature,* **354**, 56 (1991)

[5] http://online.physics.uiuc.edu/courses/phys466/fall04/projects/2000/team1/final/main.html (20 Dec 2005)

[6] S. Ijima, T. Ichihashi, *Nature,* **363,** 603 (1993)

[7] D.S. Buthune, C.H. Kiang, M.S. de Vries, G. Gorman, R. Savoy, J. Vazquez, R. Beyers, *Nature,* **363,** 605, (1993)

[8] H.W. Zhu, X.S. Li, B. Jiang, C.L. Xu, Y.F. Zhu, D.H. Wu, X.H. Chen, *Chem Phys. Lett.*, **366,** 664, (2002)

[9] http://www.science.widener.edu/science/bucky.html (20 Dec. 2005)

[10] A. Thess, R. Lee, P. Nikolaev, H. Dai, P. Petit, J. Robert, C. Xu, Y.H. Lee, S.G. Kim, A.G. Rinzler, D.T. Colbert, G.E. Scuseria, D. Tomanek, J.E. Fischer, R.E. Smalley, *Science,* **273,** 483, (1996)

[11] M.J. Yacaman, M.M. Yoshida, L. Rendon, J.G. Santiesteban, *Appl. Phys. Lett.*, **62,** 202, (1993)

[12] S. Iijima, T. Ichiashi, Y. Ando, *Nature,* **356,** 776, (1992)

[13] T.W. Ebbesen, P.M Ajayan, *Nature,* **358,** 220, (1992)

[14] C. Journet, W.K. Maser, P. Bernier, A. Loiseau, M. Lamy de la Chapelle, S. Lefrant, P. Deniard, R. Lee, J.E. Fisher, *Nature,* **388,** 756, (1997)

[15] http://students.chem.tue.nl/ifp03/synthesis.html (20 Dec 2005)

[16] Z.F. Ren, Z.P. Huang, J.W. Xu, J.H. Wang, P. Bush , M.P. Siegel, P. Provencio, *Science,* **282**, 1105, (1998)

[17] Z.F. Ren, Z.P. Huang, D.Z. Wang, J.G. Wen, J.W. Xu, J.H. Wang, L.E. Calvet, J. Chen, J.F. Klemic, M.A. Reed, *Appl. Phys. Lett.*, **75**, 1086, (1999)

[18] S.B.Sinnott , R. Andrews, D. Qian, A.M. Rao, Z. Mao, E.C. Dickey, F. Derbyshire. *Chem. Phys. Lett.* **315,** 25, (1999)

[19] http://inisjp.tokai.jaeri.go.jp/ACT99E/06/0604.htm (20 Dec 2005)

[20] T. Guo, B. Nikolaev, A.G. Rinzler, D. Tomanek, D.T. Colbert, R.E. Smalley, *J. Phys. Chem.*, **99,** 20694, (1995)

[21] J.C. Charlier, A. de Vita, X. Blasé, R. Car, *Science,* **275,** 646, (1997)

[22] J.C. Charlier, X. Blasé, A. de Vita, R. Car, *Appl. Phys. A.*,**68,** 267, (1999)

[23] Y.H. Lee, S.G. Kim, P. Jund, D. Tomanek, *Phys. Rev. Lett.*, **78,** 2393, (1997)

[24] A. Maiti, C.J. Brabec, J. Bernholc, *Phys. Rev. B,* **55,** 6097, (1997)

[25] http://www.pa.msu.edu/cmp/csc/ntproperties/equilibriumstructure.html (20 Dec 2005)

[26] W.G.J. Wilder, L.C. Venema, A. G. Rinzler, R. E. Smalley, C. Dekker, *Nature,* **391**, 59, (1998)

[27] http://www.phys.jyu.fi/research/nanotech/CNT.htm (20 Dec 2005)

[28] R. He, H. Jin, J. Zhu, Y. Yan, X. Chen, *Chem. Phys. Lett.,* **298,** 170, (1998)

[29] G.S. Duesberg, I. Loa, M. Burghard, K. Syassen, S. Roth, *Phys. Rev. Lett.,* **85,** 5436, (2000)

[30] A.M. Rao, A. Jorio, M.A. Pimenta, M.S.S. Dantas, R. Saito, G. Dresselhaus, M.S. Dresselhaus, *Phys. Rev. Lett.,* **84,** 1820, (2000)

[31] http://www.apexnanomaterials.com/images.htm (20 Dec 2005)

[32] T. Belin, F. Epron, *Materials Science & Engineering,* **119,** 105, (2005)

[33] U. Kuhlmann, H. Jantoljak, M. Pfander, P. Bernier, C. Journet, C. Thomsen, *Chem. Phys. Lett.,* **294,** 237, (1998)

[34] J. Kastner, T. Pichler, H. Kuzmany, S. Curran,W. Blau, D.N. Weldon, M. Delamesiere, S. Draper, H. Zandbergen, *Chem. Phys. Lett.*, **221**, 53
(1994)

[35] P. Eklund, J. Holden, R. Jishi, *Carbon,* **33,** 959, (1995)

[36] R. Saito, K. Matsushige, K. Tanaka, *Physica. B,* **323,** 280, (2002)

[37] R. Droppa, P. Hammer, A. Carvalho, M. Dos Santos, F. Alvarez, *Non-Cryst. Solids,* **299,** 874, (2002)

[38] Y. Lee, T. Cho, B. Lee, J. Rho, K. An, Y. Lee, *J. Fluorine Chem.,* **120**, 99, (2003)

[39]E. Dujardin, T. W. Ebbesen, A. Krishnan, P. N. Yianilos, M. M. J. Treacy, *Phys. Rev. B,* **58,** 14013, (1998)

[40] M.M.J. Treacy, T.W. Ebbesen, J.M. Gilson, *Nature,* **381,** 678, (1996)

[41] E.W. Wong, P.E. Sheehan, C.M. Lieber, *Science,* **277,** 1971, (1997)

[42] E. Herna´ndez, C. Goze, P. Bernier, A. Rubio, *Phys. Rev. Lett.* **80**, 4502 (1998)

[43] M.F. Yu, O. Lourie, M.J. Dyer, K. Moloni, T.F. Kelly, R.S. Ruoff, *Science,* **287,** 637, (2000)

[44] S. Garaj, T. Kambe, L. Forro, A. Sienkiewica, M. Fujiwara, K. Oshima, *Appl. Phys. Lett.*, **83,** 4622, (2003)

[45] A. Kis, G. Csanyi, J.P. Salvetat, L. Thein-Nga, E. Couteau, A.J. Kulik, W. Benoit, J. Brugger, L. Forro, *Nature Mat,* **3,** 153, (2004)

[46] M.F. Yu, B.S. Files, S. Arepalli, R.S. Ruoff, *Phys. Rev. Lett.*, **84**, 5552, (2000)

[47] J. Liu, A.G. Rinzler, H.J. Dai, J.H. Hafner, R.K. Bradley, P.J. Boul, A. Lu, T. Iverson, K. Shelimov, C.B. Huffman, F. Rodriguez-Macias, Y.S. Shon, T.R. Lee, D.T. Colbert, R.E.Smalley, *Science,* **280,** 1253, (1998)

[48] J. Liu, M.J. Casavant, M. Cox, D.A. Walters, P. Boul, W. Lu, A.J. Rimberg, K.A. Smith, D.T. Colbert, R.E. Smalley, *Chem. Phys. Lett.*, **303**, 125, (1999)

[49] J. Hone, M. Whitney, A. Zettle, *Synthetic Metals,* **103,** 2498, (1999)

[50] J. Che, T. Cagin, W.A. Goddard, *Theor. Chem. Acct.*, **102**, 346 (1999)

[51] W. Yi, L. Lu, D.L. Zhang, Z.W. Pan, S.S. Xie, *Phys. Rev. B,* **59,** 9015, (1999)

[52] P. Kim, L. Shi, A. Majumdar, P.L. McEuen, *Phys Rev.Lett.*, **87,** 215502, (2001)

[53] S. Frank, P. Poncharal, Z.L. Wang, W.A. de Heer *Science,* **280,** 1744,(1998)

[54] S. Sanvito, Y.K. Kwon, D. Tomanek, C.J. Lambert, *Phys. Rev. Lett.*, **84,** 1974, (2000)

[55] M. Aizawa, M.S.P. Shaffer, *Chem. Phys. Lett.*, **368,** 121, (2003)

[56] P.J. Boul, J. Liu, E.T. Mickelson, C.B. Huffman, L.M. Ericson, I.W. Chiang, K.A. Smith, D.T. Colbert, R.H. Hauge, J.L. Margrave, R.E. Smalley, *Chem. Phys. Lett.*, **310,** 367, (1999)

[57] S. Chen, W. Shen, G. Wu, D. Chen, M. Jiang, *Chem. Phys. Lett.*, **402,** 312, (2005)

[58] X. Wel, X. Song, J. Xu, Y. Ni, P. Zhang, *Mat. Chem. and Phys.*, **92,** 159, (2005)

[59] K. Hernadi, E. Ljubovic, J.W. Seo, L. Forro, *Acta Materialia,* **51,** 1447, (2003)

[60] A. Gouloumis, S.Liu, A. Sastre, P. Vazquez, L. Echegoyen, T. Torres, *Chem. Eur. J.*, **19,** 107, (2000)

[61] H. Xu, H. Chen, M. Shi, R. Bai, M. Wang, *Mat. Chem. and Phys.*, **94,** 322, (2005)

[62] A.A. Koos, Z.E. Horvath, Z. Osvath, L. Tapaszto, K. Niesz, Z. Konya, I. Kiricsi, N. Grobert, M. Ruhle, L.P. Biro, *Mat. Sci. and Eng.*, **23,** 1007, (2003)

[63] C. Zhao, L. Ji, H. Liu, G. Hu, S. Zhang, M. Yang, Z. Yang, *J. of Solid State Chem.*, **177,** 4394, (2004)

[64] A. Garg, S. B. Sinnott, *Chem. Phys. Lett.*, **295,** 273, (1998)

[65] M. Holzinger, J. Steinmetz, D. Samaille, M. Glerup, M. Paillet, P. Bernier, L. Ley, R. Graupner, *Carbon,* **42,** 941, (2004)

[66] R. Barthos, D. Mehn, A. Demortier, N. Pierard, Y. Morciaux, G. Demortier, A. Fonseca, J.B. Nagy, *Carbon,* **43,** 321, (2005)

[67] Q. Li, J. Zhang, H. Yan, M. He, Z. Liu, *Carbon,* **42,** 287, (2004)

[68] J. Fan, M. Wan, D. Zhu, B. Chang, Z. Pan, S. Xie, *Synthetic Metals,* **102,** 1266, (1999)

[69] M.S. P. Shaffer, K. Kozoil, *Chem. Commun.,* 2074, (2002)

[70] X. Jiang, Y. Bin, M. Matsuo, *Polymer,* **46,** 7418, (2005)

[71] Z. Yang, H. Pu, J. Yin *Materials lett.,* 59, 2838, (2005)

[72] A. Eitan, K. Jiang, D. Dukes, R. Andrews, L. Schadler, *Chem. Matter.,* **15,** 3198, (2003)

[73] S. Banerjee, T. Hemraj-Benny, S.S. Wong *Adv. Mater.,* **17,** 17, (2005)

[74] M.J. Biercuk, M.C. Llaguano, M. Radosvljevic, J.K. Hyun, A. T. Johnson, *Appl. Phys. Lett.,* **80,** 15, (2002)

[75] D.T. Colbert, *Plastic Additives Comp.,* **18**, (2003)

[76] B.E. Kilbride, J.N. Coleman, J. Fraysse, P. Fournet, M. Cadek, A. Drury, S. Hutzler, S. Roth, W.J. Blau, *J. Appl. Phys.,* **92,** 4024, (2002)

[77] M. Biercuk, M.C. Llanguno, M. Radosavljevic, J.K. Hyun, J.E. Fischer, A.T. Johnson, *Appl. Phys. Lett.,* **80,** 2767, (2002)

[78] M. Shaffer, I.A. Kinloch, *Comps. Sci, and Tech.,* **64,** 2281, (2004)

[79] M.S.P. Shaffer, X.Fan, A.H. Windle, *Carbon,* **36,** 1603, (1998)

[80] M.S.P. Shaffer, A.H. Windle, *Adv. Mater.,* **11,** 937, (1999)

[81] D.E. Hill, Y. Lin, A.M. Rao, L.F. Allard, Y.P. Sun, *Macromolecules,* **35,** 9466, (2002)

[82] D. Qian, E.C. Dickey, R. Andrews, T. Rantell, *Appl. Phys. Lett.,* **76,** 2868, (2000)

[83] R. Andrews, D. Jacques, D. Qian, T. Rantell, *Acc. Chem. Res.,***35,** 1008, (2002)

[84] R. Haggenmueller, H.H. Gommans, A.G. Rinzler, J.E. Fischer, K.I. Winey, *Chem. Phys. Lett,* **330,** 219, (2000)

[85] P.Potschke, T.D. Fornes, D.R. Paul, *Polymer,* **43,** 3247, (2002)

[86] M. Sennett, E. Welsh, J.B. Wright, W.Z. Li, J.C. Wen, Z.F. Ren, *Appl. Phys. A,* **76,** 111, (2003)

[87] M. Cochet, W.K. Maser, A.M. Benito, M.A. Callejas, M.T. Martinez, J.M. Benoit, J. Schreiber, O.Chauvet, *Chem. Commun.,* 1450, (2001)

[88] S.L. Ruan, P.Gao, X.G.Yang, T.X. Yu, *Polymer,* **44,** 5643, (2003)

[89] A.B. Dalton, S. Collins, E. Munoz, J.M. Razal, V.H. Ebron, J.P. Ferraris, *Nature,* **423,** 703, (2003)

[90] E. Assouline, A. Lustiger, A.H. Barber, C.A. Cooper, E. Klein, E. Wachtel, *J. Polym. Sci: Part B. Polym. Phys.*, **41,** 520, (2003)

[91] A. Peigney, E. Flahaut,C. Laurent, F. Chastel, A. Rousset, *Chem. Phys. Lett.*, **352,** 20, (2002)

[92] E. Kymakis, G.A.J. Amaratunga, *Appl. Phys. Lett.*, **80,** 112, (2002)

[93] G.D. Zhan, J.D. Kuntz, J.L. Wan, A.K. Mukherjee, *Appl. Phys. Lett.*, **83,** 1228, (2003)

[94] T.Seeger, T. Koehler, T. Frauenheim, N. Grobert, M. Ruele, M. Terrones, G. Seifert, *Chem. Commun.*, 34, (2002)

[95] T. Seeger, G.De La Fuente, W.K. Maser, A.M. Benito, M.A. Callejas, M.T. Martinez, *Nanotech*, .**14,** 184, (2003)

[96] N. Venkatesan, J. Yoshimitsu, Y. Ito, N. Shibata, K. Takada, *Biomaterials,* **26,** 7154, (2005)

[97] X. Yu, D. Chattopadhyay, I. Galeska, F. Papadimitrakopoulos, J.F. Rusling, *Electrochem. Commun.*, **5,** 408, (2003)

[98] S.H. Lim, J. Wei, J. Lin, Q. Li, J.K. You, *Biosens. Bioelectron.*, **20,** 2341, (2005)

[99] X.H. Chen, C.S. Chen, H.N. Xiao, X.H. Chen, W. Li, L. Xu, *Carbon,* **43,** 1778, (2005)

Chapter 2

Preparation, Purification and Metalation of Carbon Nanotubes

2.1 Introduction

Carbon nanotubes can be synthesised by three main methods: arc discharge, laser ablation and chemical vapour deposition (CVD)[1]. Recently new modified techniques have been employed such as the method by Zhu *et al.* [2] who used the arc discharge method under water. The approach employed in our work was the original arc discharge method using the Kratschmer-Huffman generator which was originally used to make Fullerenes in large amounts. This technique involved creating an electrical arc under pressure in an inert gas atmosphere.

Once the nanotubes have been synthesised the next step is purification. Nanotubes when formed are found amongst considerable amounts of amorphous carbon material, in the region of 70%. There are many different methods of purification, we employed only a few.

Primarily and traditionally the nanotubes have been purified by oxidation using two strong acids, nitric and sulphuric. It has been published that nanotubes have been purified from the other amorphous carbon material by using a column of glass balls however this method was not followed here.[3] The result of applying the acid purification method is that the acid severs the tip from the terminus of the nanotubes leaving the tubes open ended as is shown in the figure 2.1.

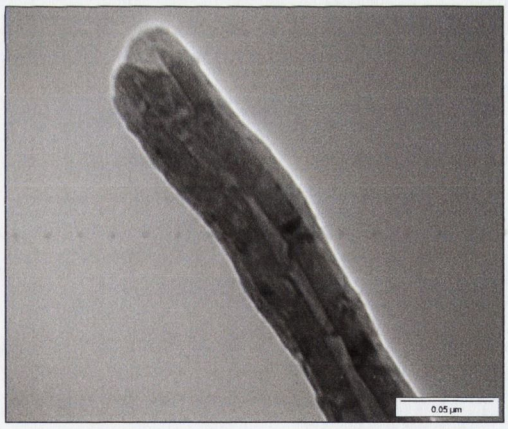

Figure 2.1 TEM image of a tip opened MWNT

Another method of purification that was employed was the use of a polymer that has considerable aromaticity and hence affinity for the nanotubes. The π-π interaction holds the nanotubes in solution and lets the amorphous carbon material fall out of solution over time.

Many applications involving carbon nanotubes require chemical modification of the carbon nanotubes to make them more amenable to rational and predictable manipulations. One of the most innovative aspects of this project is the development of a new method of chemical functionalisation of carbon nanotubes. Until now the routes that have been traditionally taken by chemists followed organic chemistry approach. For example Georgakilas *et al.* reported functionalising single walled carbon nanotubes with various different long chain carboxylic functional groups[4]. Holzinger *et al.* reported the addition of nitrenes to form alkoxycarbonylaziridino-SWNT[5]. Our work here focuses on chemical modification of carbon nanotubes through an organometallic approach. This chapter describes our work on nanotube production, subsequent purification and also nanotube metallation.

2.2 Aims of this work

First of all obtaining pure carbon nanotubes was paramount for this project and therefore our initial task was to purify nanotubes, produced in TCD by arc discharge, using a selection of methods that were published previously. Ultimately our aim was the identification of the most efficient method of purification to produce the required reactant for this work. The next objective of this part of our work was to develop a new organometallic approach for chemical functionalisation and metallation of carbon nanotubes.

On choosing a route for the chemical modification of carbon nanotubes and realising the difficulties of analysis it was important to obtain products that could be characterised by all available methods. In order to prove that there is interaction between butyl-lithium and carbon nanotubes it was recognised that the most easily identifiable and stable bonds between a nanotube and any other species was that of metal carbide bonds which has been well documented and studied by XPS, IR and Raman spectroscopy. On this basis, a selection of metal (tin, lead, germanium and gold) halides and silicon halide were chosen. We expect that this research will contribute to the development of two very important areas in nanotechnology: doping of carbon nanotubes with metals or non-metals and forming metal nanoparticles and nanowires using nanotubes as templates.

2.3 Results and Discussion

2.3.1 Production of Carbon Nanotubes

Multiwalled carbon nanotubes (MWNT) were made using a Kratschmer-Huffmann generator the basic design of which was shown in figure 1.2.

Two graphite carbon electrodes were placed in a chamber that had been evacuated and then put in a helium atmosphere (500 atm). An electric current was passed through and the nanotubes were formed and deposited on the cathode as a hard deposit inter-mixed with other graphite and amorphous material.

The optimum parameters, 24 mg/min, when the current is supplied at 190 A/cm and pressure is 500 atm, for this method were published by M. Cadek *et al.*[6] The deposit was opened and the soft fibrous internal material was removed and divided into a fine powder.

2.3.2 Purification of Carbon Nanotubes

TEM images of the impure sample of the nanotubes found in the arc-discharge deposit are shown in figure 2.2. The nanotubes can be seen here as the fibrous material amongst clearly quite a large amount of amorphous material. One of the main problems when using carbon nanotubes is their purity and the involved with large scale purification; this is also the reason for their great expense.

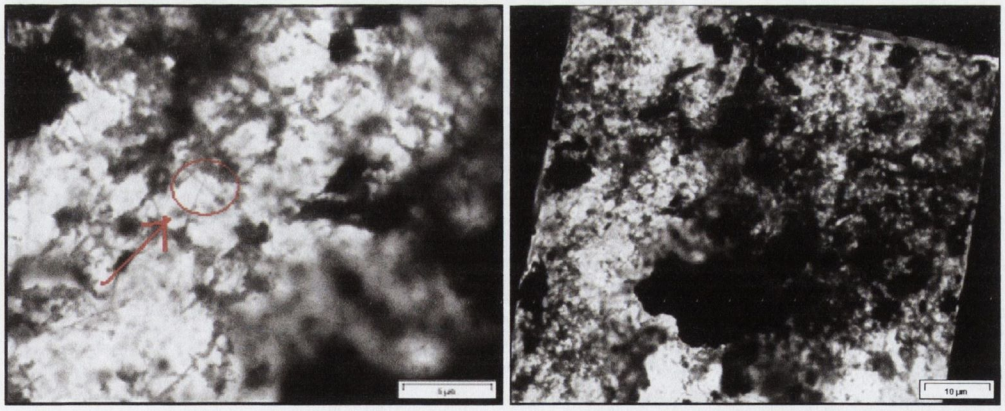

Figure 2.2 TEM images of carbon nanotubes found in the deposit before purification

In order to separate the nanotubes from the amorphous carbon material three different types of previously published purification techniques were undertaken, the advantages and disadvantages of the techniques along with each technique's characteristic procedure are

outlined below. These main techniques were employed coming from two different ideologies: those of purification by oxidation and purification by filtration.

The technique, published by Smalley *et. al.*[7], for purification of SWNT using strong acids results in the removing of graphite chunks and the opening of the nanotube tips. A modification of this technique reported by Hou and Bai *et al.*[8] involved heating the carbon nanotube graphite mixture with bromine water under reflux, followed by refluxing the mixture with sulphuric and nitric acid for six hours. Another technique which involved annealing the mixture at a high temperature was reported by Soo Park and Chul Choi *et al.*[9].

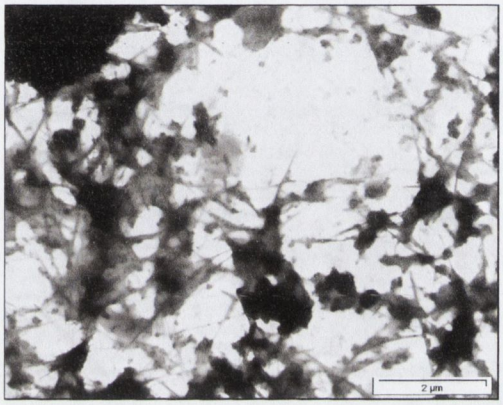

Figure 2.3 TEM image of HBr purified arc discharge carbon nanotubes

It can be seen in figure 2.3 that there has been a large removal of graphitic material and the nanotubes are much more noticeable in this image than in figure 2.2. However, this method did not produce nanotubes of sufficient purity for the reactions in which it was intended that they would be used.

The strong acid treatment removes the majority of graphite and the metal catalyst, *e.g.* iron. This is not so important for the purification of the arc discharge nanotubes since no metal catalyst is used in their production. Some papers state that the nanotubes are filtered after refluxing with acids and this adds an extra dimension where more impurities can enter into the mixture and can also lead to much greater loss of nanotubes through inevitable waste. The nanotubes become etched by this type of purification. The main site for etching is at the tips of the nanotubes. Functional groups such as carboxylic acid groups and hydroxide groups are formed on the open tips of the nanotubes. Depending on the type of experiments planned for the nanotubes this can be seen as an advantage or disadvantage. These groups may be removed later by annealing of the nanotubes, but this can lead to a further reduction in yield.

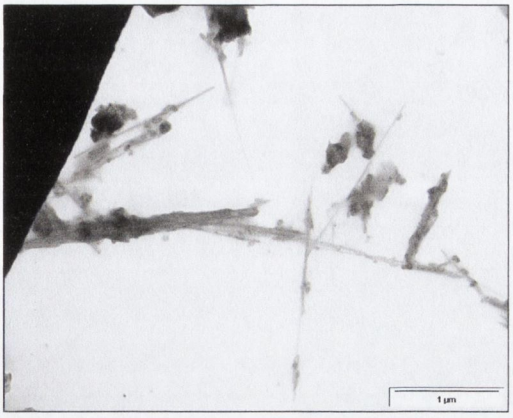

Figure 2.4 TEM image of the acid treated arc discharge nanotubes

Figure 2.4 shows acid purified nanotubes. As can be seen this has quite some degree of success at removing the amorphous carbon material. With the addition of the carboxyl groups to the end of the nanotubes and the large amount of wastage due to the use of the sintered funnel, it was felt that perhaps an alternative method could first be researched before using the acid purification method.

The other type of purification was the method involving the polymer poly *m*-phenylenevinylene-co-2,5-dioctyloxy-*p*-phenylenevinylene (PPV). The basis for this method, as described by the authors,[6] is that the polymer has an affinity for the aromatic electrons on the nanotube because the polymer also has two aromatic functional groups. Hence the polymer wraps around the nanotube holding it in solution and allowing the smaller amorphous material to fall out of solution. On removal of the polymer pure nanotubes are left. The advantage of this technique is that the nanotubes are left untouched with the tips of the nanotubes still intact.

After all of these techniques had been attempted it was decided that the best route would be to use the PPV based method. This was the best technique, as there was no etching of the tips by strong acids and no addition of extra functional groups. However, even after purification was carried out some traces of graphite residue were still visible. The TEM image of the nanotubes after the purification is shown in figure 2.5.

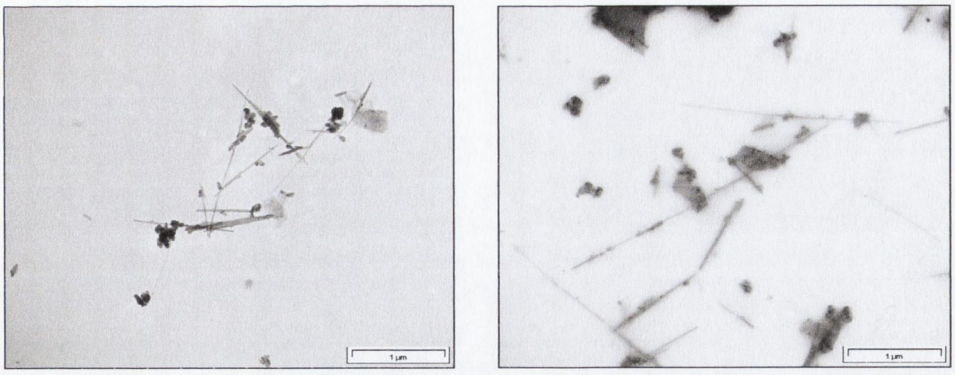

Figure 2.5 TEM images of arc discharge nanotubes after purification using PPV

The purification of the arc discharge nanotubes above allowed us to prepare pure straight multiwalled carbon nanotubes on a milligram scale.

Once the purification techniques were analysed, the ultimate yields and time taken to obtain these yields. It was realised that the amount of nanotubes supplied would not be sufficient for the project. As a result some of the valuable properties of using arc-discharge nanotubes had to be sacrificed to allow reactions to be performed on a larger, milligram scale. The Nanocyl Company reduced the price of their CVD nanotubes as they were able to produce good quality highly purified nanotubes at lower cost, 1g ~50 euro.

Subsequently curly, CVD, MWNTs were purchased from Nanocyl (figure 2.6). The disadvantage of these CVD nanotubes is that they are considerably curly due to the presence of defects in the side walls of the nanotubes which are formed during their production. The fact that they are highly flawed means that the relative strength of these tubes as compared with the, perfectly straight arc discharge nanotubes, is reduced. Also, analysis of these tubes by TEM is much more difficult as any structural differences are difficult to attribute to either a chemical modification or just how the nanotubes have been manufactured.

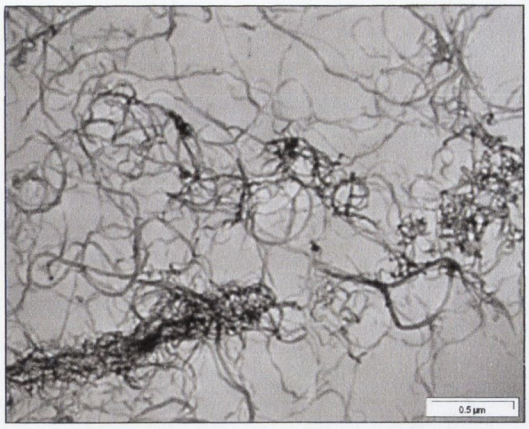

Figure 2.6 TEM image of the curly MWNT purchased from Nanocyl

The Nanocyl MWNTs have been purified by acid treatment. Then the carboxylic acid groups attached to the nanotube surface were removed by annealing under argon in the CVD machine (scheme 2.1) at 500 °C for 1 hour. After thermal treatment the nanotubes were allowed to cool under argon for two hours. IR analysis, of the sample has shown the absence of the signal at 3417 cm^{-1} and 1668 cm^{-1} attributed to CO groups in the sample before annealing, appendix 2.1.

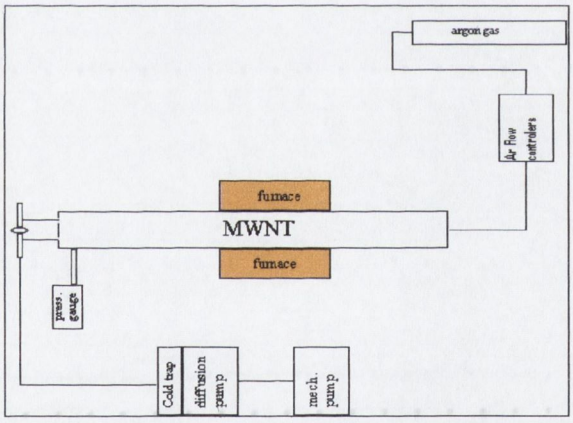

Scheme 2.1 A CVD machine set used for annealing of nanotubes

Once annealed, these nanotubes are suitable for the suggested organometallic functionalisation. Annealing is critical for organometallic reactions because the carboxy groups will be the first to react with the butyl-lithium. Once these groups are removed the nanotubes are susceptible to reacting directly with the butyl-lithium.

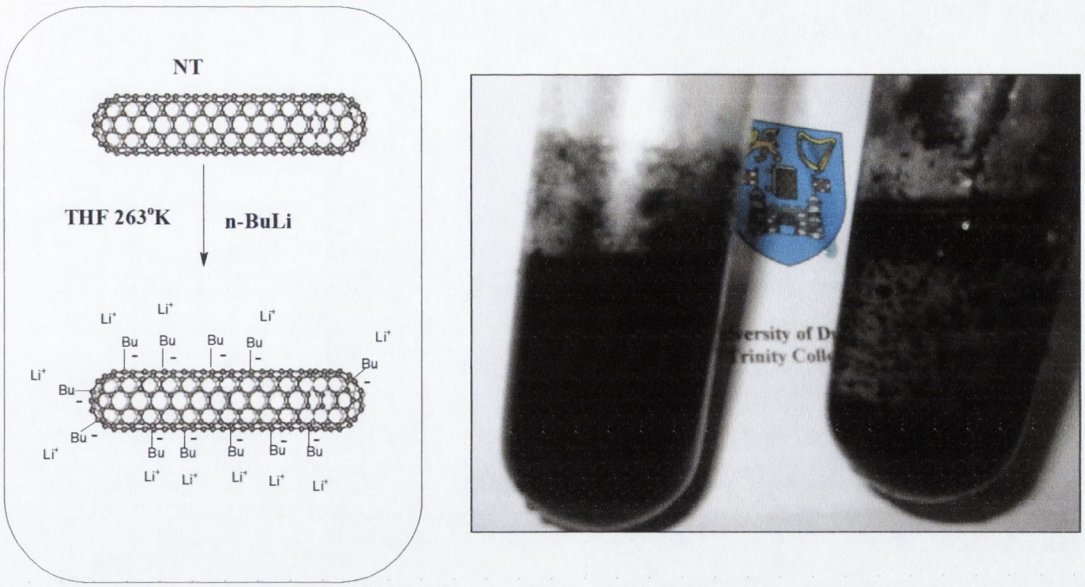

Figure 2.7 Schematic representation of the lithiation reaction (left) and an image of the dispersion of the lithiated and non-lithiated nanotubes (right). The Schlenk on the left side of the image contains a dispersion of lithiated MWNTs in THF and on the right one contains a suspension of pure annealed pristine MWNTs.

We suggest that at a low concentration of BuLi the metalation proceeds mainly at the tips and other non-hexagonal regions due to the steric stresses that the carbon atoms here are under. As the amount of BuLi is increased, these sites saturate resulting in side wall functionalisation. Additionally, depending on the electronic properties (*e.g.* metallic, semi conducting) of each nanotube, a partial or complete charge delocalisation in the nanotube could occur. This may result in some nanotubes being more susceptible to functionalisation with alkyl groups and Li atoms along the entire body of MWNTs. Lithiated nanotubes were extremely air and moisture species to be studied by any of the available methods. Therefore the lithiated nanotubes have been hydrolysed and then studied by IR spectroscopy, appendix 2.2. The IR spectrum of the sample contains characteristic alkyl (CH) bands at 2927 cm^{-1} and 1450 cm^{-1}.

As well as reacting the nanotubes with *n*-BuLi, a reaction was performed with *t*-BuLi in the same conditions to compare the reactivity of different lithium alkyls and correspondent degree of functionalisation of carbon nanotubes. Results of the, C, H, N elemental analysis of annealed, *n*-BuLi and *t*-BuLi functionalised nanotubes were compared. It was found that *n*-BuLi functionalised nanotubes have shown a higher content of both hydrogen and carbon thus it can be deduced that there was a larger amount of functionalisation by the *n*-BuLi. In the elemental analysis of annealed pristine nanotubes the amount of hydrogen present as a percentage of carbon is 0.48% compared to 1.65% for *t*-BuLi functionalised nanotubes which

increases to a significant 3.29% for *n*-BuLi functionalised nanotubes. This shows that the degree of functionalisation is approximately twice as high for the reaction with *n*-BuLi. The most plausible explanation for this is steric hindrance. The *t*-butyl is a more sterically demanding group and fewer groups are needed to cover the nanotube surface, as result the lithiation degree is lower for *t*-BuLi functionalised carbon nanotubes.

2.3.4 Interaction of lithiated carbon nanotubes and metal halides

We expected that the lithiated nanotubes should be susceptible to metathetic exchange reactions with any halogenated species *via* elimination of lithium halides, scheme 2.2. To test this idea the lithiated carbon nanotubes have been treated with different metal halides in dry THF.

Reactions with $AuBr_3$, $SnCl_4$, $SnBr_2$, $PbBr_2$, $GeCl_4$ and $SiCl_4$ have been performed in this work. We anticipated that the reactions with $SnCl_4$, $SnBr_2$, $PbBr_2$, $GeCl_4$ and $SiCl_4$ would result in products with stable metal-carbon or silicon-carbon bonds. This should allow us to investigate these new materials without using special handling techniques (high vacuum or extra clean and dry inert gases). Products have been analysed using TEM, HRTEM, EDX, XPS, IR and Raman spectroscopy.

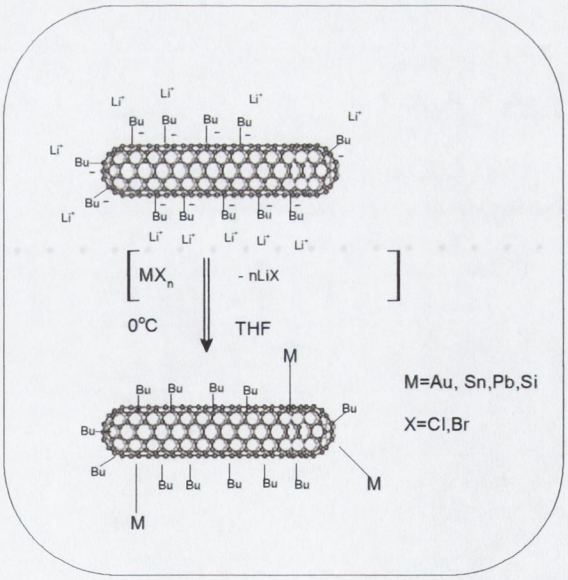

Scheme 2.2 Reaction of lithiated NTs with metal halide resulting in loss of lithium halide and metal to nanotube bond formation.

The procedures were carried out for both multi-walled and single walled lithiated nanotubes. The SWNT have a tendency to form very strong bundles, which are very difficult to split into individual nanotubes and provide an effective functionalisation of SWNTs. The problems of analysis can be seen in figure 2.8 where a sample of MWNTs and a sample of SWNT are pictured. What can be seen is a single MWNT and SWNTs at comparable magnification. The SWNTs are bound together in a bundle and hence observing small changes to the external surface of SWNTs is exceptionally difficult. In the MWNT sample it is easy to identify one nanotube and it is nearly possible to observe the walls of the nanotube.

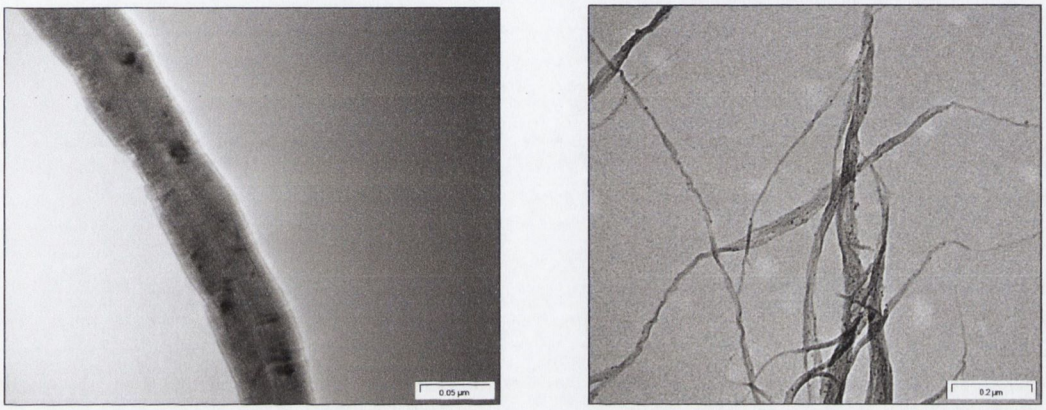

Figure 2.8 Shown here are TEM images of MWNT (left) and SWNTs bundles (right) at comparable magnification.

2.3.4.1. Reaction of lithiated MWNTs and $AuBr_3$

It has been previously demonstrated that non-functionalised SWNTs can spontaneously reduce some metal ions (Au and Pt) from their solutions with the formation of metal nanoparticles on sidewalls.[12] The formation of Au particles on SWNT sidewalls was attributed to direct redox reaction between nanotubes and metal ions. We expect that the lithiated carbon nanotubes should be extremely strong reducing agents. We also believe that the lithiated nanotubes could act as a large electron donor reducing "ligands".

Lithiated MWNTs were treated with $AuBr_3$ with a weight ratio of 1:10 in THF at -10 °C for 16 hrs. The reactions resulted in reduction of gold(III) species into gold metal and formation of gold nanoparticles on the surface of the carbon nanotubes.

TEM images of the MWNT with gold nanoparticles are shown in figure 2.9. The gold nanoparticles can be seen as black dots on the walls of the nanotubes.

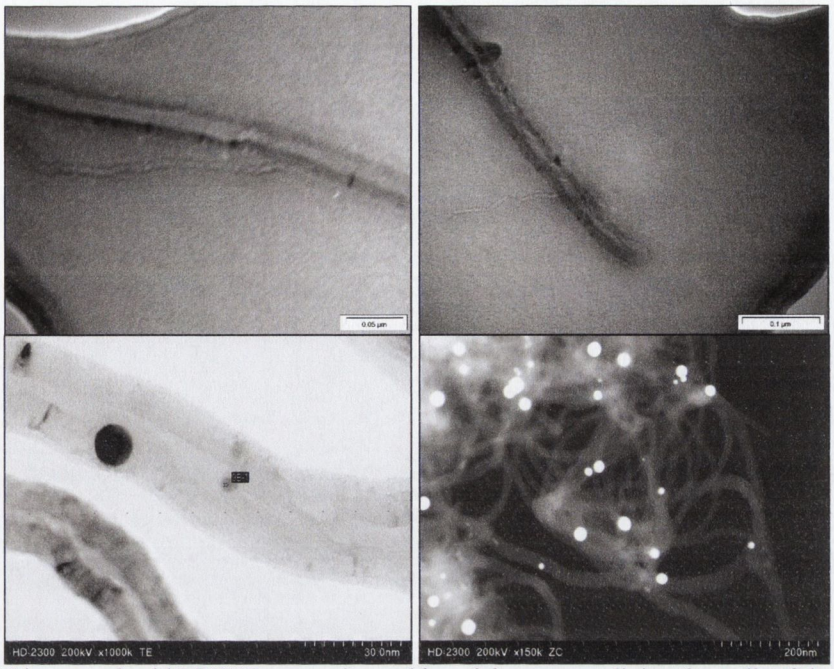

Figure 2.9 TEM images of gold-MWNT composites gold particles are seen lining the walls of the tubes as black dots the bottom right image is a dark field image where the particles are white.

These dots have been identified as gold nano-particles through the use of dark field imaging and the identification of gold through the use of diffraction patterns, all done with the use of HRTEM in Japan.

Figure 2.10 below shows the Raman spectra of the gold-nanotube composites. The I_G and I_D bands are more pronounced which might be explained by increased conductivity of the metalated carbon nanotubes. The I_G/I_D bands arise due to scattering from graphite-like and disordered forms of sp^3 bonded carbon. In the lower wave number region of the spectrum there is a new peak at 350 cm^{-1} with peak broadening. The IR spectrum, appendix 2.3, shows the spectrum for the Au functionalised MWNTs sample. The sample was also analysed by EDX using the high resolution TEM, where the EDX (appendix 2.4) clearly shows the gold peak and notably no presence of a bromine peak. This allows us to conclude that the halide has been removed as the lithium salt, resulting in the reduction of gold(III) to the gold metal on the nanotube surface.

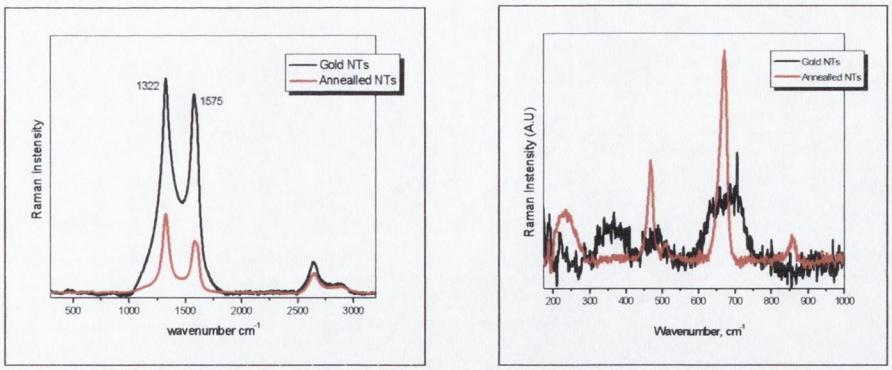

Figure 2.10 Raman spectra of the gold MWNTs composites.

2.3.4.2. Reaction of lithiated MWNTs and $SnCl_4$

Interaction of lithiated MWNT with $SnCl_4$ in a ratio of 1:14 by weight in THF gave the new tin containing nanotube composites. TEM image of the coated MWNT composites is shown figure 2.11.

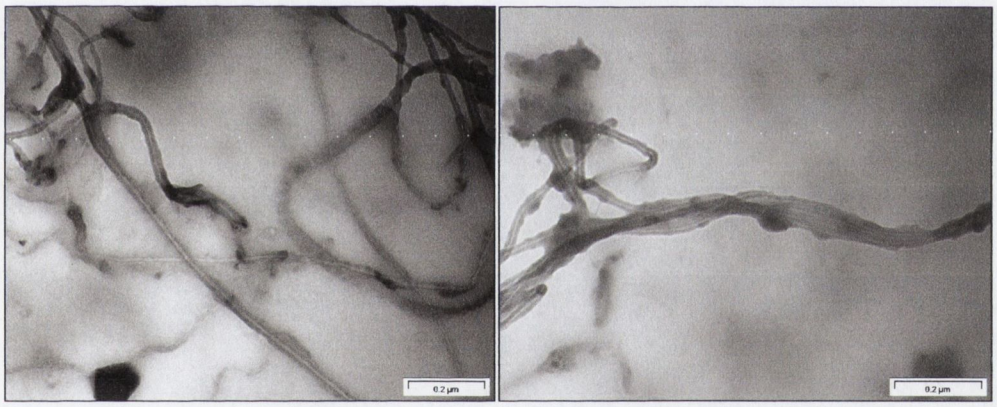

Figure 2.11 TEM image of tin containing MWNT composites

Some dark-field images (Figure 2.12 left) were taken to confirm the presence of tin in the coating of the walls of the tubes. The diffraction pattern of tin atoms was identified and subsequently this was used for dark field imaging, the nanotubes shown as white in this image due to the tin containing coating.

As can be seen from the Raman spectrum, figure 2.12, there is a shift in the peaks found by comparing with the reference sample and also a broadening of some peaks, as well as two new peaks found at 809 cm^{-1} and 351 cm^{-1}. The effect on the graphitic and defect, I_G and I_D bands has also been examined. The defect region of the sample becomes more pronounced. This is

due to the fact that the carbon atoms are deviating from the sp^2 hybridisation because they are bound to the metal atoms and are hence becoming more sp^3 hybridised. The IR spectrum of the tin MWNT composites clearly shows the presence of Sn-C bands at 652 cm^{-1} and 385 cm^{-1} in the sample, appendix 2.5.

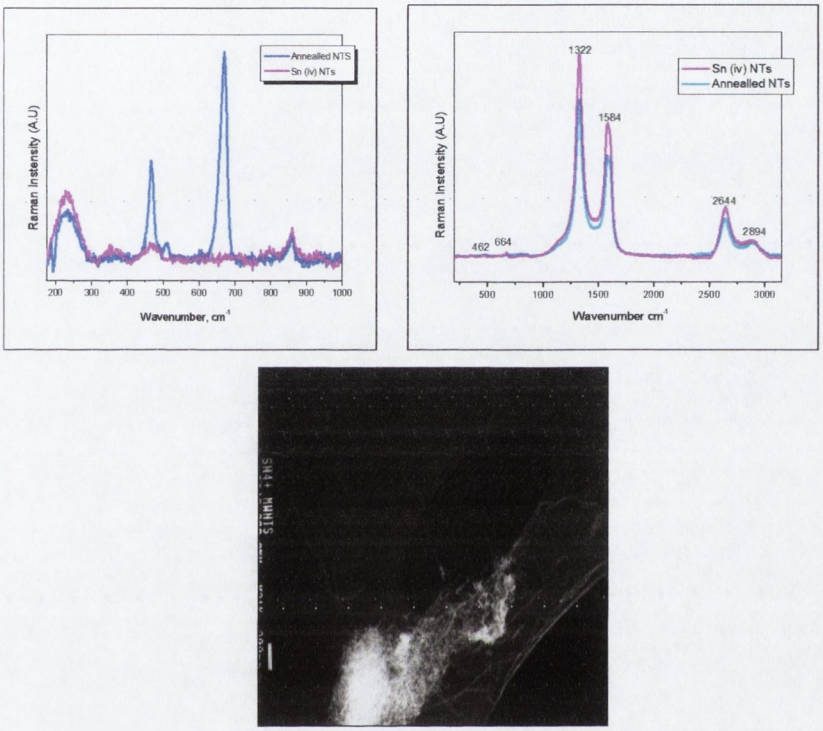

Figure 2.12 Dark-field HRTEM image of tin-MWNT and the Raman spectra, low region middle and high region far right, of tin-MWNT composites

These peaks indicate that the reaction resulted in the formation of Sn-C bonds thus with the inclusion of the EDX spectrum, appendix 2.6, right it can be deduced that the Sn is bound to the nanotubes.

This sample was analysed by XPS and the composition of this sample was calculated by quantitative analysis of the XPS spectra. The composition of the sample was as follows C 94.5%, Sn 1.4%, O 3.4% and Cl 0.8%. The presence of chlorine and oxygen indicates on the occurrence of unreacted Sn-Cl bonds, which might also be partially hydrolysed giving tin oxychloride species. The IR spectra also showed a carbonyl band, which is likely to have

arisen from the oxidation of metalated nanotubes after the sample was washed and exposed to the air.

In figure 2.13 a peak with B.E. at 487 eV can be attributed to a Sn-C bond as it is reported in the literature.[13] In general metal carbides are found in the C1s spectra at 283 eV binding energy.[14,15] The subsequent spectrum analysed was that of the C1s which had a typical carbide peak at 284.2 eV. The full width at half maximum (FWHM) was compared between the peaks of the annealed sample and the tin(IV) sample. The FWHM for the annealed sample was considerably lower than the tin sample at 1.53 eV compared to 1.8 eV this would suggest that the bonding of the carbon in the tin sample is quite different to that of the annealed sample. Comparing the bonding and shape of the C1s peak of both samples the resulting two peaks can be seen, figure 2.14.

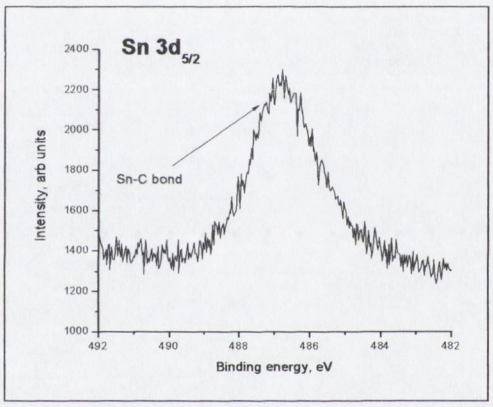

Figure 2.13 Sn 3d $_{5/2}$ region of XPS for $SnCl_4$ functionalised carbon nanotubes.

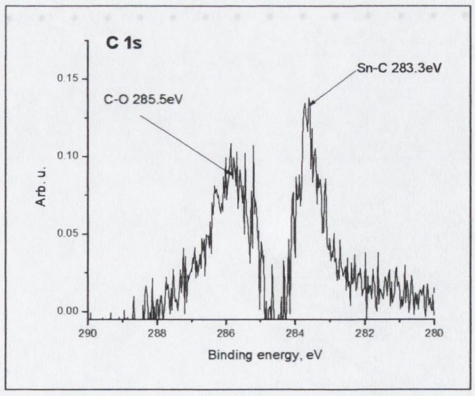

Figure 2.14 C1s region of XPS for $SnCl_4$ functionalised carbon nanotubes.

The peak at 285.5 eV is typical of a carbon oxygen bond which is likely to have originated from the oxidation after the reaction when the sample is exposed to the air. The peak at 283.3 eV is attributed to the Sn-C bond, which has been documented previously.[13]

Figure 2.15 shows the deconvolution of the signals that are present in the carbide signal of the tin sample. The signals here show C-O bonds at 286.9 eV, 285.5 eV and 288.8 eV these are representative of different forms of C-O bonding. The large signal at 284.2 eV which represents the C-C bonds of the carbon nanotube can also be seen. The signal at 283.5 eV is indicative of the C-Sn bond.

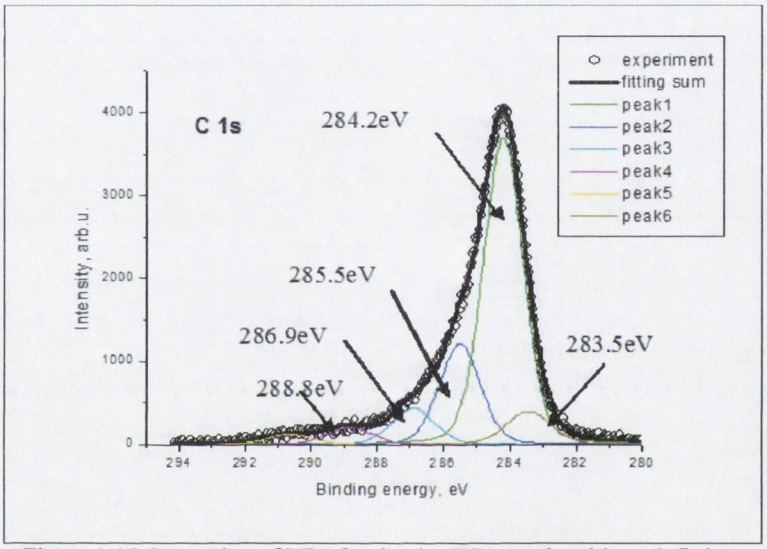

Figure 2.15 C1s region of XPS for the tin (IV) sample with peak fitting.

2.3.4.3 Reaction of lithiated MWNTs and $SnBr_2$

The treatment of the lithiated MWNTs with $SnBr_2$ in THF was performed similarly to the process with $SnCl_4$, with a weight ratio of 1:25. The TEM image of the lithiated nanotubes after treatment with $SnBr_2$ is shown in figure 2.16.

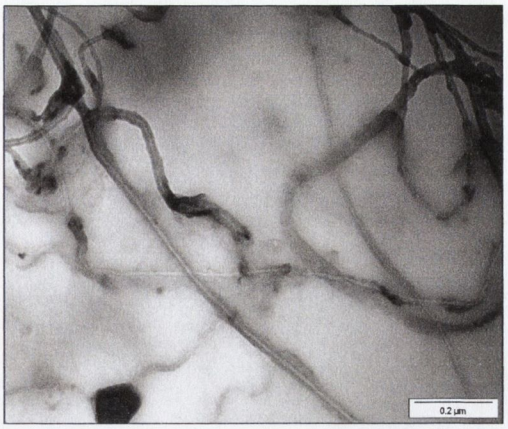

Figure 2.16 TEM image of MWNTs functionalised with tin. The tin can be seen as black dots surrounding the outside of the nanotubes.

The TEM image of the MWNTs functionalised with $SnBr_2$ also shows the coating on the MWNTs, figure 2.16. Raman spectroscopy, figure 2.17, of the sample shows peaks similar to that of the tin(IV) sample; peaks at 350 cm^{-1} and peak broadening, however, in this spectrum there is a peak at 750 cm^{-1}. IR of the sample was analogous to that above for the $SnCl_4$ lithiated MWNTs product.

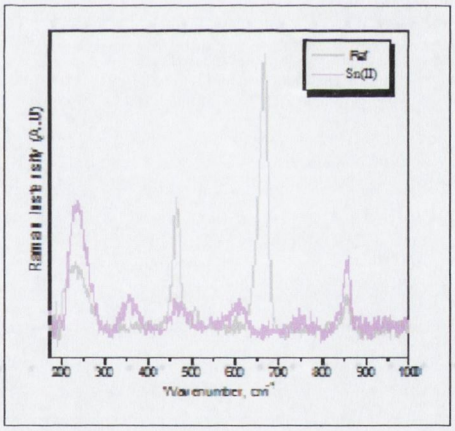

Figure 2.17 Raman spectra of $SnBr_2$ MWNT samples.

XPS analysis was carried out on this sample. The peak widths of the C1s bond signals were compared in the pure annealed MWNT sample and the tin(II) reacted sample. It was discovered that the FWHM for the tin(II) sample was greater than that of the pure MWNTs. This allowed a conclusion that the bonding of the carbon atoms in the tin sample was different. C 1s spectra of the pure annealed MWNT sample compared with the C 1s spectra of the tin(II) sample the spectra shown in figure 2.18 was observed.

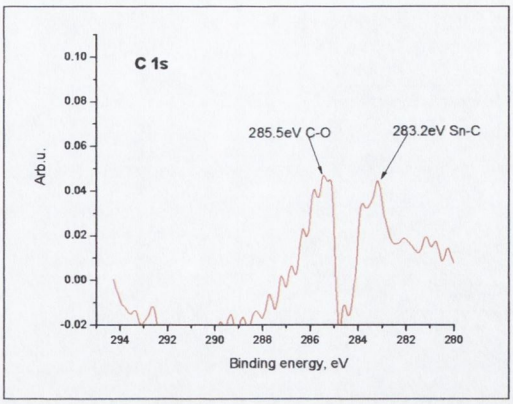

Figure 2.18 C1*s* region of XPS for tin(II) MWNT species (difference between the tin(II) minus the annealed MWNT spectra and after smoothing).

What can clearly be seen in the new spectra is that two new signals appear at 283.3 eV and at 285.5 eV. The signal at 283.3 eV is the most interesting for this sample as this is typical for a carbon metal bond according to the literature. Therefore we can conclude that the nanotube has been bound directly to the Sn *via* Sn-C bond. The other signal is typical of a carbon oxygen bond which leads us to believe that the sample becomes oxidised either over time or initially after the sample is washed. Not all of the lithium ions react with the metal halide either due to steric reasons or the nanotube supports the negative ions in an inert atmosphere. Once exposed to water or air these ions quickly react leaving the rest of the nanotube to become oxidised by water.

What is shown in figure 2.19 is the extrapolation of the bonding modes of the carbon atoms of the nanotube in the tin(II) sample. It can be easily observed that new carbon bonds have been formed after lithiation and that the tin atoms are bound to the nanotube.

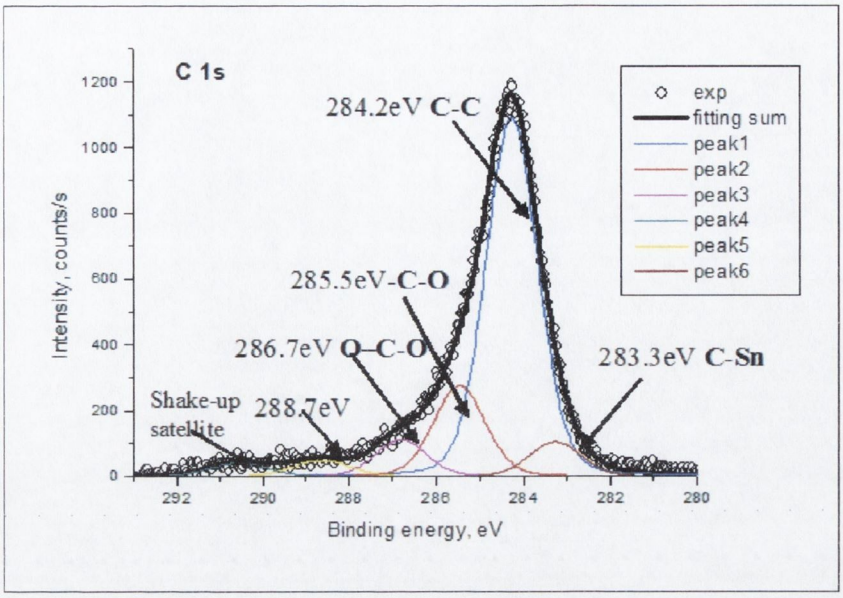

Figure 2.19 The deconvolution of the C1s region of the XPS for the $SnBr_2$ sample.

2.3.4.4 Reaction of lithiated MWNTs and $PbBr_2$

Similar reactions of lithiated MWNT with $PbBr_2$ with a weight ratio of 1:25 in THF produced new lead MWNTs nanocomposites. The TEM images of the nanocomposite are shown in figure 2.20. Most of the nanotubes were found linked to each other and coated with lead containing coating.

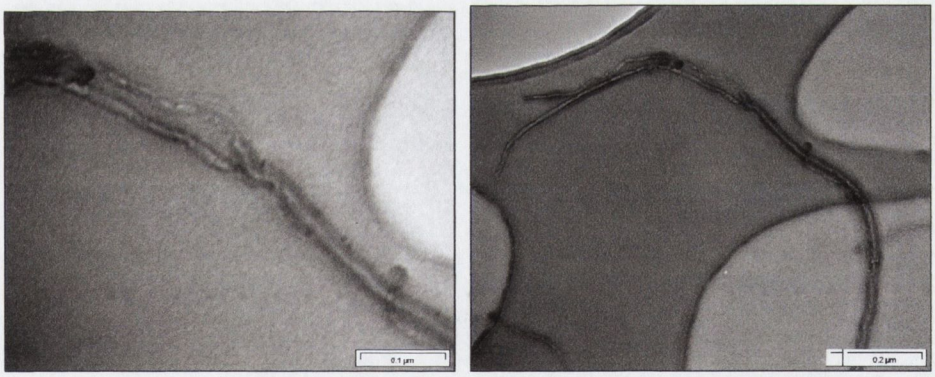

Figure 2.20 TEM images of lead functionalised nanotubes.

In the Raman spectrum the I_D/I_G ratio is more pronounced than the reference sample. However, in the lower region of the graph once again there is a shift in the peaks of the graph, with the appearance of some extra peaks towards the 1007 cm^{-1} at 903, 931 and 984 cm^{-1}. The EDX spectrum shows a lead peak and noticeably no halide peaks were observed (figure 2.21 right).

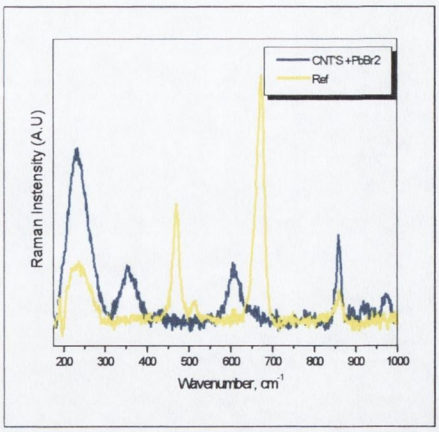

Figure 2.21 Raman spectra of Pb CNTs, left and EDX of Pb CNTs

The IR spectrum of the lead functionalised nanotubes is shown in appendix 2.7. There are a number of peaks which are typical of the functionalised nanotubes those of the nanotubes at 897, 983 and 1090 cm^{-1} and also the butyl C-H groups at 1356 cm^{-1}.

XPS data was collected for the lead carbon nanotube sample and the data was analysed. The carbon C1s spectrum (figure 2.22) for the Pb (II) sample was compared with that of the initially analysed annealed MWNT sample.

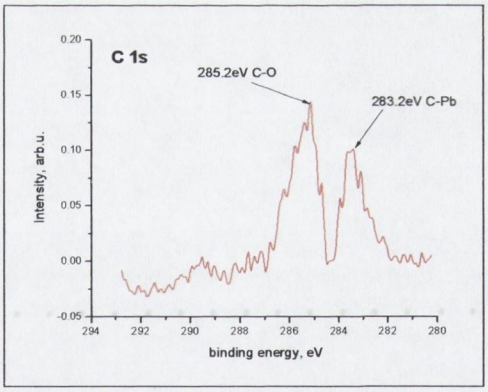

Figure 2.22 C1s region of the XPS for the Pb (II) sample minus the annealed sample after smoothing

The signal at 285.5 eV is attributed to a carbon oxygen bond formed after hydrolysis at the end of the reaction when the nanotubes are washed with water and exposed to air. The signal at 283.4 eV is typical for a carbon metal bond and is therefore attributed to the carbon lead bond. The deconvolution of the carbide bond can be seen in figure 2.23.

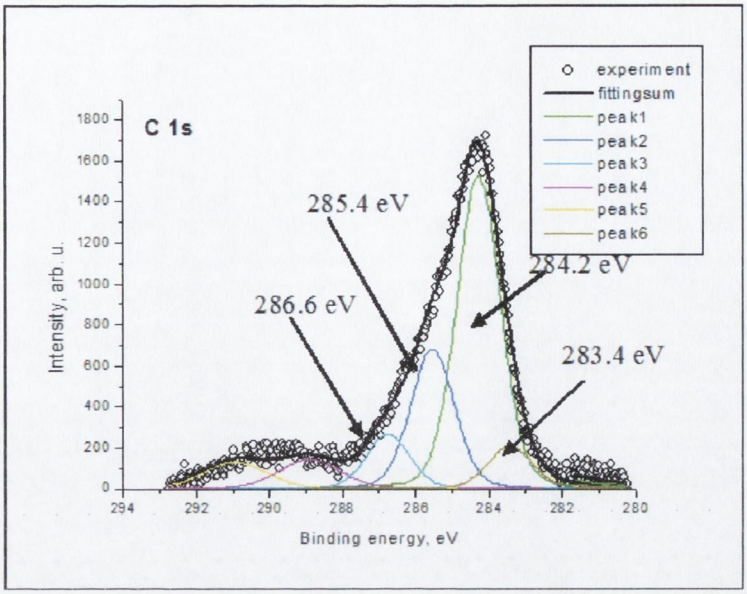

Figure 2.23 Deconvolution of the C1s spectra for the lead (II) sample

To complement this data, in the Pb $4f_{5/2}$ spectra there is a peak with B.E. at 137.3 eV, which is attributed to the lead carbon bond, see figure 2.24. The signal at 138.3 eV is representative of $Pb(OH)_2$[1617] and the signal at 138.9 eV is indicative the presence of Pb halide.

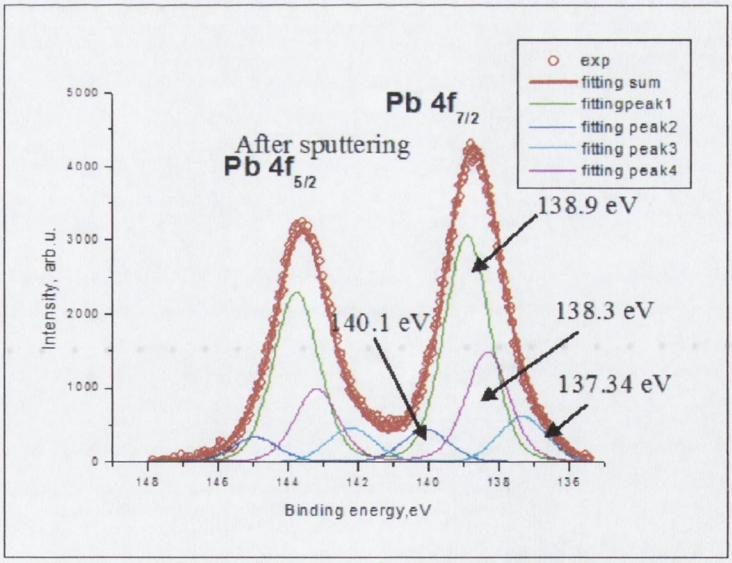

Figure 2.24 The Pb 4f5/2 spectra for the lead (II)-MWNT sample

2.3.4.5 Reaction of lithiated MWNTs and $SiCl_4$

A reaction of lithiated MWNT with $SiCl_4$ with a weight ratio of 1:19 followed by hydrolysis of the sample resulted in the formation of SiO_2 coating and nano-particles on the nanotube

surface. TEM images of the nanotubes that have been coated with SiO_2 are shown in figure 2.30. It is apparent here that the nanotubes react with $SiCl_4$ similarly to the tin halide samples above. The reaction must proceed with the elimination of LiCl and the covalent attachment of silicon chloride fragments to the nanotube surface. The unreacted Si-Cl bonds are then hydrolysed giving hydrolysed silica, resulting in a coating of the nanotubes and connecting them *via* both tip and sidewall defects of the nanotubes.

The IR spectra, appendix 2.8, of the sample have clearly shown the broad Si-O-Si stretch at 1103 cm^{-1} and a peak at 802 cm^{-1} attributed to the Si-C (sp^2) bonds.

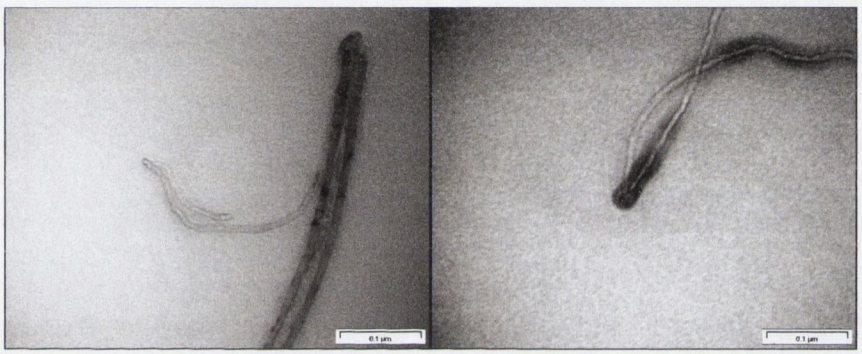

Figure 2.25 TEM images of MWNT-silica composites Silica can be seen coating the tip of the tube

Also in the Raman spectrum figure 2.26 of the silica-nanotube composites the intensity of I_G/I_D bands is quite reduced compared to the reference sample.

The EDX spectrum, appendix 2.9, of the silica-MWNT sample shows a clear peak for silicon present in the sample as well as a lack of chlorine. This indicates that the chlorine has been removed during the reactions.

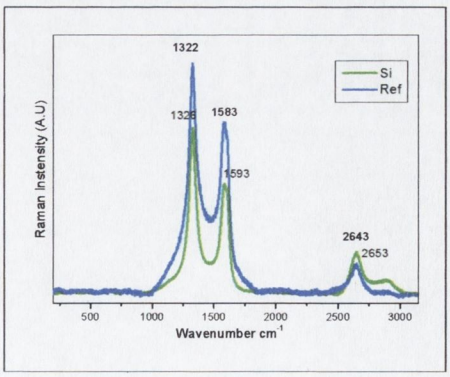

Figure 2.26 Raman spectrum of silica-MWNT composites of the silica composite

The XPS spectra of the C1s of silicon reacted nanotubes minus the annealed MWNT sample are shown in figure 2.27. It is noticeable here that, as in the previous samples of metal reacted with nanotubes; there is the appearance of the peak at 283.3 eV which is representative of a metal or metalloid carbon bond.

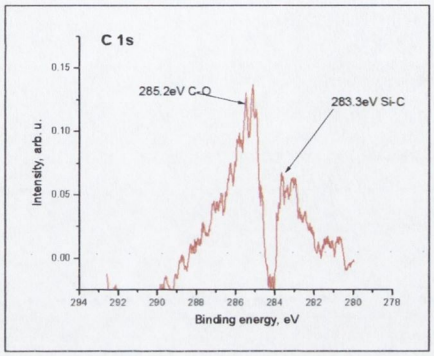

Figure 2.27 C1s region of the XPS for Si- MWNT composite sample after subtraction and smoothing

Figure 2.28 shows the total deconvolution of the C1s spectra and presence of the carbide peak at 283.3 eV in the Si-MWNT sample. The amount of total C, Si and O has been quantitatively calculated on the basis of peak area measurement. The total amount of C was 67.5%, Si was 12.3% and O was 20.2%. The amount of metalloid and oxygen are noticeably higher when compared with the total amount in the other metal nanotube experiments. It was felt that the reason for this was that the silicon became oxidised on the surface of the nanotube and resulted in more Si-O aggregating on the surface. The total amount of carbide bound to the silicon was calculated to be 10.2% which is comparable with the other metal nanotube complexes.

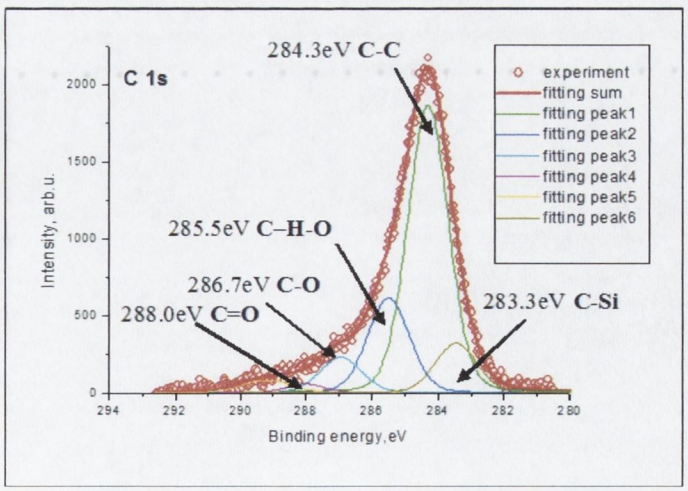

Figure 2.28 The deconvolution of the carbide peak of the C1s spectra of the Si-MWNT sample

The Si 2p spectrum, figure 2.29, of Si functionalised MWNTs shows the peaks of Si-O, Si-O-C and Si-C at 103.8, 102.7 and 101.2 eV respectively.

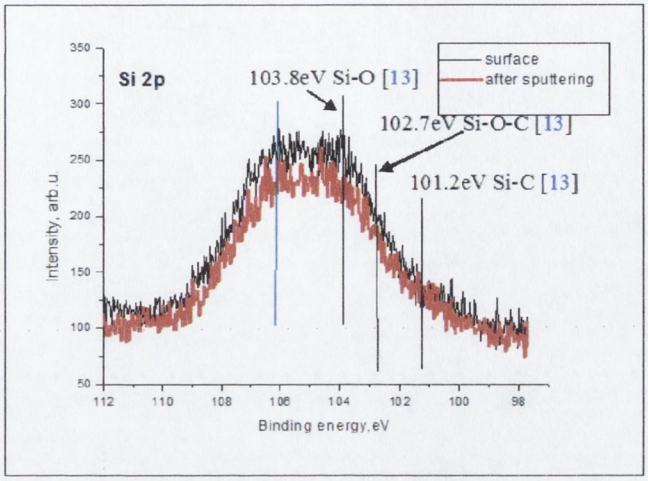

Figure 2.29 The Si 2p XPS spectrum of Si functionalised MWNTs

2.3.5 Reactions of lithiated SWNTs and group (IV) metal halides

SWNTs were reacted with butyl-lithium and subsequently with selected metal halides in analogous manner to the MWNTs. These metal halides were group(IV) metal halides: $GeCl_4$, $PbBr_2$ and $SnBr_2$.

2.3.5.1 $SnBr_2$ and lithiated SWNTs

The treatment of lithiated SWNTs with $SnBr_2$ with a weight ratio of 1:25 in THF resulted in the formation of Sn containing nanoparticles on SWNTs bundles. The products were analysed by TEM and the resulting image is pictured in figure 2.30. The tin is observed here as dark dots surrounding the SWNT which exist as bundles, this shows the difficulty in the analysis of the SWNT's due to the bundling.

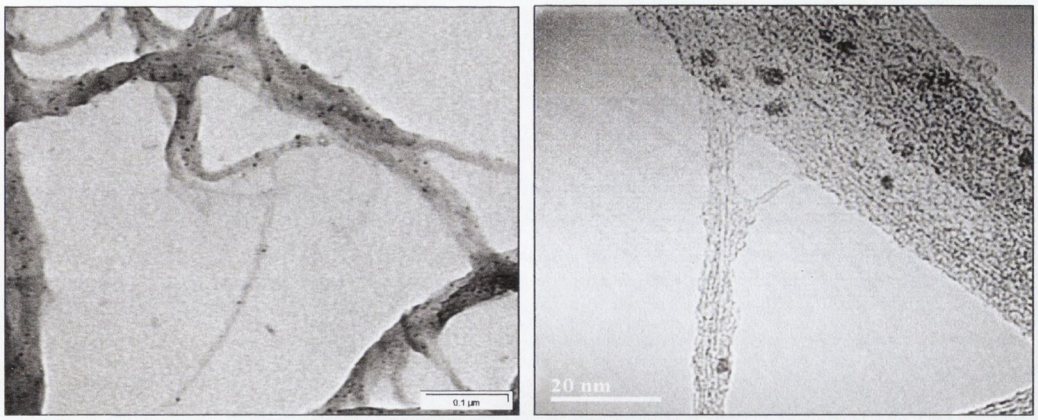

Figure 2.30 TEM images of Sn-SWNTs

An XPS spectrum of untreated SWNTs was taken and in the C1s spectrum, figure 2.31, peaks for C-C, C-H-O, C-O and a small peak at 290.6 eV which is indicative of C-H were observed.

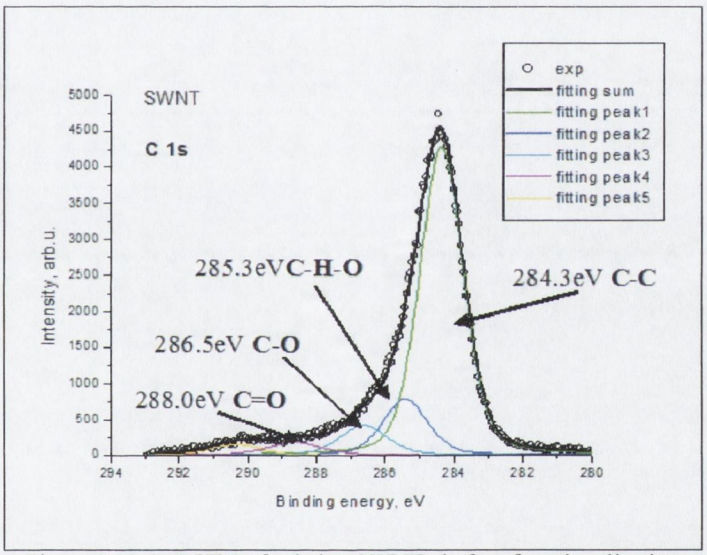

Figure 2.31 C1S XPS of pristine SWNTs before functionalisation

After this an XPS was obtained for a Sn-SWNTs sample, figure 2.32. In this sample similar peaks are observed however there are two differences between the reacted and pure SWNTs. The first difference is the appearance of a new peak at 283.4 eV which, when compared with the Sn MWNT samples is at a similar B.E. And secondly the C-H peak area has increased significantly, due to the bonding of butyl groups to the nanotubes surface upon lithiation.

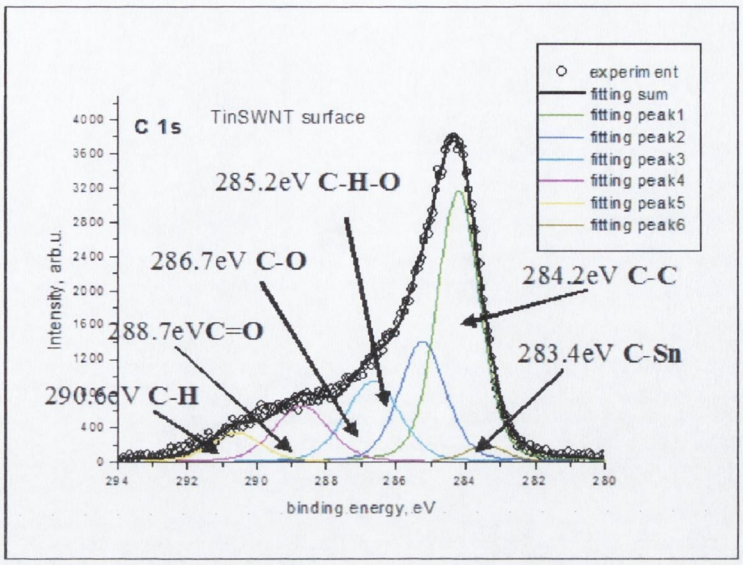

Figure 2.32 C1s region XPS of Sn-SWNT.

In the Sn 3d spectrum (figure 2.33), the peaks found at 487.6, 486.7 and 485.6 eV are attributed to tin halide, tin oxide and tin carbide respectively.

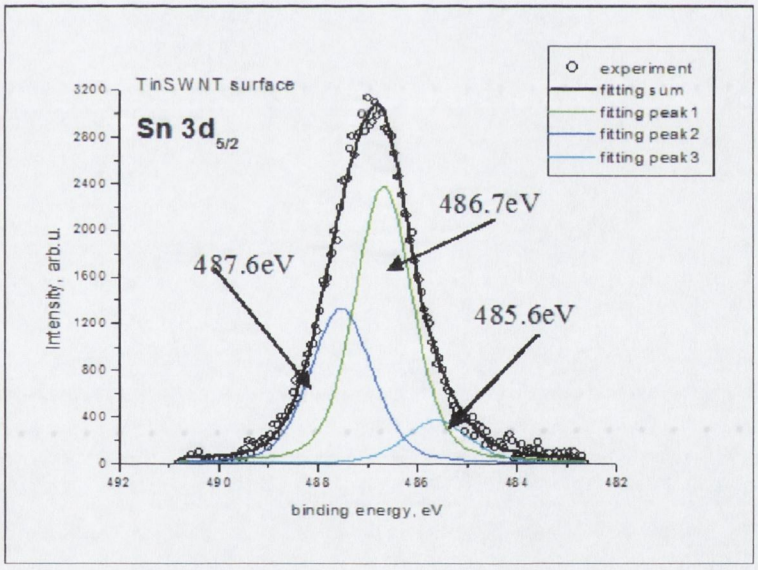

Figure 2.33 Sn 3d region of XPS for Sn functionalised SWNT sample

The Raman spectrum of the Sn functionalised SWNTs can be seen in figure 2.34. The reacted sample in blue is compared to the functionalised sample in green. The left spectrum shows the low end region, which clearly shows the radial breathing modes of the SWNTs in both cases.

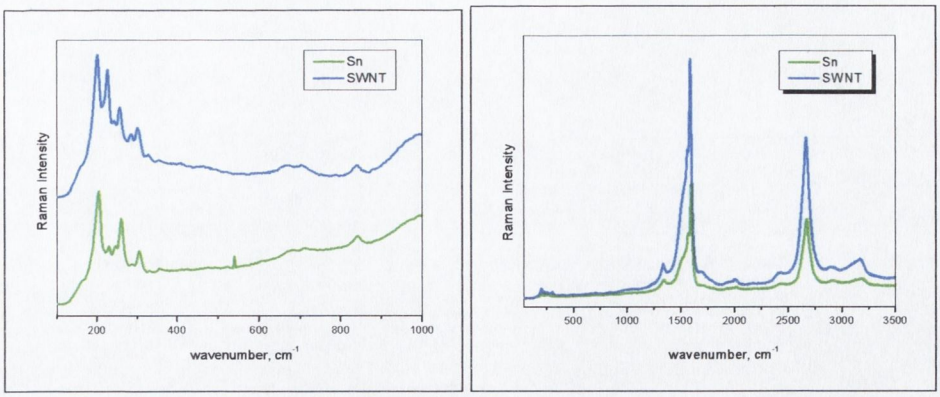

Figure 2.34 Raman spectra of Sn-SWNT sample as compared to SWNTs

The important part of this low end spectrum is that a new signal appears at 538 cm^{-1} which is well known as a Sn-C bond. Thus it can be inferred that Sn has become bound to the nanotubes upon functionalisation. Higher in the spectra there appears to be no change, however, the I_G decreases as the degree of disorder increases in the sample which is due to the functionalisation of the nanotubes graphitisation and disruption of the sp^2 to sp^3 carbons through functionalisation.

In the IR spectrum, appendix 2.10, of the Sn-functionalised nanotubes two new bands are visible. Another experiment was carried out using Raman spectroscopy to observe any differences between the pristine SWNTs, the reactants, the functionalised nanotubes and a mechanical mixture of the two; the result is shown in figure 2.35.

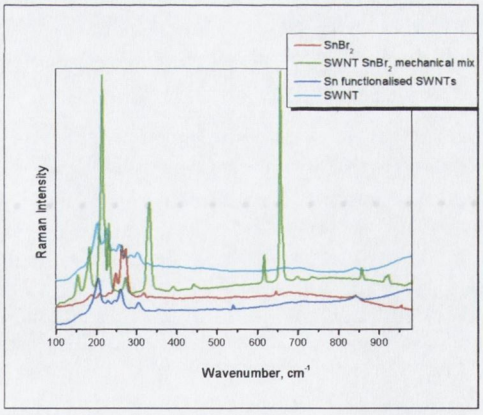

Figure 2.35 Raman spectrum of Sn functionalised SWNTS, $SnBr_2$, SWNTs and a mechanical mixture between the Sn compound and SWNTs

The Sn-C bond at 536 cm^{-1} was only present in the functionalised SWNT sample.

2.3.5.2 Reaction of lithiated SWNTs and $PbBr_2$

Lithiated SWNTs have been treated with $PbBr_2$ in THF similarly to the MWNTs considered above with a weight ratio of 1:25 nanotubes to reagent. TEM images of the Pb functionalised SWNTs were obtained and are presented in figure 2.36 which clearly exemplify the bundling problems. Lead containing nano-particles can be observed in the images as black dots coating the exterior walls of the SWNTs.

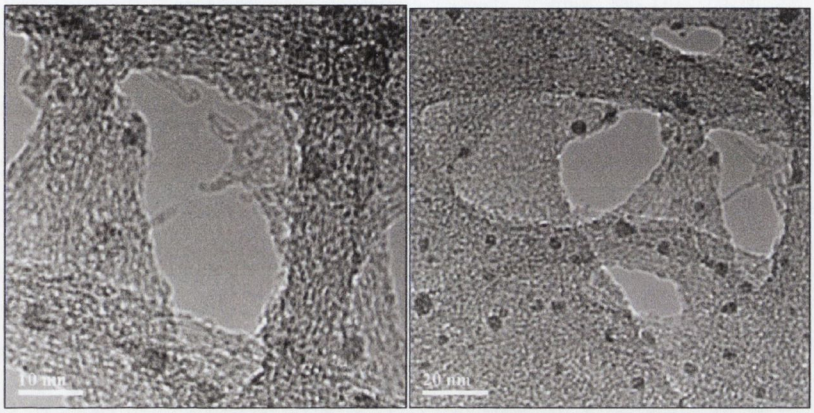

Figure 2.36 HRTEM images of Pb-SWNTs

An XPS spectrum was obtained for this sample is shown in figure 2.37. The two characteristic signs of functionalisation are observed again in the spectrum. The increase in the area of the C-H peak, at 290.6 eV, is indicative of the presence of butyl groups which arise from the lithiation step and are bound to the exterior walls of the SWNTs. Additionally the arrival of the new signal at 283.5 eV which compares well with the MWNT-Pb sample indicates the presence of Pb-C bonds.

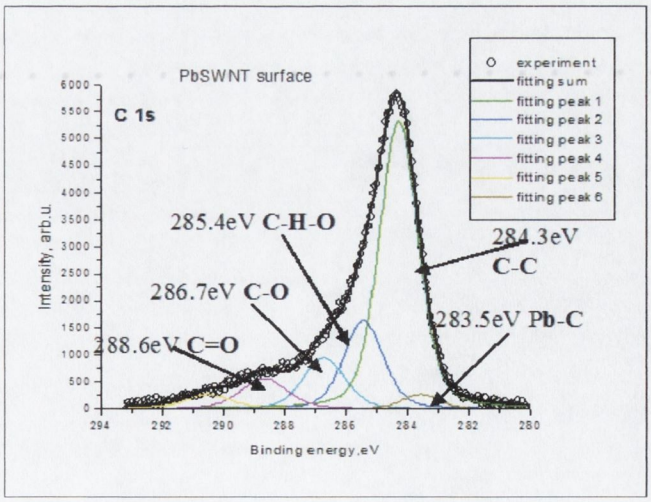

Figure 2.37 C1s region of XPS for the Pb-SWNT sample

To complement this data, a peak appears in the Pb $4f_{5/2}$ spectra at 137.3 eV this is attributed to the lead carbon bond, see figure 2.38. The signal at 138.3 eV is representative of $Pb(OH)_2$ and the signal at 138.9 eV is indicative of the excess of Pb halide used as this represents the Pb halide peak. This data is typical for both MWNT and SWNT functionalised with lead.

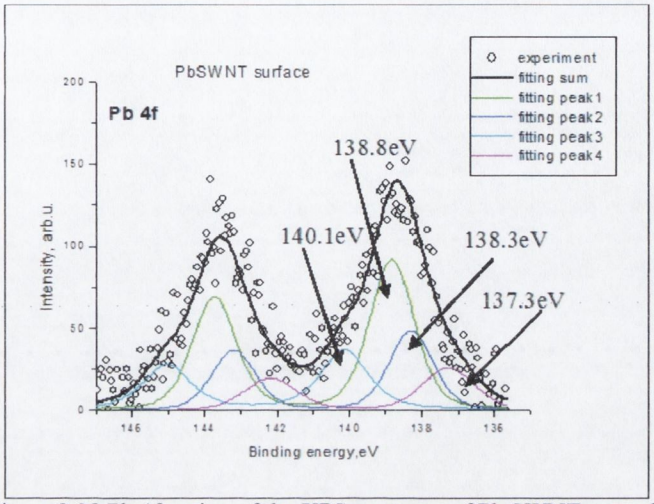

Figure 2.38 Pb 4f region of the XPS spectrum of Pb SWNTs sample

The Raman spectra for both lead bound SWNTs and pristine SWNTs are shown in figure 2.39. The spectra are divided into two regions, on the left for 250 cm^{-1} to 1000 cm^{-1}, so the RBM can be observed and the right where the entire spectrum can be seen.

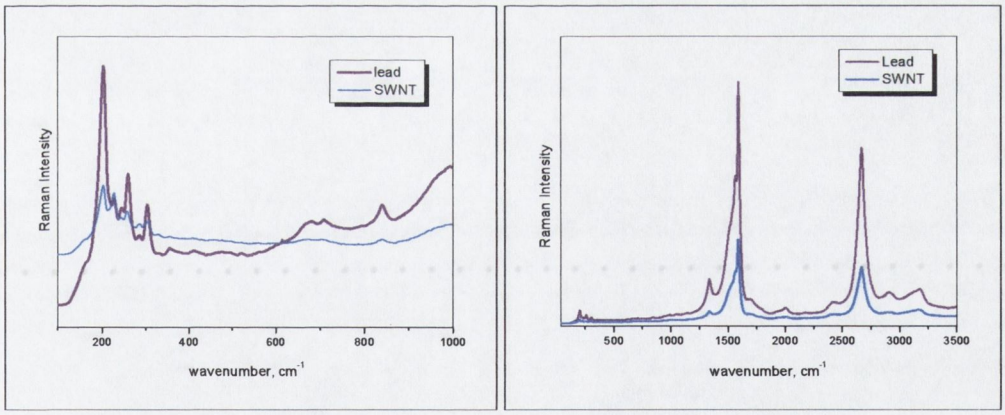

Figure 2.39 Raman spectra of SWNT-Pb as compared to SWNTs

The obvious effect of functionalisation is that the I_D band has increased in size suggesting that the functionalisation has increased the amount of sp^3 carbon present. This would be typical of addition to the nanotubes.

The Pb-SWNT IR spectrum, appendix 2.11, shows the presence of new signals of the butyl groups at 932 cm^{-1} and 1356 cm^{-1} C-C and also at 2900 cm^{-1}.

2.3.5.3 Reaction of lithiated SWNTs and $GeCl_4$

Lithiated SWNTs have been treated by $GeCl_4$ with a weight ratio of 1:19 in THF at -10 °C. After the reaction the Ge-SWNTs composites were analysed by TEM in figure 2.40. The image on the left shows an overview of the sample. The Ge species can be seen lining the outside of the nanotubes surface in the image on the right.

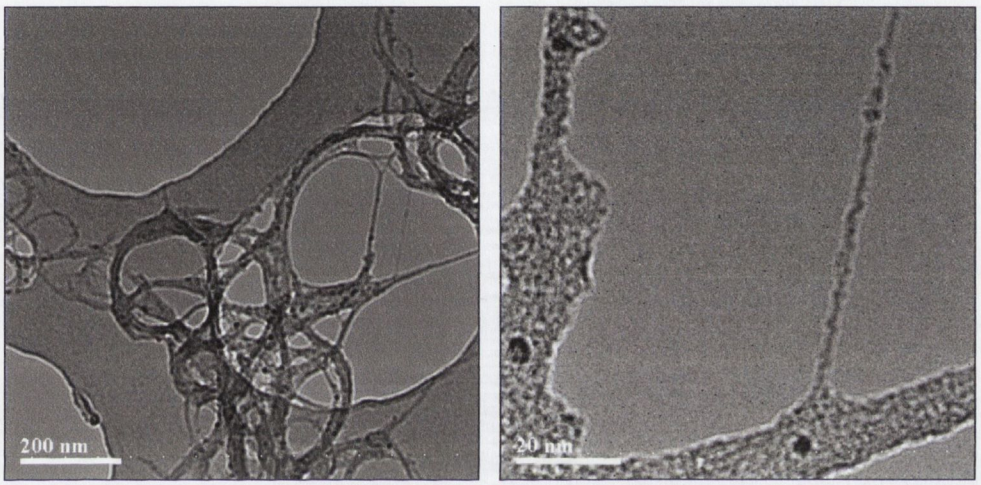

Figure 2.40 HRTEM images of SWNT-Ge composites

The Raman spectrum of the germanium functionalised SWNTs is shown in figure 2.41. It is once again divided into two with the low end spectra on the left and the entire spectrum on the right.

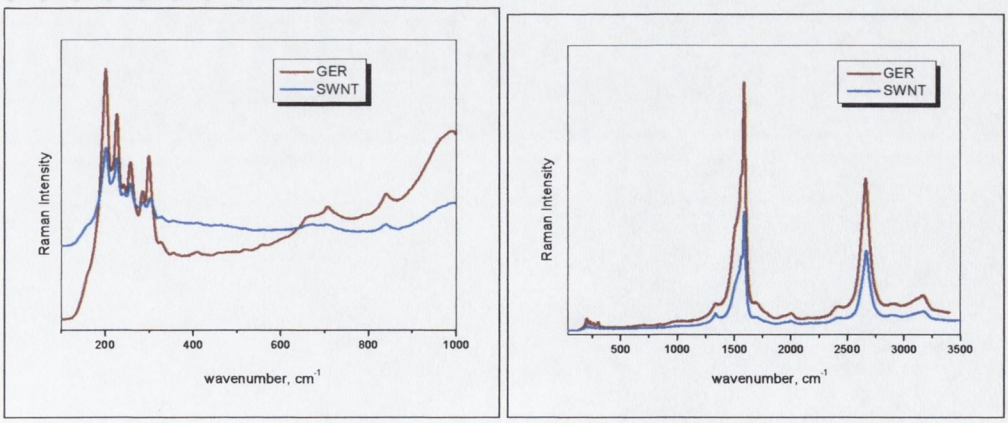

Figure 2.41 Raman spectra of Ge-SWNTs compared to pure SWNTs

There is a noticeable increase in the intensity of all the SWNT signals upon functionalisation with germanium. A new signal which is taken as the Ge-C bond is seen at 403 cm^{-1}. Once again, in the entire spectrum, an increase in signal intensities is observed.

In the IR spectrum, appendix 2.12, of the functionalised nanotubes the bands at 1357, 928 cm^{-1} and at 794 cm^{-1} are typical of the butyl groups now attached to the nanotubes.

An XPS spectrum was also obtained for this sample and the resulting C1s spectrum can be observed in figure 2.42 again there are two new points in this spectrum in comparison to the original SWNT spectrum. The area of C-H peak at 290.6 eV has increased and the butyl groups have been bound to the nanotubes surface. A new peak has been obtained at 283.5 eV which agrees well with the MWNT samples which were bound to metals. Thus this new signal is attributed to the Ge-C bond.

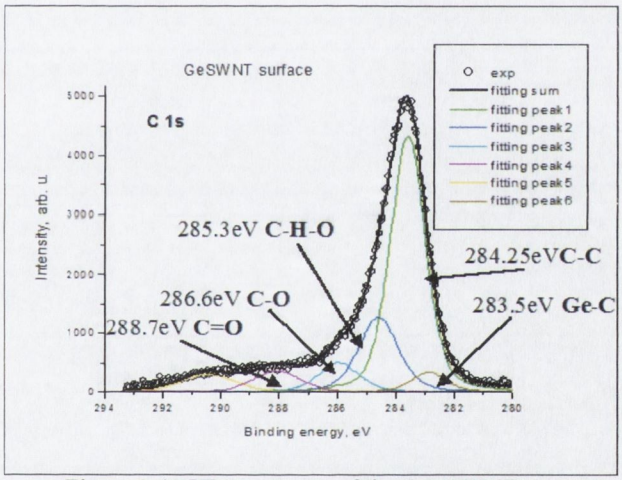

Figure 2.42 XPS spectrum of the C1s SWNT-Ge

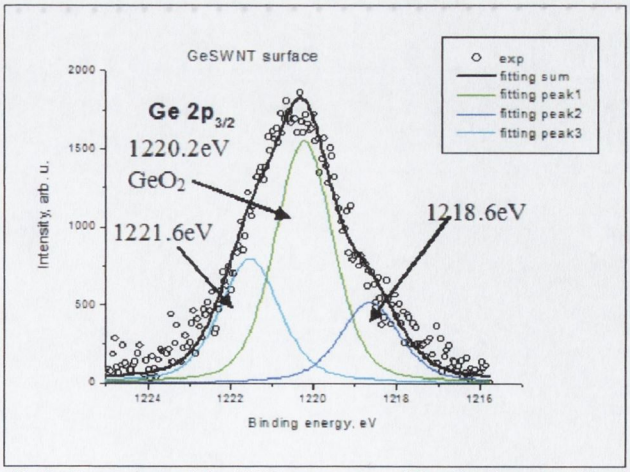

Figure 2.43 Ge 2p region of the XPS spectrum of the Ge functionalised SWNTs

In figure 2.43 there are three signals at 1221.6, 1220.2 and 1218.6eV binding energies. It is believed that the peak at 1218.6 eV corresponds to germanium carbide. The peak at 1220.2 eV is indicative of germanium oxide due to the hydrolysis and the peak at 1221.6 eV is more than likely belongs to residual germanium halide bond.

2.4 Conclusions

In this work we have identified the most suitable method of purification for arc-discharge nanotubes. This as we have shown is the purification technique involving the polymer PPV. The use of strong acids etches the nanotubes and will eventually destroy them, as well as this, it adds functional groups to the ends of the nanotubes. The technique involving PPV is more suitable for our work as it does not destroy the nanotubes in any way, thus the nanotubes are more reactive as this leaves the tips of the nanotubes intact.

We have successfully demonstrated that BuLi can react with both MWNTs and SWNTs to produce highly air and moisture sensitive and extremely reactive adducts. Hydrolysed samples of these products have been characterised by IR and Raman spectroscopy. We have lithiated MWNTs with both *t*-BuLi and *n*-BuLi. According to elemental analysis which shows a higher percentage of carbon and hydrogen for the *n*-BuLi reacted nanotubes.

This is presumably due sterical hindrance of *t*-Bu group that results in lower functionalisation degree. Thus the *n*-BuLi was found to be a better reagent for the lithiation of nanotubes.

The lithiated nanotubes are very reactive and can react with different metal and metalloid halides. These reactions result in the loss of lithium halide and the formation of metal to carbon of nanotube bonds. The products of the reactions for both MWNT and SWNT were characterised by TEM, HRTEM, IR, Raman and XPS spectroscopy. The lithiated SWNTs were treated with a range of group (IV) metals giving stable metal carbon bonds.

The reaction between the lithiated MWNTs and $SnCl_4$ resulted in the tin being bonded directly to the nanotubes surface forming an air stable Sn-C bond. This was also the case when the $SnBr_2$ was reacted with the lithiated MWNTs. The rest of the coating in the tin-nanotube composites is presumably mixture of tin oxide and partially hydrolysed tin oxychloride.

The reaction between the lithiated MWNTs and $PbBr_2$ resulted in the metal being bonded to the nanotubes surface, the resulting Pb-C bonds were particularly evident in the XPS spectra. There are also lead halide and lead oxide species in the sample due to hydrolysis and oxidation.

When $SiCl_4$ was treated with lithiated MWNTs the Si atom was covalently bound to the nanotubes however, after hydrolysis and upon exposure to air, the Si on the surface of the nanotubes became hydrolysed and oxidised. This formed Si-O bonds which are clearly visible in the IR.

Lithiated nanotubes were also found to be very strong reducing agents. The reaction between lithiated MWNTs and $AuBr_3$ resulted in the gold nano-particles being reduced on the surface of the nanotubes.

We have to admit that in each of the SWNT samples seen under HRTEM there are presence of nanoparticles of the selected metal, which indicates possible reduction reactions occur. However, also in the samples an outer coating of the SWNTs is observed and this is the metal that is bonded to the wall of the nanotube. In each case spectra of functionalised SWNTs have been compared with pristine SWNTs. Analysis has shown the presence of new metal carbon bonds which did not occur in either the original SWNTs or with a mixture of the SWNTs and the reactants. Therefore it can be concluded that the reaction between lithiated nanotubes resulted in covalent bonding of metal halides to nanotubes with the formation of metal-carbon bonds.

We believe that these studies will serve as a show case for novel application of organometallic chemistry in nanoscience that will also open up new approaches in nanotechnology.

2.5 References

[1] M Dresselhaus, Science of Fullerenes and Carbon Nanotubes, Academic Press, New York (1995)

[2] H.W. Zhu, X.S. Li, B. Jiang, C.L. Xu, Y.F. Zhu, D.H. Wu, X.H. Chen, *Chem. Phys. Lett.*, **366,** 664, (2002)

[3] G.S. Duesberg, W. Blau, H.J. Byrne, J. Muster, M. Burghard, S. Roth, *Synth. Met.*, **103,** 2484, (1999)

[4] V. Georgakilas, K. Kordatos, M. Prato, D. M. Guldi, M. Holzinger, A. Hirsch, *J. Am. Chem. Soc.*,**124,** 760, (2002)

[5] M. Holzinger, O. Vostrowsky, A. Hirsch, F. Hennrich, M. Kappes, R. Weiss, F. Jellen, *Angew. Chem. Int. Ed. Engl.*, **40,** 4002, (2001)

[6] M. Cadek, R. Murphy, B. McCarthy, A. Drury, B. Lahr, R.C. Barklie, M. in het Panhuis, J.N. Coleman, W. J. Blau, *Carbon,* **40,** 923, (2002)

[7] J. Liu, A.G. Rinzler, H. Dai, J.H. Hafner, R.K. Bradley, P.J. Boul, A. Lu, T. Iverson, K. Shelimov, C.B. Huffman, F. Rrodriguez-Macias, Y.S. Shon, T.R. Lee, D.T. Colbert, R.E. Smalley, *Science*, **280**, 1253, (1998)

[8] P.X. Hou, S. Bai, Q.H. Yang, C. Liu, H.M. Cheng, *Carbon*, **40,** 81 (2002)

[9] Y.S. Park, Y Chul Choi, K.S. Kim, D.C. Chung, D.J. Bae, K.H. An, S.C. Lim, X.Y. Zhu, Y.H. Lee, *Carbon,* **39,** 655, (2001)

[10] A.Hirsch, A. Soi, H.R. Karfunkel, *Angew. Chem. Int. Ed. Engl.*, **31,** 766, (1992)

[11] P.J. Fagan, P.J. Krusic, D.E. Evans, S.A. Lerke, E. Johnston, *J. Am. Chem. Soc.*, **114,** 9697, (1992)

[12] H.C. Choi, M. Shim, S. Bangsaruntip, H. Dai, *J. Am. Chem. Soc.*, **124**, 9058, (2002)

[13] Y. Inoue, T. Komoguchi, H. Nakata, O. Takai, *Thin Solid Films,* **322,** 41, (1998)

[14] W.F. Bergerson, J.A. Mulder, R.P. Hsung, X.Y. Zhu, *J. Am. Chem. Soc.,* **121,** 454, (1999)

[15] J.F. Moulder, W.F. Stickle, P.E. Sobol, K.D. Bomben, *Handbook of X-ray Photoelectron Spectroscopy,* J. Chasrain, R.C. King, Jr., Eds., Physical Electronics, Perkin Elmer Corp., (1995)

[16] C-H Park, Y-G Son, M-S Won, *Microchem. J.,* **80,** 201, (2005)

[17] L.J. Chen, S.M. Zhang, Z.S. Wu, Z.J. Zhang, H.X. Dang, *Mat. Lett.*, **59,** 3119, (2005)

Chapter 3

Reactions of Lithiated Carbon Nanotubes with Alkylhalides

3.1 Introduction

To date most of the work on the solubilisation of carbon nanotubes has been undertaken through non-covalent interactions. The focus of research has involved π-π stacking interactions. This form of functionalisation is attractive as the surfactants can later be removed leaving pure nanotubes. Nanotubes have been stabilised in aqueous media through the use of amphiphilic molecules[1,2]. However the research applied here focuses on covalent solubilisation and one of the earliest examples of sidewall functionalisation of SWNTs with alkyls was performed by P.J. Boul *et al*[3]. They prepared alkyl functionalised SWNTs by reaction of sidewall fluorinated nanotubes with alkyl-magnesium bromides (a typical Grignard reagent). On functionalisation, the authors noticed a significant increase in the solubility of nanotubes in a range of organic solvents. In 2005, R. Barthos,[4] functionalised CVD SWNTs with alkyl halides by ball milling the nanotubes in an atmosphere of the chosen alkyl halide. They analysed these nanotubes with TGA and TEM. Recently Pupysheva *et al.*[5] studied the theoretical interaction between organic amines with sizable alkyls. They found that these groups could be used as purify agents for SWNTs with ultra sonic treatment. M.A, Hamon *et al.*[6] and J. Chen *et al.*[7] functionalised the carboxyl moieties of acid purified nanotubes with thionyl chloride and subsequently reacted them with amines.

However, the alkyl functionalisation of carbon nanotubes and development of applications for these nanocomposites are still among one of the most significant challenges in carbon nanotube science. In this project we propose an approach to address these problems, using lithiated multiwalled nanotubes and selected alkyl hallides.

3.2 Aims of this work

The main aim of this part of our work is to investigate reactions between lithiated carbon nanotubes and different halogenated alkyls. It is expected that the halogen will be removed as the lithium salt and the alkyl chains will remain covalently bound to the nanotubes. One of the goals is to bind nanotubes to each other and in order to link them together using alkyl di-hallide chains containing halogen groups at the ends. These halogen groups would then be substituted for the nanotubes, leaving them bound directly to each other via the bridging

alkyl chain (Scheme 3.1). The prepared carbon nanotube composites will be investigated by FTIR spectroscopy and TGA. Sedimentation studies will be performed in order to evaluate the solubility of functionalised nanotubes in an organic solvent. The functionalised nanotubes are expected to be more stable in an organic solvent, e.g. THF, which could be used for preparation of nanotube solutions and their further modification.

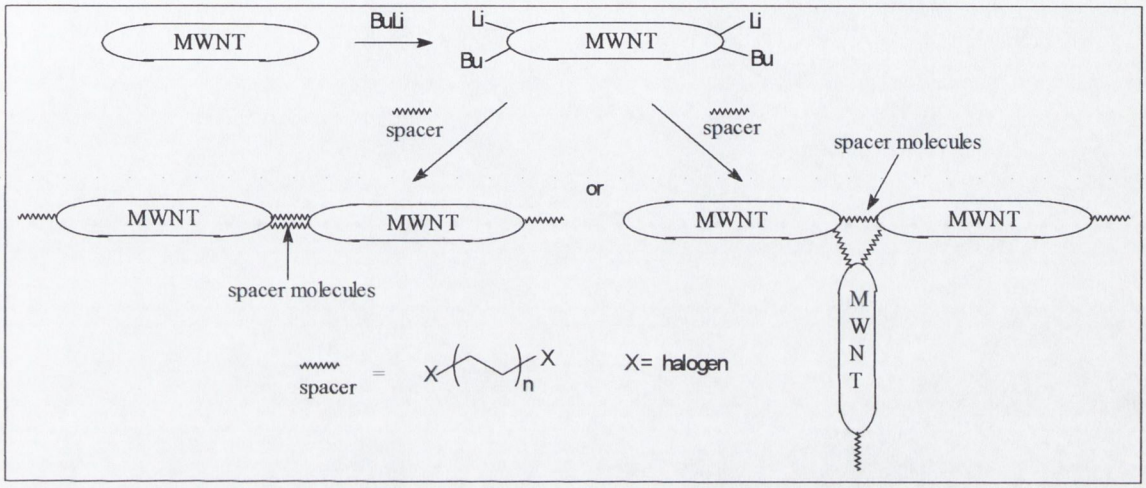

Scheme 3.1 Schematic presentation of the preparation of tip and near tip functionalised MWNT and their chemical interconnection using alkyl spacers.

3.3 Reactions of lithiated carbon nanotubes with mono-halogenated alkyl species

This work will be to prepare alkyl functionalised MWNTs and investigate their properties including their solubility in THF.

3.3.1 Reaction of lithiated nanotubes with 1-bromooctane

Lithiated MWNTs were reacted with 1-bromooctane in a 1:15, weight ratio or 1:1 molar ratio of carbon to 1-bromooctane according to scheme 3.2. The reaction was expected to result in the formation of pseudo 'flagella' as shown in scheme 3.2. This would enable the nanotubes to be more stable in organic solvents once the 'flagella' had been formed.
The lithiated nanotubes were freshly prepared and stored in THF solution under argon in a Schlenk vessel. The lithiated nanotubes were then treated with an excess of degassed

solution of 1-bromooctane in THF at 263 K. The mixture was allowed to warm to room temperature and then it was stirred for twelve hours at ambient temperature. The solvent was then removed under vacuum. In order to remove the excess of unreacted material the product was washed twice with dry hexane, then with THF and finally washed twice with water. The method of washing with selected solvents involved placing the solvent in the reaction vessel and then sonicating the vessel for 5 minutes in an ultrasonic bath followed by removing the excess of solvent *via* cannula filtration. The residue was then dried in vacuum. Due to the limited number of suitable characterisation techniques (FTIR, NMR, elemental analysis, TEM) investigation of these products is quite difficult. NMR was attempted on many occasions as the nanotubes would become stable in solvents after functionalisation. Due to the fact that the nanotubes are not soluble they cannot be studied by NMR spectroscopy. However, the products have been effectively characterised by TGA, IR and elemental analysis.

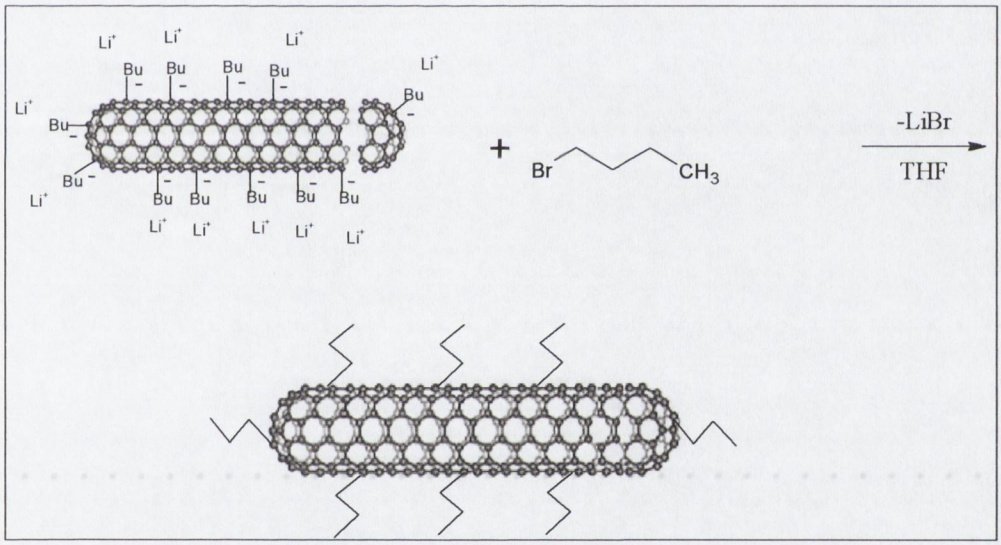

Scheme 3.2 Schematic representation of the reaction between lithiated nanotubes and mono substituted alkylhalide.

Figure 3.1 shows the TGA curves of pristine MWNTs and the octyl functionalised MWNTs TGA is shown in figure 3.2. It can be seen that the MWNT peak has shifted to a lower temperature (452 °C) due to the fact that the nanotubes have been covalently functionalised and therefore their graphitic structure has been weakened. There is also another peak at 509

°C which is believed to be the unfunctionalised inner core of the MWNTs as the peak is still at a significantly lower temperature than pristine MWNTs.

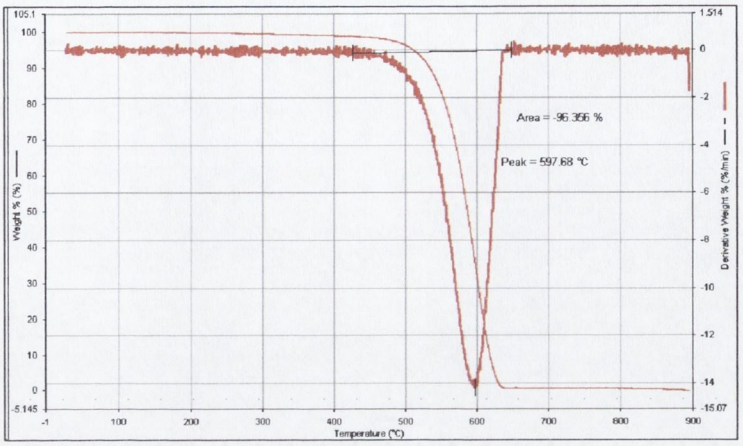

Figure 3.1 TGA of pristine CVD MWNTs

There is a peak at 232 °C which can be attributed to the octyl-groups. According to TGA results the content of octyl-groups was 3.5% by mass.

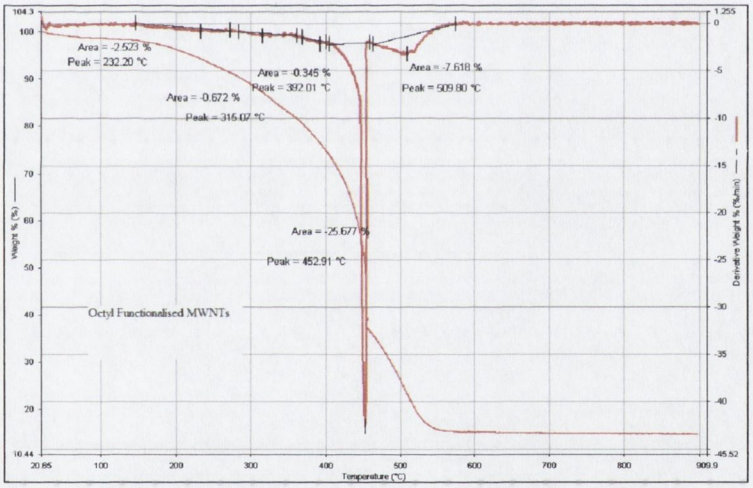

Figure 3.2 TGA of octyl-functionalised MWNTs

The band at 879 cm^{-1} would be typical of the MWNTs, as well as the signal at 1589 cm^{-1}. There are then some characteristic peaks of the alkyl chains which are observed at 1342, 1421 and 962 cm^{-1}. There should also be a band or shoulder attributed to CH stretches at 2900 – 3000 cm^{-1} which is obscured by the large broad peak, appendix 3.1.

Elemental analysis of the sample showed the presence of 2.8% of hydrogen. This shows a double in value when compared to 1.4% of hydrogen of the butyl groups in the initial sample of, hydrolysed, lithiated nanotubes.

3.3.2 Reaction of lithiated nanotubes and 1-bromodecane

To prepare decyl functionalised nanotubes the lithiated nanotubes were reacted with an excess 1:17 weight ratio of degassed 1-bromodecane following the same procedure as for 1-bromooctane discussed above. The product was prepared for analysis by TGA, IR and elemental analysis.

Figure 3.3 shows the TGA result with derivative. This TGA curve shows that again the nanotube peak has shifted to a lower temperature of 459 °C suggesting that the nanotubes are now functionalised. There is a peak at 233 °C with 2.64 % by weight which is attributed to the decyl groups.

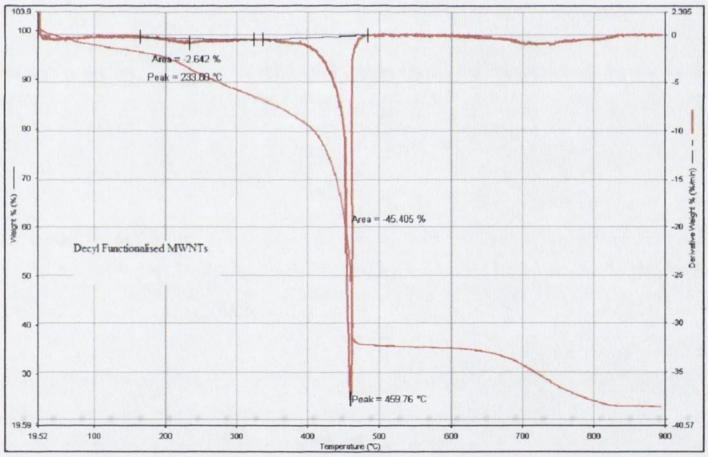

Figure 3.3 TGA of decyl functionalised MWNTs

The IR spectrum of decyl functionalised MWNTs was analogous to that of octyl functionalised MWNTs and contained a number of characteristics bands corresponding to the MWNTs at 883, 1027 and 1573 cm^{-1}, as well as the bands at 1415 and 1340 cm^{-1} and a broad shoulder at 2900 – 3000 cm^{-1} , which can be assigned to the alkyl chains attached to the surface of the MWNTs.

Elemental analysis of the decyl functionalised MWNTs gave 3.89% of hydrogen. This value again shows an increase in hydrogen percentage when compared with the octyl functionalised and initial hydrolysed, lithiated nanotubes samples.

3.3.3 Reaction of lithiated nanotubes and 1-bromohexadecane

The aim of this experiment was to prepare the hexadecyl functionalised nanotubes. The lithiated nanotubes were reacted with a degassed solution of 1-bromohexadecane in THF at 263 K in a similar manner as described above in a 1:30 weight ratio. The hexadecyl functionalised nanotubes were now highly soluble in THF which had to be removed by vacuum. The product was then washed twice with dry hexane, THF and water. In each case the solvent was removed by cannula filtration. The sample was then allowed to dry and prepared for analysis by TGA, IR and elemental analysis.

Once again in the TGA, figure 3.4, it is possible to discern the peak for the hexadecyl substituents at 227 °C which is 2.1% of the mass and for the functionalised nanotubes that has shifted from the higher temperature of 597 °C to 437 °C.

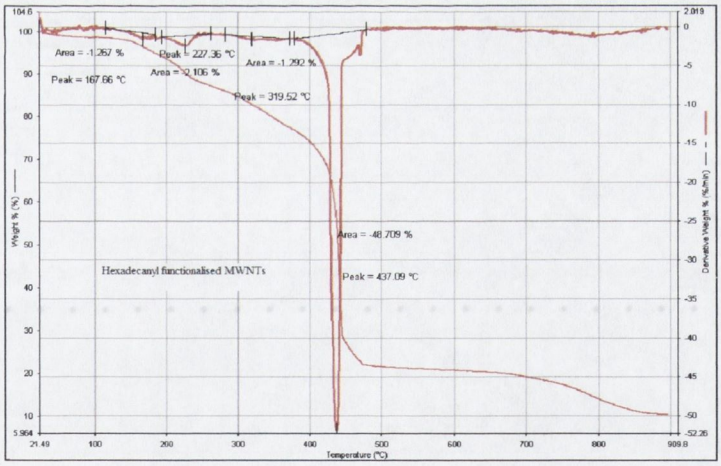

Figure 3.4 TGA of hexadecyl functionalised MWNTs

The IR spectrum of the hexadecyl functionalised MWNTs which was analogous to octyl functionalised MWNTs, has shown several bands at 896, 1016 and 1560 cm^{-1}, which are typical for the MWNTs. There are also bands of the alkyl chains at 811, 954 and 1326 and around 2950 cm^{-1}.

Elemental analysis of this sample gave 4.46% of hydrogen. Once again this shows an anticipated increase in the hydrogen content. When compared to the previous alkylated MWNTs it is close to a double hydrogen percentage to compare with the octyl sample. This is in agreement with an expected double increase due to the double chain length and hydrogen content in hexadecyl.

3.3.4 Reaction of nanotubes and 1-bromodocosane

To prepare docosanyl functionalised nanotubes, lithiated nanotubes were treated with 1-bromodocosane in a degassed solution of dry THF just as performed above procedure with 1-bromooctane in a 1:36 weight ratio. Then the product was prepared for TGA, IR and elemental analysis.

The TGA in figure 3.5 shows the presence of the functionalised nanotubes at a lower than usual temperature of 438 °C. The peak at 240 °C with 11% of the total mass of the sample corresponds to the alkyl chain of docosanyl.

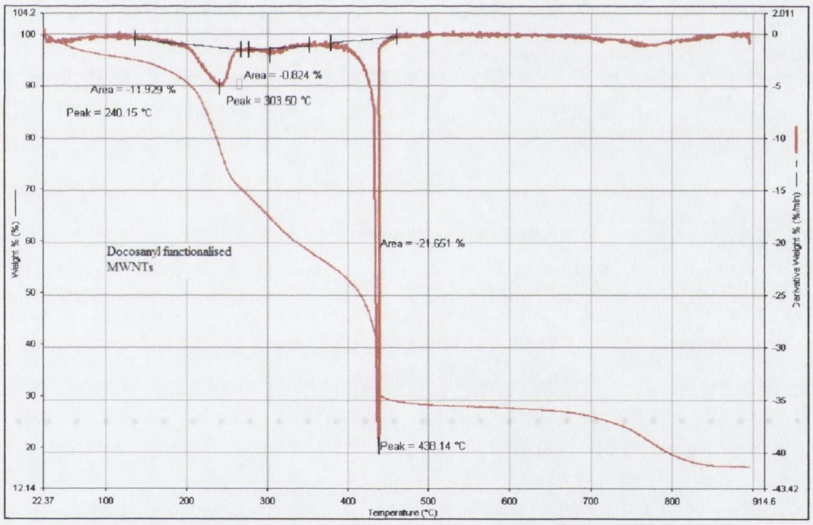

Figure 3.5 TGA of docosanyl functionalised MWNTs

The IR spectrum of the docosanyl functionalised nanotubes which was analogous to the octyl functionalised MWNTs exhibits some characteristic bands of alkyl groups at 835, 973 and 1357 and around 2950 cm^{-1} . There are also the typical MWNT peaks at 879, 1076 and 1589 cm^{-1}.

Elemental analysis was carried out on the docosanyl functionalised nanotubes and the total amount of hydrogen as a percentage of carbon was 9.59% which again was approximately double that of the decyl functionalised nanotube sample.

3.3.5 Comparison of TGA results

In order to properly analyse the TGA data it was necessary to compare them with those of pristine MWNTs and also the hydrolysed sample of lithiated nanotubes. On the left of figure 3.6 a TGA of pristine unreacted nanotubes is shown. There is only one very broad peak with the degradation temperature at 598 °C. The TGA curve on the right is that of hydrolysed lithiated nanotubes. There is a peak at 210 °C that corresponds to the degradation of the butyl substituents. The temperature of degradation of the lithiated nanotubes is substantially lower at 443 °C when compared to the pure nanotubes.

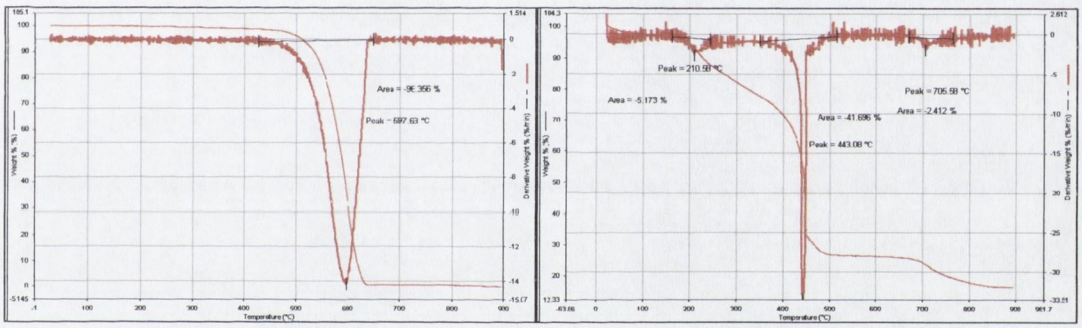

Figure 3.6 TGA analysis of pristine CVD MWNTs and hydrolised lithiated CVD MWNTs

TGA was performed on pure unreacted alkylbromide derivatives the results of which are shown in figure 3.7.

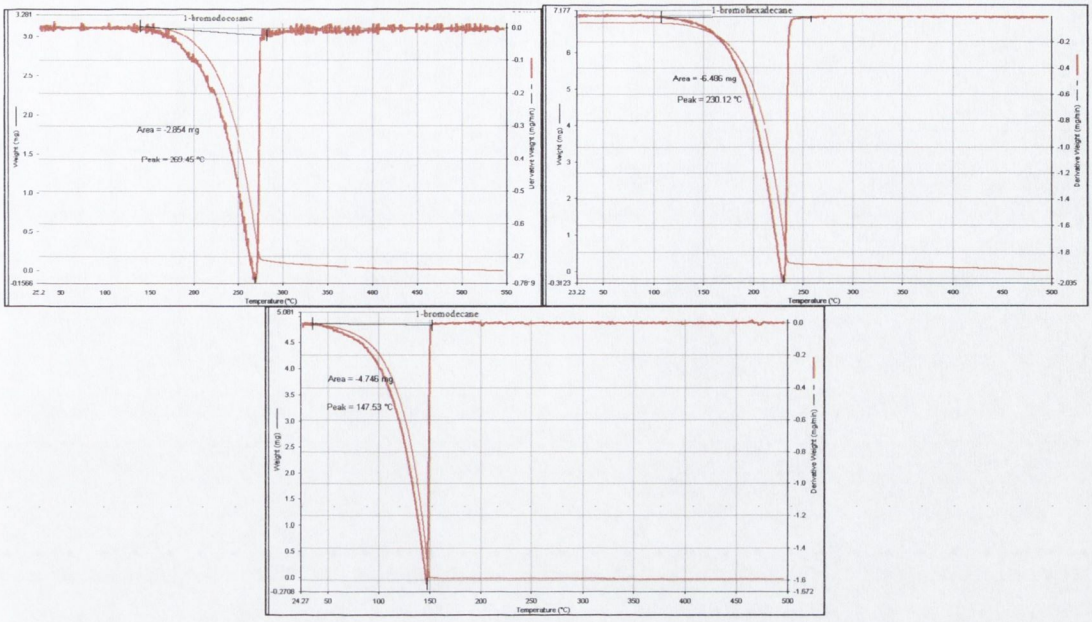

Figure 3.7 TGA analysis of 1-bromodocosane, 1-bromohexadecane and 1-bromodecane

The TGA of 1-bromodocosane shows a broad peak at 269 °C and also a peak for 1-bromohexadecane at 230 °C. However, in the case of 1-bromodecane the temperature drops significantly to 147 °C which would not be typical for this chain length. In the case of 1-bromodecane it can be observed that there is evaporation that is exemplified by the fact that the degradation appears to begin at 30 °C which is inconsistent with its appropriate degradation temperature. For this reason it was impossible to obtain a TGA for 1-bromodecane and any of the shorter chain lengths derivatives.

Finally it was important to analyse a mechanical, non-reacted, mixtures of the alkylbromides and pristine MWNTs. The mechanical mixture of nanotubes and alkylbromides were prepared in an analogous way to the reaction of the lithiated nanotubes above. The mixture was cooled to 263 K and then the alkyl chain was added in a molar ratio of 5:4 alkyl bromide to nanotubes in a dry THF solution. This was allowed to stir for twelve hours and then the mixing was stopped. The mixture was also washed in an identical manner as the products of reactions with lithiated nanotubes. Then the samples were prepared for TGA. The results of the TGA are shown in figure 3.8 below.

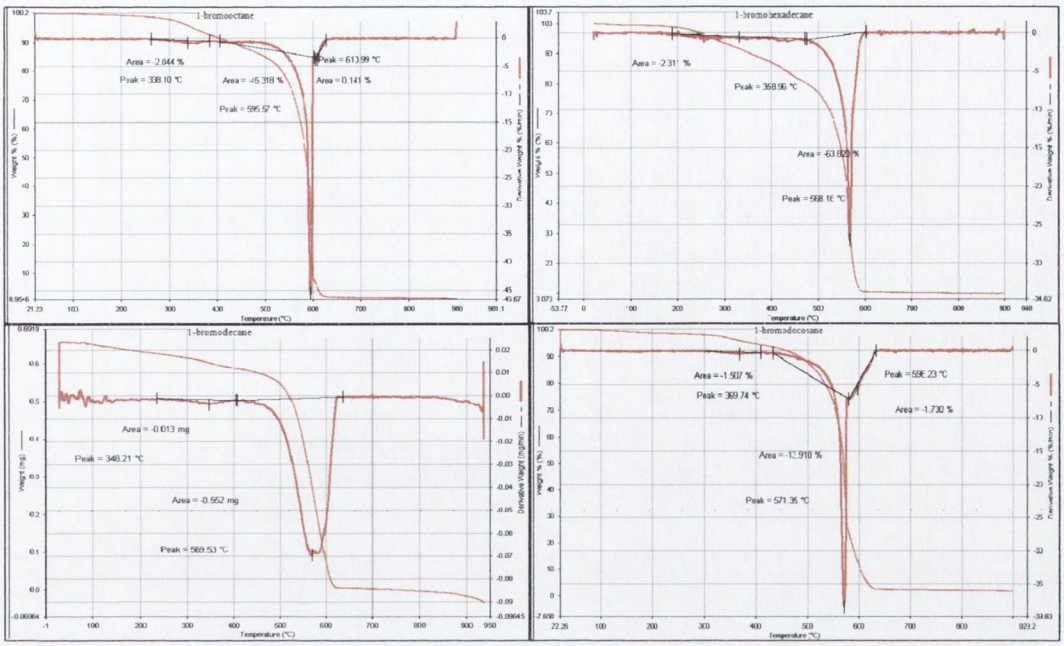

Figure 3.8 TGA results of mechanical mixture of brominated alkyl chains and MWNTs 1-bromooctane, 1-bromodecane, 1-bromohexadecane and 1-bromodocosane

In each of the cases it is possible to identify where the alkyl chain is removed and the effect of the presence of the alkyl chain of the degradation temperature of the nanotubes by comparing these TGA with those in figure 3.9. In all of the cases the degradation temperature of the nanotubes remains the same and close to 600 °C with some exception of 1-bromohexadecane where there is a slight shift in the temperature to 570 °C.

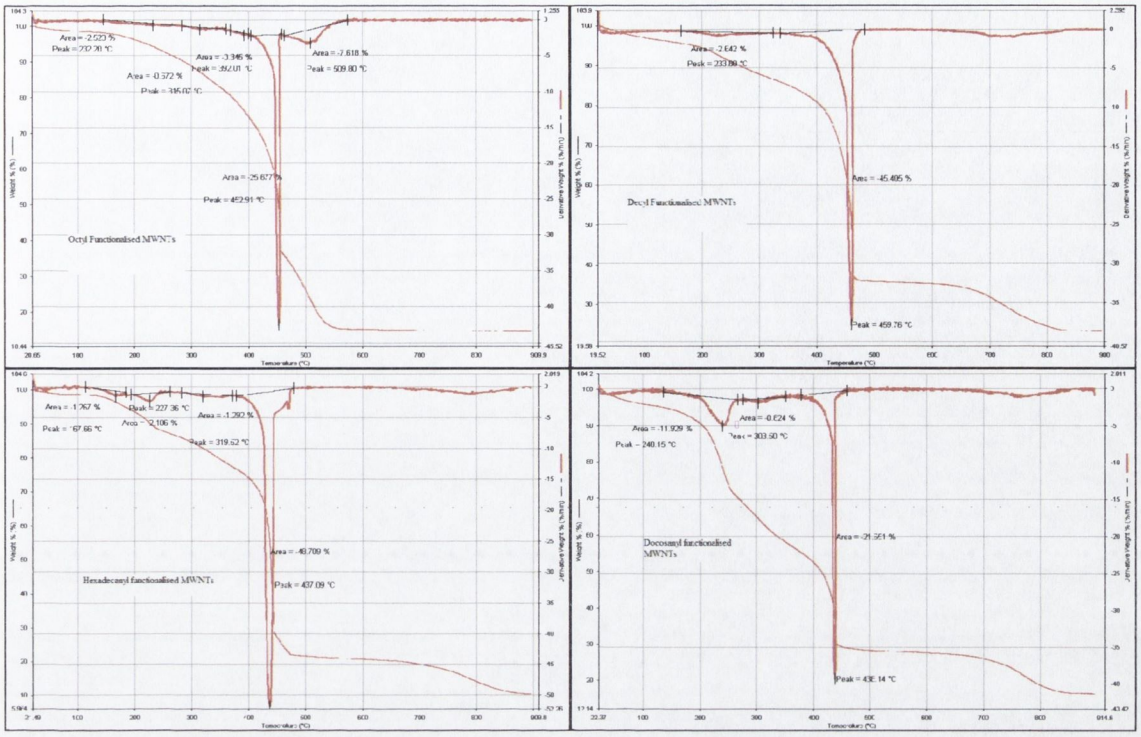

Figure 3.9 Combined TGA spectra of the alkyl functionalised MWNTs -octyl, -decyl, -hexadecyl and -docosanyl

Approximately 2% by mass of the sample is alkylbromides which is believed to become adsorbed onto the surface of the nanotubes. The degradation temperatures of the alkylbromides physically absorbed on the nanotubes are 338 °C for 1-bromooctane, 348 °C for 1-bromodecane, 358 °C for 1-bromohexadecane and for 369 °C 1-bromodocosane.

3.3.6 Sedimentation studies

Sedimentation studies were necessary to examine the solubility and stability of the alkyl functionalised nanotubes in THF. Nanotubes would not normally be soluble in this solvent without functionalisation. A sample of nanotubes was taken and sonicated under the sonic tip for five minutes. This was then transferred as quickly as possible to a 1 cm quartz cuvette. The sample was then placed in a sedimentation machine and the transmitted light was recorded. This machine flashes an intermittent light beam through the samples. There is a recorder which measures the total light transmitted and allows sedimentation graph to be obtained.

In figure 3.10 the rate at which nanotubes fall out of a THF solution is shown.

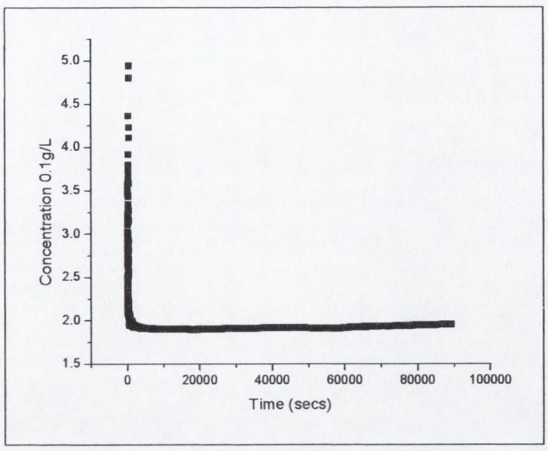

Figure 3.10 Sedimentation curve of pristine MWNTs in THF over time

It can be seen in the graph that the nanotubes fall out very quickly after as little as 5 minutes.

Figure 3.11 shows the sedimentation graph of hydrolysed lithiated nanotubes in THF solution. Lithiated nanotubes before hydrolysis are very well stable in THF. However, on hydrolysis the nanotubes become insoluble in THF. This is demonstrated by the graph in figure 3.11 where the nanotubes do not stay in solution.

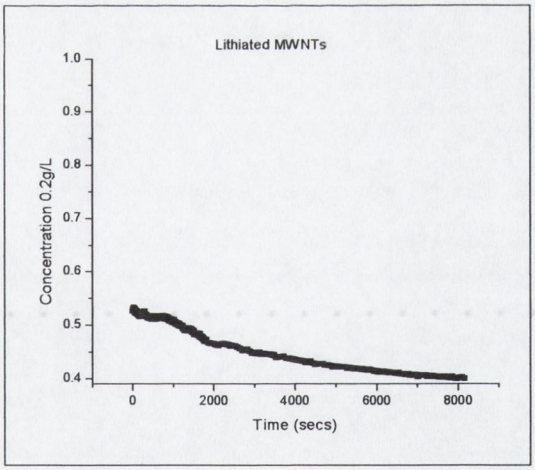

Figure 3.11 Sedimentation curve of lithiated MWNTs in THF over time

Figure 3.12 shows the sedimentation graph of octyl functionalised MWNTs. The octyl chain functionalisation of nanotubes results in increased solubility in THF. It takes in the region of twenty three hours to precipitate and reach the same concentration as the

unreacted MWNTs. This suggests that the pseudo 'flagella' of the alkyl chains are significantly increasing the stability of the nanotubes in solution.

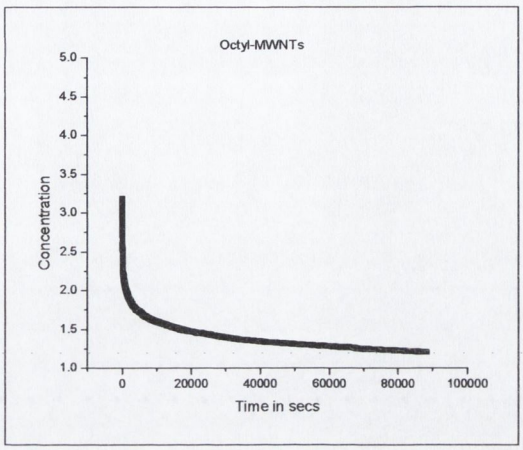

Figure 3.12 Sedimentation curve of octyl functionalised MWNTs in THF over time

Figure 3.13 shows the sedimentation curve of decyl functionalised MWNTs in a solution of THF. It is clearly visible that the longer chain length is really improving the stability of the nanotubes in solution.

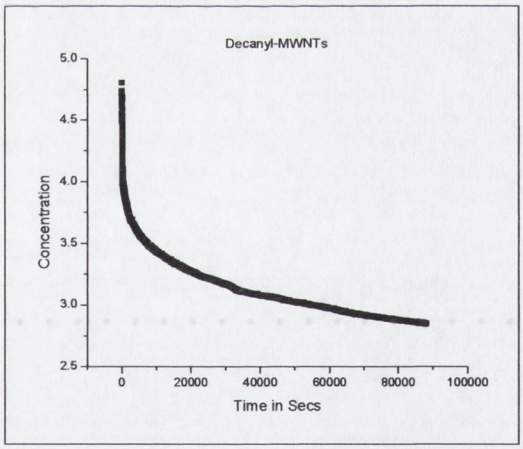

Figure 3.13 Sedimentation curve of decanyl functionalised MWNTs in THF over time

After 24 hours of sedimentation the concentration of the nanotubes in solution increased by twice that of the octyl functionalised MWNTs which is also twice the concentration of pure MWNTs in THF.

Figure 3.14 shows the sedimentation graph of hexadecyl functionalised MWNTs in THF over a 24 hour period. The concentration of nanotubes left in solution after the twenty four hour period is now three and a half times that of the pure MWNTs. As well as this, the initial concentration of nanotubes is also double that of the pure MWNTs.

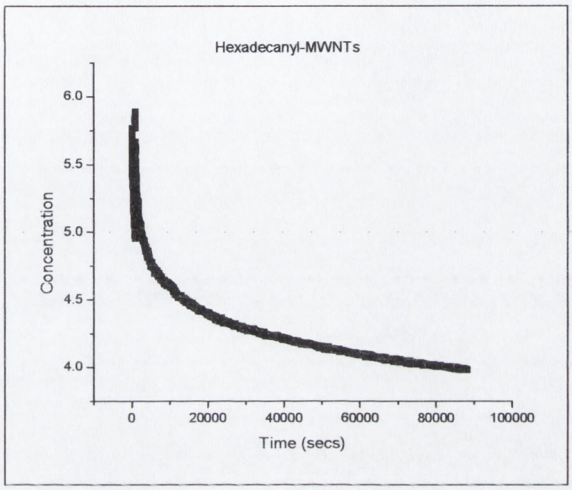

Figure 3.14 Sedimentation curve of hexadecanyl functionalised MWNTs in THF over time

Figure 3.15 shows the sedimentation curve for docosanyl functionalised MWNTs in THF. Again it is clear here that the nanotubes with longer alkyl chains are much more stable in solution than the unreacted non functionalised nanotubes. However, the docosanyl chain is not as good at stabilising the nanotubes in solution as the hexadecanyl. Presumably the solubility is reduced for the longer chain length due to thermodynamical reasons. Obviously, there is an optimum alkyl chain length, which provides the best solubility of nanotubes in THF.

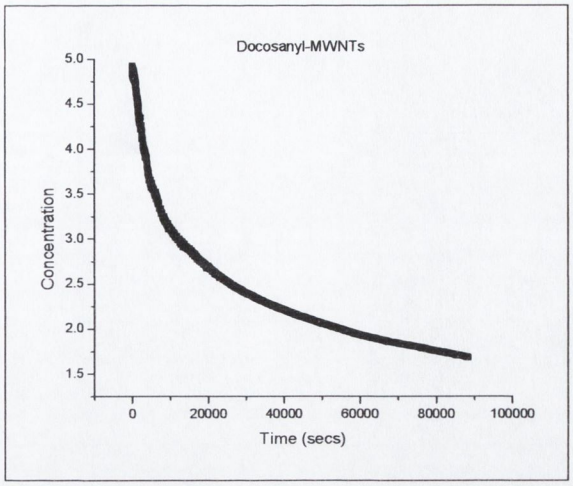

Figure 3.15 Sedimentation curve of docosanyl functionalised MWNTs in THF over time

Figure 3.16, shows the extent to which functionalisation increases the stability of the nanotubes in THF. With the hexadecanyl functional groups providing an overall 2.2 fold increase in the amount of nanotubes that stay in solution due to the alkyl functional groups.

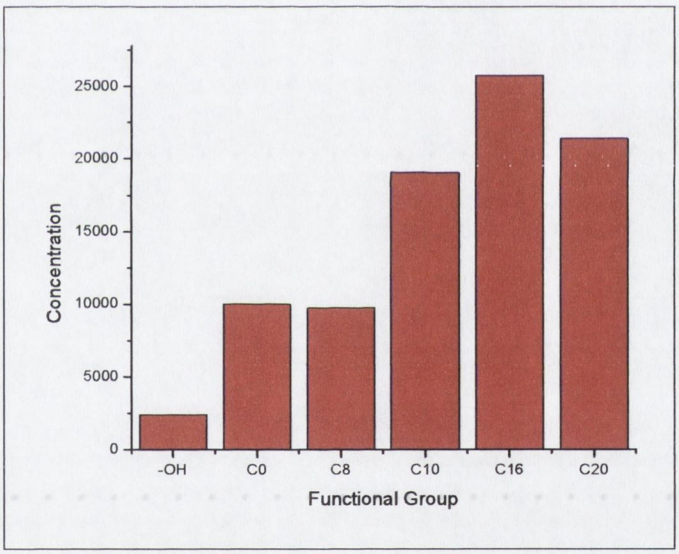

Figure 3.16 Integral of the area under each of the chain length sedimentation curves

3.4 Reactions of lithiated carbon nanotubes with dihalogenated alkyl species

The conventional methods for the preparation of nanotube arrays and connections are arc discharge, laser ablation and chemical vapour deposition (CVD) which normally produce carbon nanotubes in randomly tangled states. It remains a great challenge to find an

effective way to organise or connect nanotubes into well-ordered arrays or structures through chemical functionalisation. We believe that the organometalic modification and linking of MWNT with an appropriate length molecular spacer will enable us to find workable solutions to these problems.

The aim of this work was to connect nanotubes directly to each other so as to fabricate nano-wires interconnects made from nanotubes using lithiated MWNTs described in Chapter 2 as a starting material. Lithiated nanotubes are expected to react with halogenated alkyls resulting in the loss of lithium salt with the alkyl becoming bonded directly between two nanotubes as presented in schemes 3.1 and 3.3. It is likely that the tips of MWNTs are the most reactive areas in the nanotubes. Therefore tip-to-tip junctions of the MWNTs were expected as products. 1,6-dibromohexane and 1,12-dibromododecane were used to link the lithiated MWNTs. There is also a possibility of binding of both ends of the alkyl chain to the same nanotube and wall to wall cross linking of nanotubes as it shown in the scheme 3.3. The nano-composites have been investigated by FTIR spectroscopy, TGA, TEM and HRTEM.

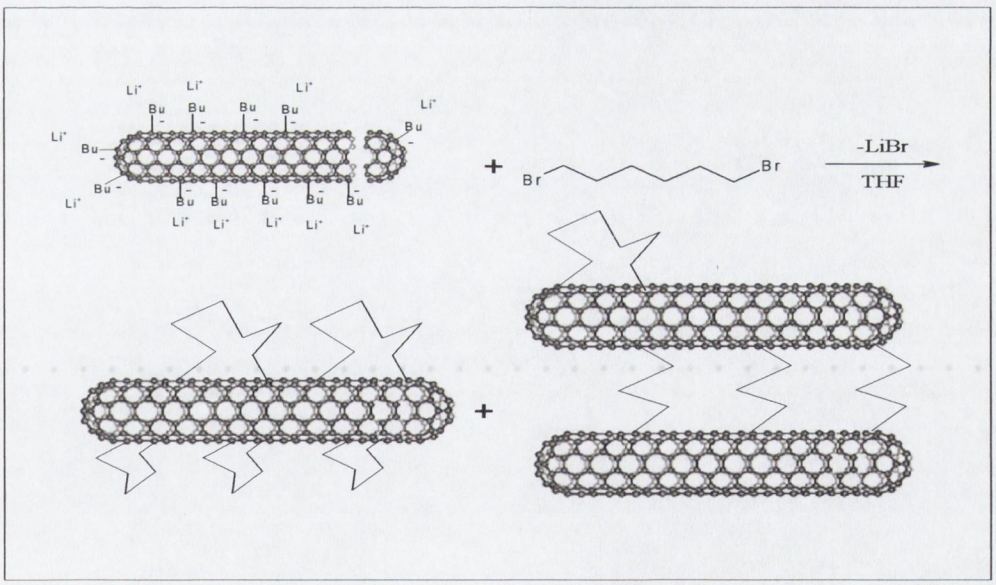

Scheme 3.3 Schematic representation of possible products after the interaction between lithiated nanotubes and di-substituted alkyls.

3.4.1 Reaction of MWNTs with 1,6 di-bromohexane

Freshly prepared and washed lithiated nanotubes were placed in dry THF and an excess with a weight ratio of 1:6 of dry degassed 1,6-dibromohexane was added to the mixture under stirring. The resulting product was washed twice with hexane and THF and dried under vacuum. FTIR spectrum of the product showed the presence of C-H stretches at 835, 973, 1357, and 2920 cm^{-1} characteristic for both the hexyl chain now bound to the nanotubes as well as any residual butyl groups after the lithiation.

A selection of TEM images of the lithiated carbon nanotubes treated with 1,6 di-bromohexane is shown in figure 3.17. In each of the images a red circle highlights the connecting points in nanotube assemblies. In the first and last images nanotubes connect *via* their tips highlighted by the red circle. In the middle image the nanotubes are connecting tip to sidewall (T or Y junctions) and are highlighted by a green colour. The presence of tip to sidewall junctions is an indication that the lithiation is not purely selective for the tips of the nanotubes but also affects the nanotubes sidewalls.

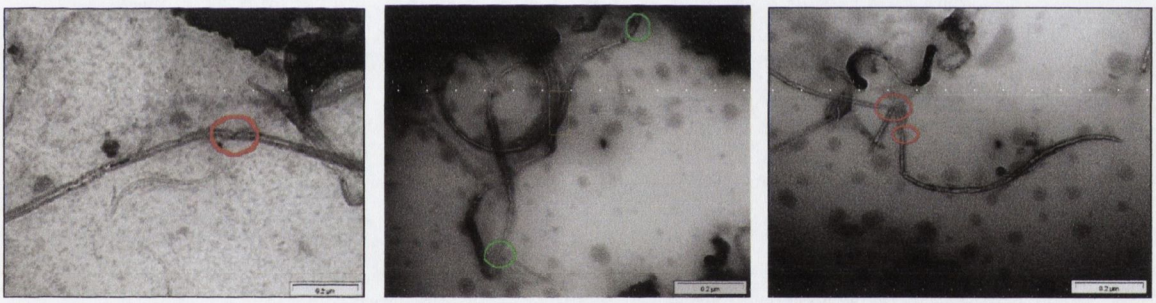

Figure 3.17 TEM image of the tip to the tip junction of MWNTs the joining is highlighted by the red circle

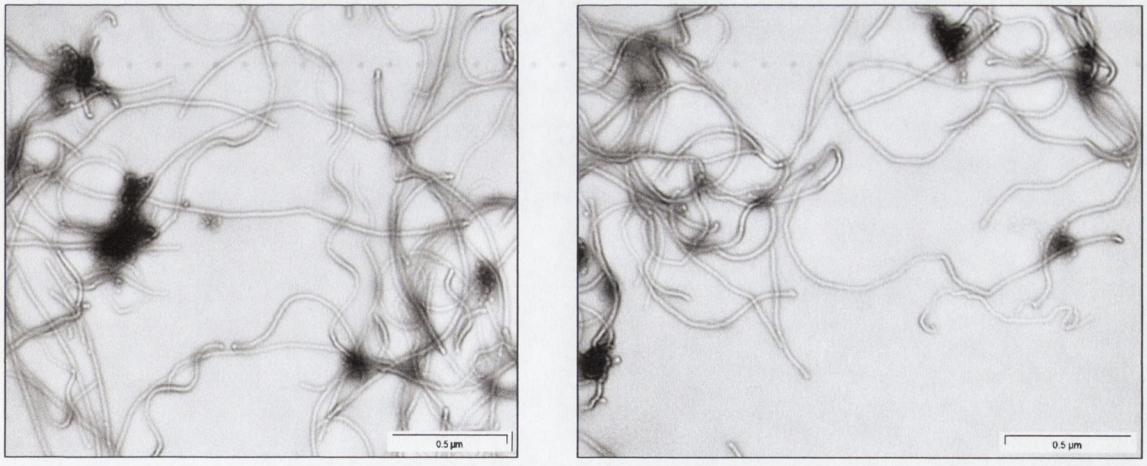

Figure 3.18 Initial MWNTs used for the reaction which show no clear signs of connection

The FTIR spectrum of hexanyl-functionalised MWNTs was analogous to the octyl functionalised MWNTs which show a number of characteristics bands corresponding to the MWNTs at 883, 1027 and 1573 cm^{-1}. There are then the peaks which are indicative of the alkyl chains attached to the surface of the MWNTs at 1415 and 1340 cm^{-1}.

The TGA (figure 3.19) exhibits the distinct peaks which are typical for alkyl functionalised nanotubes. Firstly there is the peak at 291 °C which is indicative of the alkyl chain being degraded. Secondly the peak at 458 °C represents the degradation temperature of functionalised nanotubes.

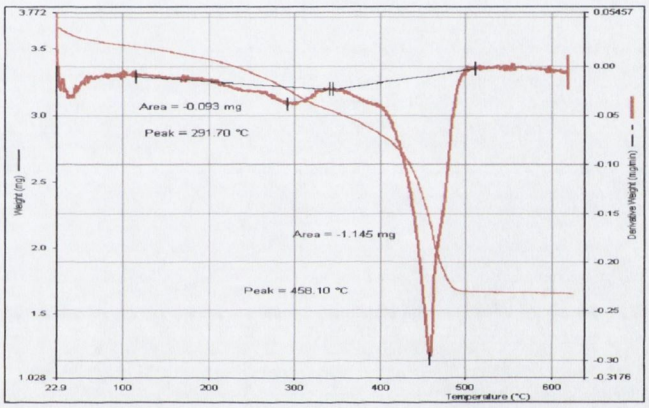

Figure 3.19 TGA of nanotubes reacted with 1,6 dibromohexane

3.4.2 Reaction of MWNTs with 1, 12-di-bromododecane

After the experiment with the hexane linker above, it was thought that a larger linker such as dodecane can be used to increase the spacing between cross-linked nanotubes. For example, it is important to have a sufficient distance between the connected nanotubes to avoid the tunnelling of electrons. The reaction was performed again in an analogous fashion using 1,12 di-bromododecane, with a 1:8 weight ratio, in place of the 1,6 di-bromohexane. FTIR was carried out, but unfortunately NMR analysis was impossible due to the reasons mentioned above. The TEM images of MWNTs linked using 1,12-dibromododecane are shown in figure 3.20.

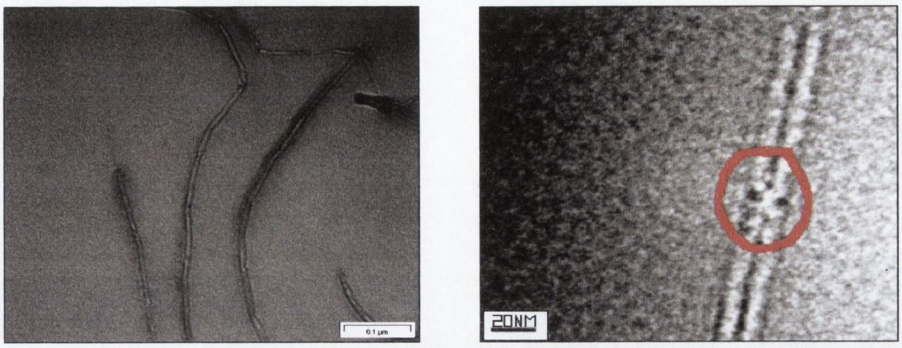

Figure 3.20 TEM (left) and HR TEM (right) images of the dodecyl linked MWNT composites junctions are highlighted by the red circles.

Similar to the hexane linker, tip-tip junctions are observed in the TEM images of the dodecane MWNT sample highlighted using red circles. Shown in the image on the right of figure 3.20 is a high resolution TEM image of the MWNT linked *via* the dodecane spacer this gap is comparable to the distance of the actual length of a dodecane chain length at 1.8 nm in size.

In the FTIR spectrum of the dodecyl linked MWNT was analogous to the octyl functionalised MWNTs and contained a number of characteristics bands corresponding to the MWNTs at 883, 1027 and 1573 cm^{-1}. Also there are peaks which are characteristic for the alkyl chains attached to the surface of the MWNTs at 1340, 1415 and 2900 cm^{-1}.
The TGA (figure 3.21) again shows the peaks which are indicative of alkyl functionalised nanotubes. There is the peak at 242 °C which corresponds to the alkyl chain, then the peak at 472 °C is attributed to the degradation of functionalised nanotubes.

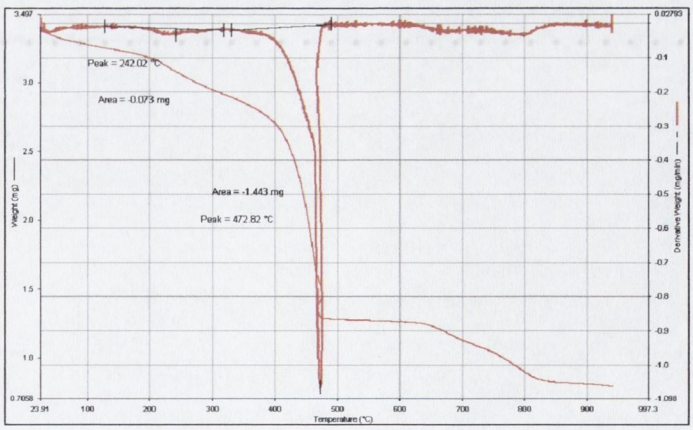

Figure 3.21 TGA of 1,12 dibromododecane functionalised nanotubes

3.5 Conclusions

Lithiated carbon nanotubes have been shown to be very good precursors for covalent functionalisation of the carbon nanotube surfaces. Functionalisation of nanotubes with different alkyl chains yielded new interesting nano-composites. TGA results have shown that the decomposition temperature of alkyl functionalised nanotubes is substantially lower than one for initial non-functionalised nanotubes. This demonstrates that functionalisation of nanotubes results in the partial damaging and weakening of the nanotubes structure and reduces its thermal stability. As expected the hydrogen content in the alkylated nanotubes rose proportionally with increasing alkyl chain length.

Sedimentation studies have shown that the solubility of nanotubes in THF increase with alkyl chain length reaching an optimum for C_{16} (hexadecanyl). Hexadecanyl functionalised nanotubes exhibit the greatest degree of stability in THF at over twice the concentration of nanotubes in solution as compared to pristine nanotubes. However, there is a reduction in solubility for docosanyl functionalised nanotubes presumably due to thermodynamic reasons.

We have demonstrated that reactions of di-halogenated alkyls with lithiated carbon nanotubes can result in the formation of tip to tip and tip to wall junctions cross-linking different nanotubes. We believe that this approach might be used for the preparation of nanotube interconnects for nanoelectronics.

3.6 References

[1] S. Bandow, A.M. Rao, K.A. Williams, A. Thess, R.E. Smalley, P.C. Eklund, *J. Phys. Chem. B,* **101,** 8839, (1997)

[2] G.S. Duesberg, M. Burghard, J. Muster, G. Philipp, S. Roth, *Chem. Commun,* 435, (1998)

[3] P.J. Boul, J. Liu, E.T. Mickelson, C.B. Huffman, L.M. Ericson, I.W. Chiang, K.A. Smith, D.T. Colbert, R.H. Hauge, J.L. Margrave, R.E. Smalley, *Chem. Phys. Lett.,* **310,** 367, (1999)

[4] R. Barthos, D. Mehn, A. Demortier, N. Poerard, Y. Morciaux, G. Demortier, A. Fonseca, J.B. Nagy, *Carbon,* **43,** 321, (2005)

[5] O.V. Pupysheva, A.A. Farajian, H. Nejo, H. Mizuseki, Y. Kawazoe, *Thin Solid Films,* article in press

[6] M.A. Hamon, J. Chen, H. Hu,, Y. Chen, A.M. Rao, P.C. Eklund, R.C. Haddon, *Adv. Mater.,* **11**, 834 (1999)

[7] J. Chen, A.M. Rao, S. Lyuksyutov, M.E. Itkis, M.A. Hamon, H. Hu, R.W. Cohn, P.C. Eklund, D.T. Colbert, R.E. Smalley, R.C. Haddon, *J. Phys. Chem, B,* **105,** 2525, (2001)

Chapter 4

Alkyl functionalised Carbon Nanotubes for Polymer Reinforcement

4.1 Introduction

There is great potential for polymer reinforcement using carbon nanotubes. The manufacture of new light weight super-strong materials will offer cheaper and stronger options, for example providing the potential to make lighter aircraft, lighter and better bullet proof clothing. Nanotubes have reported break strengths of in the region of 200 GPa and a Young's modulus of 1 TPa.[1,2,3,4,5] To put that into perspective, if it was possible to construct a cable the diameter of a shoe lace out of steel/titanium alloy, carbon fibre and single walled nanotubes the alloy could lift a standard sized car, the Carbon fibre a 4x4 off road vehicle and the nanotubes two Boeing 737 aeroplanes.[6] So however ridiculous the talk about constructing an elevator to the moon may sound the theory certainly supports the idea.[7]

To date the main research developments in this area were based mostly on mechanical mixing of polymers and carbon nanotubes. There has been very little work done on the chemical modification of nanotubes with a view for mechanical reinforcement. An early approach applied by researchers in Trinity College Dublin was to combine nanotubes with PPV in an attempt to observe the electrical conductance of the composite material which was achieved by ten orders of magnitude.[8] The same team from TCD were able to increase the Young's modulus of composite materials by a factor of two by mechanically mixing nanotubes with a polymer.[9] A recurrent problem that occurs in much of the research that is carried out on composites with nanotubesnis that researchers are not getting the levels of reinforcement expected from the nanotubes.[10,11,12] The main difficulties are related to non homogeneous distribution of carbon nanotubes in polymer matrices and very weak interaction between polymer chains and carbon nanotubes. As a result there is little interfacial stress transfer between the nanotubes and the polymer material. Thus, in order to increase the stress transfer between the nanotubes and the polymer matrix the surface of the nanotubes needs to be modified accordingly, providing the strong interaction of nanotubes and polymer.

The basic concept which we intended to use dates from 1860 when concrete was reinforced with steel by Joseph Monier. He discovered that concrete reinforced with steel rods was

considerably stronger. He found that the concrete took the compression while the steel rods endured the tension. The vital requisite of the steel rod is that they are grooved as they allow the concrete to grip to the steel thus straight steel rods are unsuitable for this task. Our method was an adaptation of Monier's work where the nanotubes represent steel while the polymer acts as the concrete. In order to form grooves on the nanotubes they were chemically modified by a group that was inert and could interact with the matrix in which it was. To achieve this we intended to use alkyl chains of varying lengths.

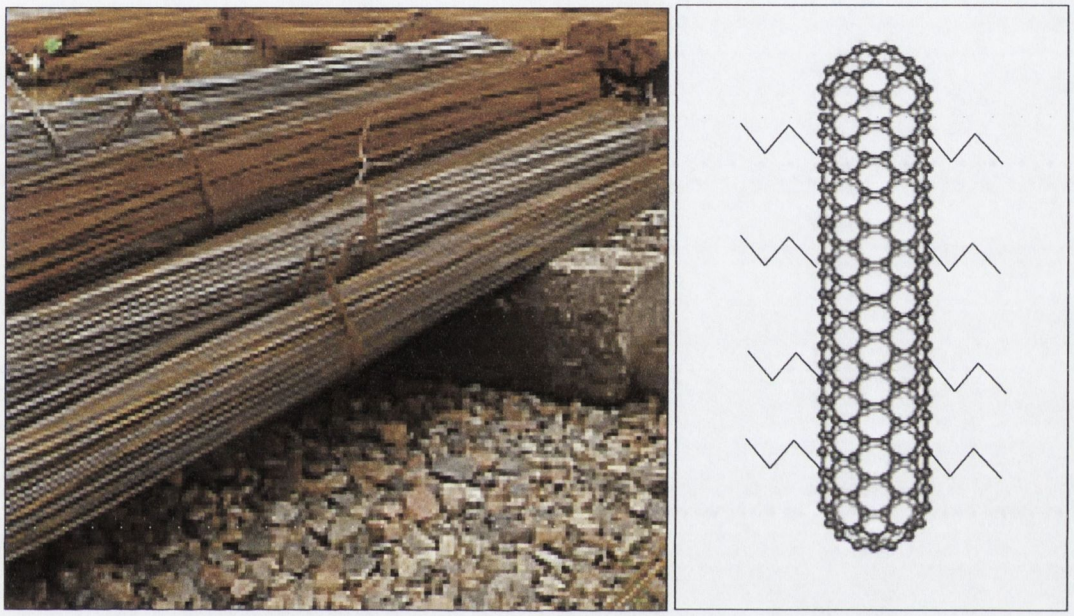

Figure 4.1 Left is steel used for reinforcing concrete and on the right is our adaptation with nanotubes

4.2 Aims of this work

The main aim of this part of the work is to investigate a range of alkyl functionalised carbon nanotubes with varying alkyl chain lengths as new additives for polymer reinforcement. We believe that that the alkyl functionalised nanotubes should have an increased solubility in polymer solution and will intertwine and entangle with the polymer molecules in the polymer matrix. It was expected that the shorter alkyl chains attached to the nanotubes should have less effect on polymer reinforcement than the longer chains. It was also anticipated that very long alkyl chains might align along the side of the nanotube walls and would therefore not impart good interfacial stress transfer between the nanotubes and the polymer.

The ultimate objective is to identify the optimal alkyl chain length for nanotube functionalisation and the most efficient interfacial stress transfer in a range of selected polymers. The polymers chosen were chlorinated polypropylene (CPP), chlorinated polyethylene (CPE), polyvinylchloride (PVC) and polystyrene (PS). These polymers were selected because they are widely used in modern technology.

Experimentally the amount of nanotubes chosen are selected by weight percent however in order to calculate the effective modulus of functionalised nanotubes and the interfacial stress transfer between the nanotubes and composite volume percentage must be calculated. To convert mass fraction to volume fraction for the amount of nanotubes present in the composite material Equation 4.1 must be examined.

$$\text{Equation 4.1} \quad V_F = \frac{1}{1 + \frac{\rho_{NT}}{\rho_P}\left(\frac{1 - m_f}{m_f}\right)}$$

Where V_f is the volume fraction, m_f is the mass fraction, ρ_f is the density of the polymer and ρ_{NT} is the density of nanotubes.

If Krenchel's rule of mixtures, Equation 4.2, is examined it will be possible to deduce the effective modulus for the functionalised nanotubes;

$$\text{Equation 4.2} \quad Y_{c_{\parallel}} = v_f Y_f + v_m Y_m, \quad Y_{c_{\perp}} = \frac{Y_f Y_m}{Y_m v_f + Y_f v_m}$$

where Y_c, Y_f, and Y_m are the composite, filler and matrix moduli, V_f and V_m are the respective volume fractions. This equation assumes that any stress applied to the system will equally affect both parts however as this is unlikely to be true in the case of two very different elements there will be considerable error in this equation.

Cox's shear lag theory must then be examined for short fibers, as it is more applicable to nanotubes in polymers. Cox assumed that the fibre and matrix remain elastic in their mechanical response;[13]

Equation 4.3 $$Y_c = Y_m(1-v_f) + Y_f v_f \left(1 - \frac{\tanh\left(\frac{\beta l}{2}\right)}{\left(\frac{\beta l}{2}\right)}\right)$$

where l is the fibre length, Y_m is the modulus of the matrix and β is given by;

Equation 4.4 $$\beta = \sqrt{\frac{-4G}{r^2 Y_f \ln(v_f)}}$$

where V_f is the volume fraction and G is the polymer sheer modulus which is found using the expression G=Y/2(1+v) where v is the Poisson's ratio. Applying these values to equation 4.3 and substituting the value η_l represents the fibre length correlation factor and η_0 is the Krenchel orientation efficiency factor;

Equation 4.5 $$Y_c = Y_p(1-v_f) + \eta_l \eta_0 Y_{nt} v_f$$

It has been found that l and Y_f are highly correlated to one another[14] and values have not been calculated there for Y_{eff} was defined as $Y_{eff} = \eta_l Y_{NT}$ therefore the actual value of YNT will be a low estimate as η_l will be less than one. By substitution Y_{eff} can be defined as;

Equation 4.6 $$Y_{eff} = \frac{\frac{dY_c}{dv_f} + Y_p}{\eta_o}$$

Y_p has been measured as the polymer's modulus and $\eta_0 = 0.38$[15] for random planar orientation[16] and dY_c/dv_f can be calculated by a linear fit of a graph of modulus versus V_f for given alkyl chain length.

For a homogeneous matrix, that is one without crystalline domains, the theoretical ultimate tensile strength of a composite, σ_T, can be derived under the assumption that the composite has two fracture components. One such component is the bulk polymer and the other is at the polymer/filler interface. The tensile strength for such a composite, σ_c, can be expressed as:

Equation 4.7 $$\sigma_c = \left(\frac{l_{nt}\,\tau}{2r_{nt}} - \sigma_p \right) v_f + \sigma_p$$

where l_{nt} is the nanotube length, r_{nt} is the nanotube radius, v_f is the nanotube volume fraction and σ_p is the ultimate tensile strength of the neat polymer film. The interfacial stress transfer, τ, can therefore be calculated from a plot of σ_T against v_f.

4.3 Results and discussion

4.3.1 Alkylated MWNTs in CPP

The preparation of carbon nanotubes functionalised with different alkyl chains was described in Chapter 3. In this part of the work, the alkyl functionalised carbon nanotubes were mixed with CPP in THF solution in an attempt to make new reinforced polymer composites. Polymer films were prepared using the layer by layer technique, which was described by Cadek *et al.*[9]. This involved making a solution of pure polymer and blending that by adding different amounts of functionalised nanotubes. This solution was deposited on to Teflon disks which are 3 cm in diameter. The polymer solution was dropped on to the disk 1 ml at a time and the solvent was allowed to evaporate this is then repeated four times in total. This resulted in a thin film on the disk that could be easily peeled off. This thin film was then cut into strips which are analysed using the Zwick 100 tensile tester. Tensile measurements were carried out to evaluate the relationship between composite morphology and mechanical performance. The data was used to calculate; Young's modulus (Y) which is the ratio of linear stress to linear strain, tensile strength (σ_T) or energy to break and toughness (T), the amount of energy that can be absorbed before a material breaks, values.

The concentration of polymer in solvent was 30 g/l. Following this a selection of weight percentages were chosen for nanotube concentration, for example: 0.25%, 0.5% and 1%. Previous research has shown that the use of higher concentrations of nanotubes results in the formation of aggregates of nanotubes which do not impart any mechanical strength

increases as they are not interacting efficiently with the polymer matrix. The lack of linear increase in strength with increase in vol.% is contrary to what the rule of mixtures would predict and typically anything over a 10 vol.% deviates from this rule, [10,11,12] this is more than likely due to the aggregation.

It was intended to find the optimum alkyl chain length to reinforce the composites to the highest degree. To facilitate this, a range of different alkyl derivatives was chosen. The abbreviations and their definitions are listed in Table 4.1.

Table 4.1 Abbreviations and definitions for alkylated nanotubes

Alkane chain length	**Name**
C0	Pristine nanotubes
C4	Butyl functionalised nanotubes
C8	Octyl functionalised nanotubes
C10	Decanyl functionalised nanotubes
C12	Dodecanyl functionalised nanotubes
C16	Hexadecanyl functionalised nanotubes
C22	Docasanyl functionalised nanotubes

In order to compare the reinforcing properties of pure nanotubes it was also planned to add pristine nanotubes to the CPP solution in THF. However, after the 12 hour settling period all of the nanotubes had precipitated to the bottom of the sample tube. The reason for this is that the nanotubes did not form stable soluble composites with the polymer. This makes impossible to study the reinforcing properties of the pure nanotubes in chlorinated polypropylene.

On functionalisation with the alkyl chains however the nanotubes form a stable suspension with the polymer. Initially butyl functionalised (initially reacted with BuLi and then hydrolysed) nanotubes were analysed and the properties of the composite are shown in table 4.2.

Table 4.2 Mechanical properties of C4 functionalised MWNT in CPP

Vol % Of MWNT	Young's modulus [GPa]	Ultimate Tensile Strength [MPa]	Toughness [KJ/m^3]
0	0.011 +/- 0.0021	12.2 +/-3.52	5.6 +/- 2.3
0.1	0.0087 +/- 0.0018	9.9 +/-0.81	2.9 +/-0.22
0.2	0.0068 +/-0.0007	13.7 +/-1.39	5.7+/-1.04
0.4	0.0082 +/-0.0007	12.5 +/- 5.5	8.58 +/-4.0

According to data presented in Table 4.2, there is no any significant change in the mechanical properties for butyl functionalised MWNTs polymer composites when compared to the pure polymer. Only a slight increase in the ultimate tensile strength (UTS) and the toughness was observed for higher concentrations of nanotubes. The tensile modulus showed some decrease, which is most likely due to the fact that the nanotubes are not incorporated well within the matrix of the polymer and are not transferring their mechanical properties to the polymer.

Table 4.3 presents the mechanical properties of octyl functionalised nanotubes in CPP. There is a slight increase in the Young's modulus as well as a two fold increase in toughness and UTS at the nanotube content of 0.2 %. Thus the octyl chain appears to reinforce the polymer to a small degree. Presumably the octyl functionalised nanotubes have a limited solubility in CPP polymer solution and the higher concentrations of nanotubes do not provide necessary homogeneous distribution of nanotubes in the polymer matrix.

Table 4.3 Mechanical properties of C8 functionalised MWNT in CPP

Vol % Of MWNT	Young's modulus [GPa]	Ultimate Tensile Strength [MPa]	Toughness [KJ/m³]
0	0.011 +/- 0.0021	12.2 +/-3.52	5.6 +/- 2.3
0.1	0.014 +/- 0.0033	16 +/- 0.6	7.1+/-2.02
0.2	0.0068+/- 0.0003	21.5 +/- 0.4	12.3 +/-0.95
0.4	0.015 +/-0.0052	15 +/- 2.5	4.5 +/- 1.38

The mechanical properties of decyl functionalised MWNTs are shown in Table 4.4. Again there are no significant changes in the mechanical properties for decanyl functionalised MWNTs at lower concentrations of nanotubes. There is a slight increase in the Young's modulus of 45% at 0.2 % nanotube content. Again the mechanical properties worsen at the higher concentrations of nanotubes and return to those of the original polymer.

Table 4.4 Mechanical properties of C10 functionalised MWNT in CPP

Vol % Of MWNT	Young's modulus [GPa]	Ultimate Tensile Strength [MPa]	Toughness [KJ/m³]
0	0.011 +/- 0.0021	12.2 +/-3.52	5.6 +/- 2.3
0.1	0.009 +/- 0.0014	14.6 +/- 4.9	6.03 +/- 4
0.2	0.016 +/- 0.0035	11.4 +/- 4.28	3.4+/- 1.6
0.4	0.015+/- 0.0034	7.03 +/- 3.1	1.91 +/-1.54

Hexadecanyl chains (Table 4.5) appear not to change the Young's modulus nor do they impart any increase in the toughness or UTS of the composite material. As a result, it looks as though the chain is too long thus relaxing against the side of the nanotube and not interacting with the polymer matrix. It is therefore not imparting any mechanical improvements to the composite material.

Table 4.5 Mechanical properties if C16 functionalised MWNT in CPP

Vol % Of MWNT	Young's modulus [GPa]	Ultimate Tensile Strength [MPa]	Toughness [KJ/m^3]
0	0.011 +/- 0.0021	12.2 +/-3.52	5.6 +/- 2.3
0.1	0.011 +/- 0.0009	12.4 +/- 2.5	4.9 +/- 1.8
0.2	0.009 +/- 0.0025	10.8 +/- 1.8	4.2 +/-1.9
0.4	0.011 +/- 0.0034	15.2 +/- 4.6	6.3 +/- 3.5

Finally, docosanyl functionality (Table 4.6) again does not show any increase in the mechanical properties of CPP-nanotube composites.

Table 4.6 Mechanical properties of C22 functionalised MWNT- CPP composites

Vol % Of MWNT	Young's modulus [GPa]	Ultimate Tensile Strength [MPa]	Toughness [KJ/m^3]
0	0.011 +/- 0.0021	12.2 +/-3.52	5.6 +/- 2.3
0.1	0.0098 +/- 0.0009	8.0 +/- 2	1.5 +/- 0.73
0.2	0.011 +/- 0.01	10.3 +/- 0.6	2.43 +/- 0.5
0.4	0.010 +/- 0.05	6.4 +/- 1.7	1.4 +/- 0.77

The relative change for Young's modulus, UTS and toughness was plotted against the alkyl chain length (figure 4.2). Thus the most efficient increase in Young's modulus was achieved for the nanotubes functionalised with the ultimate alkyl chain length of twenty carbons at 0.2 and 0.4 vol%. However, an optimum increase in both UTS and toughness is observed for C8 alkyl functionalised nanotubes at the optimal concentration of nanotubes to be 0.2 %. It is believed that the longer and shorter alkyl chains are most likely aligned along the side of the nanotubes and do not interact efficiently with the polymer matrix.

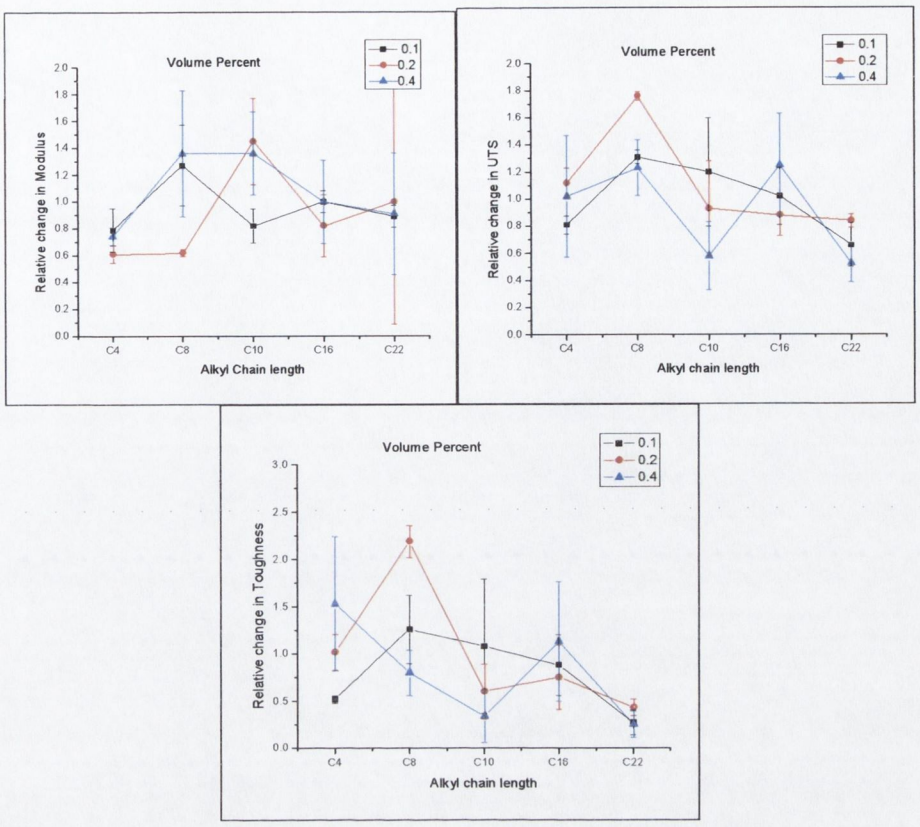

Figure 4.2 Relative change in mechanical properties of the CPP nanotube composites compared to the pure polymer for the 0.2 volume percent

4.3.2 Chlorinated Polyethylene (CPE) and alkylated nanotubes

The alkylated nanotubes were mixed with CPE in THF solution in order to identify their reinforcing characteristics. CPE was chosen as it is much more soluble as compared with pure polyethylene. As a control pure unreacted nanotubes were also combined with the polymer and were adequately stable over the twelve hour settling period.

Table 4.7 shows the change in mechanical properties of pristine nanotubes combined with chlorinated polyethylene as compared with the pure polymer. The modulus of the polymer increases significantly by a factor of 2.6. The UTS increases by a factor of 0.5 as well as the toughness increasing by a factor of 1.5 at the 0.57 % nanotube content. This sets a high target for the alkylated nanotubes for reinforcement, as the pure nanotubes have already increased the mechanical properties significantly.

Table 4.7 Mechanical properties of pristine MWNT CPE composites

Vol % Of MWNT	Young's modulus [MPa]	Ultimate Tensile Strength [MPa]	Toughness [KJ/m^3]
0	1.16 +/-0.18	6.12 +/-0.51	17 +/- 2.8
0.14	2.19 +/-0.15	8.24 +/-0.24	23.4 +/-0.8
0.28	2.01 +/-0.75	3.85 +/- 1.58	21.1 +/-1.02
0.57	3.01 +/-0.63	9.12 +/-2.87	26.2 +/-0.9

Table 4.8 Mechanical properties of C4 functionalised MWNT in CPE

Vol % Of MWNT	Young's modulus [MPa]	Ultimate Tensile Strength [MPa]	Toughness [KJ/m^3]
0	1.16 +/-0.18	6.12 +/-0.51	17 +/- 2.8
0.14	1.74 +/-0.43	2.96 +/-0.68	5.66 +/-2.54
0.28	1.74 +/-0.12	2.74 +/-0.93	5.51 +/-1.81
0.57	2.97 +/-0.16	3.58 +/-1.03	6.16 +/-2.86

Table 4.8 presents the mechanical properties of the composites of CPE and butyl functionalised nanotubes. Even on quick inspection it can be seen that the mechanical properties are not at all increased as significantly as for the pristine nanotubes. The Young's modulus is increased by 256% as compared to the pure polymer but this equals only the reinforcement of the pristine nanotube composites. The UTS decreases by nearly half as does the toughness also which decreases by over half. This demonstrates that the butyl groups do not influence the solubility of nanotubes and the butyl groups do not adequately reinforce the composites. Thus there is not sufficient interfacial stress transfer between nanotube surface and polymer matrix.

Table 4.9 presents the mechanical properties of octyl-functionalised carbon nanotubes in CPE. Again the two fold increase with a 0.57 vol% of nanotubes in CPE, whilst great, remains less significant than in the case of the pristine nanotube composites.

Again the UTS and toughness decrease by close to half that of the pure polymer. These results as well as the results for the butyl bound nanotubes do not bode well for alkylated nanotube reinforcement in this polymer.

Table 4.9 Mechanical properties of C8 functionalised MWNT in CPE

Vol % Of MWNT	Young's modulus [MPa]	Ultimate Tensile Strength [MPa]	Toughness [KJ/m^3]
0	1.16 +/-0.18	6.12 +/-0.51	17 +/- 2.8
0.14	1.44 +/-0.22	2.51 +/-0.95	6.38 +/-4.02
0.28	1.73 +/-0.11	3.38 +/-1.57	6.97 +/-3.24
0.57	2.39 +/-0.17	4.52 +/-2.32	9.27 +/-5.13

Fortunately the results in Table 4.10 present a more optimistic outlook for the hexadecanyl functionalised nanotubes in CPE the Young's modulus increases by a large factor of 3.6 which is significantly higher than that of the pristine nanotubes (2.6 fold increase). The UTS increases by a factor of 1.5 which, whilst not outstanding, is comparable with the pure nanotubes and the toughness increases by 34% which is close to the increase in the pristine nanotube composites.

Table 4.10 Mechanical properties of C16 functionalised MWNT in CPE

Vol % Of MWNT	Young's modulus [MPa]	Ultimate Tensile Strength [MPa]	Toughness [KJ/m^3]
0	1.16 +/-0.18	6.12 +/-0.51	17 +/- 2.8
0.14	2.6 +/-0.093	3.65 +/-1.49	6.91 +/-4.59
0.28	3.1 +/-0.6	3.61 +/-0.14	7.4 +/-1.96
0.57	4.12 +/-0.21	9.01 +/-0.995	22.8 +/-3.4

Table 4.11 highlights the measured mechanical properties of docosanyl functionalised nanotubes in CPE. It can be clearly seen here that the nanotubes whilst still imparting mechanical reinforcing properties, their results are not as good as for the pristine and hexadecanyl functionalised nanotubes. The modulus increases by a factor of 2 and the UTS shows a slight increase of 18% as well as an increase of 37% for the toughness.

Table 4.11 Mechanical properties of C22 functionalised MWNT CPE composites

Vol % Of MWNT	Young's modulus [MPa]	Ultimate Tensile Strength [MPa]	Toughness [KJ/m^3]
0	1.16 +/-0.18	6.12 +/-0.51	17 +/- 2.8
0.14	2.02 +/-0.185	3.61 +/-0.245	9.81 +/-0.19
0.28	2.37 +/-0.045	7.2 +/-4.2	23.4 +/-1.49
0.57	2.07 +/-0.255	6.68 +/-1.86	18.4 +/-0.62

Figure 4.3 presents the percentage increases for each of the chosen mechanical properties for different nanotube content and alkyl chain length.

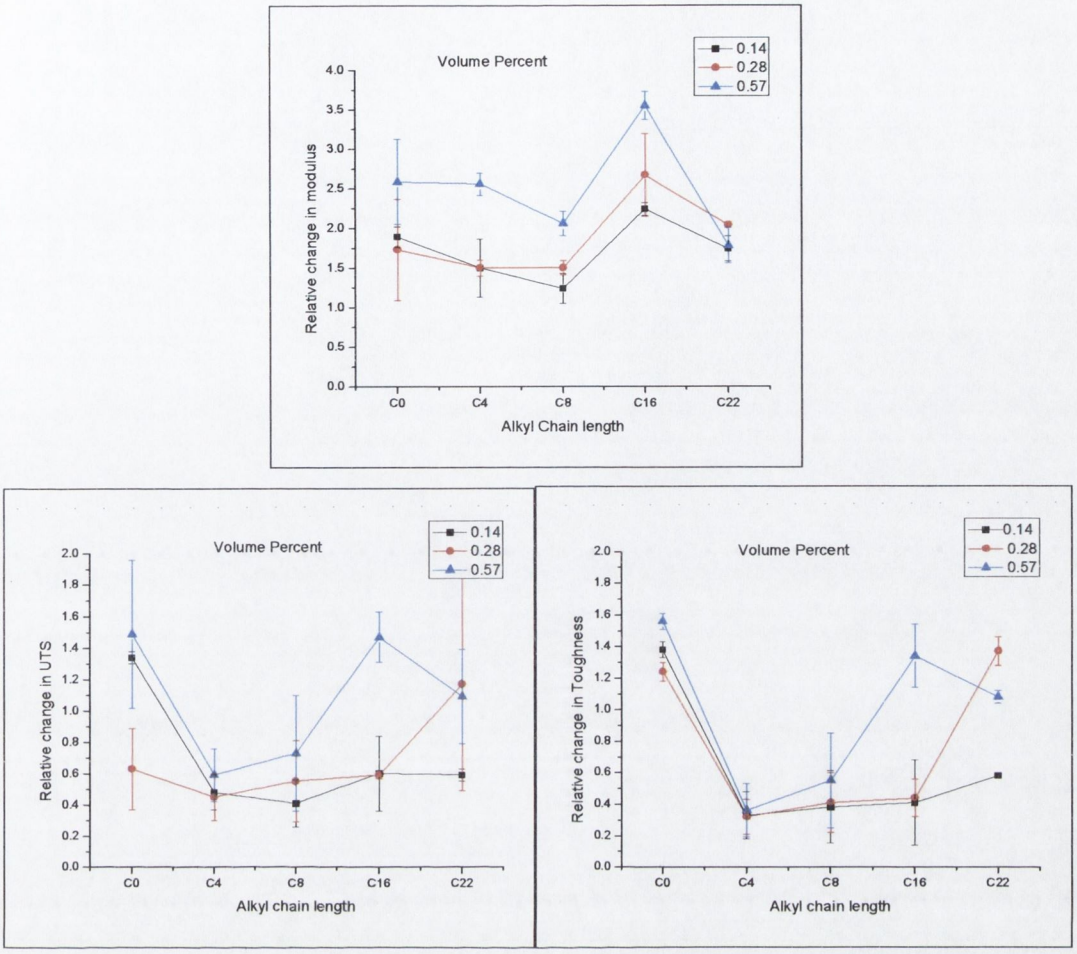

Figure 4.3 Relative change in Young's modulus, UTS and toughness of CPE nanotube composites compared to pure polymer

According to Figure 4.3, the optimum chain length for Young's modulus is hexadecyl functionalised nanotubes. They gave a 2.5 increase in modulus compared to the pure polymer. For the UTS again hexadecanyl reinforces to the greatest extent as compared to the other alkylated nanotubes. Finally in the toughness both hexadecanyl and docosanyl give an increase of 0.4 which is comparable to the pure nanotubes at 0.5.

4.3.3 Alkylated nanotubes in Polyvinyl Chloride (PVC)

Alkylated nanotubes were mixed with PVC in THF solution and films of PVC nanotube composites have been prepared by solution casting for mechanical testing. This time the

pristine unreacted nanotubes were sufficiently stable in the polymer solution in THF over the twelve hour settling period to allow composites to be compared to the base material.

In Table 4.12 the reinforcing characteristics are shown for pristine nanotubes. It is immediately noticeable that the mechanical characteristics of the PVC composite deteriorated. The reason for this is that the nanotubes are disrupting the polymer's natural crystalline structure, thus weakening the material. The nanotubes are likely to be causing large defects in the polymer structure causing fracture points which would give rise to low or negative changes in mechanical properties.

Table 4.12 Mechanical properties of pristine MWNT PVC composites

Vol % Of MWNT	Young's modulus [GPa]	Ultimate Tensile Strength [MPa]	Toughness [KJ/m^3]
0	0.56 +/-0.07	15.6 +/-0.5	5.5 +/-2.11
0.16	0.44 +/-0.17	13.8 +/-2.26	3.9 +/-1.5
0.32	0.19 +/-0.04	14.3 +/-1.92	3.1 +/-0.4
0.65	0.39 +/-0.07	12.5 +/-1.68	5.9 +/-3.65

The addition of the butyl functionalised nanotubes to PVC causes the nanotubes to significantly improve the mechanical characteristics of the polymer composite as shown in Table 4.13.

Table 4.13 Mechanical properties of C4 functionalised MWNT in PVC

Vol % Of MWNT	Young's modulus [GPa]	Ultimate Tensile Strength [MPa]	Toughness [KJ/m^3]
0	0.56 +/-0.07	15.6 +/-0.5	5.5 +/-2.11
0.16	0.94 +/-0.047	16.6 +/-1.9	5.1 +/-1.4
0.32	0.44 +/-0.042	13.3 +/-0.36	3.23 +/-0.6
0.65	0.95 +/-0.2	23.1 +/-5.02	11.2 +/-2.64

With only a 0.16 vol% there is close to a two fold increase in Young's modulus. Further more this increases to 0.65 vol% and there is 1.5 times increase in UTS and a two fold increase in toughness coupled with the large increase in modulus. This shows that the butyl functionalised nanotubes reinforced the polymer to some degree when compared to the pristine nanotubes.

For octyl-functionalised nanotubes (in Table 4.14) with a low volume percent there is a significant increase in modulus, 0.16% gives rise to a 1.6 fold increase. However the other parameters do not increase as significantly as for the butyl-functionalised nanotubes. While once again there is a significant increase if compared with the pristine nanotubes in PVC.

Table 4.14 Mechanical properties of C8 functionalised MWNT in PVC

Vol % Of MWNT	Young's modulus [GPa]	Ultimate Tensile Strength [MPa]	Toughness [KJ/m^3]
0	0.56 +/-0.07	15.6 +/-0.5	5.5 +/-2.11
0.16	0.91 +/-0.15	17.8 +/-2.84	3.9 +/-0.82
0.32	0.61 +/-0.07	16.7 +/-0.18	9.2 +/-3.08
0.65	0.72 +/-0.13	17.9 +/-1.84	6.2 +/-1.5

Table 4.15 presents the mechanical properties of the hexadecyl-functionalised nanotubes in PVC. In this case the smallest volume percent showed the most significant increase in modulus with an increase of 75%. The UTS this time also increases by approximately 50% and the toughness shows the highest seen increase with a 400% increase in overall toughness for a 0.65 vol.%. This is a very significant result especially as this dramatic increase is brought about with a relatively small amount of nanotubes present.

Table 4.15 Mechanical properties of C16 functionalised MWNT in PVC

Vol % Of MWNT	Young's modulus [GPa]	Ultimate Tensile Strength [MPa]	Toughness [KJ/m³]
0	0.56 +/-0.07	15.6 +/-0.5	5.5 +/-2.11
0.16	0.98 +/-0.048	23.9 +/-1.53	18.5 +/-1.77
0.32	0.53 +/-0.1	19.4 +/-2.4	15.9 +/-1.71
0.65	0.77 +/-0.075	20.2 +/-1.5	22 +/-1.3

Finally, table 4.16 presents the mechanical properties for PVC reinforced with docosanyl-functionalised nanotubes. In the 0.65 vol.% there is a slight increase of the modulus. However this increase is very slight and the other volume percents are equivalent or close to equivalent with the original polymer. This trend is followed for the UTS, both of the lower volume percents decrease or remain close to the polymer with the highest volume percent increasing slightly. The toughness levels for the two highest volume percents show a reasonable increase. However, none of the increases in the docosanyl nanotube composite material represent as large a jump as was exhibited in the other chain lengths. This suggests that the mechanical properties are going back to the same level as the original polymer and that this is the longest chain length, which was used for reinforcement.

Table 4.16 Mechanical properties of C22 functionalised MWNT in PVC

Vol % Of MWNT	Young's modulus [GPa]	Ultimate Tensile Strength [MPa]	Toughness [KJ/m³]
0	0.56 +/-0.07	15.6 +/-0.5	5.5 +/-2.11
0.16	0.53 +/-0.22	13.7 +/-3.3	3.32 +/-0.6
0.32	0.53 +/-0.004	15 +/-0.99	9.5 +/-0.372
0.65	0.69 +/-0.12	17.2 +/-3.12	8.7 +/-0.371

Figure 4.4 presents the percentage increases for each of the chosen mechanical properties for different nanotube content and alkyl chain length.

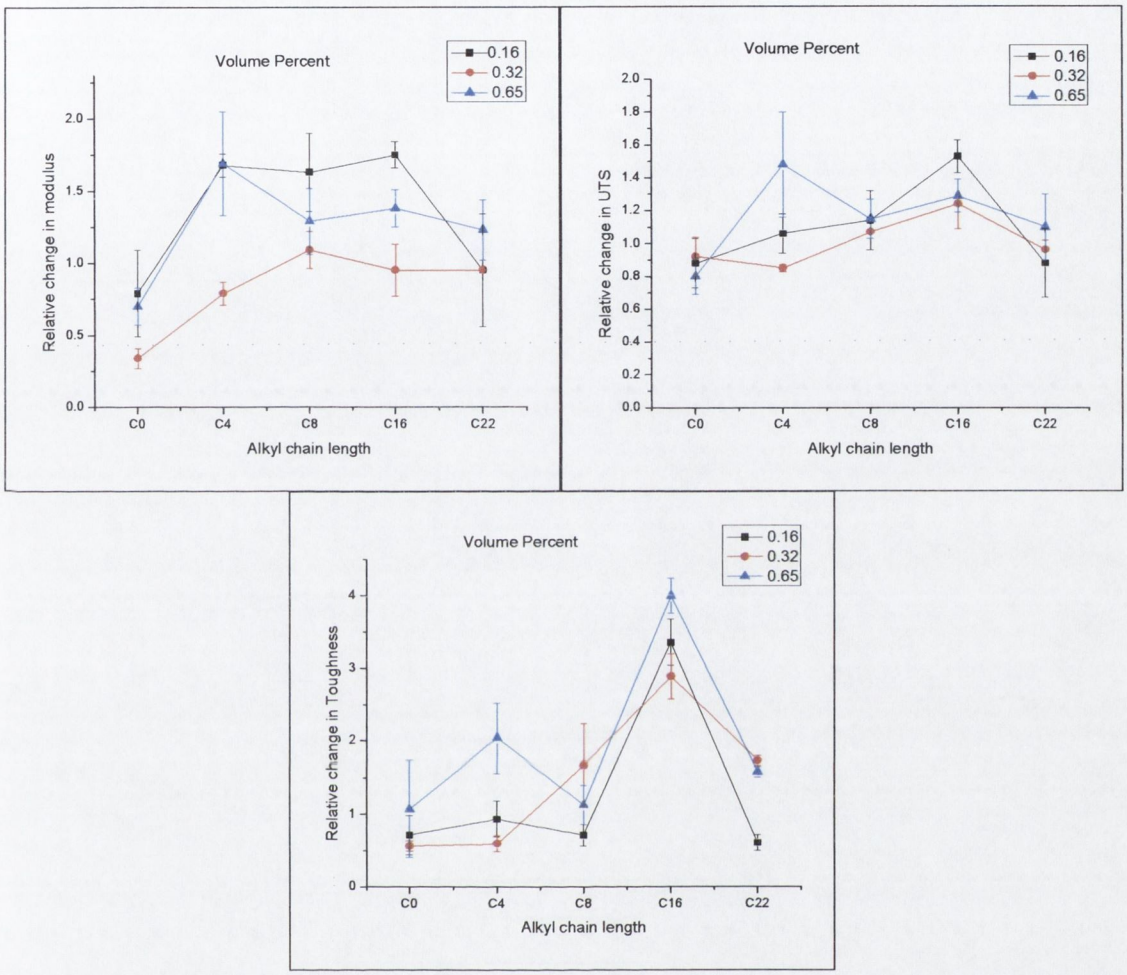

Figure 4.4 Relative change in modulus, UTS and toughness for PVC nanotube composites

Once again it can be seen from figure 4.4 that the optimum chain length for increasing the mechanical properties are sixteen carbons, which is analogous to CPE and also a mid range chain length as was the case in CPP. Docosanyl functionalised nanotubes appear to aggregate and thus do not allow for efficient interfacial stress transfer from the nanotubes to the polymer.

4.3.4 Alkylated nanotubes in Polystyrene (PS)

The final polymer chosen to reinforce with the alkylated nanotubes was polystyrene. It was 350,000 Mw purchased from Aldrich. The polymer was readily soluble in THF which led to good film formation. Polystyrene was dissolved in THF and to this solution varying masses of the alkylated nanotubes were added. With PS it was possible to suspend larger volume fractions of pristine nanotubes for a sufficient period to allow for the corresponding composites to be prepared.

Table 4.17 presents the mechanical properties of PS reinforced with pristine nanotubes. The lowest two volume fractions were not sufficiently stable in the polymer solution. What is shown is that the Young's modulus of the PS polymer is slightly reinforced by pure nanotubes. The polymer has aromatic groups which mediate nanotube suspension in solution *via* the π-π interaction between the polymer and the nanotubes. This enables an increase in tensile modulus and toughness of the PS polymer composite slightly at 0.51 % nanotube content. However, the UTS decrease dramatically. The reason the initial polymer has such a small toughness value is because the polymer is brittle even though it has a large modulus value. On addition of the nanotubes, the brittleness of the composites increases this explains why there is a substantial decrease in UTS and toughness values.

Table 4.17 Mechanical properties of pristine MWNT in PS

Vol % Of MWNT	Young's modulus [GPa]	Ultimate Tensile Strength [MPa]	Toughness [KJ/m^3]
0%	0.568 +/-0.037	15.6 +/- 5.36	0.3 +/- 0.15
0.51%	1.19 +/-0.44	6.38 +/-2.89	0.64 +/-0.19
2.5%	0.974 +/-0.3	10.2 +/-3.06	0.252 +/-0.17

Table 4.18 shows the mechanical properties of the composite materials of butyl-functionalised nanotubes combined with PS and compared to the original polymer. These results exhibit an increase in modulus which is higher again than the pristine nanotube

composites. The increase shown here is a significant increase of 338% compared to the original polymer. As well as this the other mechanical properties of the composite are not reduced as they were in the pristine nanotube composites. The reason for this is that the alkyl chains surrounding the nanotubes are hindering the crystallisation of the polymer and ultimately reducing the brittleness of the composite material. While there are no dramatic increases in the UTS and toughness the effect is clearly noticeable if compared to Table 4.17.

Table 4.18 Mechanical properties of C4 functionalised MWNT in PS

Vol % Of MWNT	Young's modulus [GPa]	Ultimate Tensile Strength[MPa]	Toughness [KJ/m^3]
0%	0.568 +/-0.037	15.6 +/- 5.36	0.3 +/- 0.15
0.13%	1.59 +/-0.23	22.4 +/-4.35	0.27 +/- 0.12
0.26%	1.89 +/-0.11	18.8 +/-3.9	0.12 +/- 0.04
0.51%	1.92 +/-0.09	24.5 +/-1.5	0.11 +/- 0.045
2.5%	1.74 +/-0.05	21.7 +/-0.86	0.15 +/- 0.05

Increasing the chain length to octyl (table 4.19) results in a large increase in Young's modulus, however has less significant impact on the UTS and toughness.

Table 4.19 Mechanical properties of C8 functionalised MWNT in PS

Vol % Of MWNT	Young's modulus [GPa]	Ultimate Tensile Strength [MPa]	Toughness [KJ/m^3]
0%	0.568 +/-0.037	15.6 +/- 5.36	0.3 +/- 0.15
0.13%	1.96 +/-0.14	22.9 +/-7.82	0.29 +/-0.05
0.26%	1.2 +/-0.13	14.7 +/-3.02	0.13 +/- 0.04
0.51%	0.85 +/-0.24	8.24 +/-3.74	0.55 +/-0.03
2.5%	0.86 +/-0.08	8.33 +/-1.49	0.66 +/-0.02

The mechanical properties of the composites containing nanotubes functionalised with the longer hexadecanyl chain are shown in Table 4.20. It can be clearly seen that there is a very significant increase in Young's modulus of 375% compared to the original polymer. The UTS again demonstrated a stable value of ~20 MPa compared to 15.6 MPa for pure PS. However the real potential of the alkylated nanotube composite increase can only be realised by comparing it to the pristine nanotube composites where the UTS dropped significantly. Also the toughness showed quite significant increase at over 5 times for 0.51 vol.% of nanotube content.

Table 4.20 Mechanical properties of C16 functionalised MWNT in PS

Vol % Of MWNT	Young's modulus [GPa]	Ultimate Tensile Strength [MPa]	Toughness [KJ/m^3]
0%	0.568 +/-0.037	15.6 +/- 5.36	0.3 +/- 0.15
0.13%	2.07 +/-0.21	20.9 +/-2.14	1.3 +/-0.02
0.26%	2.02 +/-0.11	16.2 +/-3.37	0.76 +/-0.03
0.51%	2.13 +/-0.25	20.4 +/-3.54	1.6 +/-0.04
2.5%	2.08 +/-0.07	21.9 +/-2.3	1.4 +/-0.02

The dramatic increase at this chain length correlates well with the results for the other polymers where the optimum reinforcement was seen at a chain length of ten up to sixteen carbons.

The results for docosanyl functionalised nanotube composites are shown in Table 4.21 are. It is clearly visible that there is a large modulus increase of 463% when compared to the pure polymer. As well as this the UTS shows an improvement with an increase of 175% for 0.13 vol% which is the largest increase in any of the alkylated nanotube polymer composites. The toughness again demonstrated very significant increase over 6 fold at lower vol.% of nanotubes.

Table 4.21 Mechanical properties of C22 functionalised MWNT in PS

Vol % Of MWNT	Young's modulus [GPa]	Ultimate Tensile Strength [MPa]	Toughness [KJ/m^3]
0%	0.568 +/-0.037	15.6 +/- 5.36	0.3 +/- 0.15
0.13%	2.45 +/-0.38	27.4 +/-3.7	1.94 +/- 0.02
0.26%	2.63 +/-0.23	23.8 +/-3.6	1.5 +/- 0.04
0.51%	2.04 +/-0.18	21.1 +/-2.2	1.28 +/-0.02
2.5%	1.48 +/-0.29	13 +/-1.85	0.698 +/-0.01

As we can see docosanyl-functionalised nanotubes are still reinforcing in PS but do not demonstrate that in other polymers above. The most plausible explanation for this fact is that the aromatic groups of the PS polymer competitively interact with carbon nanotube surface and the alkyl chains for surface adhesion. Due to the strong π-π interaction between the polymer and the nanotube this prevents the alignment of alkyl chains along the nanotube's surface. This allows the longer alkyl chains to expand into the polymer matrix providing a strong interaction between the alkylated nanotubes and the polymer.

Figure 4.5 summarises data on mechanical testing PS composites. According to these data, the sixteen carbon alkyl chain functionalised nanotubes provide the greatest reinforcement. For the modulus however, it appears as though the optimum length has not yet been reached but it is clearly apparent that the longer chain lengths offer greater reinforcement. This characteristic is also seen in UTS however in toughness the longer chain lengths and higher nanotube content do not demonstrate the best reinforcement. It should be noted that the reinforcing is not as high as the pure polymer, as the percentage increases are under 100%. These experiments clearly demonstrate that the higher vol% inhibits good mechanical reinforcement which is likely due to aggregation.

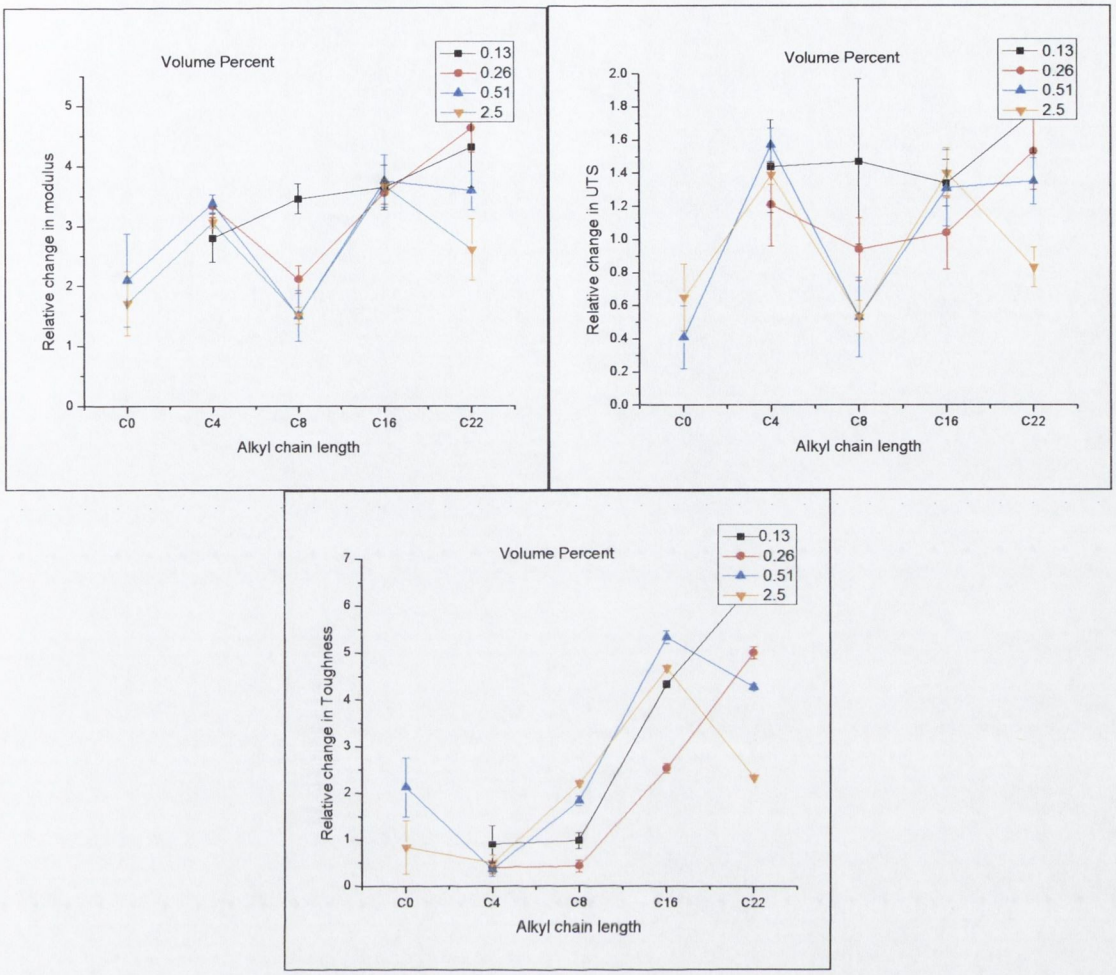

Figure 4.5 Relative change in modulus, UTS and toughness for PS nanotube composites compared to pure polymer

4.4 Analysing Y_{eff} and interfacial stress transfer for alkylated nanotubes in selected polymers

Applying the theory suggested at the beginning of this chapter and Equation 4.6 it is possible to calculate the nanotubes effective modulus, Y_{eff}, used in composite formation. This should allow us to compare the functionalised nanotubes to the pristine nanotubes, with the exception of CPP. For the case of both CPP and CPE the values, in table 4.22, for the functionalised MWNTs show reasonably low values for CVD MWNTs however the reason they are low is due to inadequate interfacial stress transfer between the nanotubes and the polymer. The PVC composites show very reasonable values for Y_{eff} of CVD nanotubes in the ~100 GPa region. And finally the PS composites show Y_{eff} which is comparable to the theoretical values for MWNTs.

Figure 4.6 shows a plot of the effective Young's modulus versus alkyl chain length in the case of CPE and PVC composites Y_{eff} increases to an optimum and then decreases for docosanyl functionalised MWNTs. The PS composites however, do not reach an optimum and continue increasing up to an very high value for Y_{eff}.

Table 4.22 Y_{eff} for the alkylated and pristine MWNTs in selected polymer all units are expressed in GPa

	Pristine MWNT	C4	C8	C16	C22
C.P.P.	N/A	5.42 +/- 2.66 GPa	2.95 +/- 2.95 GPa	2.29+/- 4.27 GPa	2.84+/- 5.85 GPa
C.P.E.	1.11 +/- 0.27 GPa	0.846 +/- 0.11 GPa	0.571 +/- 0.12 GPa	2.5 +/- 0.36 GPa	1.06 +/- 0.16 GPa
P.V.C.	71.2 +/- 41 GPa	254 +/- 31 GPa	50.4 +/- 56 GPa	85.3 +/- 43 GPa	54.1 +/- 57.7 GPa
P.S.	48.9 +/- 33.1 GPa	1.37 +/- 114 TPa	991 +/- 128 GPa	1.6 +/- 115 TPa	2.23 +/- 87 TPa

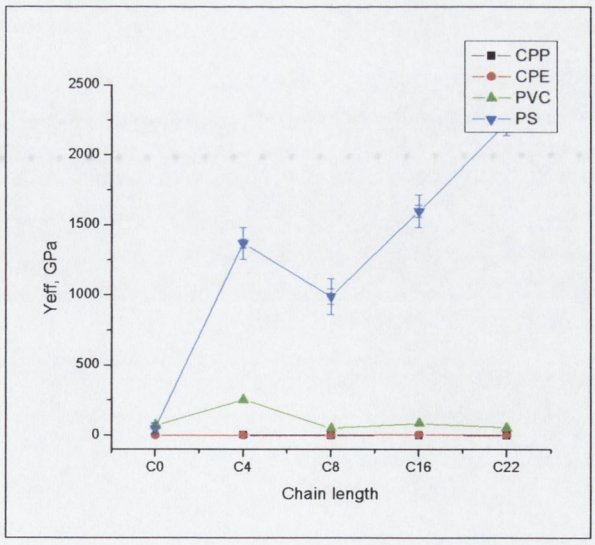

Figure 4.6 Graph of effective modulus of functionalised nanotubes versus alkyl chain length

Barber *et al.*[17] have suggested that the interfacial stress transfer of nanotubes not covalently bound to the composite should be in the region of 10 MPa. The values observed in table 4.24 agree well with this theory, with all values being close to but bellow the 10 MPa value. In each of the samples the values for τ are greater for the functionalised MWNTs than the un-functionalised. This supports the theory that the alkylated nanotubes allow for better interfacial stress transfer than the unfunctionalised nanotubes.

Table 4.24 Values of interfacial stress transfer,τ, in MPa for unfunctionalised and functionalised MWNTs in a range of polymers

	Pristine MWNT	C4	C8	C16	C22
C.P.P.	N/A	5.98+/- 2.96 MPa	7.47+/- 4.15 MPa	1.52 +/- 4.01 MPa	2.245 +/- 1.45 MPa
C.P.E.	1.5 +/- 1.94 MPa	0.34 +/- 0.97 MPa	1.14 +/- 1.89 MPa	3.91 +/- 1.12 MPa	1.74 +/- 1.45 MPa
P.V.C.	0.83 +/- 1.29 MPa	0.3 +/- 2.22 MPa	0.66 +/- 1.28 MPa	1.61 +/- 1.04 MPa	1.65 +/- 2.05 MPa
P.S.	0.45 MPa	2.63 +/- 2.43 MPa	7.3 +/- 3.97 MPa	0.581 +/- 2.57 MPa	3.54 +/- 2.46 MPa

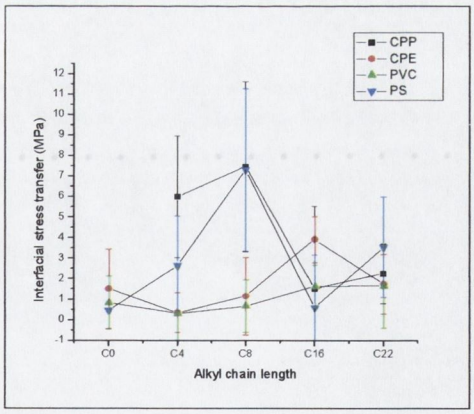

Figure 4.7 Graph of Interfacial stress transfer versus alkyl chain length

Figure 4.7 shows a graph of the interfacial stress transfer and alkyl chain length of the functionalised MWNTs. In the case of CPP and PS the interfacial stress transfer increases

to the octyl functionalised nanotubes and then decreases with higher chains. In the case of CPP and PS the interfacial stress transfer increases to the octyl functionalised nanotubes and then decreases with higher chains.

4.5 Conclusion

We have found the mechanical properties of alkylated carbon nanotube polymer composites strongly depend on the nature of polymer, length of the alkyl chain and vol.% of nanotubes.

In general, for the selected polymers and alkyl chains studied, hexadecanyl functionalised nanotubes provide the optimum alkyl chain length for overall polymer reinforcement. In the case of PS docosanyl functionalised nanotubes have showed the largest increase in modulus which is most likely due to the fact that the aromatic groups in the polymer prevent the alignment of longer chains along the nanotube surface and as result provide better interaction of alkyl chains with the polymer matrix.

Observing increases in mechanical properties, as a general rule, the vol.% concentration which showed the most significant increase in all mechanical properties was that of the lower vol.% of nanotubes. With the exception of CPE and CPP which showed a higher increase in mechanical properties for the higher vol.% of nanotubes.

Comparisons of Y_{eff} of the functionalised nanotubes in the CPP and CPE only have a small value more than likely due to the fact that the nanotubes in these polymers are not imparting good interfacial stress transfer. In the case of PVC the value for Y_{eff} is reasonable as the nanotubes are reinforcing the polymer to a certain degree. However in the case of PS the nanotubes are showing values for Y_{eff} which are close to the theoretical value for nanotubes.

Calculating, τ provides good values for the interfacial stress transfer of functionalised nanotubes to the pure polymer especially when compared to pure MWNTs in the selected polymers.

4.6 References

[1] K.T. Lau, D. Hui, *Composites Part B,* **33,** 263, (2002)

[2] E. Dujardin, T.W. Ebbesen, A. Krishnan, P.N. Yianilos, M.M.J. Treacy, *Phys. Rev. B.,* **58**, 14013, (1998)

[3] M.F. Yu, B.S. Files, S. Arepalli, R.S. Ruoff, *Phys. Rev. Lett.,* **84**, 5552, (2000)

[4] M.J. Beircuk, M.C. Llaguno, M. Radosavjevic, J.K. Hyun, J.E. Fischer, A.T. Johnson, *Appl. Phys. Lett.,* **80**, 2767, (2002)

[5] C. Wei, D. Srivastava, K. Cho, *Nano. Lett.,* **2**, 647, (2002)

[6] http://www.aldila.com/nanotubes.html, aldila, (17 Feb. 05)

[7] http://www.space.com/businesstechnology/technology/space_elevator_020327-1.html, Imaginova Corp, (17 Feb. 05)

[8] J.N. Coleman, S. Curran, A.B. Dalton, A.P. Davey, B. Mc Carthy, W.J. Blau, R.C. Barklie, *Synthetic Metals,* **102,** 1174, (1999)

[9] M. Cadek, J.N. Coleman, V. Barron, K. Hedicke, W.J. Blau, *Appl. Phys. Lett.,* **81,** 5123, (2002)

[10] M.C. Weisenberger, E.A. Grulke, D. Jacques, T Rantell, R. Andrews, *Journal Nanoscience and Nanotechnology,* **6,** 3, (2003)

[11] J.Bai, *Carbon*, **41,** 1325, (2003)

[12] C.W. Nan, Z. Shi, Y. Lin, *Chem. Phys. Lett.,* **375**, 666, (2003)

[13] .L. Cox, *Brit. J. Appl. Phys.* **3**, 72 (1952)

[14] J.N. Coleman, M. Cadek, R. Blake, V. Nicolosi, K.P. Ryan, C. Belton, A. Fonseca, J.B. Nagy, Y. Gun'ko, W.J. Blau, *Adv. Funct. Mat.* **14**, 791 (2004)

[15] H. Krenchel, Akademisk Forlag, Copenhagen (1964)

[16] L. Valentini, J. Biagiotti, J.M. Kenny, S. Santucci, *Comps. Sci. and Tech.,* **63**, 1149, (2003)

[17] A.H. Barber, S.R. Cohen, H.D. Wagner, *Appl. Phys. Lett.,* **82,** 4140, (2003)

Chapter 5

Bonding of Carbon Nanotubes to Polymers and Investigation of the Mechanical Properties of the Composites

5.1 Introduction

Nanotubes have a Young's modulus in the region of 1 TPa, which is five times stronger than that of steel[1] and an ultimate tensile strength of 30 GPa[2] as compared to steel's which is 420 MPa. In the past it has been suggested that the most important applications of nanotubes will lie in the mechanical reinforcement and/or electrical enhancement of plastics.[3] Doping of the polymer has been shown to increase the polymer's conductivity by ten orders of magnitude. It also has the added benefit of purifying the nanotubes from the initial mixture of amorphous carbon.[4] Carbon nanotubes, CNTs, have the potential to be used in numerous manufacturing materials from the construction of lightweight aeroplanes to bullet-proof shirts. New high strength and light weight structural materials are also becoming increasingly important for the aerospace industry. The impressive mechanical properties of nanotubes coupled with their low density makes them ideal reinforcement materials.

Most of the previous research on nanotube-polymer composites has focused either on the mechanical mixing of nanotubes[5] and polymers by solution casting or melt processing or *in situ* polymerisation in the presence of nanotubes.[6] There were also attempts to include the nanotubes in the polymer by the spinning process.[7] While extensive progress has recently been made in this area,[4] only a few polymers were found to form adequately strong interfaces with nanotubes. The mechanical properties of mechanically mixed carbon nanotubes with polymers have fallen short of predicted values. Yet given the magnitude of the CNT's mechanical properties, significant improvement on current composites is eminently possible provided that an appropriate means to harness the CNT's unique attributes as exhibited at the nanoscale can be transferred to the macro scale. This essentially defines the fundamental challenge for applied CNT/polymer composites research. A better understanding of the relationships between processing, interfacial stress transfer, and composite properties is a major goal of this area of research, which may lead to exciting opportunities for the optimal reinforcement of polymer matrices with CNTs.

We believe that nanotubes covalently bound to a polymer matrix should result in better polymer-nanotube interfacial stress/strain transfer and provide an access to ultra-strong

composite materials. In this work we are going to develop strong covalent bonding of carbon nanotubes to polymers and explore the potential of these new nano-composites for polymer reinforcement.

5.2 Aims of this work

The main aim of this part of the project was to prepare new ultra-strong polymer composite materials using new chemically modified carbon nanotubes as additives and as a result provide an efficient bonding of nanotubes to the polymer matrix and good interfacial stress transfer. An organometallic approach using BuLi is proposed for carbon nanotube modification with subsequent binding of the lithiated nanotubes to chlorinated polypropylene and polyvinyl chloride. Then the functionalised carbon nanotubes will be used to reinforce chlorinated polypropylene (CPP), polystyrene (PS), polyvinylchloride (PVC) and chlorinated polyethylene (CPE). The polymers selected for the work are the most commonly used every day polymers. The preparation of new polymer composites is to be achieved by mixing the pure polymer with an optimal amount of polymer grafted carbon nanotubes in an appropriate organic solvent and by the preparation of films for nanotube polymer composites. It was then planned to investigate the mechanical properties of the composites using a Zwick-100 tensile tester. It is our contention that through the interaction between the grafted polymer chain and surrounding chains, interfacial stress transfer will be enhanced.

DSC tests will be undertaken to analyse the thermal transitions of the nanotube polymer composites to see if the nanotubes affect the crystallinity of the polymers.

The successful outcome of this research should contribute to the development of both nanoscale Physics and Chemistry of nanotubes have expected to result in development of novel ultra strong composite materials.

5.3 Synthesis and characterisation of CPP carbon nanotube composites

The reaction used to bind the polymers and the nanotubes was a coupling reaction between lithiated nanotubes discussed above in Chapter 2, and halogenated polymer. First both SWNT and MWNTs were reacted with n-butyllithium in THF as has been reported earlier. Then the lithiated nanotubes were treated with a degassed solution of chlorinated polypropylene in dry THF at -10 °C using an acetone ice bath. It is important that the polymer solution is degassed before the reaction to remove any possible contaminants which may be residual from the production of the polymer; these contaminants could include chlorine gas or air both of which would be detrimental to the reaction. The resulting product is nanotubes that are covalently bound to chlorinated polypropylene whilst the lithium was removed in the form of lithium chloride. Scheme of the reaction is shown in figure 5.1

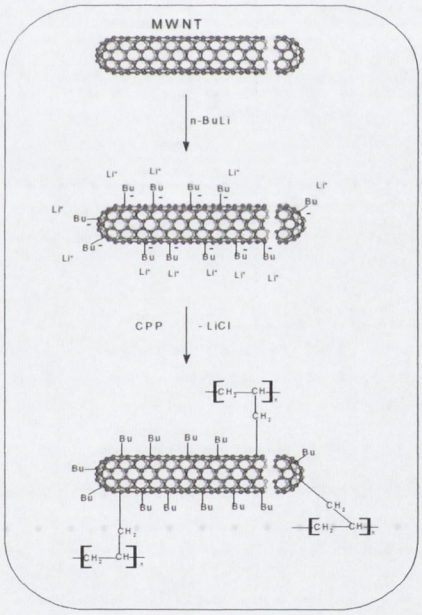

Figure 5.1 Schematic representation of the covalent binding of nanotubes to polymer

Analysis of the products is problematic due to the limited number of characterisation techniques, which can be used. TGA, DSC, TEM, Raman and IR spectroscopy have been performed to investigate the new nanotubes derivatives. As well as this mechanical strength experiments have been carried out on the polymer films blended with polymer grafted nanotubes.

TEM images (figure 5.2) shows the nanotubes that are bound and intertwined directly with the polymer, a coating can be observed surrounding the outside of the nanotubes.

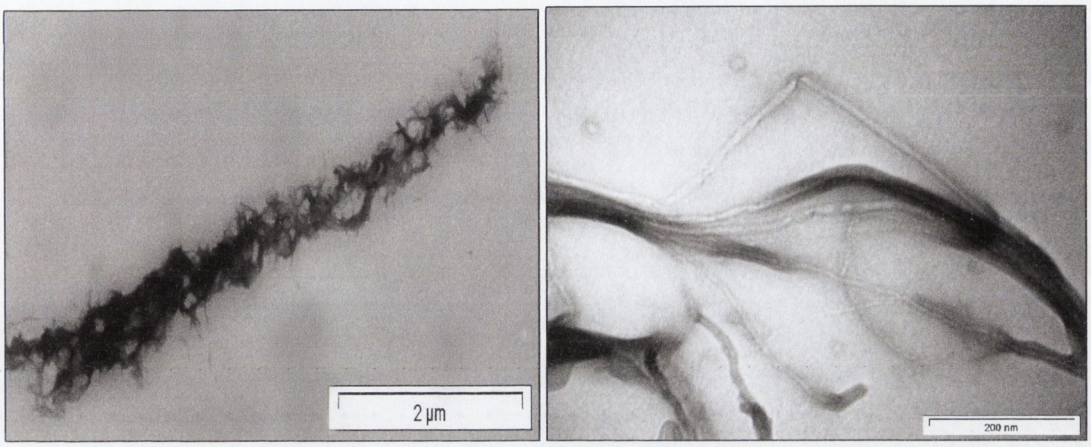

Figure 5.2 TEM images of MWNTs grafted with chlorinated polypropylene.

Of course chemical bonding can not be identified from these images but it is clear that the end product is very different from the initial polymer and nanotube materials, figure 5.3.

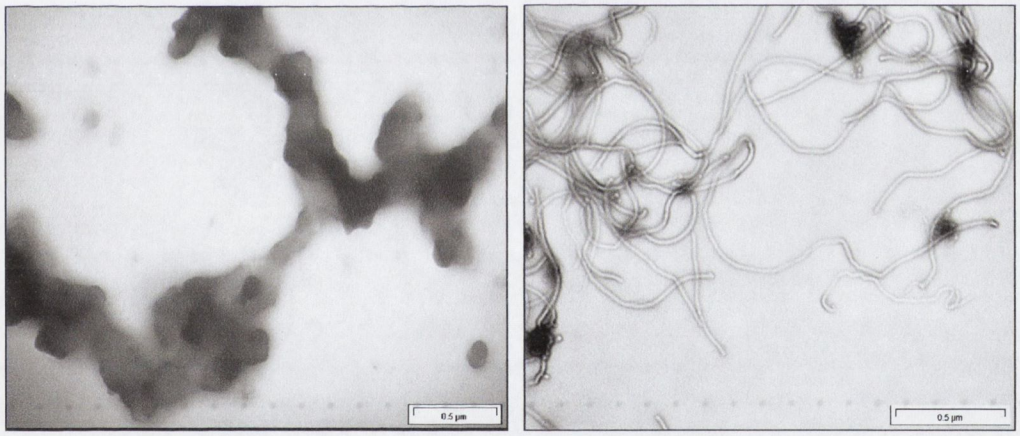

Figure 5.3 TEM images of pure chlorinated polypropylene under TEM (left) and original nanotubes (right)

TGA studies of CPP grafted nanotubes showed the presence of two different temperature peaks one at 315 °C and the other at 535 °C (figure 5.4). The peak at 535 °C is indicative of carbon nanotubes. This can be identified by comparison with the TGA of the pure MWNTs with the peak at 597.7 °C. The decomposition temperature of nanotubes is lower than one for nanotube polymer composites. This can be caused by several factors. Firstly it is well known that chemical functionalisation damages carbon nanotubes[8] resulting in lower

degradation temperatures. Another factor is that the polymer in the grafted nanotubes might assist the heat transfer directly to the nanotubes allowing the nanotubes to decompose more rapidly and at a lower temperature. The other peak that appears at a much lower temperature (315 °C) corresponds to the polymer. The calculated content of polymer was found to be 31%.

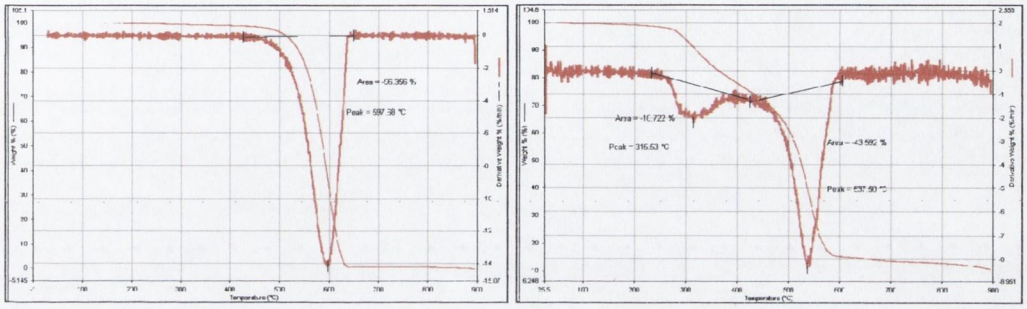

Figure 5.4 TGA of pristine nanotubes (left) and CPP grafted nanotubes (right).

In order to test the mechanical strength of the polymer grafted nanotubes and their possible potential for plastics reinforcement it was decided to blend the new PVC grafted nanotubes with the original polymer. Samples with various ratios of nanotube material to pure polymer have been prepared from 0.125% to 1% by weight of grafted nanotubes. A 30 g per litre concentration of pure chlorinated polypropylene was prepared in THF. 10 mls of this solution was added to the relevant amount of polymer grafted nanotubes material. The mixture was then ultrasonically treated for 5 minutes using the sonic tip and followed by 2 hours treatment in the sonic bath. The mixture was left to settle for 12 hours to allow any unreacted nanotubes or residual impurities to fall out leaving only the polymer bound nanotubes in solution. The resulting suspension was then decanted from the deposit. 1ml was taken from this solution and put on to Teflon disks which were 3cm in diameter and the solvent was allowed to evaporate at room temperature this was repeated three subsequent times leaving a film which was allowed to dry on the disk for a further 12 hours. The film was carefully removed from the disk using a thin blade and placed in a sample holder. A digital picture of some of the resulting films is shown in figure 5.5.

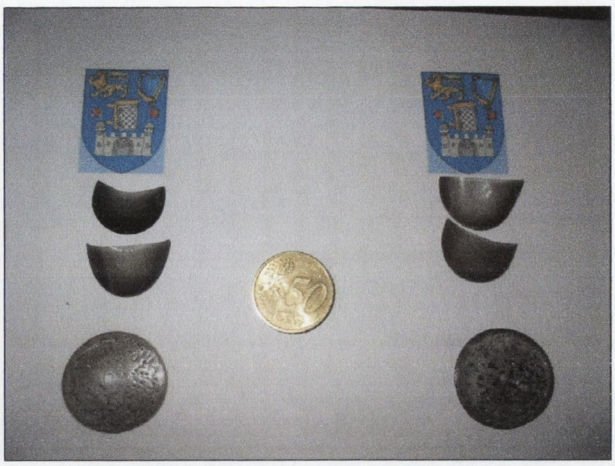

Figure 5.5 A photograph of examples of nanotube-polymer composite films.

Solutions of unfunctionalised nanotubes with chlorinated polypropylene were prepared by the same method using the same concentration of polymers and nanotubes. However, after the twelve hour settling period all pristine nanotubes fell out of solution indicating that they do not form a stable suspension with the polymer. This is shown in figure 5.6 where the difference in nanotube polymer solution stability can be seen between unreacted and chlorinated polypropylene grafted nanotubes. The unreacted original nanotubes aggregate together and fall out of the polymer solution, where as the grafted nanotubes are readily stable in the solution. The unreacted nanotubes are shown in the vial to the far left and the CPP grafted nanotubes are the other three. This is unfortunate as the mechanical properties of the pristine nanotubes in the polymer can not be investigated. However it does show that the non functionalised pristine nanotubes are inherently different in properties from the functionalised nanotubes.

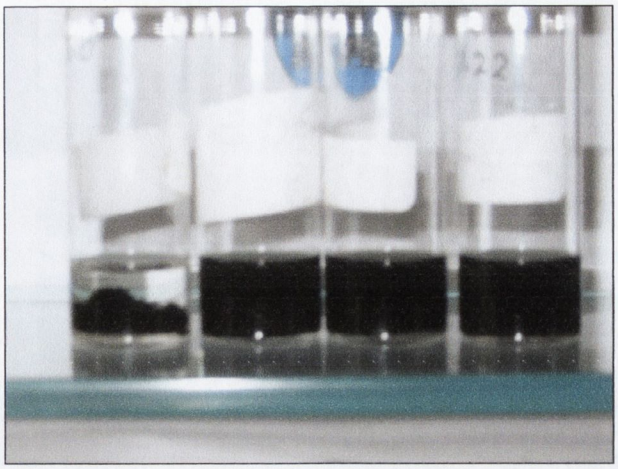

Figure 5.6 A digital image of the difference in THF suspensions for: from the left pure nanotubes in CPP, and varying concentrations of CPP grafted nanotubes to the right

After the polymer nanotube films were prepared, they were cut into strips of 3 and 4 mm in width and ~ 15 mm in length. The mechanical properties of these polymer strips were examined on a Zwick Z100 tensile testing machine. In order to obtain a reference for the pure polymer a 30 g/l solution was made up in an identical fashion to the composite materials. The mechanical properties of the pure polymer were studied initially and the stress/strain graph can be seen in figure 5.7.

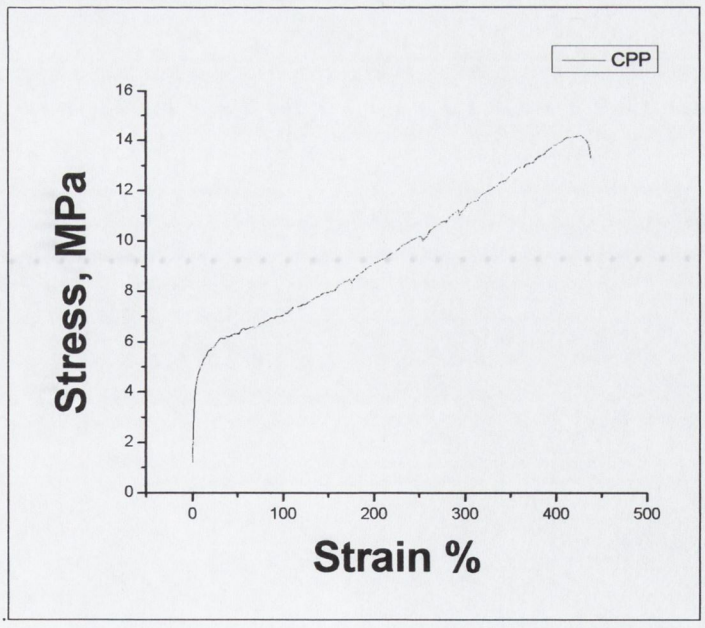

Figure 5.7 Stress strain curve for chlorinated polypropylene.

Chlorinated polypropylene has a Young's Modulus of 0.22 GPa, toughness of 3.6 KJ/m^3 and an UTS, of 14 MPa. The stress strain curve of the original unmodified polymer is shown in figure 5.7. This polymer has the ability to stretch to up to four and a half times its original size this imparts a large toughness value as toughness is a function of modulus and elongation. Upon addition of the CPP functionalised nanotubes to the pure polymer these mechanical properties increase significantly, as can be seen in the stress strain curves in figure 5.8 and table 5.1.

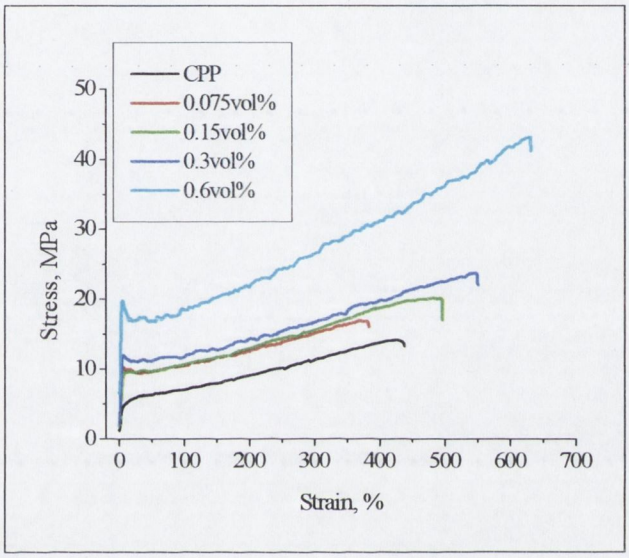

Figure 5.8 Stress strain curves for pure CPP and nanotube-CPP composite materials with a range of nanotube volume fractions.

Table 5.1 Results of mechanical testing for CPP-MWMT composite thin films for each volume fraction (5 films were tested and the results were averaged)

Vol % Of MWNT	Young's modulus [GPa]	Tensile strength [MPa]	Toughness [KJ/m^3]
0	0.22+/-0.26	6.3 +/-0.23	3.6 +/-1.1
0.08	0.21+/-0.14	9.5 +/-0.62	6.7 +/-3.2
0.15	0.30+/-0.03	11.1 +/-0.36	7.5 +/-1.6
0.30	0.32+/-0.6	10.7 +/-0.52	10.6 +/-4.3
0.60	0.68+/-0.11	17.3 +/-0.13	14.0 +/-3.2

A substantial improvement in mechanical properties is observed as the nanotube concentration is increased. On average, as the nanotube content is increased to 0.6 vol.%, the Young's Modulus increases by a factor of 3 compared to the pure polymer from 0.22 to 0.68 GPa. This is significant when compared with previous results. Moreover, both the tensile strength and the toughness (energy required to break) also increase by factors of 3.8 (from 13 to 49 MPa) and 4 (from 27 J/g to 108 J/g), respectively.

As can be seen in figure 5.8, the addition of even very small amounts of the functionalised polymer grafted nanotubes to the polymer matrix causes significant changes in physical properties of the polymer. These results show that the covalent functionalisation of carbon nanotubes enables to achieve both efficient dispersion and excellent interfacial stress transfer. The fact that the pristine nanotubes fell out of CPP in THF solution leads to the conclusion that the un-reacted nanotubes do not form a stable dispersion with the polymer unlike the nanotubes that have reacted with the polymer.

Young's moduli, Yc, for the nanotube CPP composite films as a function of volume fraction are shown in figure 5.9.

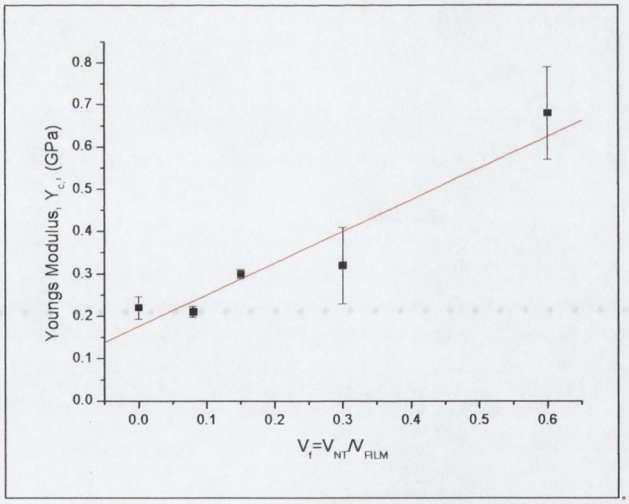

Figure 5.9 Young's modulus as a function of volume fraction for CPP grafted nanotubes.

The modulus increases almost linearly from 0.22 GPa for the pure polymer to 0.68 GPa for the 0.6 vol % sample with a slope of $dY/ dV_f = 0.75$ GPa. At such low concentrations of nanotubes these represent tremendous increases in modulus. Applying Krenchel's rule of

mixtures for short fibre composites as in Chapter 4 (equations 4.1 - 4.5) allows the effective nanotube modulus to be calculated using $Y_{eff} = \eta_l Y_{NT}$. This analysis gives the modulus for CVD nanotubes as 253 ± 20 GPa.

Applying similar methodology, the UTS of the composite materials, σ_c, a graph of σ_c as a function of volume fraction is shown in figure 5.10. The strength increases linearly from 12.5 ±3.0 MPa for the pure polymer to 49 ± 10 MPa for the 0.6% vol sample with a slope of $d\sigma/ dV_f$ = 6.8 ± 0.9 MPa. The increase here is a factor of 3.9 and represent, again, a significant increase for the amount of nanotubes present.

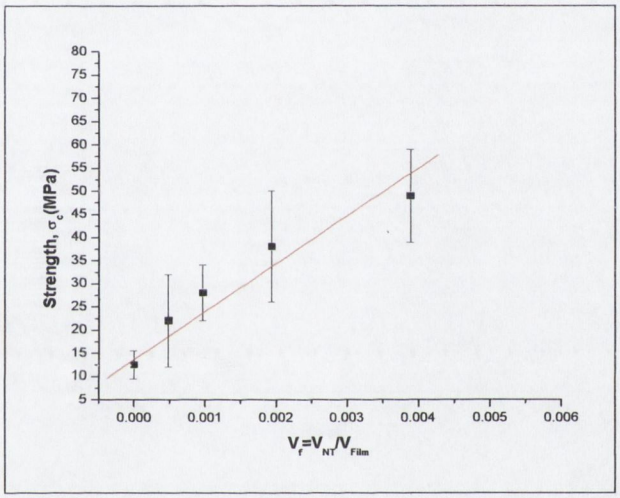

Figure 5.10 UTS as a function of volume fraction for CPP grafted nanotubes.

For the composite materials the UTS increases linearly from 12.5 ± 3.0 MPa for the pure polymer to 49 ± 10 MPa for the 0.6 vol% sample with a slope of $d\sigma/dV_f$ 10.3 ± GPa.

The interfacial stress transfer, τ, can therefore be calculated from a plot of σ_T against v_f, equation 4.6, chapter 4. The outcome of the application of equation 4.6 is that the interfacial stress transfer is 23.9 MPa.

The toughness as a function of volume fraction of the chlorinated polypropylene grafted MWNT increases as shown in figure 5.11

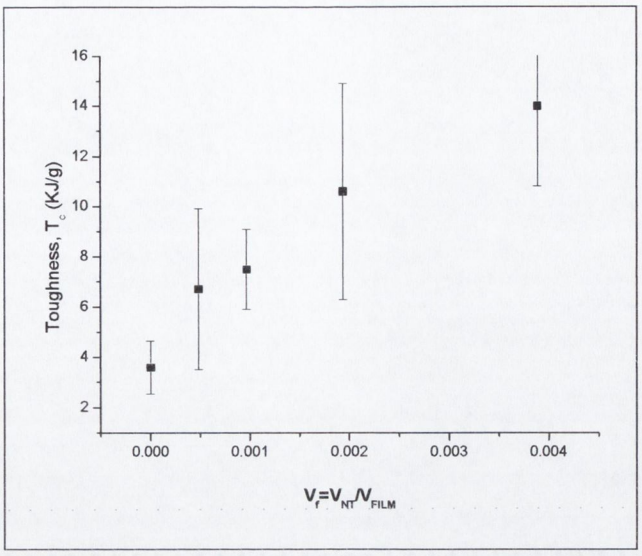

Figure 5.11 Toughness as a function of volume fraction for CPP grafted MWNT in CPP

The toughness increased from 43 ± 10.5 Jg^{-1} for the pure chlorinated polypropylene to a substantial 168 ± 32 Jg^{-1} for the 0.6% composite. This is a 4 fold increase in the overall toughness.

Thus, our studies have clearly demonstrated that MWNTs can be effectively functionalised using *n*-butyllithium and then chemically bonded to chlorinated polypropylene. They have also shown that with the covalent bonding of the polymer to nanotubes not only do the nanotubes become more soluble and stable in solution but also the mechanical properties of the polymer improve significantly.

5.3.1 CPP grafted MWNTs and other polymers composites

After the preparation and investigation of nanotube CPP composites above, other commercially available polymers were blended with the CPP grafted carbon nanotubes. These polymers were polyvinyl chloride (PVC), polystyrene (PS) and chlorinated polyethylene (CPE). The main reasons for the choice of these three other polymers were their wide range of technological applications and high commercial value. Polyvinyl chloride is a very important material for the manufacture of doors, windows, conservatories, building components etc. and any possible increase in mechanical properties would have immediate implications in the construction industry. Polyethylene is

also very technologically important polymer, but it is a difficult polymer to cast from solution due to its very limited solubility in all known solvents. Therefore CPE, which has much better solubility and close in its properties to polyethylene, was chosen. Finally, polystyrene was selected because it is again a very popular and technologically important polymer, which is well soluble in many organic solvents and can be easily processed by solution casting technique.

The objective of this work was to demonstrate the universality of our techniques and to extend it for a wide range of polymer materials. We also planned to compare the CPP grafted nanotubes with pristine nanotubes as additives for reinforcement of different polymer materials.

5.3.1.1 CPP grafted MWNTs in PVC composites

PVC composite materials were prepared in exactly the same manner as for the chlorinated polypropylene composites above. The weight percent concentrations chosen were also the same. The properties of the polypropylene grafted nanotubes in PVC are just as impressive as can be seen in table 5.2.

Table 5.2 Mechanical results for CPP-MWNTs in PVC

Vol % Of MWNT	Young's modulus [GPa]	Ultimate Tensile Strength [MPa]	Toughness [KJ/m³]
0%	0.559 +/-0.07	15.6 +/-0.5	5.46 +/-2.11
0.16%	0.645 +/-0.05	28 +/-5.6	45.3 +/-33.9
0.33%	0.937 +/-0.067	22.6 +/-2.69	14 +/-5.67
0.65%	0.593 +/-0.19	30.6 +/-2.12	56.5 +/-27.9

It was possible to analyse the pristine MWNTs in PVC as they were sufficiently stable in this polymer solution over the twelve hour settling time period. The solvent used for the

film formation was THF which enabled the production of films easily, as THF is a volatile solvent.

Once again applying the equations which we have used previously we can calculate the Y_{NT} of the PPC grafted MWNT in PVC this should be comparable to their value in PPC. The modulus of the nanotubes was calculated as discussed previously, using dY/dV_f from the graph shown in figure 5.12. The calculated Y_{NT} was 328 ± 92 GPa which is comparable to the modulus calculated previously. The point at 0.65 vol % is significantly lower than the other data indicates. This is due to the fact that there is an aggregation of nanotubes at this concentration that results in decrease of the modulus.

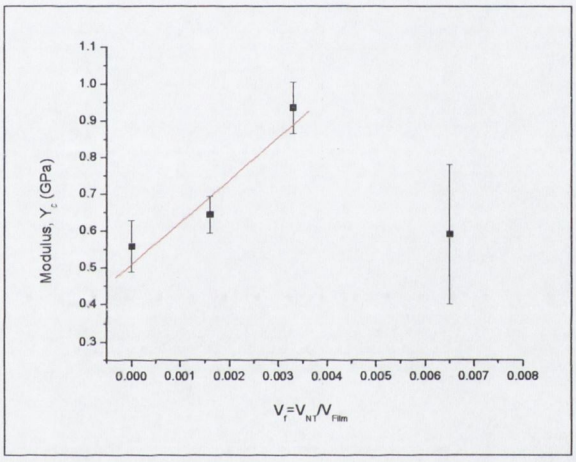

Figure 5.12 Young's modulus as a function of volume fraction for CPP grafted MWNTs in PVC composites.

The plot of the UTS of the PPC grafted nanotubes in PVC composites as a function of volume fraction is shown in figure 5.13. Again the strength increases from 15.6±0.5 MPa to an impressive 30.6± 2.12 MPa which represents a two fold increase compared to the strength of the initial polymer. From this graph $d\sigma/dV_f$ can be calculated to give 2.3± 0.3GPa. The calculated value of τ is 5.36 MPa.

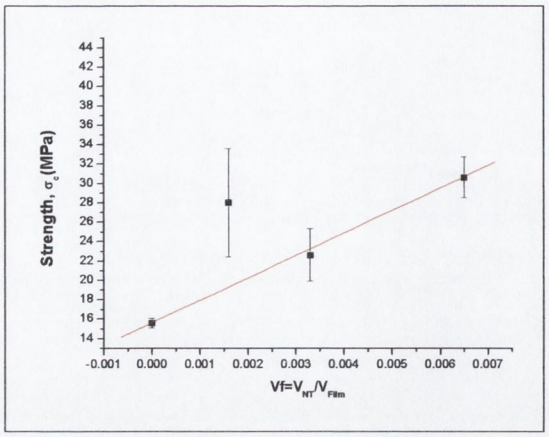

Figure 5.13 UTS graph of CPP grafted nanotubes in PVC composites versus volume fraction.

As is seen in figure 5.14 the toughness of the PVC composites reinforced with CPP grafted nanotubes increases steadily from 0.546 KJ/m^3 to a high 5.65 KJ/m^3. This represents more than a ten fold increase in the toughness of the films.

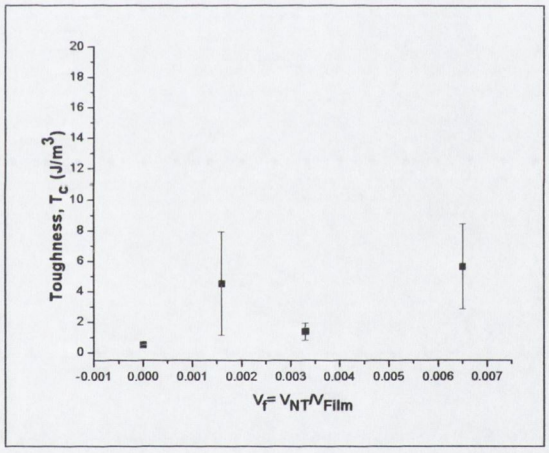

Figure 5.14 Toughness of CPP grafted nanotubes in PVC composite versus volume fraction.

Similar preparations and tests have been performed for pristine MWNTs. As we can see from the table 5.3 and figure 5.15, there is a slight decrease in all mechanical characteristics of PVC composites containing pristine nanotubes. This is more than likely due to the fact that the nanotubes add defects to the polymer matrix and weaken it. In contrast, the addition of the CPP grafted nanotubes (table 5.2) showed a considerable increase in all cases. The Young's modulus increases by a factor of two, the ultimate tensile strength increases by a factor of two and most impressively the toughness increases by a factor of ten. Therefore,

the presence of the CPP grafted nanotubes significantly increases the strength of the composites due to the strong covalent bonding of nanotubes to polymer which provides excellent interfacial stress transfer between nanotubes and polymer matrix.

Table 5.3 Mechanical test results for pristine MWNTs in PVC composites.

Vol % Of MWNT	Young's modulus [GPa]	Ultimate Tensile Strength [MPa]	Toughness [KJ/m^3]
0%	0.559 +/-0.07	15.6 +/-0.5	5.46 +/-2.11
0.16%	0.442 +/-0.17	13.8 +/-2.26	3.88 +/-1.5
0.33%	0.189 +/-0.04	14.3 +/-1.92	3.13 +/-0.4
0.65%	0.389 +/-0.06	12.5 +/-1.68	5.89 +/-3.65

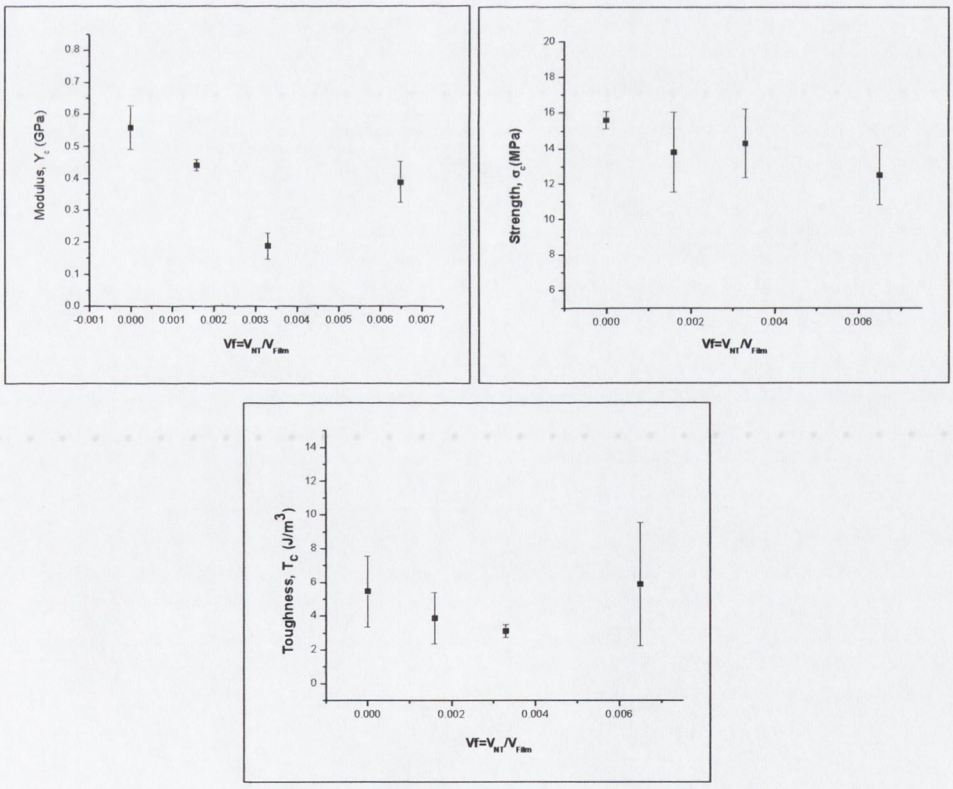

Figure 5.15 Representation of the modulus, UTS and toughness of pristine MWNTs in PVC composites.

5.3.1.2 CPP grafted MWNTs polystyrene composites

Polystyrene nanotube composites have been prepared similarly to above by blending PS solutions in THF with CPP grafted nanotubes. Results of mechanical testing of PS nanotube composites are presented in table 5.4.

Table 5.4 Mechanical test results for CPP-MWNT PS composites.

Vol % Of MWNT	Young's modulus [GPa]	Ultimate Tensile Strength [Mpa]	Toughness [KJ/m³]
0%	0.568 +/-0.04	15.6 +/-5.35	0.3 +/-0.15
0.13%	0.842 +/-0.12	18.2 +/-1.95	0.235 +/-0.02
0.26%	1.16 +/-0.0935	29.3 +/-0.9	0.24 +/-0.09
0.51%	0.846 +/-0.024	17.8 +/-1.82	0.107 +/-0.13

Overall, as we can see from the results in table 5.4, there are no very significant changes in mechanical characteristics of PS nanotube composites in contrast to the nanotube polymer composites considered before. As is shown in figure 5.16 there is a slight increase in Young's modulus of the PS nanotube composite materials. The slope of the graph dY/dV_f allows Y_{NT} to be calculated which is 515 ± 88 GPa this is higher than for the other polymers. This again is well within the expected values for CVD nanotubes.

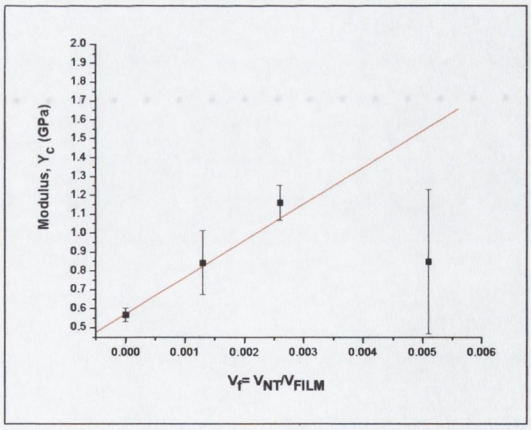

Figure 5.16 Youngs modulus vs volume fraction for CPP grafted nanotubes in PS.

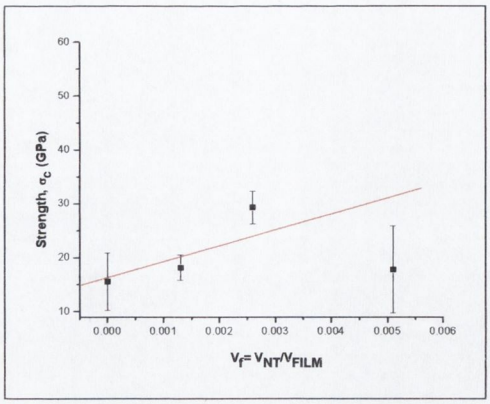

Figure 5.17 The UTS of the composite films versus volume fraction.

Again here in figure 5.17 the UTS increases from 15.6 ± 5.35 MPa for the pure polymer to 29.3 ± 3MPa for 0.26 vol% representing almost a doubling in the UTS. The UTS then returns to near the value for the pure polymer for the 0.51 vol.% however noticeably this vol.% has large error bars therefore this decrease could be due to overloading of nanotube content and aggregation of the nanotubes. Using the line fit and taking the slope of the graph, giving $d\sigma_c/dV_f$, τ is calculated as 6.8 MPa.

The graph of toughness versus volume fraction shows no noticeable change in the size of toughness for any of the composites. Thus the CPP grafted nanotubes do not appear to reinforce polystyrene as strongly as for CPP and PVC polymers. The most plausible explanation for this fact is that PS contains aromatic groups, which are not compatible with CPP coating on the nanotubes. And does not result in an efficient interaction between CPP grafted nanotubes and PS matrix.

A table of pristine MWNTs in PS was presented in chapter 4, table 4.17, and from this table the modulus of the pristine MWNTs in PS increased by close to a factor 2; however both the UTS and toughness decreased.

5.3.1.3 CPP grafted MWNTs in CPE

The CPE composite films were made using chloroform which is quite volatile, making film preparation easy. Once again the composite materials were made in an analogous manner to previously discussed polymers using the same concentrations. The Young's Modulus of the

CPP grafted nanotubes in CPE composites show an increase in modulus of approximately 40%, table 5.5, which is a reasonable increase in modulus but is not as exceptional as would be expected from previous results. The graph in figure 5.18 shows a steady increase in modulus over the concentration range.

Table 5.5 Mechanical test results for CPP-MWNTs in CPE

Vol % Of MWNT	Young's modulus [MPa]	Ultimate Tensile Strength [MPa]	Toughness [KJ/m^3]
0%	3.56 +/-0.175	4.78 +/-0.5	9.17 +/-2.82
0.14%	1.74 +/-0.14	7.74 +/-1.58	19.7 +/-4.05
0.28%	4.68 +/-0.2	8.78 +/-1.6	17.3 +/-3.51
0.57%	4.98 +/-0.4	14.57 +/-1.81	46.3 +/-5.73

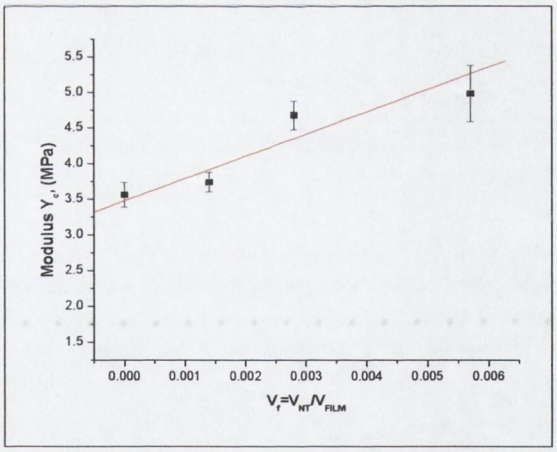

Figure 5.18 Graph of modulus versus volume fraction for CPP grafted nanotubes in CPE.

The UTS steadily increases over the concentration range up to a highly significant 305% when compared to the original polymer, figure 5.19.

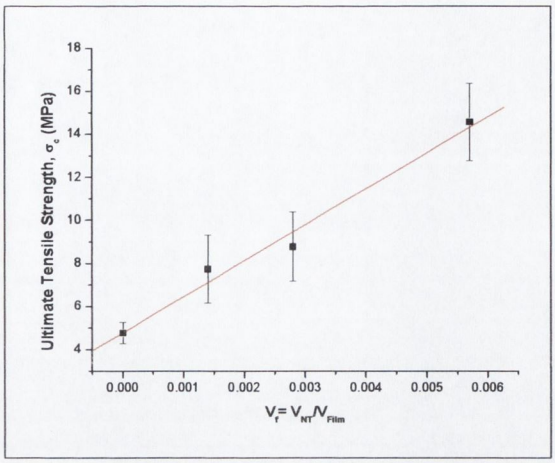

Figure 5.19 Graph of UTS versus Volume fraction.

Once again in the graph of toughness versus volume fraction, figure 5.20 there is a very significant increase as high as 505%. The CPP functionalised carbon nanotubes appear to be reinforcing the CPE to a high degree.

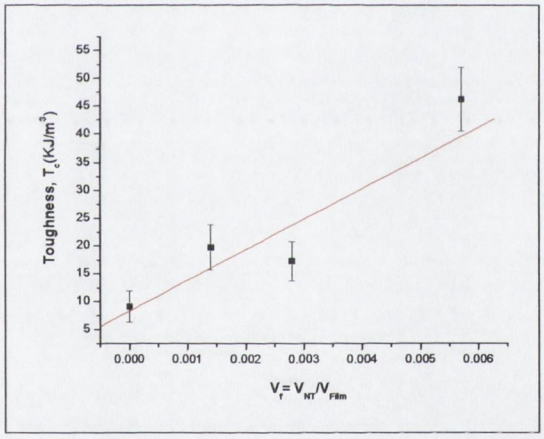

Figure 5.20 graph of toughness versus volume fraction for CPP grafted nanotubes

Samples were also prepared of pure polymer and CPE and the results are listed in table 5.6. The results shown in table 5.6 have figures that are more or less consistent with those of the CPP grafted nanotubes.

Table 5.6 Mechanical results for pristine MWMT in CPE

Weight % Of MWNT	Young's modulus [MPa]	Ultimate Tensile Strength [MPa]	Toughness [KJ/m³]
0%	3.56 +/-0.175	4.78 +/-0.5	9.17 +/-2.82
0.25%	2.19 +/-0.15	8.24 +/-0.24	23.4 +/-0.83
0.5%	2.01 +/-0.75	3.85 +/-1.58	21.1 +/-1.02
1%	3.01 +/-0.63	9.12 +/-2.87	26.2 +/-0.93

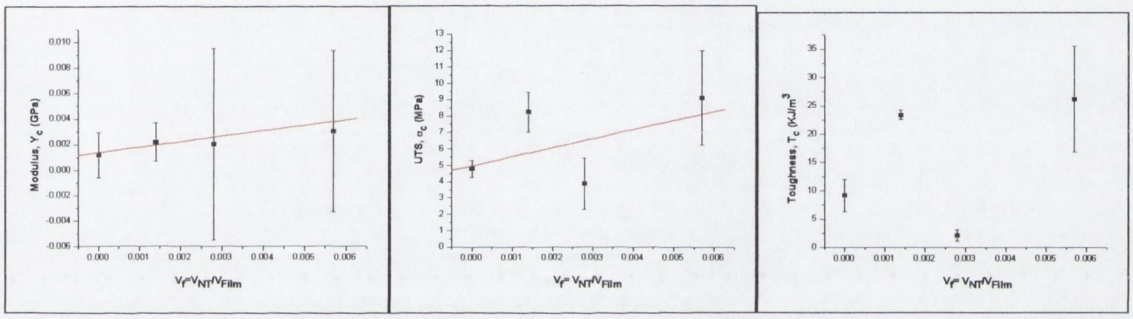

Figure 5.21 modulus, UTS and toughness versus volume fraction for pristine nanotubes in PEC

As is shown in figure 5.21 and table 5.6 there appears to be a slight increase in modulus of the pure nanotubes in CPE as compared to the pure polymer. However, the error bars present are too large to attribute a large increase in modulus due to the nanotubes. There is an apparent increase in strength on the addition of nanotubes which increases by 190%. Again there are large error bars for the composite material which could represent a smaller increase. The significant increases in the mechanical properties of the CPP grafted nanotubes reinforced CPE films must be attributed to the fact that the nanotubes are covalently bonded to the CPP which is interacting with the CPE to a large degree.

5.3.1.4. Differential Scanning Calorimetry (DSC) results

DSC was performed on the polymer composite samples of PS, PVC and CPE in order to make sure that addition of carbon nanotubes to the polymer did not change the crystallinity that would result in dramatic changes in mechanical properties.

In each case polymer DSC was carried out on; the pure polymer and the polymer with CPP grafted MWNTs. Each nanotube polymer composite tested by DSC had the highest mass percentage of nanotubes in polymer. The DSC curves are presented in appendix 5.1. The curves were analysed and the thermal transitions of the polymer and nanotube-polymer composites were measured. These include the glass transition temperature (T_g), crystalline temperatures (T_c), and melting temperatures (T_m) shown in table 5.7.

Table 5.7. DCS results for selected nanotube-polymers composites

Polystyrene	
Type of sample	Tm °C
Pure polymer	104
Polymer with CPP functionalised carbon nanotubes	102
Poly (vinyl chloride)	
Pure polymer	88
Polymer with CPP functionalised carbon nanotubes	88
Chlorinated polypropylene	
Pure polymer	98
Polymer with CPP functionalised carbon nanotubes	98

Any molecular parameter affecting chain mobility affects the T_m. As we can see from the results there is no significant change in the glass transition of the polymer when pristine MWNTs and CPP grafted MWNTs were added separately to the polymer. The addition of the nanotubes does not change the crystallinity of the polymer which in turn may affect the mechanical strength of the composite. It has been shown that an increase in NTs in a selected polymer can lead to an increase in the polymer's crystallinity which will reinforce a polymer by up to a factor of 4.[9] It is now known that any change in mechanical properties of the polymers is due to the addition of the NTs.

The melting process is a first order endothermic thermal transition and causes a much more dramatic change in the DSC curve than the glass transition. Another transition which can

sometimes occur between the glass transition and melting is called cold crystallization and the temperature at which this occurs is denoted T_c. This represents a net output in energy resulting in an exothermic peak. There are no significant changes in the melting point or the cold crystallisation when the polymer CPP grafted MWNTs were added to the polymer. This shows again that the physical properties of a substance when measured as a function of temperature do not change upon addition of functionalised NTs.

Appendix 5 shows the DSC graphs taken for the range of polymers. We can see the thermal transitions occur at the same temperature.

5.3.2. PVC grafted nanotubes

5.3.2.1 Preparation of PVC grafted MWNTs

The aim of this experiment was to prepare PVC grafted MWNTs. The lithiated MWNTs were reacted with PVC in the same way as for the CPP functionalised nanotubes. Freshly prepared and washed lithiated nanotubes were treated with a solution of degassed PVC in THF at 263 K. Then the mixture was allowed to warm to room temperature over twelve hours. The precipitate was then washed with dry THF and then with deionised water until the water was colourless. The remaining powder was dried in vacuum for 10 hrs.

TEM analysis of the product (figure 5.22) showed polymer coated carbon nanotubes. The second image on the right shows that of the pure polymer under TEM. It can be easily seen that the polymer forms quite smooth and uniform coating on the nanotubes. By contrast mechanical mixture of PVC and pristine nanotubes gave non uniform coating of PVC on the nanotubes with the formation of polymer globules the walls of the nanotubes. (figure 5.23).

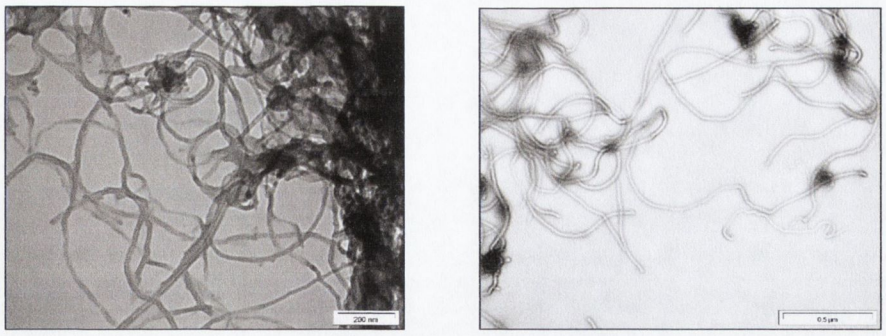

Figure 5.22 TEM images of PVC grafted MWNTs (left) and pure untreated nanotubes (right).

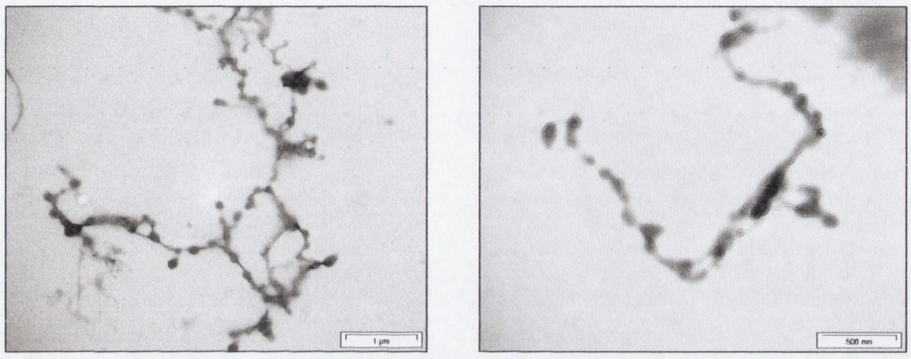

Figure 5.23 TEM images of mechanical mixure of pure polymer with pristine nanotubes.

Elemental analysis of a sample of PVC grafted nanotubes has shown 2.88% of hydrogen. This was identified as the polymer's and butyl group's hydrogen. IR spectroscopy has shown C-H bands at 1425, 1345 and 2920 cm^{-1}. TGA (figure 5.24) showed the presence of two peaks one at 184 °C which represents the polymer and the other at 440 °C which is attributed to the MWNTs. Noticeably the MWNT peak has shifted down from the original 559 °C due to the functionalisation of the nanotubes.

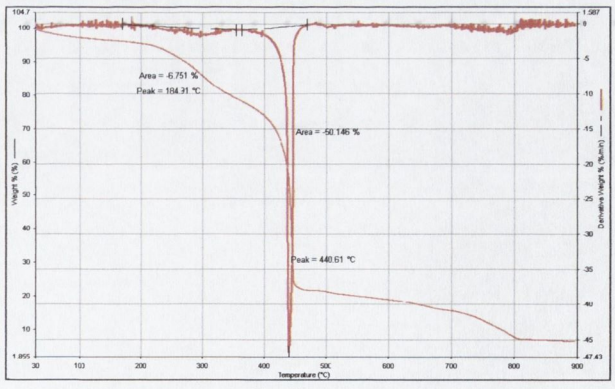

Figure 5.24 TGA curve of PVC grafted MWNTs.

The PVC grafted nanotubes were then mixed, in the same manner as for CPP grafted nanotubes, with the pure PVC polymer in THF at the same concentrations. As well as this there was an attempt to use the PVC grafted nanotubes as additives to other polymers: CPP, PS and CPE. However, it was not possible to produce films of suitable quality for mechanical testing for these polymers. The reason of that was very poor solubility of the PVC grafted nanotubes in the polymers solutions.

5.3.2.2 PVC grafted nanotubes in PVC

The PVC grafted nanotubes were mixed with the pure PVC and polymer composite films have been prepared in the same manner as described above for the CPP grafted nanotubes. The results of mechanical testing are presented in the table 5.7. The increase, observed, in Young's modulus (table 5.8) was not as impressive as was expected; an addition of 0.16% of PVC grafted nanotubes gave a 36% increase in the Young's modulus.

Table 5.8 Mechanical properties of PVC grafted nanotubes in PVC

Weight % Of MWNT	Tensile modulus [GPa]	Ultimate Tensile Strength [MPa]	Toughness [KJ/m^3]
0%	0.559 +/-0.07	15.6 +/-0.5	5.46 +/-2.11
0.16%	0.762 +/-0.055	21.2 +/-2.67	17.9 +/-4.93
0.33%	0.65 +/-0.05	16.2 +/-2.46	7.91 +/-3.02
0.65%	0.427 +/-0.09	14.4 +/-2.66	36.7 +/-2.39

The values for Young's modulus were plotted against volume fraction dY/dV_f (figure 5.25). The calculated Y_{NT} the modulus of the PVC functionalised was found to be 50 GPa. The data point for 0.65% vol is significantly lower than the other points as well as being associated with large error bars. This is disappointingly low as compared with the CPP grafted nanotubes however still within the value for CVD nanotubes.

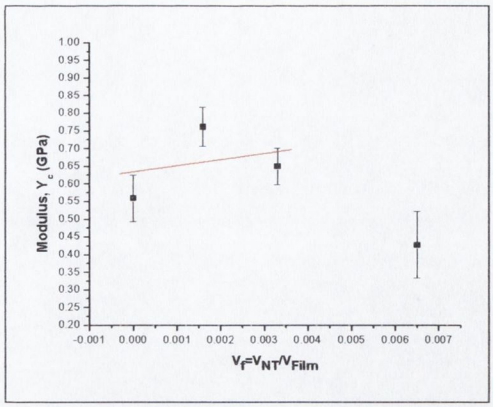

Figure 5.25 Modulus versus volume fraction for PVC grafted nanotubes in PVC

The UTS also fails to increase as much as expected, with the 0.25% concentration of PVC grafted MWNTs there is an increase in UTS of just 36%. After considering the graph of strength versus the volume fraction (figure 5.26) it is easy to see that the low volume fraction has large error bars and that the overall trend in the samples is that there is no increase in the overall strength of the composites.

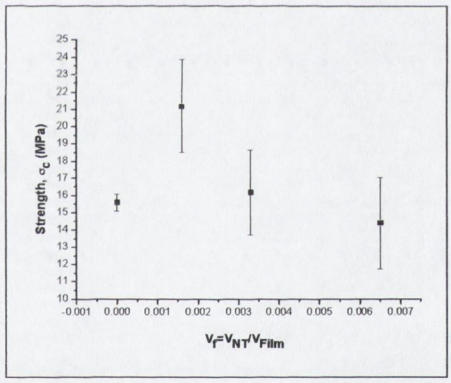

Figure 5.26 Tensile strength versus volume fraction for PVC grafted nanotubes in PVC.

The large increases are present in toughness where in the 0.16% there was a 328% increase in toughness and in the 0.65% volume concentration there was a 672% increase in toughness. Again plotting these values against the volume fraction it can be seen, figure 5.27, that there is an increase in the overall toughness even though there are large errors associated with these values. Although there is an increase in the mechanical properties of the grafted PVC composites the increase is not as substantial as that of the CPP grafted nanotube composites. This is possibly due to the fact that the chlorine of the PVC molecule

is not very reactive and can not be readily substituted as that of the chlorinated polypropylene. Therefore there is a lack of covalent bonding between polymer and nanotubes which results in poor interfacial stress transfer.

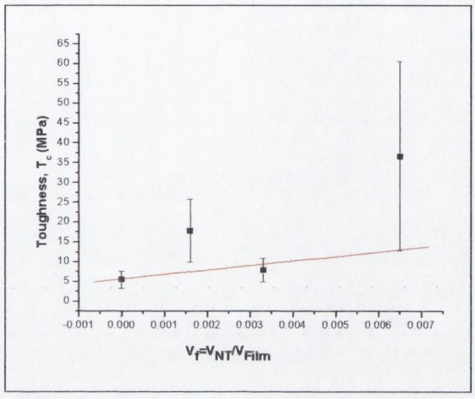

Figure 5.27 Toughness versus volume fraction for PVC grafted nanotubes in PVC.

The mechanical properties of pristine MWNT in PVC are presented in table 5.9 and in figure 5.28. As we can see the mechanical characteristics of PVC pristine nanotubes composite are in general worse than those of the pure polymer. The pristine MWNT in PVC seem to be disrupting the polymer matrix and decreasing the strength of the composite as was identified previously.

Table 5.9 Mechanical properties of pristine MWNT in PVC

Vol % Of MWNT	Tensile modulus [GPa]	Ultimate Tensile Strength[GPa]	Toughness [KJ/m^3]
0%	0.559 +/-0.07	15.6 +/-0.5	5.46 +/-2.11
0.16%	0.442 +/-0.17	13.8 +/-2.26	3.88 +/-1.5
0.33%	0.189 +/-0.04	14.3 +/-1.92	3.13 +/-0.4
0.65%	0.389 +/-0.06	12.5 +/-1.68	5.89 +/-3.65

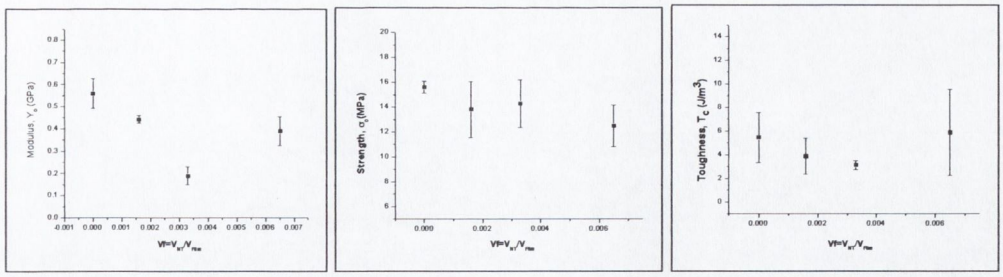

Figure 5.28. Representation of the modulus, UTS and toughness of pristine nanotubes in PVC

5.3.3 Chlorinated polypropylene grafted SWNTs

SWNTs are expected to impart greater strength to polymers than their multi walled counterparts. The reason for this is that they are more structurally sound than the MWNTs because they are a pure single tube as opposed to the multi-tube structure of MWNTs. Therefore, CPP grafted SWNTs have been prepared in similar manner and investigated as additives for polymer reinforcement. The SWNT were lithiated using an excess of n-butyl lithium in THF at 263 K in an inert atmosphere and allowed to heat to room temperature over a twelve hour period. Once lithiated the nanotubes were washed with dry hexane and THF. The nanotubes were then placed in dry THF and reacted with a degassed solution of CPP. The IR spectrum was similar to that of the multi-walled nanotubes. Characteristic CH bands of the polymer and butyl groups were found at 1430, 1350 and 2980 cm^{-1}.

The TGA (figure 5.29) shows two peaks at 325.5 and 557.5 °C corresponding to the polymer and the nanotubes respectively.

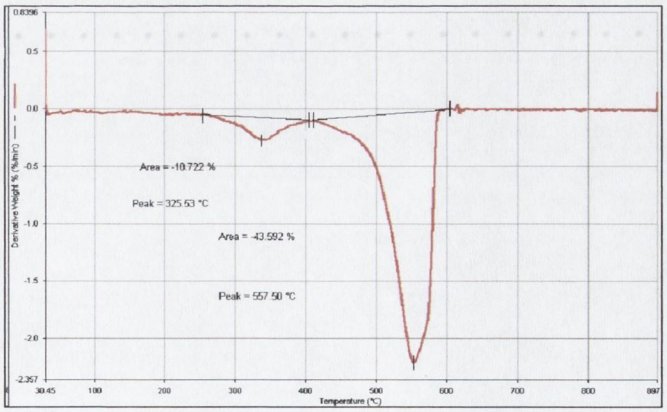

Figure 5.29 TGA of CPP grafted SWNTs

TEM images of CPP grafted SWNTs are shown in the figure 5.30. There is a clear coating of polymer around the SWNT ropes, however no single nanotubes can be identified in these images.

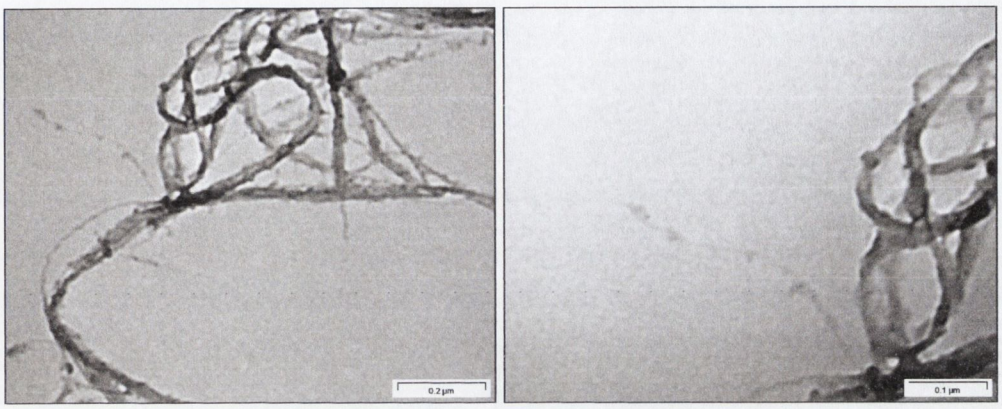

Figure 5.30 TEM images of SWNT-CPP bound ropes.

Composites of CPP grafted SWNTs in CPP were prepared in the same fashion as for the MWNTs using the same solvent and concentrations. However, as can be seen from table 5.10 of mechanical strength results, the expectations of good mechanical properties from SWNTs were ill founded.

Table 5.10 Mechanical test results for CPP-SWNT composite thin films. For each volume fraction, 5 films were tested and the results averaged.

Vol % On MWNT	Tensile modulus GPa]	Tensile strength[MPa]	Toughness [KJ/m^3]
0	0.22 +/- 0.26	6.3 +/- 0.23	3.6 +/- 1.1
0.08	0.17 +/- 0.13	5.1 +/- 0.89	4.1 +/- 1.4
0.15	0.26 +/- 0.09	5.9 +/- 0.29	3.1 +/- 0.78
0.30	0.26 +/- 0.16	6.3 +/- 0.14	3.5 +/- 1.6
0.60	0.19 +/-28	6.8 +/- 0.56	3.2 +/- 1.2

The explanation for the uninspiring results was that single walled nanotubes have a tendency to form strong bundles via π -π interaction.[10] When stress is applied to SWNT ropes, the nanotubes slide inside in the bundles, this results in very poor mechanical properties. According to G. Viswanathan *et al*[11] sec-butyl lithium has the ability to disrupt

bundles by charging each of the nanotubes which then repel each other. It was thought that this repulsion would keep them apart and that after they had reacted with the polymer they would be held apart by the polymer matrix. However, it seems the lithiation of nanotubes did not debundle SWNTs enough or after reaction with the halogenated polymer the charge disappears and the nanotubes bundle. Therefore, when SWNTs react with the halogenated polymer this resulted in the polymer coating the SWNT bundles, but not individual nanotubes. This was also confirmed by TEM images above.

Due to the reasons above and the uninspiring initial results of mechanical testing it decided to abandon work on SWNT composites.

5.4 Conclusions

We have demonstrated that carbon nanotubes can be functionalised using halogenated polymers and subsequently used as additives to improve the mechanical properties of different polymers. Lithiated carbon nanotubes have been shown to be very good precursors for functionalisation of the carbon nanotube surfaces and for the preparation of nanotube polymer composite materials.

Polymer samples of CPP, PVC, PS and CPE were chosen for the preparation and characterisation of CPP grafted nanotube polymer composites. DSC tests on these CPP grafted nanotube polymer films showed that the addition of the nanotubes did not change the crystallinity of the polymer, which in turn may affect the mechanical strength of the composite. It is now known that any change in the mechanical properties of the polymers is due to the addition of the functionalised NTs.

Plots of mechanical characteristics of CPP grafted nanotube-polymer composites versus mass fraction of nanotubes have shown that there is possibly a critical mass fraction for an optimum increase in tensile strength for every polymer type. CPP grafted nanotubes demonstrated the most significant increase in the mechanical properties of all polymers. In general the increase was much higher than for pristine nanotubes in polymer composites. However, we found that the effect of polymer grafted nanotubes on mechanical properties strongly depends on the nature of the polymer material selected.

The addition of CPP functionalised nanotubes in the CPP polymer improved all its mechanical characteristics at least by a factor of three. In PVC the CPP functionalised nanotubes improve the polymers mechanical characteristics by close to a factor of two. Again in PS the CPP functionalised nanotubes increase the polymer by close to a factor of two. In CPE the CPP functionalised nanotubes increase the polymers mechanical properties only slightly.

The addition of PVC functionalised nanotubes slightly improved the mechanical properties of the pure PVC polymer, but did not have such a strong impact as CPP grafted nanotubes.

We believe that the reaction between lithiated nanotubes and PVC does not provide sufficient covalent bonds between PVC and carbon nanotube surface, due to the low reactivity of chlorine in PVC. This and also low solubility of PVC grafted nanotubes result in poorer performance of these nanotubes in polymer reinforcement comparatively to CPP grafted nanotubes.

In this project we have also affirmed the theory that SWNTs are unsuitable for polymer reinforcement due the SWNTs affinity for bundle formation, which does not allow sufficient stress transfer due to sliding of SWNTs in the bundles.

5.7 References

[1] E. Dujardin, T.W. Ebbesen, A. Krishnan, P.N. Ylanilos, M.M.J. Treacy, *Phys. Rev. B Solid State,* **58,** 14013, (1998)

[2] M.F. Yu, B.S. Files, S. Arepalli, R.S. Ruoff, *Phys. Rev. Lett.* **84**, 5552, (2000)

[3] B. Dalton, S. Collins, E. Muñoz, J.M. Razal, V.H. Ebron, J.P. Ferraris, J.N. Coleman, B.G. Kim, R.H. Baughman, *Nature,* **423**, 703, (2003)

[4] M. Cadek, R. Murphy, B. McCarthy, A. Drury, B. Lahr, R.C. Barklie, M. in het Panhuis, J.N. Coleman, W.J. Blau, *Carbon,* **40,** 923, (2002)

[5] J.N. Coleman, D.F. O'Brien, M. in het Panhuis, A.B. Dalton, B. McCarthy, R.C. Barklie, W.J. Blau, *Synth. Met.,* **121,** 1229, (2001)

[6] M.S.P. Shaffer, K. Koziol, *Chem. Commun.*, 2074, (2002)

[7] D. Hulicova, K. Hosoi, S. Kuroda, H. Abe, A. Oya, *Adv. Mater.*, **14**, 452, (2002)

[8] A. Garg, S.B. Sinnott, *Chem. Phys. Lett.*, **295,** 273, (1998)

[9] K. P. Ryan *PhD Thesis,* Trinity College Dublin, (2005)

[10] A. Thess, R. Lee, P. Nikolaev, H. Dai, P. Petit, J. Robert, C. Xu, Y.H. Lee, S.G. Kim, A.G. Rinzler, D.T. Colbert, G.E. Scuseria, D. Tomanek, J.E. Fischer, R.E. Smalley, *Science,* **273,** 483, (1996)

[11] G. Viswanathan, N. Chakrapani, H. Yang, B. Wei, H. Chung, K. Cho, C. Ryu, P. Ajayan, *J. Am. Chem. Soc.,* **125,** 9258, (2003)

Chapter 6

Experimental Procedures

6.1 General procedures

The transmission electron microscopy (TEM) images were taken on a Hitachi H-7000 microscope. The TEM was operated at a beam voltage of 100 kV. Samples for TEM were prepared by deposition and drying of a drop of the powder dispersed in ethanol onto a formvar coated 400 mesh copper grid. Samples for high resolution transmission electron microscopy (HRTEM) were analysed on a Tecnai F 20. The samples were prepared by dropping solutions of either ethanol or chloroform on lacey carbon grids. The scanning electron microscopy (SEM) images of the samples were obtained using an Hitachi S-4300 scanning electron microscope, which was operated at 5.0 kV. Room temperature Raman and PL spectra were measured with a Renishaw 1000 micro-Raman system. The excitation wavelength was 514.5 nm from an Ar^+ ion laser (Laser Physics Reliant 150 Select Multi-Line) with a typical laser power of ~ 20 mW in order to avoid excessive heating. The 100x magnifying objective of the Leica microscope was capable of focusing the beam into a spot of approximately 1 μm diameter. Fourier transform infrared (FT-IR) measurements were performed in transmission mode using a Digilab FTS-6000 spectrometer with the sample placed in the main chamber, using Perkin-Elmer micro-sampling attachment, and in the positional stage of UMA 500 IR microscope. For measurements in the main chamber a wide band Mercury Cadmium Telluride (MCT) detector in the wave number range of 450-6000 cm^{-1} and a resolution of 2 cm^{-1} and 8 cm^{-1} was used. A narrow band MCT detector with spectral range of 4500-750 cm^{-1} was used in the UMA 500 IR microscope. Thermo-gravimetric analysis (TGA) was carried out on a Perkin Elmer Pyris 1 TGA machine the temperature range was from 30 ° to 900 °C under flowing air and the temperature was increased by 10 ° every minute. Morphology and thermal properties of the composites were studied by differential scanning calorimetry (DSC) using a Perkin Elmer Diamond DSC power compensation instrument. Scanning rate was 40 K/min where 10 mg of each sample was measured and analyzed. The sedimentation machine is composed of four LED lights which were held in position in a box which can fit a $1cm^3$ cuvette. Through this there is a light detector which was connected to a program on a computer. This program would record light received against time. The frequency of the light emitter could be changed by the user as well as the duration of the program. I_0 was calculated by using a solution of pure THF.

XPS measurements were carried out using LAS-3000 (RIBER, France) in Vilnius University. The residual pressure in analysis chamber was 2 10^{-10} torr. The photoelectrons were excited by Al K_α radiation (hν=1486.6 eV). The photoelectrons were analyzed with MAC 2 analyzer system (double-pass cylindrical mirror analyzer). The analyzer energy scale was calibrated using the spectrometer work function such that Au $4f_{7/2}$ = 83.8 eV. In this case the position of C 1s was 284.6 eV (adsorbed surface contamination on Au). Graphite sample (fresh cleaved surface) was analysed first and found C 1s line position to be at binding energy 284.3 eV (bond C-C). This binding energy was taken as the reference for all samples. An energy step width of 30 meV and dwell time of 200 ms was used for narrow scan of peaks Sn 3d, Pb 4f, Si 2p C 1s. An energy step width of 50 meV and dwell time of 200 ms was used for narrow scan of peaks Cl 2p, O 1s. Typically 5 scans were accumulated for each spectrum. Fitting and deconvolution of the spectra were performed by XPSPEAK41 software.

6.2. Experimental for Chapter 2: Preparation, purification and metallation of carbon nanotubes

6.2.1 Preparation and purification of nanotubes

Nanotubes were prepared using the arc-discharge method in a Kratschmer Huffmann generator. The optimum conditions that have been published by Cadek *et al.*[1] were followed. The Kratschmer generator consisted of a cylindrical steel chamber with dimensions of 300 mm in length and 100 mm in diameter. Two graphite electrodes were enclosed in the chamber. The anode was a larger electrode of 99.5% purity and 6.1 mm in diameter. The moveable cathode was graphite of 99.998% purity and was 4.6 mm in diameter. The chamber was water cooled evacuated and filled with He gas and maintained at the current pressure of 500 Torr. A DC current was applied to the electrodes while they were touching before separating them in order to form the arc. The electrodes were separated until there was a drop of 23 V and this was maintained by constantly and consistently separating the electrodes. The nanotubes are formed by sublimation of carbon from the cathode, and deposited on the anode. The quality of the nanotube production can

be estimated at this stage. If the deposit contains a high concentration of nanotubes it will be silver in colour and have a series of repeating parallel groves around the outside of the deposit. The hard deposit was removed from the anode and cut open using a blade. The soft black inner core is then removed and divided into a consistent fine powder by removing as many large erroneous particles as possible. This powder was then purified through the methods below. The curly MWNTs were purchased from Nanocyl company. Poly(m-phenylenevinylene-co-2,5-dioctyloxy-p-phenylenevinylene) (PPV) was synthesised using the Horner polycondensation method and was obtained from the Physics Department, TCD.

Purification method 1[1]

The host polymer used was poly(m-phenylenevinylene-co-2,5-dioctyloxy-p-phenylenevinylene) (PPV) and was produced using the Horner polycondensation method. PPV and toluene were mixed to give a 16.7 g/L solution. This solution was sonicated for 1 min. using a high power sonic tip and then approximately 20 mg of MWNT soot from the same batch was added. The resulting composite solution was sonicated for 1 min using the sonic tip, and then for 2 hours in a low power (60 W) sonic bath to ensure good dispersion and homogeneity. The solution was then left to settle for 48 hours to allow any impurities to fall out as sediment. For each sample the resulting suspension was separated from the sediment by decantation.

The MWNT were retrieved from the polymer using Buchner filtration using a polychlorotrifluoroethylene filter with a pore size of 0.45 microns over a sintered glass frit. The decanted solution (10 ml) was mixed thoroughly with toluene (250 ml) and sonicated for 1 minute at low power (20%). The deep green/blue solution was then quickly filtered leaving a black residue of MWNT on the filter paper and creating a yellow filtrate, indicating the presence of the polymer and the absence of MWNT. The residual PPV was then removed from the precipitate by repeated washings with toluene, until the emerging solvent was colourless. The purified MWNT were then sonicated at low power in ether, then poured into a large Petri dish and allowed to dry in air. TEM was then used to check the purity *i.e.* lack of soot. Yield in 8.6 mg and 20 wt %.

Purification method 2[2]

Raw MWNT (20 mg) soot was heated at 120 °C under reflux in a HNO_3 solution (200 ml, 2.8 M) for 12 hr. The solution was filtered using a sintered glass funnel and washed with distilled water several times, followed by drying at 100 °C for 12 hr. The dried sample was then heated in air at 550 °C for 1 hr. Yield 3.8 mg and 19 wt%. Which were then prepared for analysis by IR and TEM.

IR: 878, 1598, 1668, 3417 cm^{-1}

Purification method 3[3]

20 mg of the raw material was first ultra-sonicated and heat-treated to disperse the MWNTs, followed by immersing them in bromine water at 90 °C for 3 hr. Then the residual substance was heated in air at 520 °C for 45 min. The black product was soaked in hydrochloric acid 15 ml, 1 M at room temperature to remove iron particles. Finally, the sample was washed with de-ionised water 4x20 ml. The product was dried at 120°C for 12 hr. Yield in 6.79mg and 34 wt%

They were then prepared for analysis by IR and TEM.

IR: 869, 1586, 1663, 3417 cm^{-1}

Annealing of the nanotubes

The above purified nanotubes were placed in a porcelain boat which was put into a CVD machine that was used to anneal at 500 °C under flowing argon at 0.7 s/m for 1 hr. Then the nanotubes were allowed to cool under flowing argon for a further two hours. Yield is 99.9 wt % of initial product added. The MWNT were then prepared for analysis by IR.

6.2.2 Metallation of Carbon Nanotubes

All manipulations were carried out under a vacuum or argon atmosphere using standard Schlenk techniques. Organic solvents were dried and distilled over a sodium-potassium alloy under argon prior to use and then condensed into a reaction flask under vacuum shortly before use. The BuLi in hexane, $AuBr_3$, $SnCl_4$, $SnBr_2$, $PbBr_2$, $GeCl_4$ and $SiCl_4$

were obtained from Aldrich used without further purification and stored under argon when appropriate.

Argon gas was purchased from BOC Gases, Ireland and was dried using P_2O_5/ glass wool columns.

Lithiation of MWNTs *(Procedure 1)*

A small sample of purified annealed MWNTs (50 mg) was placed in a clean dry Schlenk vessel under argon. This was then evacuated to remove any residual air and then heated using a heat gun up to 250 °C to remove any residual water or other volatile contaminants from the reaction vessel. Dry and degassed THF, 20 ml, were added to the sample and the mixture was then sonicated for 30 min under argon in an ultrasonic bath. Then the suspension was cooled to –10 °C using an acetone ice bath. n-BuLi, 30 ml of 1.6 M-solution, was added to the suspension at –10 °C and the mixture was allowed slowly to warm to room temperature and this was stirred for 12 hours. The suspension was then allowed to settle and the THF solution was removed by cannula filtration and the precipitate was washed with dry THF, 2x25 ml, and then dry hexane, 2x25 ml. The product was dried under vacuum for 24 hr. Lithiated nanotubes were stored in THF under Ar for further use.

Lithiation of MWNTs using *t*-BuLi was carried out analogously.

Lithiation of SWNTs *(Procedure 2)*

Lithiation of SWNTs was performed analogously to MWNTs above using a sample of SWNTs as opposed to MWNTs.

Reaction of lithiated MWNTs with metal halides

Reaction with $AuBr_3$ (Procedure 3)

15 mg of the lithiated nanotubes were dispersed in dry THF, 20 ml, using an ultrasonic bath (30 min). Then $AuBr_3$ 0.16 g ($3.7*10^{-4}$ mol) was added to the lithiated nanotubes at -10 °C. The mixture was stirred for 24 hours and then it was left for precipitation for 12 hr. The THF solution was decanted and the precipitate was washed with dry THF and then with

deionised water until the water was clear. The remaining powder was dried in vacuum for 1 day. Yield was 31 mg .

Raman, IR: see section 2.3.4.1

Reaction with $SnCl_4$

Reaction was performed analogously to *procedure 3* above using $SnCl_4$, 221 mg, $0.86*10^{-3}$ mol, instead of $AuBr_3$. Yield was 26 mg.

IR, Raman: see section 2.3.4.2

Reaction with $SnBr_2$

Reaction was performed analogously to *procedure 3* using $SnBr_2$, 373 mg, $1.35*10^{-3}$ mol, instead of $AuBr_3$. Yield was 46 mg.

IR: 2913, 1421, 1356, 1090, 983, 897,363 cm^{-1}

Raman: see section 2.3.4.3

Reaction with $PbBr_2$

Reaction was performed analogously to *procedure 3* using $PbBr_2$, 381 mg, $1.04*10^{-4}$ mol, instead of $AuBr_3$. Yield was 43 mg

IR, Raman: see section 2.3.4.4

Reaction with $SiCl_4$

Reaction was performed analogously to *procedure 3* using of $SiCl_4$, 289 mg, $1.7*10^{-3}$ mol, instead of $AuBr_3$. Yield was 38 mg

IR, Raman: see section 2.3.4.5

Reaction of lithiated SWNTs with metal halides

In the case of lithiated SWNTs and metal halides all reactions were performed analogously to procedure 2 using the same quantities of reactants as for the MWNTs. As well as this the same metal halides were attached to the SWNTs: $SnBr_2$, $PbBr_2$ and $GeCl_4$

Reaction of lithiated SWNTs and $SnBr_2$

Procedure 2 was followed analogously using $SnBr_2$, 373mg, $1.35*10^{-3}$ mol. Yield was 30 mg.

IR, Raman: see section 2.3.4.7

Reaction of lithiated SWNTs and $PbBr_2$

Procedure 2 was followed analogously using $PbBr_2$, 381 mg, $1.04*10^{-4}$ mol. Yield was 38 mg.

IR, Raman: see section 2.3.4.8

Reaction of lithiated SWNTs and $GeCl_4$

Procedure 2 was followed analogously using $GeCl_4$, 279 mg, $1.3*10^{-3}$ mol. Yield was 23 mg

IR, Raman: see section 2.3.4.9

6.3. Experimental for Chapter 3: Reaction of lithiated nanotubes and alkyl halides

Reaction with 1-bromooctane (Procedure 4)

Lithiated MWNTs (50 mg) in dry THF (20 ml) were placed under ultrasound for 30 min to form a suspension. Then the mixture was cooled to -10 °C using an acetone ice-bath. 1-bromooctane 0.75 ml (0.004 mol) was added to the suspension of MWNTs. The mixture was stirred for 24 hours. The precipitate was then washed several times with dry THF and then with deionised water until the water was clear. The residue was then dried in a vacuum for 12 hr. Yield was 64 mg .

IR: 2913, 2364, 1589, 1421, 1356, 1090, 978, 897cm^{-1} **TGA:** see section 3.4.1

Reaction with 1-bromodecane

The reaction was performed analogously to *procedure 4* using 1-bromodecane 1 ml (0.005 mol) and lithiated MWNTs 50 mg. Yield was 56 mg.

IR: 2913, 2369, 1603, 1424, 1363, 1093, 978, 879cm^{-1}

TGA: see section 3.3.1.2

Reaction with 1-bromohexadecane

The reaction was performed analogously to *procedure 4* using 1-bromohexadecane 1.5ml (0.005 mol) and lithiated MWNTs 50 mg. Yield was 63 mg.

IR: 2923, 2363, 1594, 1411, 1344, 1103, 971, 873cm^{-1}

TGA: see section 3.3.1.3

Reaction with 1-bromodocosane

The reaction was performed analogously to *procedure 4* using 1-bromodocosane 1.8 g (0.005 mol) and lithiated MWNTs 50mg. Yield was 69 mg.

IR: 2921, 2368, 1591, 1413, 1367, 1084, 973, 884cm^{-1}

TGA: see section 3.3.1.4

Reaction with 1,6-dibromohexane

The reaction was performed analogously to *procedure 4* using 0.06 g (2.46*10^{-4} mol) of 1,6 di-bromohexane and lithiated MWNTs 10 mg. Yield was 23 mg.

IR, TGA: see section **3.3.1.1**

Reaction with 1, 12-dibromododecane

The reaction was performed analogously to *procedure 4* using 1,12-dibromododecane 0.08 g (2.47*10^{-4} mol). Yield was 26 mg.

IR: 2908, 2354, 1593, 1419, 1354, 1086, 967, 885cm^{-1} **TGA:** see section 3.4.2

6.4. Experimental for Chapter 4: Alkyl-functionalised carbon nanotubes for polymer reinforcement

Film preparation for the mechanical testing on Zwick Z100 tensile tester (Procedure 5)

A solution of CPP, 300 mg, in THF 10 ml was added to butyl functionalised nanotubes 3 mg. This was sonicated under a sonic tip for 5 minutes and subsequently in a sonic bath for two hours. Two more solutions were made up using of butyl functionalised MWNTs 1.5

mg and 0.75 mg in CPP 300 mg in THF. These solutions were then allowed to settle for twelve hours and the supernatant was separated from the residue by decantation. 1 ml of the supernatant was then placed on a Teflon disk 30 mm in diameter and spread evenly, the solvent was then allowed to evaporate. This was repeated until a total of 4 ml of the supernatant was placed on the disk. The film was allowed to dry on the disk for 12 hr and was then removed using a blade. This thin film was then cut into strips of 4 mm in width and 17 mm in length and stored in a sample holder. These strips were then placed in the Zwick Z100 and a holding load of 0.5 N was applied and then the sample was extruded by the machine which measured the response of the material to loads applied. This data was then plotted on a stress strain curve.

Procedure 5 was followed for the film preparation of each subsequent alkyl chain length; octyl, decyl, hexadecyl and docosanyl functionalised nanotubes as well as pristine nanotubes in CPP. As well as this *Procedure 5* was followed for alkyl functionalised nanotubes in CPE, PS and PVC. There was only one exception for CPE where the solvent was changed to chloroform.

Sedimentation studies

Sedimentation studies were carried out for hydrolysed lithiated MWNTs, pure MWNTs and all alkyl functionalised nanotubes. An appropriate concentration of MWNTs in THF was found to be 0.1 mg/ml was experimentally. The limiting chain length was hexadecyl functionalised nanotubes, as any higher concentration resulted in the beam being unable to penetrate the dark solutions.

Pure MWNTs in THF (Procedure 6)

MWNTs, 1 mg, were placed in a sample tube, to this wet THF, 10 mls, was added and sonicated under the sonic tip for 5 min. From this solution a 1 cm^3 cuvette was filled immediately after sonication. The cuvette was sealed with a cap and the cap was further sealed with Para-film^{TM} taking care not to obscure where the light emitters would transmit through. This was then immediately placed in the sedimentation machine and test time of

24 hr was run with the frequency of the light emitting set to every 10 sec for the first hour and then this was changed to once every 30 sec for the remaining 23 hr.

Alkyl functionalised MWNTs

Procedure 6 was followed analogously for all alkyl functionalised MWNTs including octyl, decanyl, hexadecanyl and docosanyl functionalised MWNTs.

Tensile testing (*Procedure 7)*

Tensile testing was carried out using a Zwick Z100 tensile tester in the Biomechanical Engineering Department of the National University of Ireland Galway University. A 100 N load cell and a cross head speed of 0.5 mm/min were used to obtain stress strain curves. The diameter and thickness of each strip was measured before the strip was placed into the Zwick machine for mechanical testing. The measurements for diameter and thickness were inputted into the machine. The machine then stretched the sample until the sample broke.

In this way the Young's modulus and the tensile strength of the film can be measured. The process was repeated approximately three times for each film so an average strength could be measured. Each of the polymer-CNTs composites had their tensile strengths measured against that of the tensile strength of the initial pure polymer.

6.5. Experimental for Chapter 5: Bonding of carbon nanotubes to polymers and investigation of mechanical properties of the composites

All manipulations were carried out under a vacuum or argon atmosphere by standard Schlenk techniques. Solvents were dried and distilled over sodium-potassium alloy under argon prior to use and then condensed into a reaction flask under vacuum shortly before use. The polystyrene (PS), chlorinated polypropylene (CPP), PVC and chlorinated polyethylene were obtained from Aldrich. The tensile testing measurements were carried out in NUIG (National University of Ireland, Galway) on a Zwick Tensile tester.

Chlorinated polypropylene functionalised MWNTs *(procedure 8)*

Lithiated MWNTs, 15 mg, in dry THF, 20ml, were ultra-sonicated for 30 min. Chlorinated polypropylene, 0.02g, was added to a Schlenk vessel containing dry THF, 10 mls. This solution was sonicated for 30 min. Once the polymer had dissolved in the solvent it was then degassed to remove any residual air or impurities. This was then added to the suspension of lithiated nanotubes by syringe. The mixture was stirred for 24 hr at room temperature. The precipitate was then washed with dry THF and then with deionised water until the water was colourless. The remaining powder was dried in vacuum for 10 hr.

A control experiment was performed using the same amounts of non-lithiated MWNTs and chlorinated polypropylene in THF. The product was treated analogously to above.

Chlorinated polypropylene functionalised SWNTs

The preparation of CPP-grafted SWNTs were performed analogously to *procedure 8* however, using lithiated SWNTs in place of MWNTs.

PVC functionalised MWNTs

The preparation of PVC-MWNT composite was performed analogously to the *procedure 8* polypropylene using PVC, 0.02g.

Composite film production

Films were produced for four different polymer matrices; Polystyrene, Chlorinated Polypropylene, Polyethylene and Polyvinyl Chloride. The nanotubes used were functionalised 'thin' CVD MWNT.

Polystyrene composites

Procedure 9

30g/l solutions of films were made in the following manner; polystyrene 0.3g was added to THF, 10 ml and this was sonicated immediately under the sonic tip for 5 min subsequently this was sonicated in a sonic bath for 2 hr. The solution was then allowed to settle for 12 hr. 1ml fractions were syringed from the solutions and placed on circular Teflon studs of 2 cm

in diameter. While this was being undertaken considerable care was used in order to inhibit the formation of air bubbles in the film which could lead to poor mechanical properties. The end of the syringe was held at a 45 ° angle directly against the surface of the stud. Care was also undertaken to ensure that the film was of homogenous nature and the entire surface of the stud was covered this was done by breaking the surface tension with the end of the syringe and leading the solution to the edge of the stud. The solvent was allowed to completely evaporate under ambient temperatures and a further 1 ml of solution was added to this. This was repeated until there were 4 layers of polymer on the stud. This was allowed to dry under ambient temperature over a 12 hr period. The polymer film was then removed from the stud with the use of TEM tweezers. The thin film was then cut into strips of ~4 mm and length of ~15 mm, these were then stored in sample tubes.

Procedure 10

Three weight percent samples were made for PPC functionalised nanotubes in PS these were 1%, 0.5% 0.25%. For 1% 3 mg of functionalised nanotubes were weighed out and placed in the bottom of a sample tube to this P.S, 0.3 g (300 mg) was added with THF, 10 ml, this was then sonicated under the sonic tip for 5 min and in the sonic bath for 2 hr. This solution was allowed to settle over a twelve hour period. The supernatant was then decanted from the sediment into another sample tube. From this 1ml of the solution was deposited on a Teflon stud 3 cm in diameter. Considerable care was again used when the films were being produced the syringe was held at a 45 ° angle to the surface of the stud whilst the solution was being deposited. Care was also undertaken to ensure that the film was of homogenous nature and the entire surface of the stud was covered this was done by breaking the surface tension with the end of the syringe and leading the solution to the edge of the stud. This was then left for 12 hr at ambient temperature to allow for full evaporation of the solvent and the polymer would set on the stud. The polymer film was then removed from the stud with the use of TEM tweezers. This was cut into strips of ~4 mm in width and ~15 mm in length. These were then placed into a sample tube. This was followed analogously for the two subsequent weight percentages except 1.5 mg and 0.8 mgs were weighed instead of 3 mg for the two lower weight percents.

Procedure 10 was followed for the PVC functionalised nanotubes in polystyrene.

Procedure 10 was followed for the formation of alkyl chain composites including 1-bromobutane, 1-bromooctane, 1-bromodecane, 1-bromohexadecane and 1-bromodocosane in polystyrene.

Chlorinated Polypropylene composites

Procedure 9 was followed for the preparation of pure chlorinated polypropylene films by substituting CPP for PS.

Procedure 10 was followed for the preparation of CPP functionalised MWNTs and SWNTs in CPP.

Procedure 10 was followed for the preparation of PVC functionalised nanotubes in CPP.

Procedure 10 was followed for the formation of alkyl chain composites including 1-bromobutane, 1-bromooctane, 1-bromodecane, 1-bromohexadecane and 1-bromodocosane in CPP.

Polyvinyl Chloride composites

Procedure 9 was followed for the preparation of pure chlorinated polypropylene films by substituting PVC for PS.

Procedure 10 was followed for the preparation of CPP functionalised nanotubes in PVC.

Procedure 10 was followed for the preparation of PVC functionalised nanotubes in PVC.

Procedure 10 was followed for the formation of alkyl chain composites including 1-bromobutane, 1-bromooctane, 1-bromodecane, 1-bromohexadecane and 1-bromodocosane in PVC.

Chlorinated Polyethylene composites

Procedure 9 was followed analogously for the preparation of pure chlorinated polyethylene films however chloroform was used as a substitute for THF as CPE was more soluble in chloroform and CPE was used instead of PS.

Procedure 10 was followed for the preparation of CPP functionalised nanotubes in CPE however chloroform was used as opposed to THF.

Procedure 10 was followed for the preparation of PVC functionalised nanotubes in CPE however chloroform was used instead of THF as a solvent.

Procedure 10 was followed for the formation of alkyl chain composites including 1-bromobutane, 1-bromooctane, 1-bromodecane, 1-bromohexadecane and 1-bromodocosane in CPE and chloroform was used instead of THF.

6.6 References

[1] M. Cadek, R. Murphy, B. McCarthy, A. Drury, B. Lahr, R. C. Barklie, M. in het Panhuis, J. N. Coleman, W. J. Blau, *Carbon,* **40,** 923 (2002)

[2] J. Liu, A.G. Rinzler, H. Dai, J.H. Hafner, R.K. Bradley, P.J. Boul, A. Lu, T. Iverson, K. Shelimov, C.B. Huffman, F. Rrodriguez-Macias, Y.-S. Shon, T.R. Lee, D.T. Colbert, R.E. Smalley, *Science*, **280**, 1253 (1998).

[3] P.X. Hou, S. Bai, Q.H. Yang, C. Liu, H.M. Cheng, *Carbon*, **40,** 81 (2002)

Chapter 7

Conclusions and Future Work

7.1 Conclusions

The first part of this work was focused on further development of the preparation of MWNTs using the Kratschmer Huffmann generator. The conditions outlined by Cadek *et al.*[1] were reexamined and were reaffirmed. As well as this the nanotubes were purified by a selection of popular purification techniques and it was realised that in order to use the nanotubes for the purpose which we intended it was necessary that the nanotubes were left unaltered. The purification technique of preference therefore was that using the polymer PPV. During the initial time of nanotube production and purification the price of MWNTs sold by the Nanocyl Company fell dramatically from 500 euro to 50 euro a gram. This rapid decrease in price meant that it was feasible to buy in adequate amounts of purified good quality CVD MWNTs. Purchasing nanotubes also enabled immediate investigation of chemical modification on MWNTs as opposed to slower production, purification and subsequent chemical modification.

Our studies have shown that both SWNTs and MWNTs can be successfully lithiated using two different alkyl lithium reagents, n-BuLi and t-BuLi. The resulting nanotube derivatives are exceptionally air and moisture sensitive. Hydrolysed samples of both of these types of reactions were analysed by IR and Raman spectroscopy. It has also been shown that n-BuLi is more effective at lithiating the nanotubes.

We have found that the lithiated nanotubes are susceptible to metathetic exchange reactions with many halogenated species *via* elimination of lithium halides. This strategy was initially applied to react lithiated carbon nanotubes with various metal halides. This resulted in the formation of carbon-nanotube composites containing metal-carbon bonds (Sn-C, Pb-C or Si-C), which have been identified by IR, Raman spectroscopy and by XPS. As well as these, electron microscopy techniques such as TEM and HRTEM were applied to characterise the new nanocomposites. Reactions of lithiated nanotubes with $AuBr_3$ resulted in reduction of the metal and in the formation of gold nano-particles on the external walls of the nanotubes.

Lithiated MWNTs have been reacted with different halogenated alkyls producing a series of interesting products. The reactions with a range of mono-halogenated alkyls gave products which improved the solubility of MWNTs in an organic solvent. It was observed that after functionalisation with alkyl chains the degradation temperature in the TGA spectrum of MWNTs decreased dramatically. This was due to two reasons the alkyl chains facilitated more rapid heat transfer to the nanotubes and also functionalised nanotubes are known to be more defective than pure unfunctionalised nanotubes as has been reported by Garg *et al.*[2]

The reaction of lithiated MWNTs with di-substituted alkyl hallides resulted in the formation of MWNTs which were connected to each other forming Y and T junctions. This technique could be used to fabricate new nanosized electronic devices based on carbon nanotubes. In the TEM images of the product of this reaction examples of nanotubes connected to each other *via* a tip to tip or a tip to wall junction have been observed.

The alkyl functionalised nanotubes that were produced in chapter 3 were added to a range of polymers in order to investigate their potential for polymer reinforcement. We have found that the mechanical properties of alkylated carbon nanotube polymer composites strongly depend on the nature of polymer, length of the alkyl chain and % of nanotubes. It was observed for the selected polymers such as PVC and PS that the hexadecyl functionalised MWNTs provide the greatest reinforcement. For the range of alkyl chains and polymers examined the polymer that the MWNTs imparted the greatest increase was PS. As a general rule, with concentrations of greater than one volume percent these would not show a good degree of reinforcement. The reason for this is that the nanotubes form aggregates which do not allow for adequate or reasonable stress transfer and also add defects to the composite material.

Following a series of known equations for nanotube volume concentration and using an applied form of the rule of mixtures allows Y_{eff} to be calculated. Applying this to the values given for the modulus of the composites made from the alkyl functionalised nanotubes. The

values obtained for Y_{eff}, correlated well with the theoretical values for functionalised nanotubes.

Also examining the interfacial stress transfer, τ, gave very good values for the functionalised nanotube composites, especially when compared to the unfunctionalised MWNT composites. This exemplifies the fact that the alkyl functionalised nanotubes are mixing with the polymer and imparting greater interfacial stress transfer than unfunctionalised nanotubes.

We have demonstrated that lithiated nanotubes can be reacted with halogenated polymers such as CPP and PVC giving correspondent polymer grafted carbon nanotubes. CPP grafted nanotubes were added to the original and other polymers and mechanical testing was carried out. Results of mechanical testing have proven that functionalised MWNT composites can significantly improve mechanical properties of polymers. The best reinforcement was achieved for the chlorinated polypropylene polymer matrix. As nanotube content is increased to 0.6 vol %, Young's modulus increased by a factor of 3, while both the tensile strength and the toughness increased by factors of 3.8 and 4, respectively. Also PVC composites reinforced with CPP grafted nanotubes demonstrated more than a ten fold increase in the toughness of the films. We have found that polymer grafted nanotubes did reinforce the other polymers to the same high extent as when mixed with the original polymer. DSC studies have shown that an addition of polymer grafted nanotubes does not affect crystallinity of selected by us polymers as contrast to that has been observed for polyvinyl alcohol (PVA), where carbon nanotubes caused polymer crystallization that resulted in its reinforcement.[5,6]

Thus we can conclude that the covalent functionalisation of nanotubes enabled us to get an efficient dispersion and excellent interfacial stress transfer, leading to new ultra strong polymer composite materials.

Lithiated SWNTs were also reacted with CPP in an attempt to prepare CPP grafted SWNTs and use the greater reinforcing properties of the SWNTs. However as has been previously observed by other researchers the SWNTs tend to form very stable bundles which are very difficult to break apart to allow for interfacial stress transfer between them and the polymer.

Overall this project contributed to the fundamental development of basic organometallic chemistry of carbon nanotubes and application of novel nanotube derivatives for polymer composite reinforcement.

7.2 Future Outlook

Our work explored the lithiation of nanotubes and reactions of lithiated nanotubes with a number of different halogenated species from metal halides to alkyl halides and polymer halide derivatives. Organometallic chemistry of carbon nanotubes is just in its infancy. We believe that lithiated carbon nanotubes can act as a bulky macromolecular ligands for organometallic chemistry. Also the use of organometallic approaches in carbon nanotube chemistry will allow several very important problems to be addressed such as: doping of carbon nanotubes with metals or non-metals and formation of metal nanoparticles and nanowires using the lithiated nanotubes as templates. Both these aspects are very important for potential application of carbon nanotubes in nanotechnology.

Future work will be to treat the lithiated nanotubes with various Si, Ge(IV), Sn(II), Sn(IV) and Pb(II) halides and some of their organometallic derivatives such as REX_3, R_2EX_2, R_3EX (R-alkyl or aryl, E – Si, Ge or Sn, X-halogen). We expect that all these reactions must result in products with the stable silicon-carbon or metal-carbon bonds. This should allow us to investigate these new materials without using special handling techniques (high vacuum or extra clean and dry inert gases). The presence of alkyl- or aryl-substituents on the organometallic species (e.g. R_3E- or R_2E-) should also result in increased solubility of the nanotube derivatives in organic solvents that should enable us to investigate the products by NMR (e.g. ^{1}H, ^{29}Si, ^{119}Sn) spectroscopy.

Another future aspect will be to develop a deposition of metal nanoparticles or nanowires using the lithiated nanotube as both a reducing agent and a template. It has been demonstrated that even non-functionalised SWNTs can spontaneously reduce some metal ions (Au and Pt) from their solutions with the formation of metal nanoparticles on sidewalls.[3] The formation of Au and Pt particles on SWNT sidewalls was attributed to direct redox reaction between nanotubes and metal ions. Our feasibility studies have shown that the lithiated carbon nanotubes are extremely strong reducing agents. We have found that they can easily reduce Au, from a $AuBr_3$ solution in an organic solvent giving the corresponding metal nanoparticles on sidewalls of nanotubes. Therefore it would be very interesting to investigate in details interactions of different transition metal (Cu, Ag, Au, Fe, Ni, Co, Ti, Zr, Cr, Mo and W) halides (Cl, Br and I) with the lithiated nanotubes. The choice of metal salts will be defined by their solubility in suitable organic solvents and their redox behaviour with the lithiated nanotubes. New nanotube metal composites will be characterised by TEM, AFM, XRD, TGA, elemental analysis and Raman spectroscopy.

Conductivity studies of the most promising selected nanocomposites from those produced above should be performed. This research will be necessary for understanding the electron transport properties of the metallated nanotubes, which are affected by the interaction with the foreign metallic structure. In addition to the direct transport along the metallic coating, the electronic carriers can also travel through the nanotube, forming a system that behaves like two resistors in parallel. The overall resistance thus depends on how conducting the metallic structure is and how good a contact there is between metal and nanotube. Conductivity measurements should be performed on polymer nanotube composite thin films and on individual metallated nanotubes.

As well as this, it may be possible to anneal the metallated nanotube composites at 700 °C to remove or burn out the carbon nanotubes. What should be left is the shell of metal which had surrounded the nanotube, essentially metal or metal oxide nanotubes. These nanotubes could then be used as nano-wires and nanointerconnects in nanoelectronics..

The work involving the lithiation of nanotubes and subsequent reactions with a range of brominated alkanes produced some promising results when they were combined with a range of polymer composites. However the resulting reinforcement was not as significant as was first expected. Progressing on this theory would be to react the lithiated nanotubes with a range of branched alkyl hallides. This may result in nanocomposites with an increased polymer interfacial stress transfer because the branched alkyls may strongly interact with the polymer matrix through their branched functional groups. This has the potential to allow for further reinforcement of composite materials. According to theoretical calculations[4] nanotubes non-covalently attached to polymers will not reinforce composite materials to the same degree as covalently bound nanotubes. However, having a material which could reinforce polymers to a high degree will offer an attractive filler material to polymer scientists and also commercial applications. The reasons for this would be; as this project has shown, and others before it,[5,6] the amount of nanotubes required to reinforce composite materials is minimal in the region of 1-2vol. %. Thus transporting a small amount of filler material is more beneficial than transporting a large amount of composite material. Also, obtaining a universal additive material which would reinforce a range of polymers to a large degree has many commercial benefits.

It is known that nanotubes reinforce polyvinyl alcohol (PVA) and improve the mechanical properties by up to a factor of four.[5,6] This was achieved by the non-covalent reinforcing of PVA through the mechanical mixing of nanotubes and PVA. As previously stated non-covalent reinforcement should not be as great as covalent functionalised. Therefore covalently binding of MWNTs to PVA should reinforce this polymer to an even higher degree. In order to covalently reinforce this polymer it would not be possible to add lithiated nanotubes to a solution of the polymer. The reason for this is that the lithium atoms will react preferentially with the hydroxyl groups of the polymer and not allow the nanotubes to react with the polymer. However, as nanotubes can be halogenated[7] it should be possible to lithiate the polymer and combine this with the halogenated nanotubes. Making composites out of these functionalised nanotubes should improve PVA composites to an even higher degree than the non functionalised nanotubes.

It is has been reported that nanotubes react with nitrogenous compounds[8] under UV light. Applying this to polymer composites it should be possible to combine nanotubes with polypyrrole as has been performed.[9] However, researchers focused mainly on the conductive properties of nanotube-polypyrrole composites. If the nanotubes were bound to the pure polymer through a Diels Alder reaction induced by UV light this should significantly increase the mechanical properties and potentially increase the conductive properties of the composite.

Overall, we believe that organometallic chemistry must have a significant impact on nanoscience in the near future. This research should also contribute to the development of relevant areas in nanotechnology. New nanotube nanocomposites can be potentially utilised in different electronic devices, computers, mobile phones, television systems as well as in fabrication of new ultra-strong composite materials. It is in the nano-world that discoveries will be made and technologies developed which are likely to change peoples' lives in the coming decades.

7.3 References

[1] M. Cadek, R. Murphy, B. McCarthy, A. Drury, B. Lahr, R.C. Barklie, M. in het Panhuis, J.N. Coleman, W. J. Blau, *Carbon,* **40,** 923, (2002)

[2] Garg, S.B. Sinnott, *Chem. Phys. Lett.*, **295,** 273, (1998)

[3] H.C. Choi, M. Shim, S. Bangsaruntip, H. Dai, *J. Am. Chem. Soc*, **124**, 9058, (2002)

[4] A.H. Barber, S.R. Cohen, H.D. Wagner, *Appl. Phys. Lett.,* **82,** 4140, (2003)

[5] M. Cadek, *PhD Thesis,* Trinity College Dublin, (2004)

[6] K.P. Ryan, *PhD Thesis,* Trinity College Dublin, (2005)

[7] E. Unger, A. Graham, F. Kreupl, M. Liebau, W. Hoenlein, *Curr. Appl. Phys.*, **2,** 107, (2002)

[8] H. Hayden, *PhD Thesis,* Trinity College Dublin, (2005)

[9] K. Jurewicz, S. Delpeux, V. Bertagna, F. Beguin, E.Frackowiak, *Chem. Phys. Lett.*, **347,** 36, (2001)

Appendix

Journal Publications

1. R. Blake, Y. K. Gun'ko, J. Coleman, M. Cadek, A. Fonseca, J.B. Nagy, W. Blau, A generic organometalic approach toward ultra-strong carbon nanotube-polymer composites, *J. Am. Chem. Soc.*, **126**, 10226, (2004)

2. J. N. Coleman, M. Cadek, V. Nicolosi, R. Blake, F. Liégeois, A. Fonseca, J. B Nagy, Y. Gun'ko and W. J Blau, High performance nanotube reinforced plastics: Understanding the mechanism of strength increase, *Adv. Functional Materials,* **14**, 791, (2004)

Oral and poster presentations:

1. Talk: Organometallic Modification of Carbon Nanotubes, at 2005, Department of Chemistry, TCD, Ireland.
2. Talk Organometallic Modification of Carbon Nanotubes, at 2005, 2nd Annual PRTLI meeting Malahide, Co. Dublin, Ireland.
3. Poster Presentation: Organometallic Modification of Carbon Nanotubes, at the 55th Irish Universities Chemistry Research Colloquium, 2004 University of Limerick, Ireland.
4. Poster Presentation: A TEM Study of Organometalically Functionalised Carbon Nanotubes to the 28th Annual meeting of the Microscopal Society of Ireland, 2004 Trinity College Dublin, Ireland
5. Poster Presentation: Organometallic Modification of Carbon Nanotubes, at the First International Annual Nanofabrication Symposium March 2004 Dundalk, Ireland.

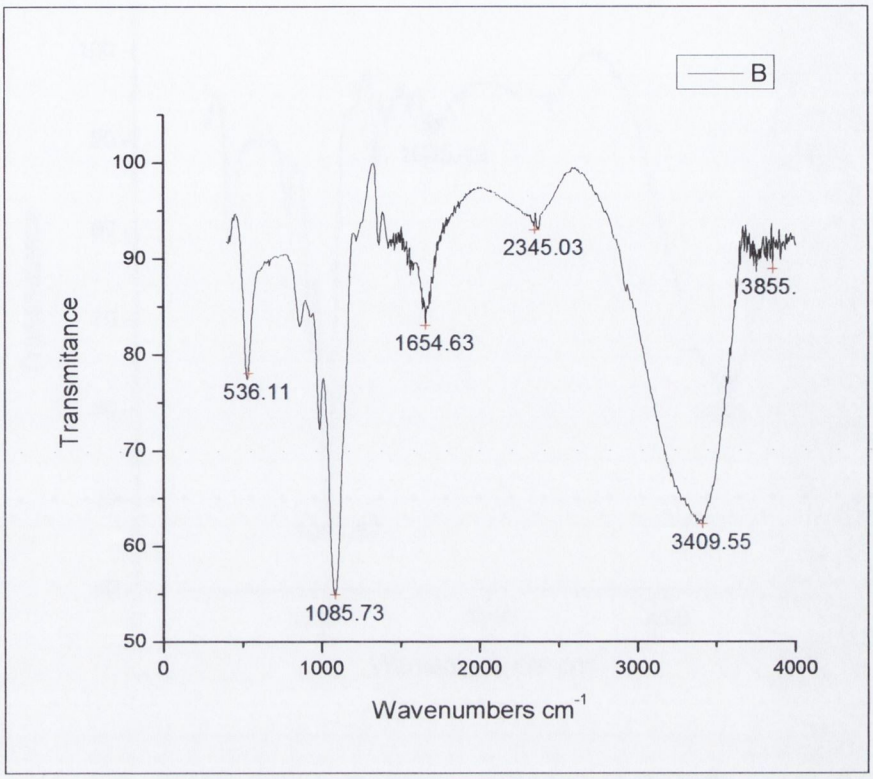

IR of untreated Nanocyl CVD MWNTs

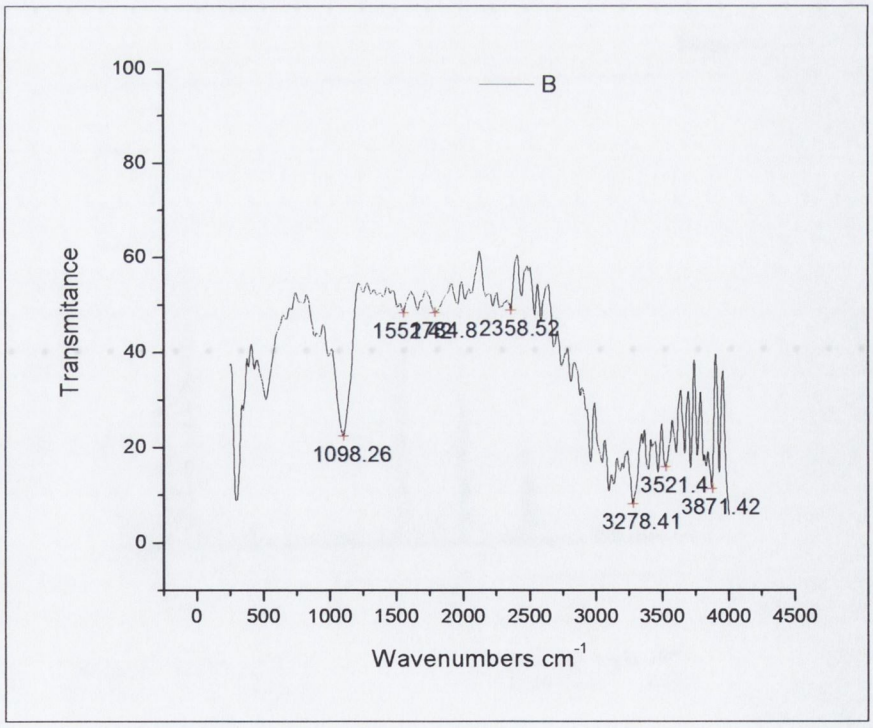

IR of annealed Nanocyl CVD MWNTs

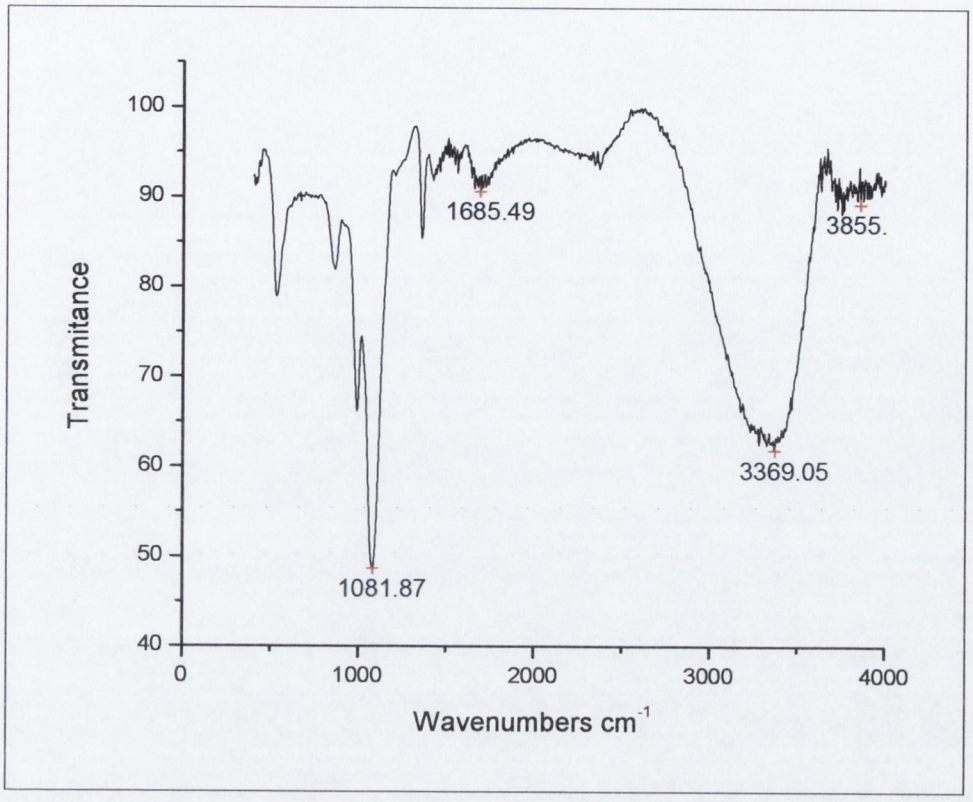

IR spectrum of hydrolysed lithiated MWNTs

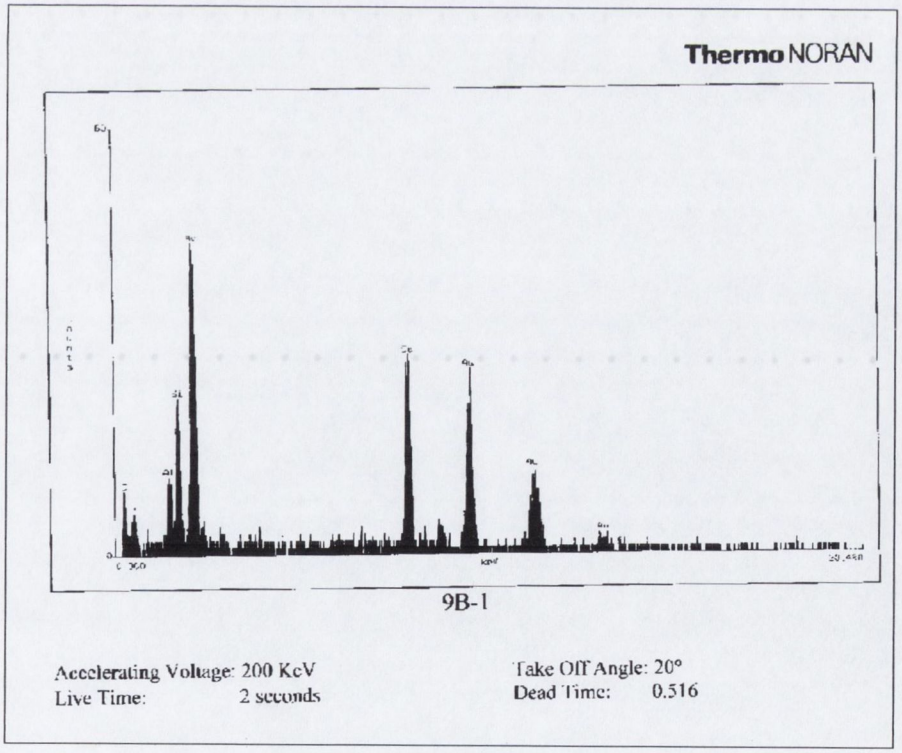

EDX spectrum of gold MWNT composites

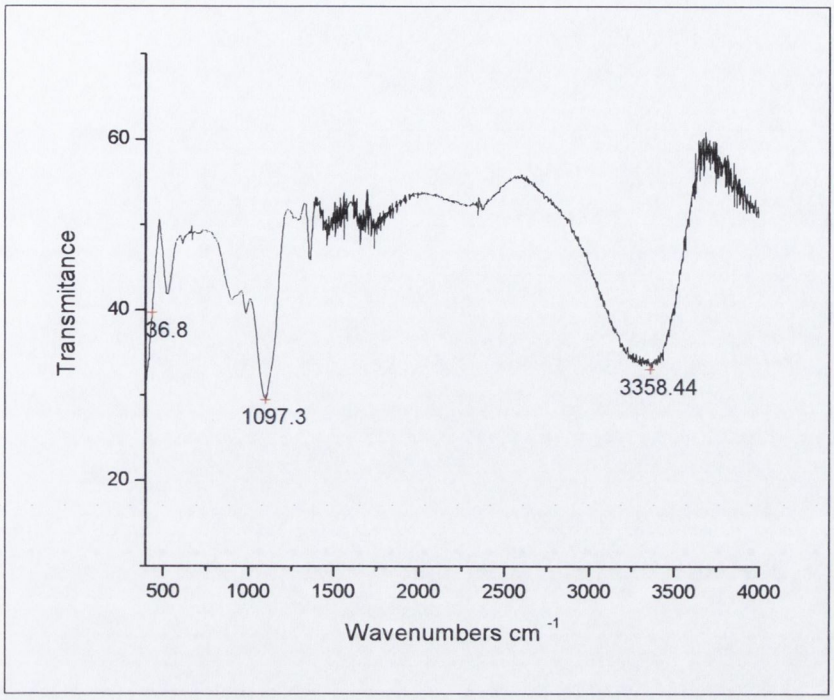

IR spectrum of Sn functionalised MWNTs

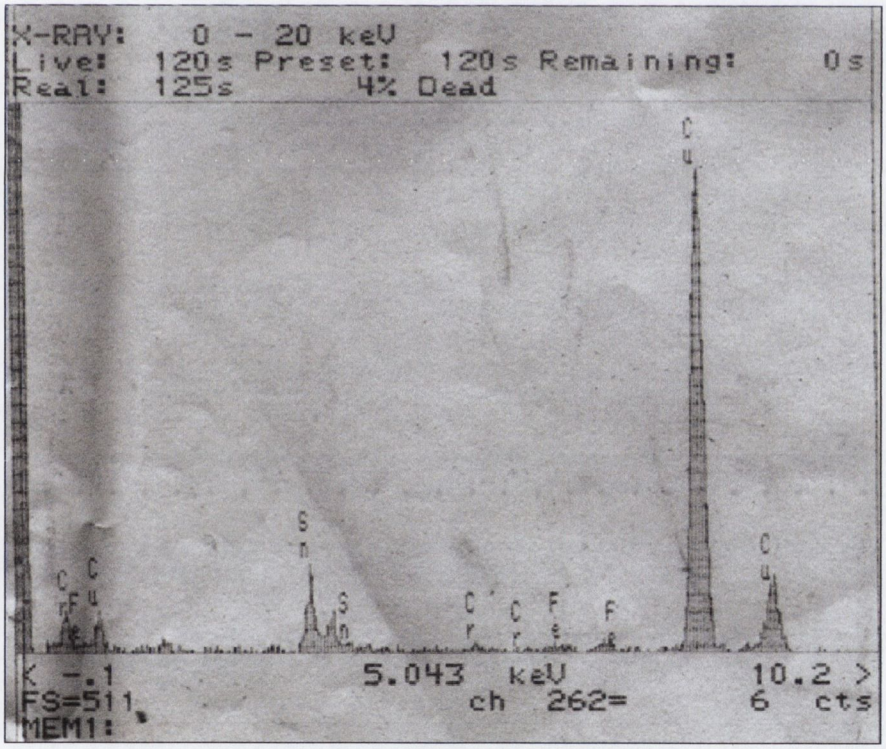

EDX spectrum Sn functionalised MWNTs

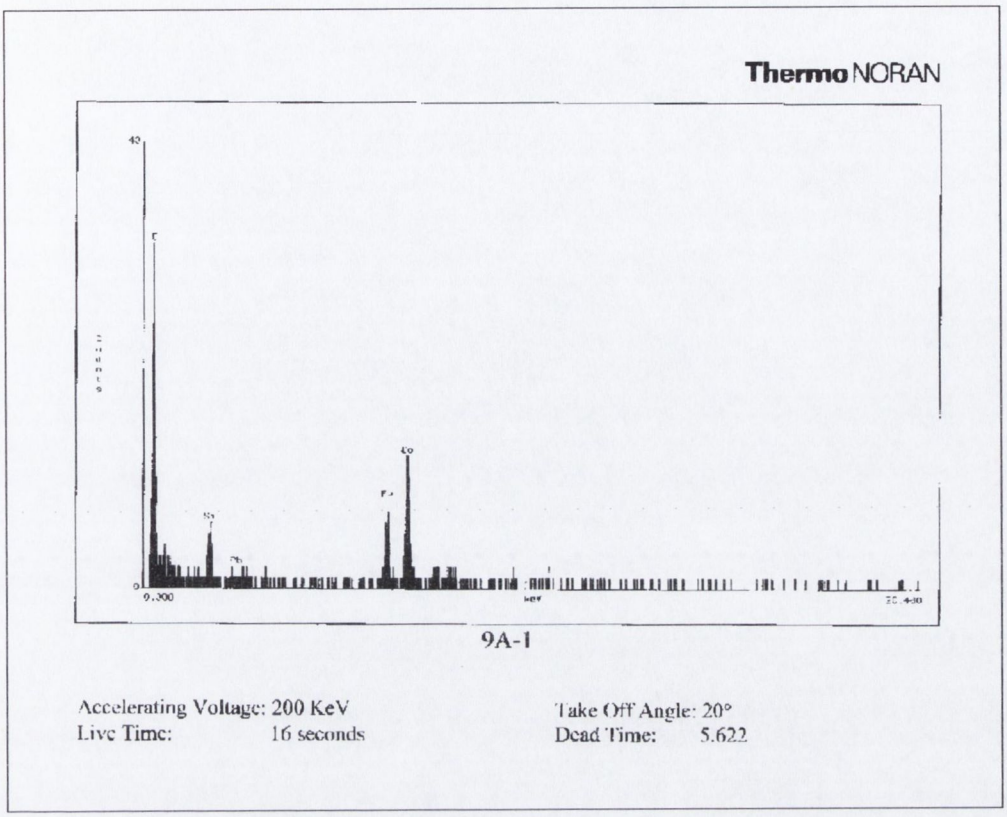

EDX spectrum Pb functionalised MWNTs

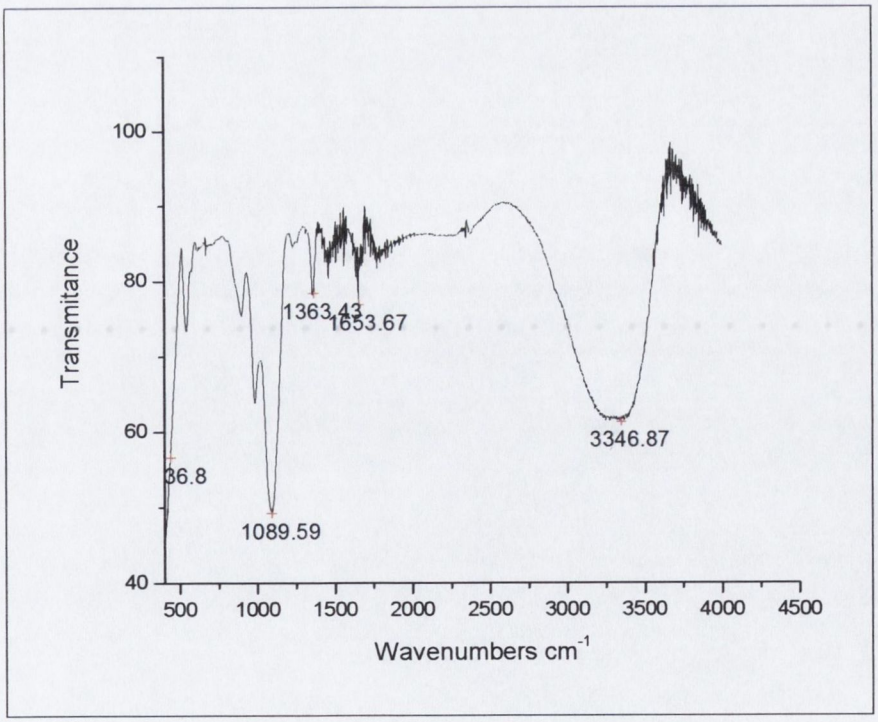

Figure 2.26 IR spectrum of Pb functionalised MWNTs

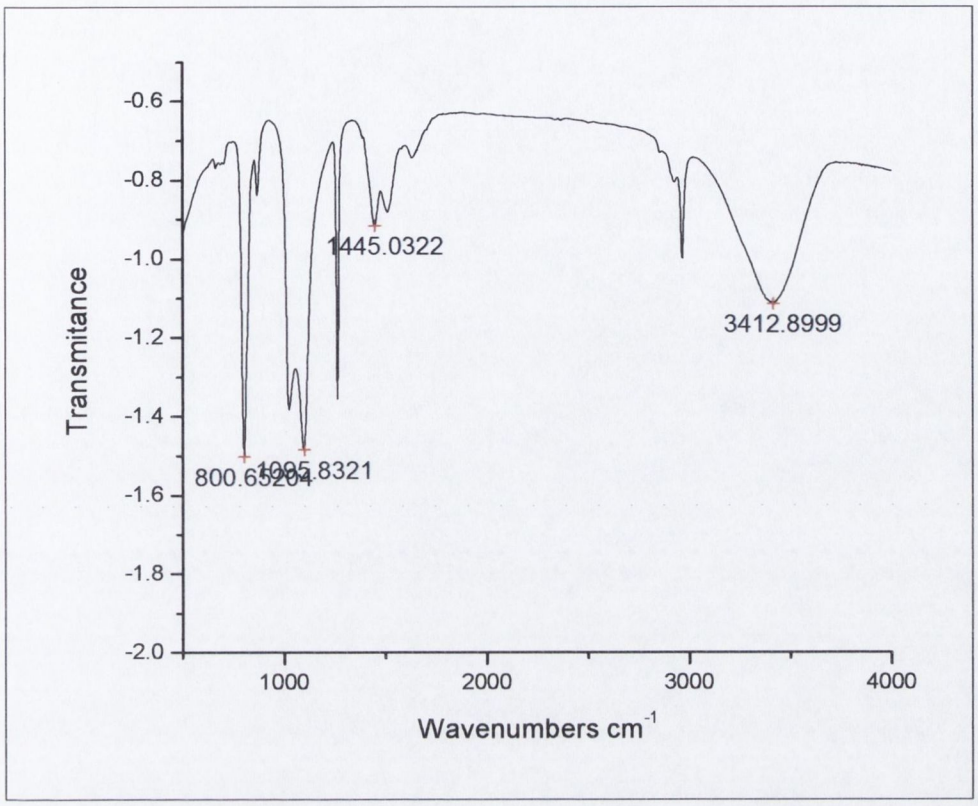

IR of pristine SWNTs

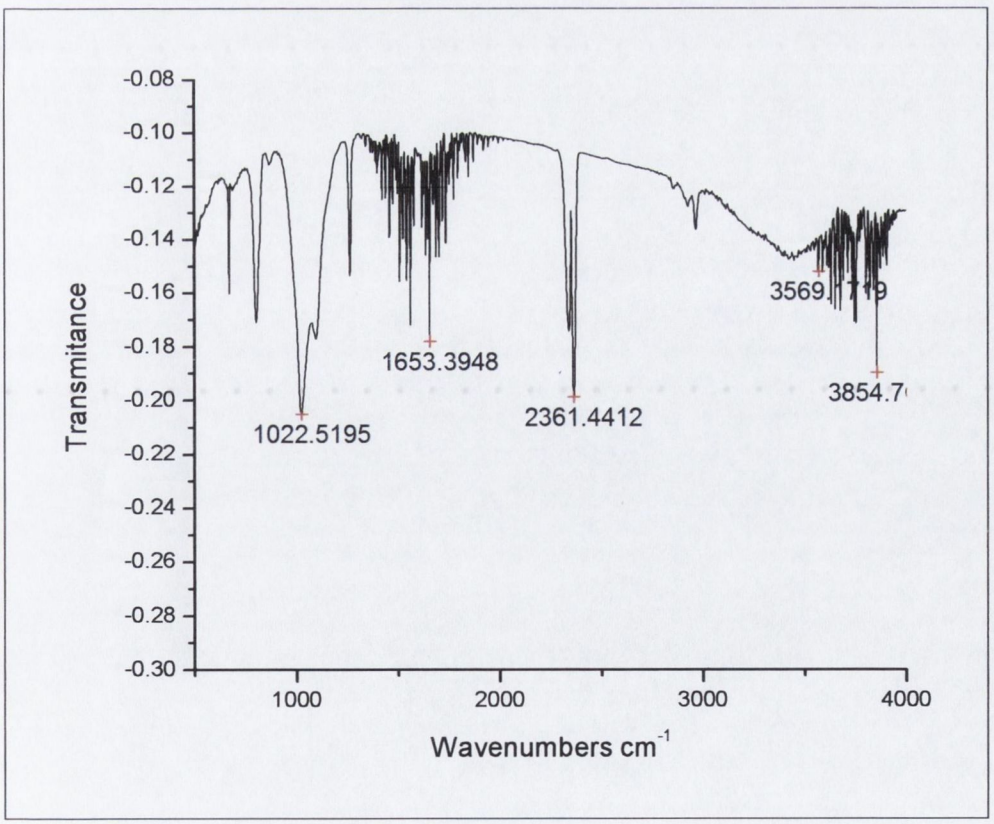

Sn-SWNTs (right)

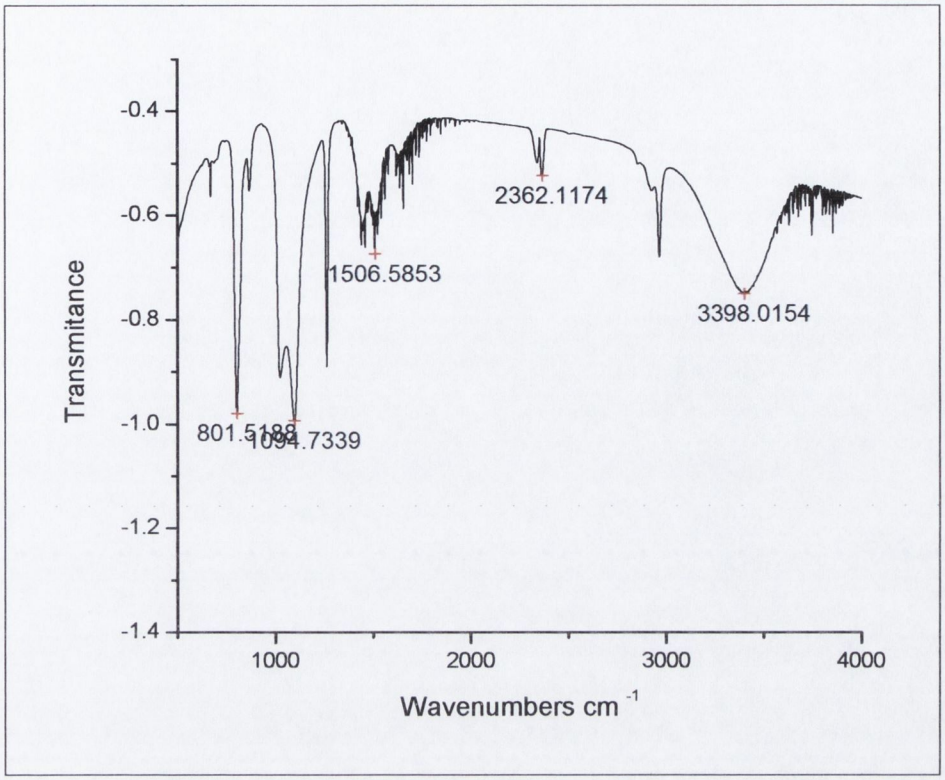

Pb-SWNTs

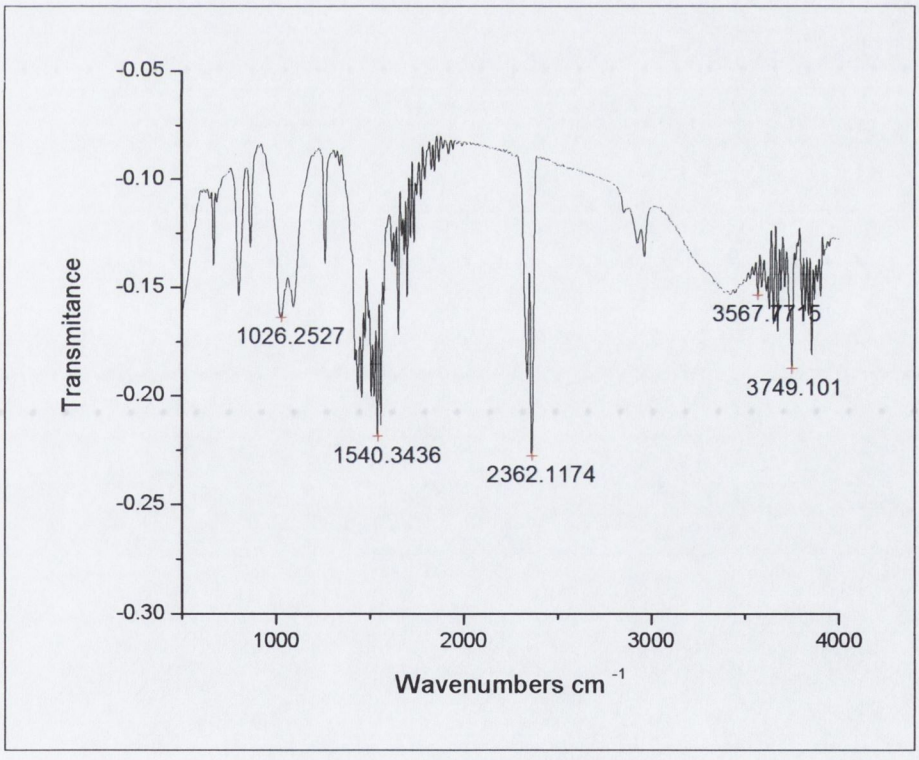

germanium functionalised SWNTs

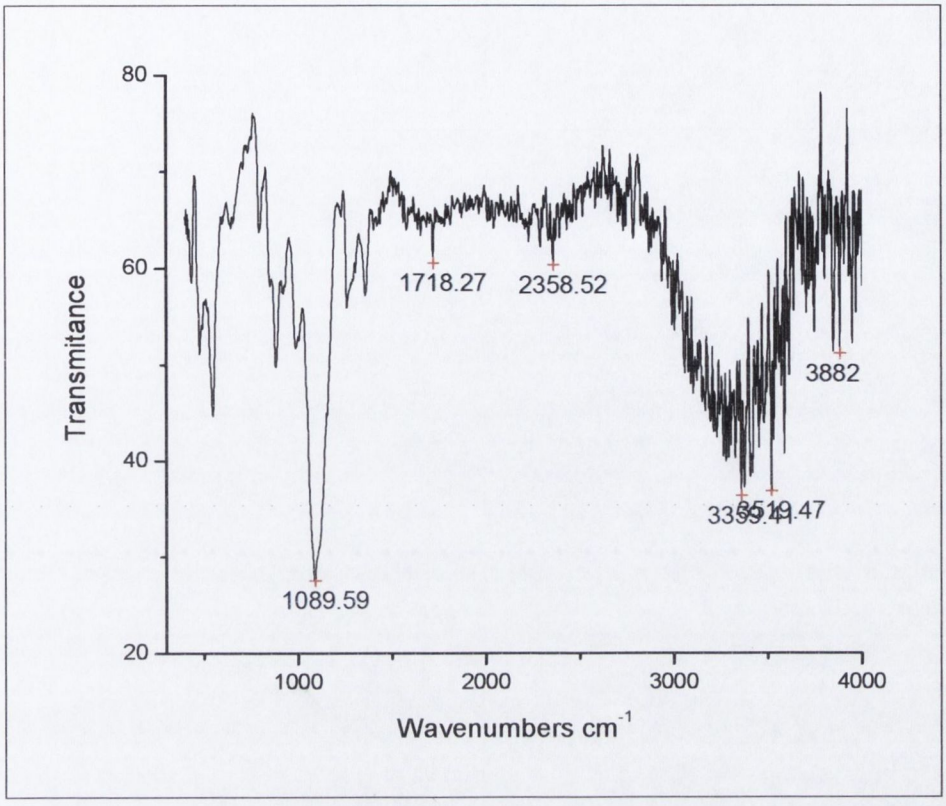

CPP grafted nanotubes

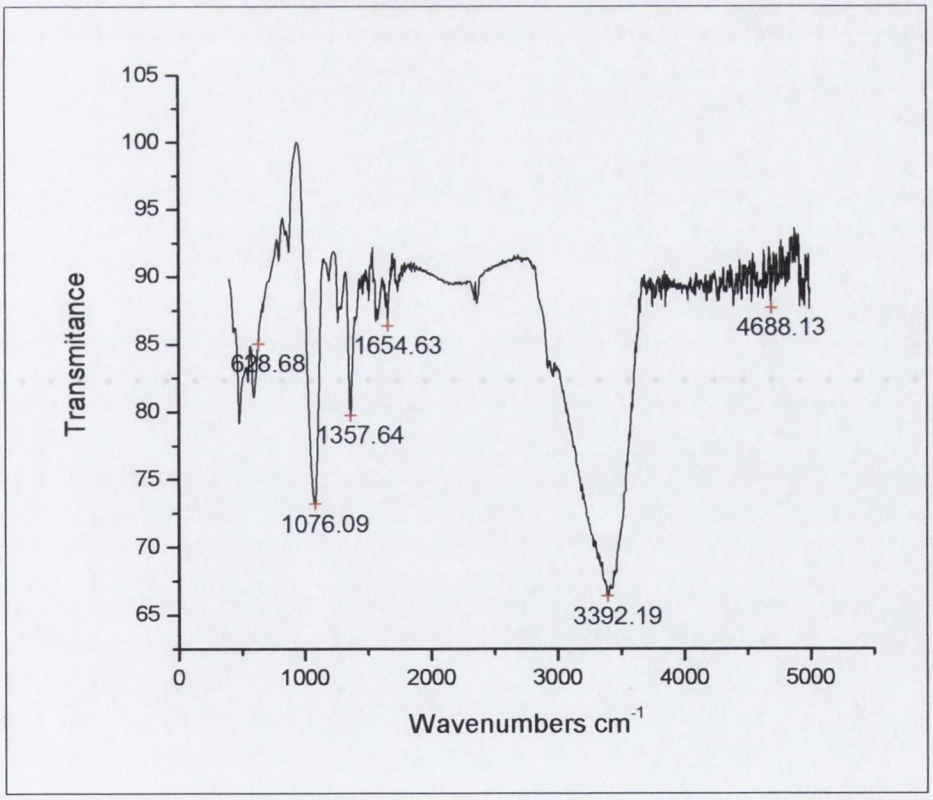

PVC grafted MWNTs

Appendix for Chapter 3

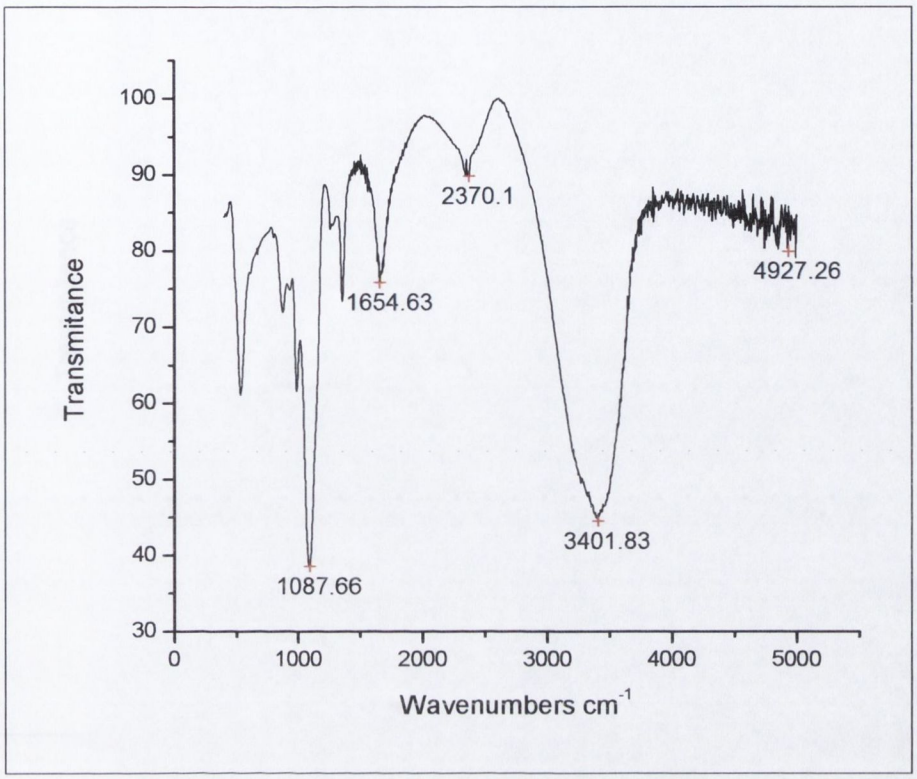

Butane functionalised MWNTs

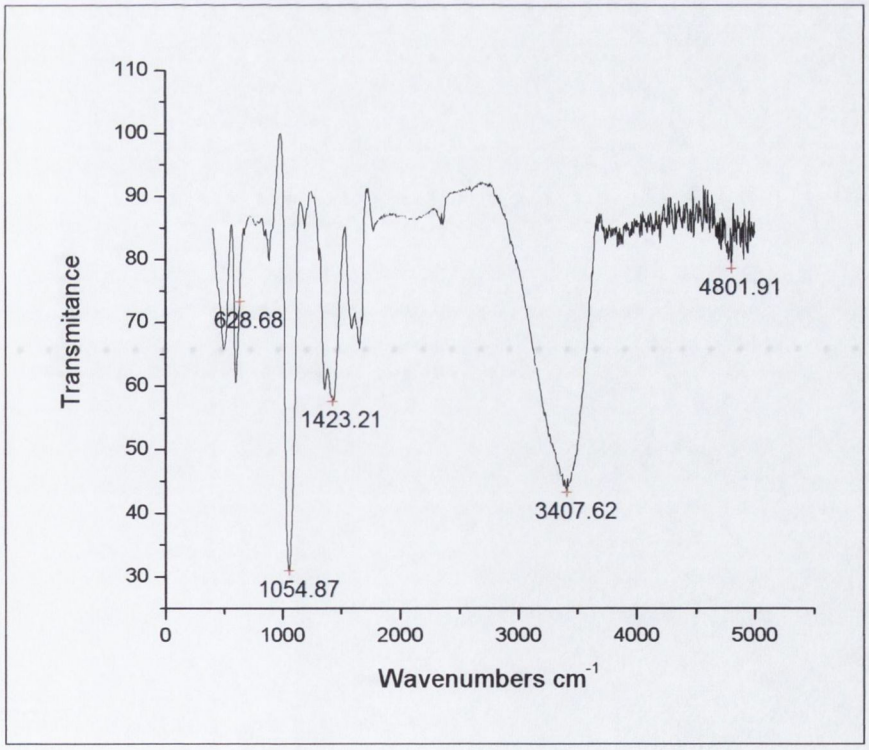

Hexyl functionalised MWNTs

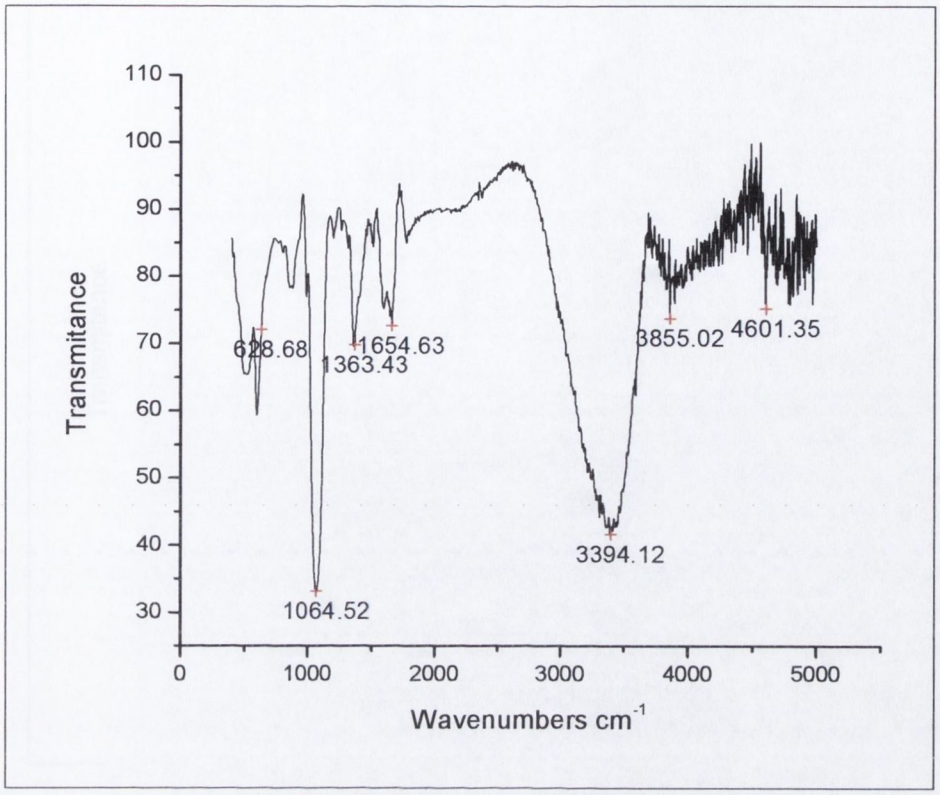

Octyl functionalised MWNTs

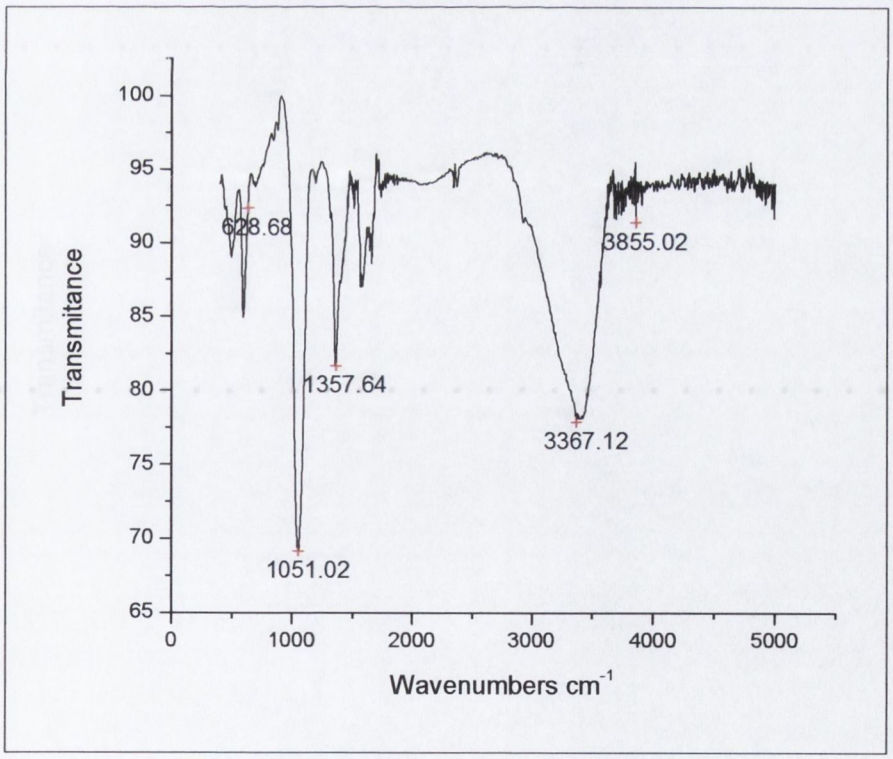

Decyl functionalised MWNTs

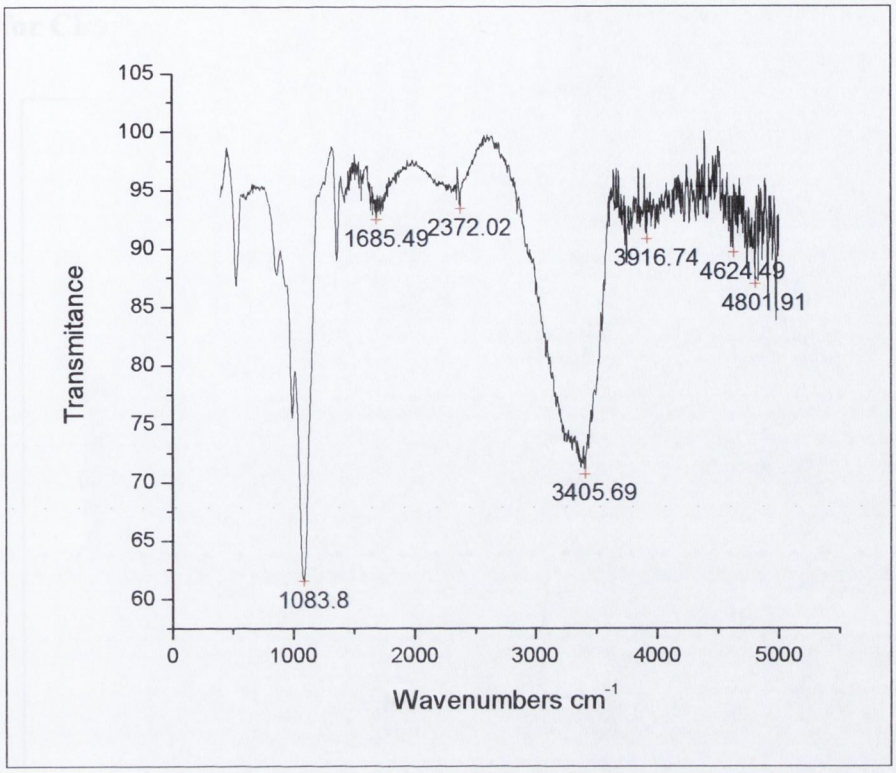

Hexadecyl functionalised MWNTs

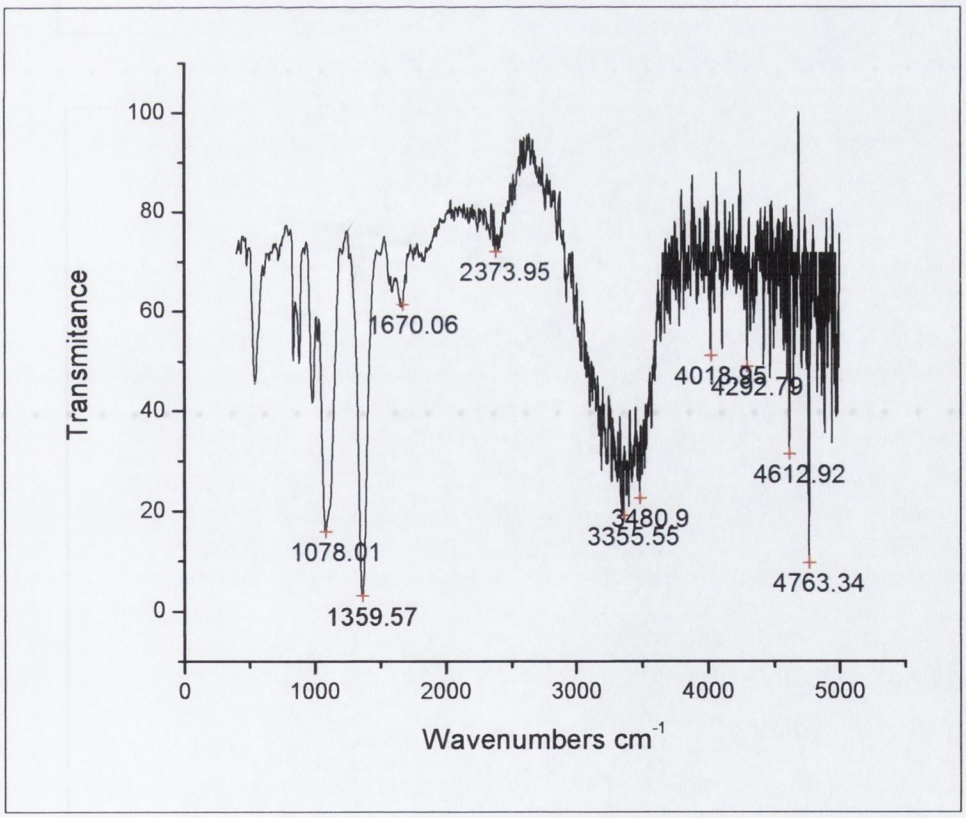

Docosyl functionalised MWNTs

Appendix for Chapter 5

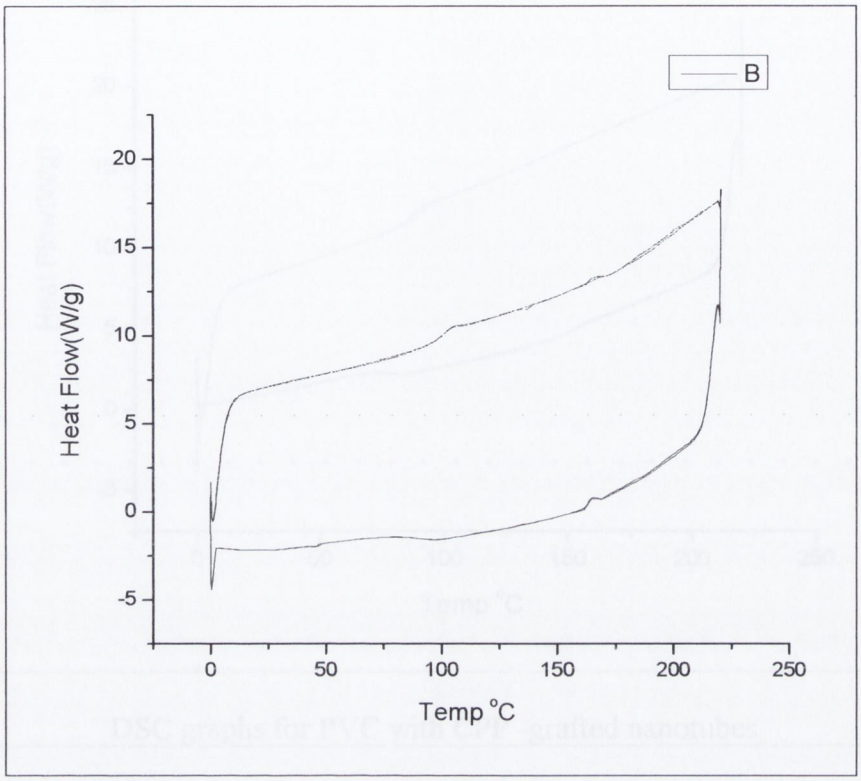

DSC graphs for polystyrene with CPP grafted nanotubes

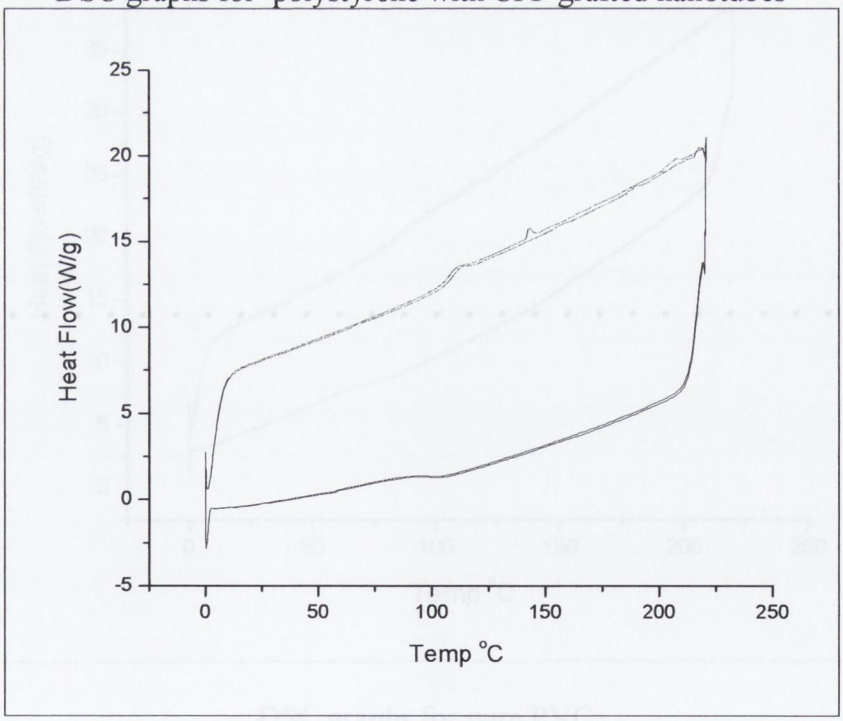

DSC graphs for pure polystyrene.

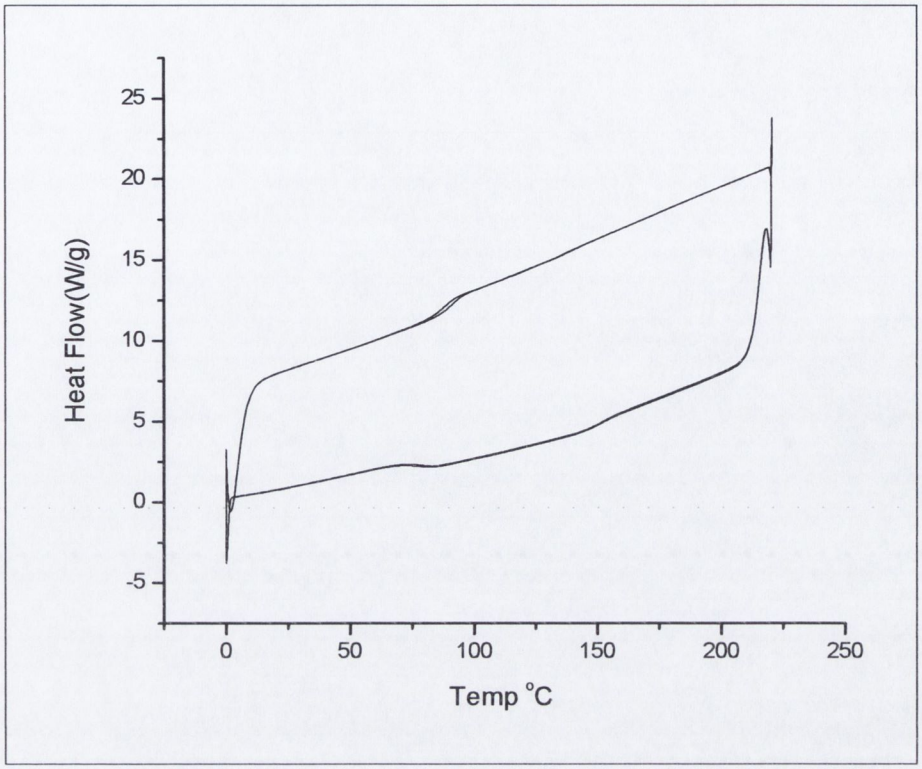

DSC graphs for PVC with CPP -grafted nanotubes

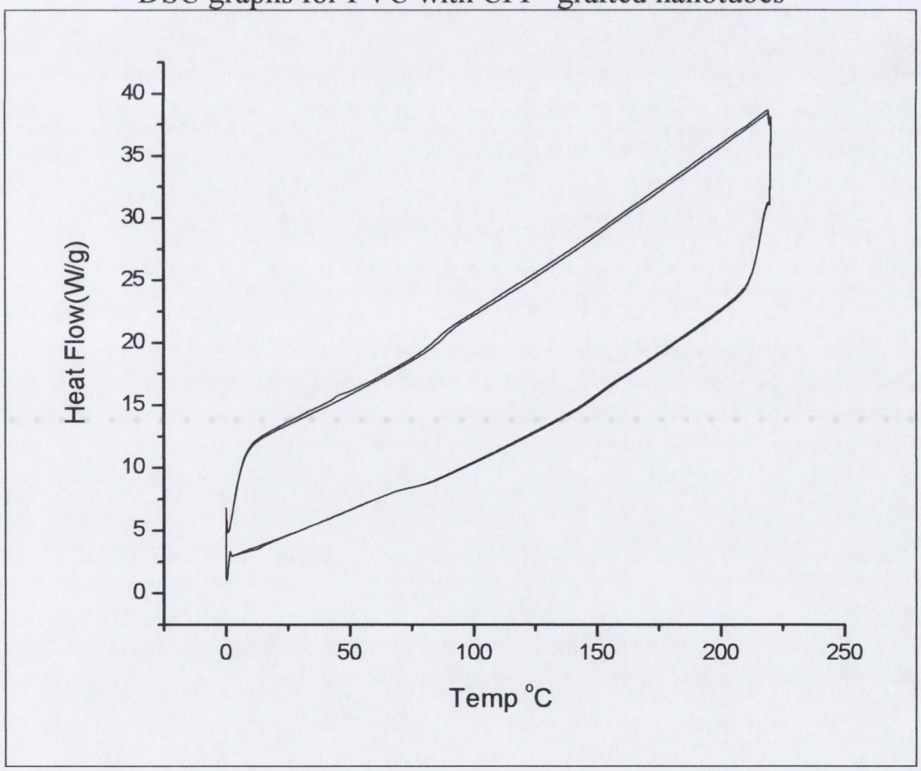

DSC graphs for pure PVC

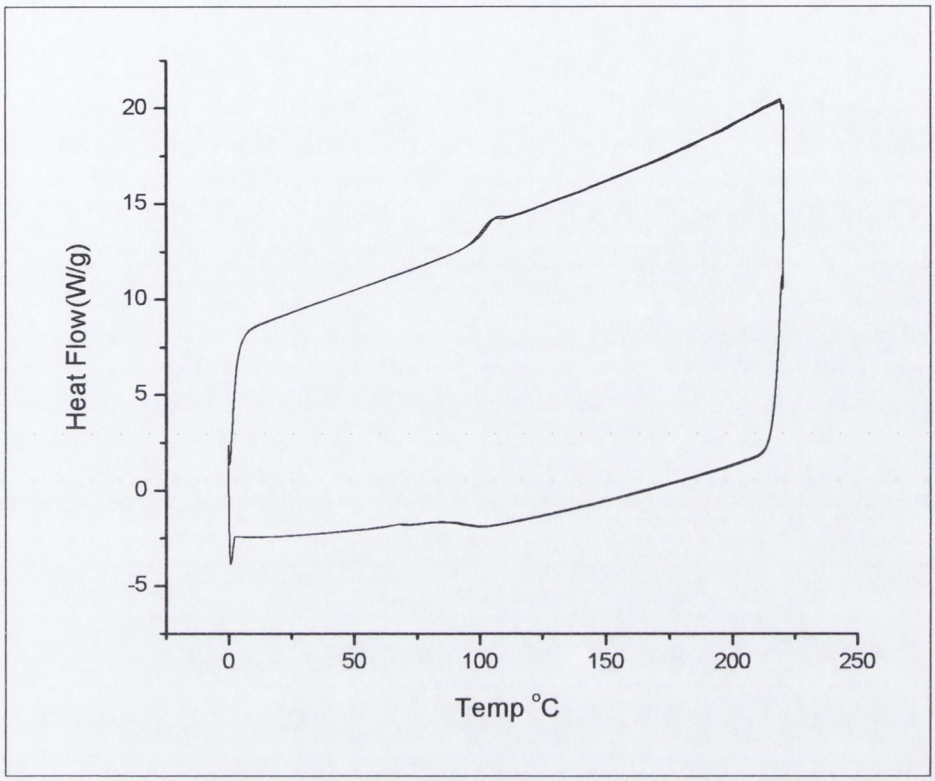

DSC graphs for CPP grafted MWNT in CPP

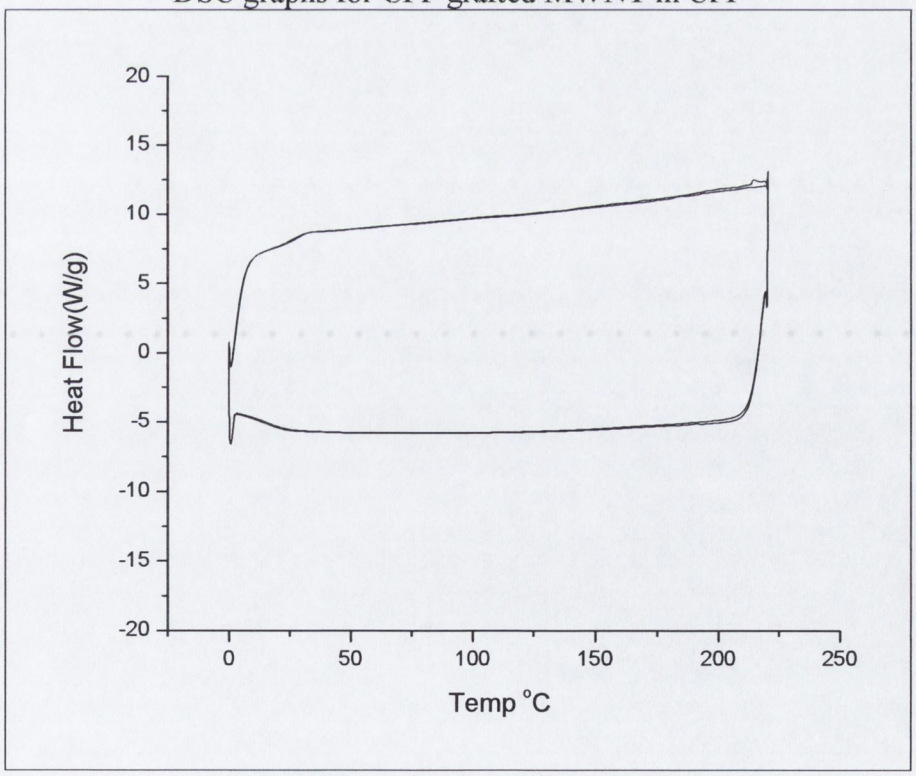

DSC graphs for pure CPP